DE GRUYTER

Tharwat F. Tadros

FORMULATION SCIENCE AND TECHNOLOGY

VOLUME 2: BASIC PRINCIPLES OF FORMULATION TYPES

Tharwat F. Tadros

Formulation Science and Technology

Also of Interest

Handbook of Colloid and Interface Science.
Volumes 1–4
Tadros, 2018
ISBN 978-3-11-054050-5

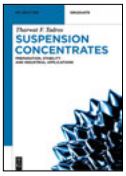

Suspension Concentrates.
Preparation, Stability and Industrial Applications
Tadros, 2017
ISBN 978-3-11-048678-0, e-ISBN 978-3-11-048687-2

Polymeric Surfactants.
Dispersion Stability and Industrial Applications
Tadros, 2017
ISBN 978-3-11-048722-0, e-ISBN 978-3-11-048728-2

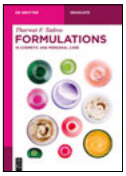

Formulations.
In Cosmetic and Personal Care
Tadros, 2016
ISBN 978-3-11-045236-5, e-ISBN 978-3-11-045238-9

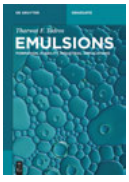

Emulsions.
Formation, Stability, Industrial Applications
Tadros, 2016
ISBN 978-3-11-045217-4, e-ISBN 978-3-11-045224-2

Tharwat F. Tadros

Formulation Science and Technology

Volume 2:
Basic Principles of Formulation Types

DE GRUYTER

Author
Prof. Tharwat F. Tadros
89 Nash Grove Lane
Workingham RG40 4HE
Berkshire, UK
tharwattadros3@gmail.com

ISBN 978-3-11-058748-7
e-ISBN (PDF) 978-3-11-058796-8
e-ISBN (EPUB) 978-3-11-058757-9

Library of Congress Control Number: 2018935454

Bibliographic information published by the Deutsche Nationalbibliothek
The Deutsche Nationalbibliothek lists this publication in the Deutsche Nationalbibliografie; detailed bibliographic data are available on the Internet at http://dnb.dnb.de.

Cover image: Nik_Merkulov / iStock / Getty Images
Typesetting: PTP-Berlin, Protago-TEX-Production GmbH, Berlin
Printing and binding: CPI books GmbH, Leck

www.degruyter.com

Preface

In Volume 1, the various interfacial phenomena, colloid stability/instability and bulk properties of formulations are described. This volume deals with the basic principles of formulation of the various systems encountered in industry. Chapter 1 describes the formulation of solid/liquid (suspension) systems that can be produced by the "bottom-up" (build-up of particles from molecular units) and "top-down" (break-up of bulk solid into smaller particles) processes. The basic factors responsible for the stability/instability of suspensions are analysed. The formulation of suspensions and the maintenance of their physical stability over long periods of time under various conditions, e.g. temperature variation, transport, etc. still remains a challenging problem to the formulation scientist or chemical engineer. This requires an understanding of the various interfacial phenomena involved in their preparation and stabilization. Once a suspension is prepared, it is necessary to control its properties on storage. Three main aspects must be considered. Firstly, control of its colloid stability which requires the presence of a repulsive energy that overcomes the everlasting van der Waals attraction. The second property that must be controlled is the process of Ostwald ripening (crystal growth) that occurs with most suspensions of organic substances. The third instability problem with suspensions is particle sedimentation that is usually reduced by addition of a thickener.

Chapter 2 deals with formulation of liquid/liquid (emulsion) systems, the role of the emulsifier and methods for selecting it. The thermodynamics of emulsion formation and breakdown processes are described and this shows the non-spontaneous formation of emulsions. The mechanism of emulsification and the role of the emulsifier are described at a fundamental level. Surfactants allow the existence of interfacial tension gradients which are crucial for formation of stable droplets and this illustrates the important role of the emulsifier to prevent coalescence during emulsification. Several procedures may be applied for emulsion preparation. Two general methods can be applied for selecting emulsifiers, namely the hydrophilic-lipophilic balance (HLB) and the phase inversion temperature (PIT) concepts. The interaction forces between emulsion droplets and factors affecting their stability are described. Several breakdown processes may occur on storage depending on droplet size distribution and density difference between the droplets and the medium; magnitude of the attractive versus repulsive forces, which determines flocculation; solubility of the disperse droplets and the particle size distribution which determine Ostwald ripening; stability of the liquid film between the droplets that determines coalescence; phase inversion, where the two phases exchange, e.g. an O/W emulsion inverting to W/O and vice versa. Phase inversion can be catastrophic as is the case when the oil phase in an O/W emulsion exceeds a critical value. The inversion can be transient when the emulsion is subjected to a temperature increase.

https://doi.org/10.1515/9783110587968-001

Chapter 3 describes the fundamental principles of foam formulations, the mechanism of stabilization and destabilization of foams. Foams can be obtained by condensation (top-down) and dispersion (bottom-up) methods. Several surface active foaming materials may be distinguished, e.g. ionic, nonionic and zwitterionic surfactants, polymers (polymeric surfactants). Particles that accumulate at the air/solution interface can also stabilize the foam. The drainage and thinning of foam films are described at a fundamental level. The theories of foam stability are described in terms of the surface viscosity and elasticity, the Gibbs–Marangoni effect, surface forces (disjoining pressure), stabilization by micelles (high surfactant concentrations > cmc), stabilization by lamellar liquid crystalline phases and stabilization of foam films by mixed surfactants. Finally, foam inhibitors, namely antifoamers that are added to prevent foam formation and deformers that are added to eliminate an existing foam, are described.

Chapter 4 deals with the formulation of gels and their rheological characteristics. The various types of gel-forming materials are described. A gel is a "semi-solid" consisting of a "network" in which the solvent is "entrapped". It may be classified as a "liquid-in-solid" dispersion. Depending on the gel strength, the system may behave as viscoelastic solid or viscoelastic liquid depending on the stress applied on the gel. Several classes of gels can be identified, namely gels produced as a result of repulsive interaction, e.g. expanded double layers, self-structured systems, whereby one induces weak flocculation to produce a "gel" by the particles or droplets; thickeners consisting of high molecular weight polymers or finely divided particulate systems that interact in the continuous phase forming a "three-dimensional" structure; self-assembled structures such as associative thickeners, crosslinked polymers (chemical gels) and liquid crystalline structures of the hexagonal, cubic or lamellar phases. The most commonly used materials to produce a gel network are polymers both natural and synthetic. However, many colloidal particulate solids can form gels by some specific interactions between the particles. High concentrations of nonionic surfactants can also produce clear gels in systems containing up to 15 % mineral oil. One of the most effective techniques to characterize a gel is to investigate its rheological (viscoelastic) behaviour, in particular under conditions of low deformation, namely stress relaxation (after sudden application of strain), constant stress (creep) and dynamic (oscillatory) measurements.

The formulation of polymer colloids (latexes) using emulsion and dispersion polymerization is described in Chapter 5 at a fundamental level. In emulsion polymerization, the monomer, e.g. styrene or methyl methacrylate that is insoluble in the continuous phase, is emulsified using a surfactant that adsorbs at the monomer/water interface. The surfactant micelles in bulk solution solubilize some of the monomer. A water-soluble initiator such as potassium persulphate $K_2S_2O_8$ is added and this decomposes in the aqueous phase forming free radicals that interact with the monomers forming oligomeric chains. The most accepted theory of emulsion polymerization is referred to as the coagulative nucleation theory where the oligomers grow by propa-

gation and this is followed by a termination process in the continuous phase. A random coil is produced which is insoluble in the medium and this produces a precursor oligomer at the θ-point. The precursor particles subsequently grow primarily by coagulation to form true latex particles. Dispersion polymerization is usually applied for the preparation of nonaqueous latex dispersions and hence it is referred to as NAD. The monomer, normally an acrylic, is dissolved in a nonaqueous solvent, normally an aliphatic hydrocarbon and an oil-soluble initiator and a stabilizer (to protect the resulting particles from flocculation, sometimes referred to as "protective colloid") is added to the reaction mixture. The most successful stabilizers used in NAD are block and graft copolymers.

Chapter 6 deals with the formulation of thermodynamically stable microemulsions. The definition of microemulsions on the basis of the second law of thermodynamics showed that the driving force of microemulsion formation is due to the ultra-low interfacial tension. The various theories that are used to account for the thermodynamic stability of microemulsions, namely the mixed film, the solubilization and the thermodynamic theories are described. The importance of using two surfactants for producing ultra-low interfacial tension is described using the Gibbs adsorption equation for multicomponent mixtures. This is followed by a section on the techniques that can be applied to characterize microemulsions, namely scattering, conductivity and NMR methods.

Chapter 7 describes the controlled-release formulations that offer a number of advantages, in particular for pharmaceuticals and agrochemicals, namely improvement of residual activity, reduction of application dosage, stabilization of the core active ingredient (AI) against environmental degradation, reduction of mammalian toxicity, reduction of phytotoxicity, reduction of fish toxicity and reduction of environmental pollution with agrochemicals. One of the main advantages of using controlled-release formulations, in particular microcapsules, is the reduction of physical incompatibility when several drugs are used and when mixtures are used with agrochemicals in the spray tank. They also can reduce biological antagonism when mixtures are applied in the field. Several types of controlled-release systems can be identified: microcapsules with particles in the size range 1–100 μm that consist of a distinct capsule wall (mostly a polymer) surrounding the active ingredient core; microparticles (size range 1–100 μm) consisting of a matrix in which the active ingredient (AI) is uniformly dissolved or dispersed; and granules with matrix particles of 0.2–2.0 mm with the active ingredient uniformly dissolved or dispersed within the matrix. Particular attention is given to the formulation of microcapsules both for liquid and solid systems.

The use of solid dosage forms such as granules and tablets, in particular in the pharmaceutical field, is described at a fundamental level in Chapter 8. Solid dosage forms are one of the most important systems used in the chemical industry, e.g. pharmaceuticals, food and speciality products. The formulation of such solid dosage forms requires the formation of the desired structure, as well as its controlled breakdown during end use by the consumer. The preparation of these systems requires an un-

derstanding of the fundamental chemistry and material science, e.g. the biological activity in a pharmaceutical product, taste in a food, etc. The material must be produced in a form that has the correct structure and on usage and delivery one must prove that this structure is correct. It is, therefore, important to obtain information on the structure by using techniques such as electron microscopy and spectroscopy. A section is devoted to agglomerated products that are frequently used in instant foods (e.g. coffee), agrochemicals and detergent powders. The structure of the agglomerated product is made up by agglomeration of smaller constituent particles. In some cases, the agglomerated product is further processed by compaction to produce a tablet as is the case with many pharmaceutical products. The next section deals with the process of compaction which is sometimes referred to as "dry agglomeration" since in this case no liquid binders are necessary for the agglomeration process. The last section describes the use of solid dosage forms in the pharmaceutical industry, namely tablets, hard and soft gelatin capsules and sustained-release pellets.

The various techniques that can be applied for assessing and predicting the long-term physical stability of formulations are listed in Chapter 9. For full characterization of the properties of formulations, three main types of investigations are needed:

(i) Fundamental investigations of the system at a molecular level, namely structure of the electrical double layer, adsorption of surfactants, polymers and polyelectrolytes and conformation of the adsorbed layers; it is important to know how each of these parameters changes with the conditions, such as temperature, solvency of the medium for the adsorbed layers and effect of addition of electrolytes.

(ii) Investigation of the state of the suspension on standing, namely flocculation rates, flocculation points with sterically stabilized systems, spontaneity of dispersion on dilution and Ostwald ripening or crystal growth, investigations of emulsion coalescence and phase inversion for the emulsions discussed. All these phenomena require accurate determination of the particle size distribution as a function of storage time and temperature.

(iii) Bulk properties of the suspension, which are particularly important for concentrated systems. This requires measuring the rate of sedimentation and equilibrium sediment height. More quantitative techniques are based on assessment of the rheological properties of the suspension (without disturbing the system, i.e. without its dilution and measurement under conditions of low deformation) and how these are affected by long-term storage. Rheological measurements provide accurate information on the state of the system, such as sedimentation or creaming and flocculation. These measurements are also applied for the prediction of the long-term physical stability of the suspension. Three type of measurements can be applied, namely steady state shear stress–shear rate, constant stress (creep) and dynamic (oscillatory) measurements. Rheological techniques can also be applied for the assessment and prediction of the physical stability of the formulation

This comprehensive text on the fundamental principles of formulation of various formulation classes provides the scientist with a rational approach for formulations of any type, rather than using the empirical trial and error method. It is certainly valuable for chemists and chemical engineers dealing with formulation both in academia as well as industrial labs.

Tharwat Tadros
May 2018

Contents

1 Formulation of solid/liquid dispersions (suspensions)

1.1 Introduction

Many chemicals are formulated as solid/liquid dispersions (to be referred to as suspensions), e.g. paints, dyestuffs, paper coatings, printing inks, agrochemicals, pharmaceuticals, cosmetics, food products, detergents, ceramics, etc. The powder particles can be hydrophobic, e.g. organic pigments, agrochemicals, ceramics or hydrophilic, e.g. silica, titania, clays [1–5]. The liquid can be aqueous or nonaqueous. The average particle size of the suspension can be within the colloid range (1 nm–1 μm) or outside the colloid range (> 1 μm). Suspensions with dimension within the colloid range are referred to as colloidal suspensions. In contrast, suspensions with dimensions outside the colloid range are generally referred to as coarse suspensions. They are to be distinguished from colloidal suspensions in the sense that the particles of coarse suspensions settle to the bottom of the container (as a result of the gravitational field on the particles) whereas with colloidal suspensions, with particle density not significantly larger than that of the medium, the very mild mixing produced by ambient thermal fluctuations and/or Brownian motion can keep the particles uniformly dispersed in the continuous medium [1]. The formulation of suspensions and maintenance of their physical stability over long periods of time under various conditions, e.g. temperature variation, transport, etc. still remains a challenging problem to the formulation scientist or chemical engineer. This requires understanding of the various interfacial phenomena involved in their preparation and stabilization [6, 7].

The concentration of a suspension is described by its volume fraction ϕ, namely the ratio between the total volume of particles to the volume of the suspension. The value of ϕ above which a suspension may be considered "dilute", "concentrated" or "solid" can be defined from a consideration of the balance between the particle translational motion (Brownian diffusion) and interparticle interaction [2, 8]. If Brownian diffusion predominates over the imposed interparticle interaction, the suspension may be described as "dilute". In this case the particle translational motion is large and only occasional contacts may occur between the particles which are then separated by the Brownian force. The particle interactions can be represented by two-body collisions. This "dilute" suspension has generally time-independent properties and if the particle size is within the colloid range and the density difference between the particles is very small, no gravitational sedimentation of particles occurs and the system maintains its properties over long periods of time. These "dilute" suspensions show Newtonian flow, i.e. their viscosity is independent of the applied shear rate [9]. In contrast, if interparticle interaction predominates over Brownian diffusion, i.e. the interparticle distance h becomes much smaller than the particle radius, the system may be described as a "solid" suspension. In this case the particles may vibrate with

https://doi.org/10.1515/9783110587968-002

a distance h that is much smaller than the particle radius. The interaction produces a specific order between the particles and a highly developed structure is reached. The resulting "solid" suspension becomes predominantly elastic with very little energy dissipation during flow [9]. Again, the properties of these elastic systems are time-independent. In between the two extremes one may define a volume fraction ϕ at which the suspension may be considered "concentrated". In this case the interparticle distance h is comparable to the particle radius and the suspension shows time-dependent spatial and temporal correlations. The particle interactions occur with many body collisions and the translational motion of the particles is restricted. These "concentrated" suspensions show viscoelastic behaviour, i.e. a combination of viscous and elastic response [9]. At low stresses the suspension may show predominantly elastic response, whereas at high stress predominantly viscous response is obtained (Chapter 14 of Vol. 1)

There are two main processes for the preparation of suspensions [1]. The first depends on the "build-up" of particles from molecular units, i.e. the so-called "bottom-up" or condensation method, which involves two main processes, namely nucleation and growth. In this case, it is necessary first to prepare a molecular (ionic, atomic or molecular) distribution of the insoluble substances; then by changing the conditions, precipitation is caused leading to the formation of nuclei that grow to the particles in question. A particular case of the condensation process is the preparation of polymer latex particles by emulsion or suspension polymerization. The second procedure for preparation of suspension concentrates is usually referred to as the "top-down" or dispersion process [2]. Dispersion is a process whereby aggregates and agglomerates of powders are dispersed into "individual" units, usually followed by a wet milling process (to subdivide the particles into smaller units) and stabilization of the resulting dispersion against aggregation and sedimentation. The larger "lumps" of the insoluble substances are subdivided by mechanical or other means into smaller units. In the whole "top-down" process, it is essential to wet both the external and internal surfaces of the aggregates and agglomerates. For hydrophobic solids dispersed in aqueous media, it is essential to use a wetting agent (surfactant) that lowers the surface tension of water (under dynamic conditions) and reduces the solid/liquid interfacial tension by adsorption on the surface of the particles. After wetting, the aggregates and agglomerates are dispersed into single particles by high-speed mixing. The resulting suspension, referred to as "mill base" is then subjected to a milling process to reduce the particle size to the desired value [1, 2].

Once a suspension is prepared, it is necessary to control its properties on storage. Three main aspects must be considered. Firstly, control of its colloid stability which requires the presence of a repulsive energy that overcomes the everlasting van der Waals attraction. Three main types of stabilization may be considered:

(i) Electrostatic repulsion produced by the presence of electrical double layers surrounding the particles [10, 11] as described in Chapter 7 of Vol. 1. These double layers are extended in solution, particularly at low electrolyte concentration and low valency

of ions forming the double layers. When two particles with these extended double layers approach each other to a separation distance h that is smaller than twice the double layer extension ("thickness") strong repulsion occurs. This repulsion G_{elec} increases with decreasing electrolyte concentration and valency. Combining G_{elec} with the van der Waals attraction G_A results in an energy–distance curve that forms the basis of the theory of colloid stability due to Deryaguin–Landau–Verwey–Overbeek (DLVO theory) [10, 11]. This energy–distance curve shows a maximum (energy barrier) at intermediate separation distances (when the 1 : 1 electrolyte concentration is $< 10^{-2}$ mol dm^{-3}). This energy barrier prevents strong aggregation of the particles thus maintaining effective stability.

(ii) Steric repulsion produced by adsorption of nonionic surfactants or polymeric surfactants as described in Chapter 8 of Vol. 1. These surfactants consist of an "anchor" chain(s) that strongly adsorbs on the particle surface and stabilizing chain(s) that remains in solution and becomes strongly solvated by the molecules of the medium [12, 13]. One can define an adsorbed layer thickness δ which increases with increasing molar mass of the stabilizing chain(s). When two particles with adsorbed surfactant or polymer layers approach to a distance h that is lower than 2δ, the stabilizing chains may overlap or become compressed resulting in an increase in the segment concentration in the overlapped or compressed layers. Provided the latter are in good solvent conditions (highly solvated by the molecules of the medium), this effect results in an increase in the osmotic pressure in these overlapped or compressed layers. Solvent molecules will now diffuse to these layers thus separating the particles. This repulsive effect is referred to as the mixing interaction energy G_{mix} (unfavourable mixing of the stabilizing chains). In the overlapped or compressed layers the configurational entropy of the chains is significantly reduced resulting in another repulsive energy G_{el} (entropic, volume restriction or elastic interaction). The sum of G_{mix} and G_{el} is referred to as G_s (steric repulsive energy). Combining G_{mix} and G_{el} with G_A gives G_T–h curves and this forms the basis of the theory of steric stabilization [12, 13]. In this case the G_T–h curve shows a shallow minimum at separation distance $h \approx 2\delta$, but when $h < 2\delta$, G_T increases sharply with any further decrease in h.

(iii) Electrosteric stabilization where G_{elec} and G_s are combined with G_A. In this case the G_T–h curve shows a shallow minimum at large h values, a maximum at intermediate distances (DLVO type maximum) and a sharp increase at distances comparable to 2δ. Electrosteric stabilization is generally produced when using polyelectrolytes to stabilize the suspension or when using a mixture of nonionic or polymeric surfactant with an ionic one.

The second property that must be controlled is the process of Ostwald ripening (crystal growth) that occurs with most suspensions of organic substances [1–3], as described in Chapter 10 of Vol. 1. Organic substances have a finite solubility in the medium that may reach several hundred ppm (parts per million). The smaller particles with higher radius of curvature have a higher solubility when compared with the larger particles. This difference in solubility between small and large particles is the driving

force for Ostwald ripening. With time, molecular diffusion occurs from the small to the large particles with the ultimate dissolution of these small particles and their molecules become deposited on the larger particles. Thus, on storage of the suspension, the particle size distribution shifts to larger particles. This will result in instability of the suspension, e.g. enhanced sedimentation. Another mechanism of Ostwald ripening is due to polymorphic changes. The particles (e.g. a drug) may contain two or more polymorphs with different solubility. The more stable polymorph has a lower solubility when compared with the metastable polymorph. With time, the more soluble polymorph gradually changes to the less soluble stable one. This Ostwald ripening problem may result in a reduction of bioavailability of the drug and hence it must be reduced or eliminated. Several methods can be applied to reduce Ostwald ripening in suspensions, e.g. incorporation of impurities that strongly adsorb on the particle surface, thus blocking the active sites for growth. Alternatively one can use strongly adsorbed polymeric surfactants, which has the same effect as the added impurities.

The third instability problem with suspensions is particle sedimentation [1–4], as described in Chapter 13 of Vol. 1, which occurs when the particle size is outside the colloid range and the density difference between the particles and the medium is significant. In this case the gravity force $(4/3)\pi R^3 \Delta\rho gh$ (where R is the particle radius, $\Delta\rho$ is the density difference between the particle and the medium, g is the gravity force and h is the height of the container) exceeds the Brownian motion kT (where k is the Boltzmann constant and T is the absolute temperature). With most practical suspensions with a wide particle size distribution, the larger particles sediment at a higher rate than the smaller particles. A particle concentration gradient of the particles occurs across the container. Several methods may be applied to reduce sedimentation, e.g. balancing the density of the disperse phase with that of the medium, reducing particle size (i.e. formation of nanosuspensions) and adding thickeners. The latter can be high molecular weight polymers such as xanthan gum or "inert" fine particles such as silica or clays. In all cases these thickeners produce a "gel network" in the continuous phase which produces a very high viscosity at low shear rates that prevents particle sedimentation.

It is now important to distinguish between "colloid" and "physical" stability. Colloid stability implies absence of particle aggregation and this requires a high repulsive energy as discussed above. However, a colloidally stable suspension may undergo separation, e.g. as a result of particle sedimentation as discussed above. Physical stability, on the other hand, implies absence of any separation, ease of redispersion on gentle shaking or dilution. In many cases "physical stability" may require weak flocculation and formation of a "gel-network structure".

An important factor that controls physical stability is the bulk rheology of the suspension.

One way to distinguish between colloid and physical stability is to consider the various states of the suspension on standing as schematically illustrated in Fig. 1.1. These states are determined by the interaction energy between the particles, the ef-

fect of gravity and addition of other components such as surfactants, polymers and thickeners [1–4].

States (a)–(c) correspond to a suspension that is stable in the colloid sense. The stability is obtained as a result of net repulsion due to the presence of extended double layers (i.e. at low electrolyte concentration), the result of steric repulsion produced by adsorption of nonionic surfactants or polymers, or the result of a combination of double layer and steric repulsion (electrosteric). State (a) represents the case of a suspension with small particle size (submicron) where the Brownian diffusion overcomes the gravity force producing uniform distribution of the particles in the suspension, i.e. $kT \gg (4/3)\pi R^3 \Delta\rho g h$.

A good example of the above case is a latex suspension with particle size well below 1 μm that is stabilized by ionogenic groups, by an ionic surfactant or nonionic surfactant or polymer. This suspension will show no separation on storage for long periods of time.

States (b) and (c) represent the case of suspensions in which the particle size range is outside the colloid range (> 1 μm). In this case, the gravity force exceeds the Brownian diffusion, i.e. $(4/3)\pi R^3 \Delta\rho g h \gg kT$.

With state (b), the particles are uniform and initially they are well dispersed, but with time and the influence of gravity they settle to form a hard sediment (technically referred to "clay" or "cake"). In the sediment, the particles are subjected to a hydrostatic pressure $h\rho g$, where h is the height of the container, ρ is the density of the particles and g is the acceleration due to gravity.

Within the sediment each particle will be acting constantly with many others, and eventually an equilibrium is reached where the forces acting between the particles will be balanced by the hydrostatic pressure on the system. The forces acting between the particles will depend on the mechanism used to stabilize the particles, for example electrostatic, steric or electrosteric, the size and shape of the particles, the medium permittivity (dielectric constant), electrolyte concentration, the density of the particles, etc. Many of these factors can be incorporated to give an interaction energy in the form of a pair potential for two particles in an infinite medium. The repulsive forces between the particles allow them to move past each other until they reach small distances of separation (that are determined by the location of the repulsive barrier). Due to the small distances between the particles in the sediment, it is very difficult to redisperse the suspension by simple shaking.

With case (c) consisting of a wide distribution of particle sizes, the sediment may contain larger proportions of the larger size particles, but still a hard "clay" is produced. These "clays" are dilatant (i.e. shear thickening) and they can be easily detected by inserting a glass rod in the suspension. Penetration of the glass rod into these hard sediments is very difficult.

States (d)–(f) represent the case for unstable, coagulated suspensions which either have a small repulsive energy barrier or its complete absence. State (d) represents the case of coagulation under conditions of no stirring in which case chain aggregates

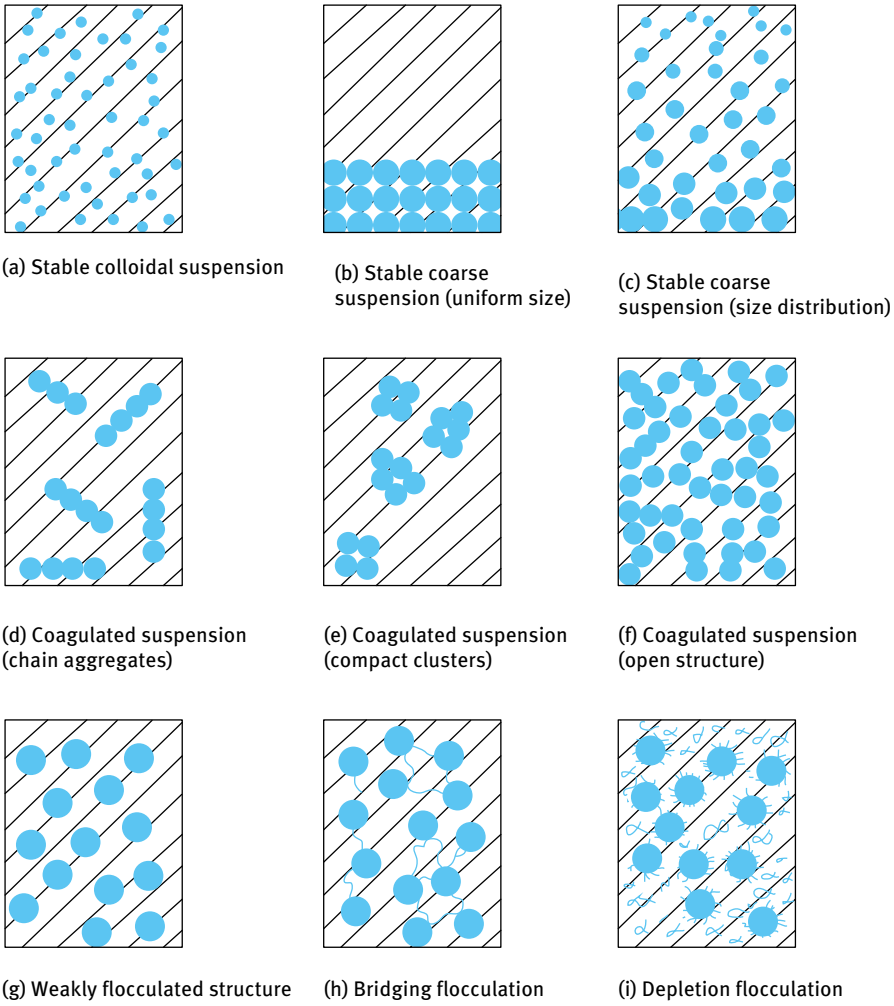

(a) Stable colloidal suspension

(b) Stable coarse suspension (uniform size)

(c) Stable coarse suspension (size distribution)

(d) Coagulated suspension (chain aggregates)

(e) Coagulated suspension (compact clusters)

(f) Coagulated suspension (open structure)

(g) Weakly flocculated structure

(h) Bridging flocculation

(i) Depletion flocculation

Fig. 1.1: States of the suspension.

are produced that will settle under gravity forming a relatively open structure. State (e) represents the case of coagulation under stirring conditions where compact aggregates are produced that will settle faster than the chain aggregates and the sediment produced is more compact. State (f) represents the case of coagulation at high volume fraction of the particles, ϕ. In this case the whole particles will form a "one-floc" structure that is formed from chains and cross chains that extend from one wall to the other in the container. Such a coagulated structure may undergo some compression (consolidation) under gravity leaving a clear supernatant liquid layer at the top of the container. This phenomenon is referred to as syneresis.

State (g) represents the case of weak and reversible flocculation. This occurs when the secondary minimum in the energy distance curve is deep enough to cause flocculation [1–4]. This can occur at moderate electrolyte concentrations, in particular with larger particles. The same occurs with sterically and electrosterically stabilized suspensions. This occurs when the adsorbed layer thickness is not very large, particularly with large particles. The minimum depth required for causing weak flocculation depends on the volume fraction of the suspension. The higher the volume fraction, the lower the minimum depth required for weak flocculation.

The above flocculation is weak and reversible, i.e. on shaking the container redispersion of the suspension occurs. On standing, the dispersed particles aggregate to form a weak "gel". This process (referred to as sol–gel transformation) leads to reversible time dependency of viscosity (thixotropy). On shearing the suspension, the viscosity decreases and when the shear is removed, the viscosity is recovered. This phenomenon is applied in paints. On application of the paint (by a brush or roller), the gel is fluidized, allowing uniform coating of the paint. When shearing is stopped, the paint film recovers its viscosity and this avoids any dripping.

State (h) represents the case in which the particles are not completely covered by the polymer chains. In this case, simultaneous adsorption of one polymer chain on more than one particle occurs, leading to bridging flocculation. If the polymer adsorption is weak (low adsorption energy per polymer segment), the flocculation could be weak and reversible. In contrast, if the adsorption of the polymer is strong, tough flocs are produced and the flocculation is irreversible. This phenomenon is used for solid/liquid separation, e.g. in water and effluent treatment.

Case (i) represents a phenomenon referred to as depletion flocculation, produced by addition of "free", nonadsorbing polymer [14, 15]. In this case, the polymer coils cannot approach the particles to a distance Δ (that is determined by the radius of gyration of free polymer R_G), since the reduction of entropy on close approach of the polymer coils is not compensated by an adsorption energy. The suspension particles will be surrounded by a depletion zone with thickness Δ. Above a critical volume fraction of the free polymer, ϕ_p^+, the polymer coils are "squeezed out" from between the particles and the depletion zones begin to interact. The interstices between the particles are now free from polymer coils and hence an osmotic pressure is exerted outside the particle surface (the osmotic pressure outside is higher than in-between the particles) resulting in weak flocculation. The magnitude of the depletion attraction free energy, G_{dep}, is proportional to the osmotic pressure of the polymer solution, which in turn is determined by ϕ_p and molecular weight M. The range of depletion attraction is proportional to the thickness of the depletion zone, Δ, which is roughly equal to the radius of gyration, R_G, of the free polymer.

In this chapter I will start by describing the process of preparation of suspensions by the "bottom-up" process. The advantage of this method over the "top-down" process is highlighted, namely the ability to control the particle size distribution. A section is devoted to the process of preparation of suspensions by precipitation. The clas-

sical theory of nucleation and growth (Gibbs–Volmer theory) is described in terms of the free energy components of the process, namely the surface free energy and the bulk energy in producing a new phase. This results in a definition of the critical nucleus size above which spontaneous particle growth occurs. The dependency of the critical nucleus size on supersaturation is described and particular reference is given to the effect of added surfactants. A section is devoted to the kinetics of precipitation and control of particle size distribution. The effect of surface modification on precipitation kinetics is described followed by other methods that can be applied for preparing suspension particles. A section is devoted to the process of emulsion and suspension particle preparation for latex suspensions.

The next section describes the methods for preparing suspensions using the top-down process. The process of wetting of powder aggregates and agglomerates (both external and internal surfaces) is described with special reference to the role of surfactants (wetting agents). Wetting of the external surface requires the presence of a surfactant that lowers the surface tension of the liquid and the interfacial tension of the solid/liquid interface. This results in lowering the contact angle at the three-phase region of solid/liquid/vapour. For adequate wetting of the external surface, a contact angle approaching zero is required. Wetting of the internal surface (pores of aggregates and agglomerates) requires adequate penetration of the liquid inside the pores. Again a low contact angle is required, but good penetration of the liquid requires a high liquid surface tension. Thus, a compromise is needed for good wetting of the external and internal surfaces, namely a low contact angle but not too much lower surface tension. This shows the difficulty of choosing the right wetting agent for any particular powder. The various methods that can be applied for measuring powder wetting are described. The different classes of surfactants for enhancing wetting are described. This is followed by a section on dispersion of the aggregates and agglomerates using high-speed stirrers. Finally the methods that can be applied for size reduction are described with reference to bead milling. The main factors responsible for the maintenance of colloid stability are described.

The next section will only give a summary of the electrostatic stabilization of suspensions, since this has been described in detail in Chapter 7 of Vol. 1. The origin of charge in suspensions and the structure of the electrical double layer was discussed in detail in that chapter. The well-known theory of colloid stability due to Deryaguin–Landau–Verwey–Overbeek (DLVO theory) [10, 11] was described in detail in Chapter 7 of Vol. 1.

The next section gives a brief description of steric stabilization of suspensions, which has been described in detail in Chapter 8 of Vol. 1. The interaction between particles containing adsorbed surfactant or polymer layers will be briefly described [12, 13].

The various processes of flocculation of electrostatically and sterically stabilized suspensions are summarized, which were described in detail in Chapter 9 of Vol. 1.

A section is devoted to the process of the Ostwald ripening (crystal growth) of suspensions and its prevention and this has been described in more detail in Chapter 10 of Vol. 1.

The last section deals with sedimentation of suspensions and prevention of formation of dilatant sediments that was described in detail in Chapter 13 of Vol. 1.

1.2 Preparation of suspension concentrates by the bottom-up process

As mentioned in the introduction, the bottom-up process for preparing suspensions involves the formation of particles from molecular units [16]. A good example is the preparation of particles of inorganic materials, such as silica, titania, ZnO, etc., i.e. the process of precipitation, nucleation and growth. Another example is the preparation of polymer colloids by emulsion or dispersion polymerization.

As mentioned above, one of the main advantages of the bottom-up process over the top-down process is the possibility to control the particle size and shape distribution as well as the morphology of the resulting particles [16]. By controlling the process of nucleation and growth it is possible to obtain suspensions with a narrow size distribution. This is particularly important for many practical applications such as photonic materials, and semiconductor colloids. However, for other processes such as in paints and ceramic processes, a modest polydispersity can be beneficial to enhance the random packing density of the spheres and, consequently, the viscosity of the mixtures is generally below that for monodisperse spheres at the same volume fraction [9].

A very important aspect of suspensions is the maintenance of their colloid stability, i.e. absence of any flocculation. This can be achieved by three different mechanisms as described in the introduction.

The precipitation method is usually applied for preparing inorganic particles such as metal oxides and nanoparticles of metals. As an illustration, ferric oxide and aluminium oxide or hydroxide are prepared by hydrolysis of metal salts [8],

$$2FeCl_3 + 3H_2O \rightarrow F_2O_3\downarrow + 6HCl, \tag{1.1}$$

$$AlCl_3 + 3H_2O \rightarrow AlOOOH + 3HCl. \tag{1.2}$$

Another example of preparing particles by precipitation is that of silica sols. These can be prepared by acidification of water glass, a strongly alkaline solution of glass (that essentially consists of amorphous silica). Acidification is necessary to achieve a highly supersaturated solution of dissolved silica. Another method for obtaining high supersaturation of silica is by a change of solvent, instead of a change in pH. In this method a stock solution of sodium-silica solution ($Na_2O.SiO_2$, 27 wt% SiO_2) is diluted with double distilled water to 0.22 wt% SiO_2. Under vigorous stirring, 0.2 ml of this water glass solution is rapidly pipetted into 10 ml of absolute ethanol. A sudden turbidity increase

manifests the formation of small, smooth silica spheres with a diameter around 30 nm and a typical polydispersity of 20–30 % [16]. A third method for preparation of silica spheres is the well-known Stober method [16]. The precursor tetraethyl silicate (TES) is dissolved in an ethanol-ammonia mixture which is gently stirred in a closed vessel. Silica spheres with a radius of about 60 nm and typical polydispersity of 10–15 % are produced.

An example of nanometal particles is the reduction of metal salt [16],

$$H_2PtCl_6 + BH_4^- + 3H_2O \rightarrow Pt\downarrow + 2H_2\uparrow + 6HCl + H_2BO_3^-. \tag{1.3}$$

To understand the process of formation of nanoparticles by the bottom-up process, we must consider the process of homogeneous precipitation at a fundaments level. If a substance becomes less soluble by a change of some parameter, such as a temperature decrease, the solution may enter a metastable state by crossing the bimodal as is illustrated in the phase diagram (Fig. 1.2) of a solution which becomes supersaturated upon cooling [16].

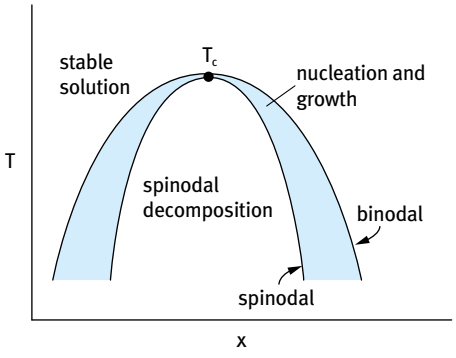

Fig. 1.2: Phase diagram of a solution which becomes supersaturated upon cooling; x is the solute mole fraction and T is the temperature.

In the metastable region, the formation of small nuclei initially increases the Gibbs free energy. Thus, demixing by nucleation is an activation process, occurring at a rate which is extremely sensitive to the precipitation in this metastable region. In contrast, when the solution is quenched into the unstable region on crossing the spinodal (Fig. 1.2) there is no activation barrier to form a new phase.

1.2.1 Nucleation and growth

Classical nucleation theory considers a precipitating particle (referred to as a nucleus or cluster) to consist of a bulk phase containing N_i^s molecules and a shell with N_i^σ molecules which have a higher free energy per molecule than the bulk. The particle is

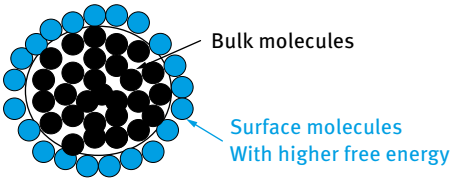

Fig. 1.3: Schematic representation of a nucleus

embedded in a solution containing dissolved molecules *i*. This is schematically represented in Fig. 1.3. The Gibbs free energy of the nucleus G^s is made up of a bulk part and a surface part [8],

$$G^s = \mu_i^s N_i^s + \sigma A, \tag{1.4}$$

where μ_i^s is the chemical potential per molecule, σ is the solid/liquid interfacial tension and A is the surface area of the nucleus.

In a supersaturated solution the activity a_i is higher than that of a saturated solution a_i(sat). As a result, molecules are transferred from the solution to the nucleus surface. The free energy change ΔG^s upon the transfer of a small number N_i from the solution to the particle is made up of two contributions from the bulk and the surface,

$$\Delta G^s = \Delta G^s(\text{bulk}) + \Delta G^s(\text{surface}). \tag{1.5}$$

The first term on the right-hand side of equation (1.5) is negative (it is the driving force) whereas the second term is positive (work has to be carried out in expanding the interface). ΔG^s(bulk) is determined by the relative supersaturation, whereas ΔG^s(surface) is determined by the solid/liquid interfacial tension σ and the interfacial area A which is proportional to $(N_i^s)^{2/3}$.

ΔG^s is given by the following expression,

$$\Delta G^s = -N_i kT \ln S + \beta \sigma N_i^{2/3}, \tag{1.6}$$

where k is the Boltzmann constant, T is the absolute temperature and β is a proportionality constant that depends on the shape of the nucleus. S is the relative supersaturation that is equal to a_i/a_i(sat).

For small clusters the surface area term dominates, whereas ΔG^s only starts to decrease due to the bulk term beyond a critical value N^*.

N^* can be obtained by differentiating equation (1.6) with respect to N and equating the result to 0 ($dG^s/dN = 0$),

$$(N^*)^{1/3} = \frac{2\sigma\beta}{3kT \ln S}. \tag{1.7}$$

The maximum in the Gibbs energy is given by,

$$\Delta G^* = \frac{1}{3}\beta (N^*)^{2/3}. \tag{1.8}$$

Equation (1.7) shows that the critical cluster size decreases with increasing the relative supersaturation S or reducing σ by adding surfactants. This explains why a high supersaturation and/or addition of surfactants favours the formation of small particles. A large S pushes the critical cluster size N^* to smaller values and simultaneously lowers the activation barrier, illustrated in Fig. 1.4, which shows the variation of ΔG with radius at increasing S.

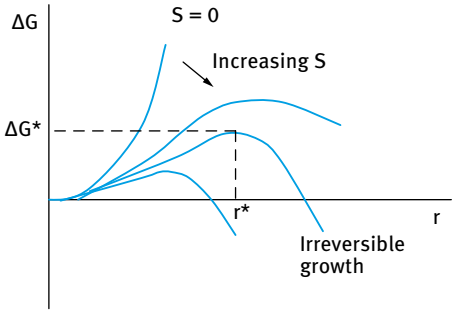

Fig. 1.4: Schematic representation of the effect of supersaturation on particle growth.

Assuming the nuclei to be spherical, equation (1.6) can be given in terms of the nucleus radius r,

$$\Delta G = 4\pi r^2\sigma - \left(\frac{4}{3}\right)\pi r^3\left(\frac{kT}{V_m}\right)\ln S, \tag{1.9}$$

where V_m is the molecular volume.

ΔG^* and r^* are given by,

$$\Delta G^* = \frac{4}{3}\pi(r^*)^2\sigma, \tag{1.10}$$

$$r^* = \frac{2V_m\sigma}{kT\ln S}. \tag{1.11}$$

When no precautions are taken, precipitation from a supersaturated solution produces polydisperse particles. This is because nucleation of new particles and further particle growth overlap in time. This overlap is the consequence of the statistical nature of the nucleation process; near the critical size particles may grow as well as dissolve. To narrow down the particle size distribution as much as possible, nucleation should take place over a short time, followed by equal growth of a constant number of particles. This can be achieved by rapidly creating the critical supersaturation required to initiate homogeneous nucleation after which particle growth lowers the saturation sufficiently to suppress new nucleation events. Another option is to add nuclei (seeds) to a solution with subcritical supersaturation. A fortunate consequence of particle growth is that in many cases the size distribution is self-sharpening.

1.2.2 Precipitation kinetics

The kinetics of precipitation in a metastable solution can be considered to follow two regimes, according to Fig. 1.4. The initial regime is that where small particles struggle with their own solubility to pass the Gibbs energy barrier ΔG^*. This passage is called a nucleation event, which is simply defined as the capture of one molecule by a critical cluster [16], assuming that after this capture, the cluster enters the irreversible growth regime upon which a new colloid is born. In this case the number I of colloids that exist per second is proportional to c_m (the concentration of single unassociated molecules) and c^* (the concentration of critical clusters),

$$I = kc_m c^*, \tag{1.12}$$

where k is the rate constant. Equation (1.12) predicts second-order reaction kinetics.

To quantify I, one must evaluate the frequency at which molecules encounter a spherical nucleus of radius a by diffusion. This can be evaluated using Smoluchowski's diffusion model for coagulation kinetics [16]. The diffusion flux J of molecules through any spherical envelope with radius a is given by Fick's first law,

$$J = 4\pi r^2 D \frac{\mathrm{d}c(a)}{\mathrm{d}a}, \tag{1.13}$$

where D is the molecular diffusion coefficient relative to the sphere positioned at the origin $a = 0$. Each molecule that reaches the sphere's surface irreversibly attaches to the insoluble sphere and it is assumed that the concentration c_m of molecules in the liquid far away from the sphere radius remains constant [16],

$$c(a - r) = 0, \quad c(a \to \infty) = c_m. \tag{1.14}$$

For these boundary conditions equation (1.13) becomes,

$$c(a - r) = 0, \quad c(a \to \infty) = c_m, \tag{1.15}$$

if it assumed that J is independent of a, i.e. if the diffusion of the molecules towards the sphere has reached a steady state. Such a state is approached by the concentration gradient around a sphere in a time of the order of r^2/D needed by the molecules to diffuse over a sphere diameter. Assuming that the sphere growth is a consequence of stationary states, one can identify the nucleation rate I as the flux J multiplied by the concentration c^* of sphere with critical radius r^*,

$$I = 4\pi D r^* c_m c^* \ [\mathrm{m^{-3}\,s^{-1}}]. \tag{1.16}$$

The concentration c^* can be evaluated by considering the reversible work to form a cluster out of N molecules using the Boltzmann distribution principle,

$$c(N) = c_m \exp\left(\frac{-\Delta G}{kT}\right). \tag{1.17}$$

$c(N)$ represents the equilibrium concentration of clusters composed of N molecules and ΔG is the free energy of formation of a cluster. Applying this result to clusters with a critical size r^*, we obtain on substitution in equation (1.16),

$$I = 4\pi D r^* c_m^2 \exp\left(\frac{-\Delta G^*}{kT}\right), \tag{1.18}$$

$$\Delta G^* = \left(\frac{4\pi}{3}\right)(r^*)^2\sigma, \tag{1.19}$$

where ΔG^* is the height of the nucleation barrier. The exponent may be identified as the probability (per particle) that a spontaneous fluctuation will produce a critical cluster. Equation (1.18) shows that the nucleation rate is very sensitive to the value of r^* and hence to supersaturation as given by equation (1.11). The maximum nucleation rate at very large supersaturation, i.e. the pre-exponential term in equation (1.18) can be obtained by substitution of D using the Stokes–Einstein equation,

$$D = \frac{kT}{6\pi\eta r^*}, \tag{1.20}$$

where η is the viscosity of the medium. This maximum nucleation rate is given by,

$$I \approx \frac{kT}{\eta} = c_m^2. \tag{1.21}$$

For an aqueous solution at room temperature with a molar concentration c_m, the maximum nucleation rate is of the order of 10^{29} m^{-3} s^{-1}. A decrease in supersaturation to values around $S = 5$ is sufficient to reduce this very high rate to practically zero. For silica precipitation in dilute, acidified water glass solutions, $S \approx 5$ and nucleation may take hours or days.

As mentioned above, when no precautions are taken, precipitation from a supersaturated solution produces polydisperse particles. Fortunately, in many cases the size distribution is self-sharpening. This can be illustrated by considering the colloidal spheres with radius r, which irreversibly grow by the uptake of molecules from a solution according to the following rate law [16],

$$\frac{dr}{dt} = k_0 r^n \tag{1.22}$$

where k_0 and n are constants. This growth equation leads either to spreading or sharpening of the relative distribution, depending on the value of n. Consider at a given time t any pair of spheres with arbitrary size from the population of independently growing particles. Let $1 + \varepsilon$ be their size ratio such that $r(1 + \varepsilon)$ and r are the radius of the larger and smaller spheres, respectively. The former grow according to,

$$\frac{d}{dt} r(1 + \varepsilon) = k r^n (1 + \varepsilon)^n \tag{1.23}$$

which can be combined with the growth equation (1.22) for the smaller spheres to obtain the time evolution of the size ratio,

$$\frac{d\varepsilon}{dt} = k_0 r^{n-1}\left[(1 + \varepsilon)^n - (1 + \varepsilon)\right], \quad \varepsilon \geq 0. \tag{1.24}$$

The relative size difference ε increases with time for $n > 1$, in which case particle growth broadens the distribution. For $n = 1$, the size ratio between the spheres remains constant, whereas for $n < 1$ it monotonically decreases with time. Since this decrease holds for any pair of particles in the growing population, it follows that for $n < 1$ the relative size distribution is self-sharpening [8]. This condition is practically realistic. For example, when the growth rate is completely determined by a slow reaction of molecules at the sphere radius,

$$\frac{\mathrm{d}r^3}{\mathrm{d}t} = k_0 r^2 \tag{1.25}$$

implying that $\mathrm{d}r/\mathrm{d}t$ is a constant, so $n = 0$. The opposite limiting case is growth governed by the rate at which molecules reach a colloid by diffusion. The diffusion flux for molecules with a diffusion coefficient D, relative to a sphere centred at the origin at $a = 0$, is given by equation (1.13). The saturation concentration is assumed to be maintained at the particle surface, neglecting the influence of particle size on $c(\mathrm{sat})$, and keeping the bulk concentration of molecules constant [16],

$$c(a = r) = c(\mathrm{sat}), \quad c(a \to \infty) = c(\infty). \tag{1.26}$$

For these boundary conditions, the stationary flux towards the sphere equals,

$$J = 4\pi D r[c(\infty) - c(\mathrm{sat})] \tag{1.27}$$

showing that the rate at which the colloid intercepts the diffusing molecules is proportional to its radius and not to its surface area. If every molecule contributes a volume v_m to the growing colloid, then for a homogeneous sphere, the volume increases at a rate given by,

$$\frac{\mathrm{d}}{\mathrm{d}t}\frac{4}{3}\pi r^3 = J v_\mathrm{m} \tag{1.28}$$

which on substitution in equation (1.27) leads to,

$$\frac{\mathrm{d}r}{\mathrm{d}t} = D v_\mathrm{m}[c(\infty) - c(\mathrm{sat})]r^{-1}. \tag{1.29}$$

With the typical scaling $r^2 \approx t$, as expected for a diffusion controlled process. Thus the exponent in equation (1.22) for diffusion controlled growth is $n = -1$, and consequently the relative width of the size distribution decreases with time.

For charged species, an electrostatic interaction may be present between the growing colloids and the molecules they consume. This will either enhance or retard growth, depending on whether colloids and monomers attract or repel each other. In this case the diffusion coefficient D of the monomers in the diffusion flux J has to be replaced by an effective coefficient of the form,

$$D_\mathrm{eff} = \frac{D}{r\int_r^\infty \exp(-[u(a)/kT]a^{-2})\,\mathrm{d}a}, \tag{1.30}$$

where $u(a)$ is the interaction energy between molecule and colloid.

If the molecules are ions with charge ze and the colloid sphere has a surface potential ψ^0, then for low electrolyte where the interaction is unscreened (upper estimate of the ion–colloid interaction), $u(a)$ is given by,

$$\frac{u(a)}{kT} = u_0 \frac{r}{a}, \tag{1.31}$$

$$u_0 = \frac{ze\psi^0}{kT} = zy^0, \tag{1.32}$$

where u_0 is the colloid–ion interaction energy and $y^0 = (e\psi^0/kT)$.

Thus the Coulombic interaction, equation (1.30), gives,

$$D_{\text{eff}} = D\frac{zy^0}{\exp(zy^0) - 1}. \tag{1.33}$$

Thus, the growth rate is slowed down exponentially by the Coulombic interaction. For example when $\psi^0 = 75$ mV, the effective diffusion coefficient for divalent ions is about $0.01D$. Addition of electrolyte screens the colloid–ion interaction and this moderates the effect of y^0 on the growth kinetics.

The interaction between charged monomers and the growing colloid within the approximation given by equation (1.33) does not change the growth equation (1.29) and, therefore, does not affect the conclusion that diffusional growth sharpens the size distribution.

The effect of Ostwald ripening on the kinetics of particle growth can be analysed using the Gibbs–Kelvin [17] equation that relates the solubility $c(r)$ of a particle with radius r to that of an infinitely large particle $c(\text{sat})$, i.e. a flat surface, by the equation,

$$\ln\left[\frac{c(r)}{c(\text{sat})}\right] = \frac{2\sigma v_{\text{m}}}{r^* kT}. \tag{1.34}$$

The increased solubility according to equation (1.34) is referred to as the Gibbs–Kelvin effect. By considering the Gibbs energy maximum of Fig. 1.4, it clear that it represents an unstable equilibrium, which can only be maintained for particles of exactly the same size. For polydisperse particles (with the same interfacial tension), there is no single, common equilibrium solubility; particles either grow or dissolve. Clearly, the largest particles have the strongest tendency to grow owing to their low solubility. This coarsening of colloids is referred to as Ostwald ripening and it is an important ageing effect which occurs with most polydisperse systems with small particles.

In a polydisperse system, the bulk concentration $c(\text{bulk})$ is not constant, but slowly decreasing in time due to the gradual disappearance of small particles. At any moment in time there is one sphere with radius r_0 which is in metastable equilibrium with the bulk concentration,

$$c(\text{bulk}) = c(\text{sat}) \exp\left[\frac{2\sigma v_{\text{m}}}{r_0 kT}\right], \tag{1.35}$$

where $c(\text{sat})$ is the solubility of a flat surface. If the local solute concentration near a sphere with radius r_i is also fixed by the Gibbs–Kelvin equation, the steady state diffusion flux for sphere I is given by,

$$J_i = 4\pi D r_i c(\text{sat})\left\{\exp\left[\frac{2\sigma v_m}{r_0 kT}\right] - \exp\left[\frac{2\sigma v_m}{r_i kT}\right]\right\}. \tag{1.36}$$

It is clear that particles with radii $r_i < r_0$ dissolve because $J < 0$, whereas for $r_i > r_0$ the particles grow. The average particle radius and the critical radius r_0 increase over time, so that the exponents in the diffusion flux can be linearized at a later stage of the ripening process. In this case, one can write for the growth or dissolution rate of sphere i the following approximate equation,

$$\frac{d}{dt} r_i^3 = 6 D r_i c(\text{sat}) \frac{\sigma v_m^2}{kT}\left[\frac{1}{r_0} - \frac{1}{r_i}\right]. \tag{1.37}$$

One limiting case of Ostwald ripening allows for a simple analytical solution, namely a monodisperse sphere with radius r, from which dissolved matter is deposited on very large particles, or a flat substrate. If that substrate controls the bulk concentration, r_0 is infinitely large and consequently,

$$\frac{dr^3}{dt} = -6 D c(\text{sat}) \frac{\sigma v_m^2}{kT}. \tag{1.38}$$

Thus, for this case the particle volume decreases at a constant rate.

The time evolution of a continuous size distribution was analysed by Lifshitz and Slesov [18] and Wagner [19] (referred to as the LSW theory) which predicts for large times the asymptotic result,

$$\frac{d\langle r\rangle^3}{dt} = \frac{8}{9} D c(\text{sat}) \frac{\sigma v_m^2}{kT} \tag{1.39}$$

which predicts that at a late stage of the ripening process, the average particle radius increases as $t^{1/3}$. The supersaturation falls as $t^{-1/3}$ and the number of spheres as t^{-1}. A remarkable finding of the LSW theory is that due to Ostwald ripening the size distribution approaches a certain universal, time-independent shape, irrespective of the initial distribution.

1.2.3 Seeded nucleation and growth

In the above analysis it is assumed that particle nucleation and growth occur in a solution of one solute. In practice this process of homogeneous nucleation is difficult to realize due to the presence of contaminants, dust, motes and irregularities on the vessel wall. This process of heterogeneous nucleation may have a dramatic effect on the kinetics. This process may be advantageous, resulting in particle size polydispersity. This process of seed nucleation was first exploited for the preparation of quite monodisperse gold colloids by using a finely divided Faraday gold sol as the seed. The latter can also differ chemically from the precipitating material, leading to the formation of core-shell colloids [16]. Good examples are the growth of silica on gold cores, and

other inorganic particles for the preparation of core-shell semiconductor particles [16]. Such well-defined composite colloids are increasingly important in materials science, in addition to their use in fundamental studies.

The efficiency of seeds or container walls to catalyse nucleation is due to the reduction of the interfacial Gibbs energy of a precipitating particle. Steps and kinks on the seed substrate may act as active sites because they enable more of the surface of the nucleus to be in contact with the seed, which lowers its surface excess Gibbs energy.

1.2.4 Surface modification

Surface modification is the deliberate attachment of a polymeric surfactant to the surface of the colloid to change its physical properties or chemical functionality [13]. This modification is permanent if the attached polymer is not desorbed by thermal motion. Such surface modification occurs either via a chemical bond or significant adsorption energy (lack of desorption). The polymeric surfactant provides steric repulsion for the particles as discussed in Chapter 8 of Vol. 1. Surface modification is generally made straightforward by choosing a molecule with a suitable chemical linker. For example for metal hydroxide particles, such as silica, one can use a linkage between the –OH group on the surface of the particles and a carboxylic group or alcohol. For example, under mild conditions the surface silane groups on silica react with silane coupling agents (SCAs) and these materials are suitable for in situ modification of the colloid in a sol. The SCAs hydrolyse to reactive silanes, which graft themselves onto silica via the formation of a silixane linkage.

Once reactive oligomers or polymers attach to a colloidal core, the core-shell particle behaves as one kinetic unit with an average kinetic energy of $(3/2)kT$ (where k is the Boltzmann constant and T is the absolute temperature). This energy has to be weighed against the replacement of a large number of solvent molecules by the adsorbed species. Even a very small Gibbs energy penalty per replacement may suffice to produce aggregates that do not break apart by thermal motion. Such aggregation can also be induced by minute changes in the nature or composition of the solvent, a subtle effect that is difficult to predict or explain. Any small change in the composition involves a large number of low-molecular species, with a net enthalpy change that easily compensates the entropy loss due to aggregation of large colloids. One obvious counterexample is any solvent adsorption on modified or unmodified colloids. Water adsorption on silica is well known, but polar organic solvents such as dimethylformamide or triethylphosphate also adsorb in significant amounts on bare silica particles, often sufficient to prevent this aggregation. It should be noted that small particles also have a disadvantage since the coagulation rate is proportional to the square of the number density. For modified, stable colloids, the small particle size becomes a benefit in view of the many functional groups per gram. One attractive option is the simultaneous synthesis and modification of inorganic colloids by nucle-

ation and growth in the presence of the modifying agent, which also influences and controls the particle size [16].

1.2.5 Other methods for preparation of suspensions by the bottom-up process

Several other methods can be applied for the preparation of suspensions using bottom-up processes of which the following are worth mentioning:

(i) Precipitation of particles by addition of a nonsolvent (containing a stabilizer for the particles formed) to a solution of the compound in question;
(ii) Preparation of an emulsion of the substance by using a solvent in which it is soluble following emulsification of the solvent in another immiscible solvent. This is then followed by removal of the solvent making the emulsion droplets by evaporation;
(iii) Preparation of the particles by mixing two microemulsions containing two chemicals that react together when the microemulsion droplets collide with each other;
(iv) Sol–gel process particularly used for preparation of silica particles;
(v) Production of polymer suspensions by emulsion or suspension polymerization;
(vi) Preparation of polymer suspensions by polymerization of microemulsions.

A brief description of each process is given below.

1.2.5.1 Solvent-antisolvent method [16]

In this method, the substance (e.g. a hydrophobic drug) is dissolved in a suitable solvent such as acetone. The resulting solution is carefully added to another miscible solvent in which the resulting compound is insoluble. This results in precipitation of the compound by nucleation and growth. The particle size distribution is controlled by using a polymeric surfactant that is strongly adsorbed on the particle surface and provides an effective repulsive barrier to prevent aggregation of the particles. The polymeric surfactant is chosen to have specific adsorption on the particle surface to prevent Ostwald ripening. This method can be adapted for the preparation of low water solubility drug suspensions. In this case the drug is dissolved in acetone and the resulting solution is added to an aqueous solution of Poloxamer (an A–B–A block copolymer consisting of two A polyethylene oxide (PEO) chains and a B polypropylene oxide (PPO) chain, i.e. PEO–PPO–PEO). After precipitation of the particles the acetone is removed by evaporation. The main problem with this method is the possibility of formation of several unstable polymorphs that will undergo crystal growth. In addition, the resulting particles may be of needle shape structure. However, by proper choice of the polymeric surfactant one can control the particle morphology and shape. Another problem may be the lack of removal of the solvent after precipitation of the particles.

1.2.5.2 Use of an emulsion

In this case the compound is dissolved in a volatile organic solvent that is immiscible with water, such as methylene dichloride. The oil solution is emulsified in water using a high-speed stirrer followed by high pressure homogenization [16]. A suitable emulsifier for the oil phase is used, which has the same HLB number as the oil. The volatile oil in the resulting emulsion is removed by evaporation and the formed suspension particles are stabilized against aggregation by the use of an effective polymeric surfactant that can be dissolved in the aqueous phase. The main problem with this technique is the possible interaction with the emulsifier, which may result in destabilization of the resulting suspension. However, by careful selection of the emulsifier/stabilizing system one can form a colloidally stable nanosuspension.

1.2.5.3 Preparation of suspensions by mixing two microemulsions [16]

Reverse microemulsions lend themselves as suitable "nonreactors" for the synthesis of particles. Inorganic salts can be dissolved in the water pools of a W/O microemulsion. Another W/O microemulsion with reducing agent dissolved in the water pools is then prepared. The two microemulsions are then mixed and the reaction between the inorganic salt and the reducing agent starts at the interface and proceeds towards the centre of the droplet. The rate limiting step appears to be the droplet diffusion. Control of the exchange can be achieved by tuning the film rigidity. This procedure has been applied for the preparation of noble metal particles that can be applied in electronics, catalysis and in potential medical applications.

1.2.5.4 Sol–gel process

This method is particularly applicable for preparation of silica particles [16]. This involves the development of networks through an arrangement of colloidal suspension (sol) and gelation to form a system in continuous liquid phase (gel). A sol is basically a dispersion of colloidal particles (1–100 nm) in a liquid and a gel is an interconnected rigid network with pores of submicron dimensions and polymeric chains. The sol–gel process, depending on the nature of the precursors, may be divided into two classes; namely inorganic precursors (chlorides, nitrates, sulphides, etc.) and alkoxide precursors. Extensively used precursors include tetramethyl silane and tetraethoxysilane. In this process, the reaction of metal alkoxides and water, in the presence of acid or base, forms a one phase solution that goes through a solution-to-gel transition to form a rigid, two-phase system comprised of metal oxides and solvent-filled pores. The physical and electrochemical properties of the resultant materials largely depend on the type of catalyst used in the reaction. In the case of silica alkoxides, the acid catalysed reaction results in weakly crosslinked linear polymers. These polymers entangle and form additional branches leading to gelation. In base-catalysed reactions, due to rapid hydrolysis and condensation of the alkoxide silanes, the system forms highly

branched clusters. The difference in cluster formation is due to the solubility of the resulting metal oxide in the reaction medium. The solubility of the silicon oxide is higher in alkaline medium, which favours the interlinking of the silica clusters, than in acidic medium. A general procedure for sol–gel includes four stages; namely hydrolysis, condensation, growth and aggregation. Complete hydrolysis to form $M(OH)_4$ is very difficult to achieve. Instead, condensation may occur between two –OH or M–OH groups and an alkoxy group to form a bridge between oxygen and a water or alcohol molecule. The hydrolysis and polycondensation reactions are initiated at numerous sites and the kinetics of the reaction can be very complex. When a sufficient number of interconnected M–O–M bonds are formed in a particular region, they interact cooperatively to form colloidal particles or a sol. With time, the colloidal particles link together to form three-dimensional networks. The size, shape and morphological features of the silica nanoparticles can be controlled by reaction kinetics, use of templates such as cationic, nonionic surfactants, polymers, electrolytes, etc.

1.3 Preparation of suspensions using the top-down process

As mentioned in the introduction, in the top-down process one starts with the bulk material (which may consist of aggregates and agglomerates) that is dispersed into single particles (using a wetting/dispersing agent) using high-speed stirrers followed by subdivision of the large particles into smaller units that fall within the required size [1–4]. This process requires the application of intense mechanical energy that can be achieved using bead milling. Finally, the resulting suspension must remain colloidally stable under all conditions (such as temperature changes, vibration, etc.) with absence of any flocculation and/or crystal growth.

A schematic representation of the dispersion process is shown in Fig. 1.5. This process requires wetting of the aggregates and agglomerates (both external and internal surfaces) by molecules of the dispersion medium. This is particularly the case with hydrophobic solids dispersed in aqueous media. As will be discussed below, wetting of hydrophobic solids in aqueous media requires the presence of a wetting agent (surfactant) that lowers the surface tension of water and adsorbs very quickly at the solid/liquid interface, thus reducing the solid/liquid interfacial tension. Once the powder is completely wetted, the aggregates and agglomerates are dispersed into single particles using high-speed stirrers and adding a dispersing agent (surfactant and/or polymer). The resulting dispersion of single particles (referred to as the “mill base”) is then subjected to a comminution (milling or particle size reduction) mostly achieved using bead mills. The final suspension must remain colloidally stable using electrostatic and/or steric stabilization as will be briefly described below.

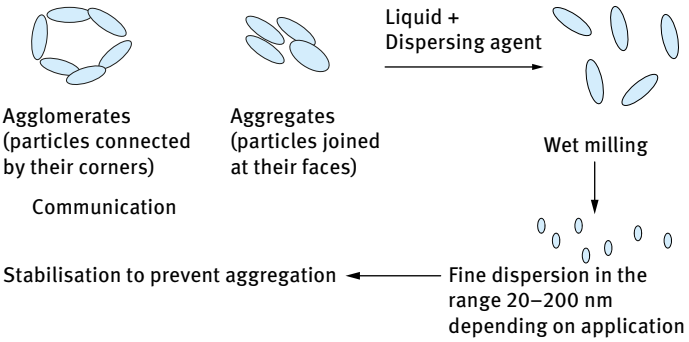

Fig. 1.5: Schematic representation of the dispersion process.

1.3.1 Wetting of the bulk powder

Wetting of powders is a prerequisite for dispersion of powders in liquids. Most chemicals are supplied as powders consisting of aggregates in which the particles are joined together with their "faces" (compact structures), or agglomerates in which the particles are connected at their corners (loose aggregates) as illustrated in Fig. 1.4. It is essential to wet both the external and the internal surface (in the pores within the aggregate or agglomerate structures) and this requires the use of an effective wetting agent (surfactant) [1–4]. Wetting of a solid by a liquid (such as water) requires the replacement of the solid/vapour interfacial tension, γ_{SV}, by the solid/liquid interfacial tension, γ_{SL}.

The equilibrium aspects of wetting can be studied at a fundamental level using interfacial thermodynamics. A useful parameter to describe wetting is the contact angle θ of a liquid drop on a solid substrate [1–4] which is the angle between planes tangent to the surfaces of solid and liquid at the wetting perimeter. If the liquid makes no contact with the solid, i.e. $\theta = 180°$, the solid is referred to as non-wettable by the liquid in question. This may be the case for a perfectly hydrophobic surface with a polar liquid such as water. However, when $180° > \theta > 90°$, one may refer to a case of poor wetting. When $0 < \theta < 90°$, partial (incomplete) wetting is the case, whereas when $\theta = 0$ complete wetting occurs and the liquid spreads on the solid substrate forming a uniform liquid film.

The utility of contact angle measurements depends on equilibrium thermodynamic arguments (static measurements) using the well-known Young's equation [1–4]. The value depends on:

(i) the history of the system;

(ii) whether the liquid is tending to advance across or recede from the solid surface (advancing angle θ_A, receding angle θ_R; usually $\theta_A > \theta_R$).

Under equilibrium, the liquid drop takes the shape that minimizes the free energy of the system. Three interfacial tensions can be identified:

- γ_{SV}, solid/vapour area A_{SV};
- γ_{SL}, solid/liquid area A_{SL};
- γ_{LV}, liquid/vapour area A_{LV}.

A schematic representation of the balance of tensions at the solid/liquid/vapour interface is shown in Fig. 1.6. Here, solid and liquid are simultaneously in contact with each other and the surrounding phase (air or vapour of the liquid). The wetting perimeter is referred to as the three-phase line or wetting line. In this region there is an equilibrium between vapour, liquid and solid.

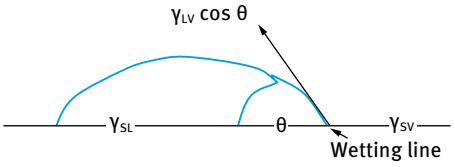

Fig. 1.6: Schematic representation of the contact angle and wetting line.

$\gamma_{SV}A_{SV} + \gamma_{SL}A_{SL} + \gamma_{LV}A_{LV}$ should be a minimum at equilibrium and this leads to the well-known Young's equation,

$$\gamma_{SV} = \gamma_{SL} + \gamma_{LV}\cos\theta, \tag{1.40}$$

$$\cos\theta = \frac{\gamma_{SV} - \gamma_{SL}}{\gamma_{LV}}. \tag{1.41}$$

The contact angle θ depends on the balance between the solid/vapour (γ_{SV}) and solid/liquid (γ_{SL}) interfacial tensions. The angle which a drop assumes on a solid surface is the result of the balance between the adhesion force between solid and liquid and the cohesive force in the liquid,

$$\gamma_{LV}\cos\theta = \gamma_{SV} - \gamma_{SL}. \tag{1.42}$$

Wetting of a powder is achieved by the use of surface active agents (wetting agents) of the ionic or nonionic type which are capable of diffusing quickly (i.e. lower the dynamic surface tension) to the solid/liquid interface and displacing the air entrapped by rapid penetration through the channels between the particles and inside any "capillaries". For wetting of hydrophobic powders in water, anionic surfactants, e.g. alkyl sulphates or sulphonates or nonionic surfactants of the alcohol ethoxylates are usually used [1–4].

A useful concept for choosing wetting agents of the ethoxylated surfactants is the hydrophilic–lipophilic balance (HLB) concept,

$$\mathrm{HLB} = \frac{\%\ \text{of hydrophilic groups}}{5}. \tag{1.43}$$

Most wetting agents of this class have an HLB number in the range 7–9.

The process of wetting of a solid of unit surface area by a liquid involves three types of wetting [1–4]: adhesion wetting, W_a; immersion wetting W_i; spreading wetting W_s. In every step one can apply Young's equation,

$$W_a = \gamma_{SL} - (\gamma_{SV} + \gamma_{LV}) = -\gamma_{LV}(\cos\theta + 1), \tag{1.44}$$

$$W_i = 4\gamma_{SL} - 4\gamma_{SV} = -4\gamma_{LV}\cos\theta, \tag{1.45}$$

$$W_s = (\gamma_{SL} + \gamma_{LV}) - \gamma_{SV} = -\gamma_{LV}(\cos\theta - 1). \tag{1.46}$$

The work of dispersion of a solid with unit surface area W_d is the sum of W_a, W_i and W_s,

$$W_d = W_a + W_i + W_s = 6\gamma_{SV} - \gamma_{SL} = -6\gamma_{LV}\cos\theta. \tag{1.47}$$

Wetting and dispersion depend on: γ_{LV}, liquid surface tension; θ, contact angle between liquid and solid. W_a, W_i and W_s are spontaneous when $\theta < 90°$. W_d is spontaneous when $\theta = 0$. Since surfactants are added in sufficient amounts (γ_{dynamic} is lowered sufficiently) spontaneous dispersion is the rule rather than the exception.

The work of dispersion of a powder with surface area A, W_d, is given by [1–4],

$$W_d = A(\gamma_{SL} - \gamma_{SV}). \tag{1.48}$$

Using Young's equation (1.40),

$$W_d = -A\gamma_{LV}\cos\theta. \tag{1.49}$$

Equation (1.49) shows that W_d depends on γ_{LV} and θ, both of which are lowered by addition of surfactants (wetting agents). If $\theta < 90°$, W_d is negative and dispersion is spontaneous.

Wetting of the internal surface requires penetration of the liquid into channels between and inside the agglomerates. The process is similar to forcing a liquid through fine capillaries. To force a liquid through a capillary with radius r, a pressure p is required that is given by,

$$p = -\frac{2\gamma_{LV}\cos\theta}{r} = \left[\frac{-2(\gamma_{SV} - \gamma_{SL})}{r\gamma_{LV}}\right]. \tag{1.50}$$

γ_{SL} has to be made as small as possible; rapid surfactant adsorption to the solid surface, low θ. When $\theta = 0$, $p \propto \gamma_{LV}$. Thus for penetration into pores one requires a high γ_{LV}. Thus, wetting of the external surface requires low contact angle θ and low surface tension γ_{LV}. Wetting of the internal surface (i.e. penetration through pores) requires

low θ but high γ_{LV}. These two conditions are incompatible and a compromise has to be made: $\gamma_{SV} - \gamma_{SL}$ must be kept at a maximum. γ_{LV} should be kept as low as possible but not too low.

The above conclusions illustrate the problem of choosing the best dispersing agent for a particular powder. This requires measurement of the above parameters as well as testing the efficiency of the dispersion process.

The contact angle of liquids on solid powders can be measured by application of the Rideal–Washburn equation. For horizontal capillaries (gravity neglected), the depth of penetration l in time t is given by the Rideal–Washburn equation [1–4],

$$l = \left[\frac{rt\gamma_{LV} \cos\theta}{2\eta} \right]^{1/2}. \tag{1.51}$$

To enhance the rate of penetration, γ_{LV} has to be made as high as possible, θ as low as possible and η as low as possible. For dispersion of powders into liquids one should use surfactants that lower θ while not reducing γ_{LV} too much. The viscosity of the liquid should also be kept at a minimum. Thickening agents (such as polymers) should not be added during the dispersion process. It is also necessary to avoid foam formation during the dispersion process.

For a packed bed of particles, r may be replaced by $K(= r/k^2)$, which contains the effective radius of the bed r and a tortuosity factor k, which takes into account the complex path formed by the channels between the particles, i.e.,

$$l = \left(\frac{Kt\gamma_{LV} \cos\theta}{2\eta} \right)^{1/2}. \tag{1.52}$$

Thus a plot of l^2 versus t gives a straight line and from the slope of the line one can obtain θ. The Rideal–Washburn equation can be applied to obtain the contact angle of liquids (and surfactant solutions) in powder beds. K should first be obtained using a liquid that produces zero contact angle. A packed bed of powder is prepared, say in a tube fitted with a sintered glass at the end (to retain the powder particles). It is essential to pack the powder uniformly in the tube (a plunger may be used in this case). The tube containing the bed is immersed in a liquid that gives spontaneous wetting (e.g. a lower alkane), i.e. the liquid gives a zero contact angle and $\cos\theta = 1$. By measuring the rate of penetration of the liquid (this can be carried out gravimetrically using for example a microbalance or a Kruss instrument) one can obtain K. The tube is then removed from the lower alkane liquid and left to stand for evaporation of the liquid. It is then immersed in the liquid in question and the rate of penetration is measured again as a function of time. Using equation (1.52), one can calculate $\cos\theta$ and hence θ.

For efficient wetting of hydrophobic solids in water, a surfactant is needed that lowers the surface tension of water very rapidly (within few ms) and quickly adsorbs at the solid/liquid interface [1–4]. To achieve rapid adsorption the wetting agent should be either a branched chain with central hydrophilic group or a short hydrophobic chain with hydrophilic end group.

The most commonly used wetting agents are the following:

Aerosol OT (diethylhexyl sulphosuccinate)

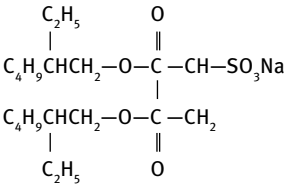

The above molecule has a low critical micelle concentration (cmc) of 0.7 g dm^{-3} and at and above the cmc the water surface tension is reduced to ≈ 25 mN m^{-1} in less than 15 s.

Several nonionic surfactants such as the alcohol ethoxylates can also be used as wetting agents. These molecules consist of a short hydrophobic chain (mostly C_{10}) which is also branched. A medium chain polyethylene oxide (PEO), mostly consisting of 6 EO units or lower is used. These molecules also reduce the dynamic surface tension within a short time (< 20 s) and they have reasonably low cmc. In all cases one should use the minimum amount of wetting agent to avoid interference with the dispersant that needs to be added to maintain the colloid stability during dispersion and on storage.

1.3.2 Breaking of aggregates and agglomerates into individual units

This usually requires the application of mechanical energy. High-speed mixers (which produce turbulent flow) of the rotor-stator type [1, 2] are efficient in breaking up the aggregates and agglomerates, e.g. Silverson mixers, Ultra-Turrax. These are the most commonly used mixers for dispersion of powders in liquids. Two main types are available. The most commonly used toothed device (schematically illustrated in Fig. 1.7) is the Ultra-Turrax (IKA Works, Germany).

Toothed devices are available as both in-line as well as batch mixers, and because of their open structure they have a relatively good pumping capacity. Therefore, in batch applications they frequently do not need an additional impeller to induce bulk flow even in relatively large mixing vessels.

Batch radial discharge mixers such as Silverson mixers (Fig. 1.8) have a relatively simple design with a rotor equipped with four blades pumping the fluid through a stationary stator perforated with differently shaped/sized holes or slots.

They are frequently supplied with a set of easily interchangeable stators enabling the same machine to be used for a range of operations e.g. blending, particle size reduction and de-agglomeration. Changing from one screen to another is quick and simple. Different stators/screens used in batch Silverson mixers are shown in Fig. 1.9.

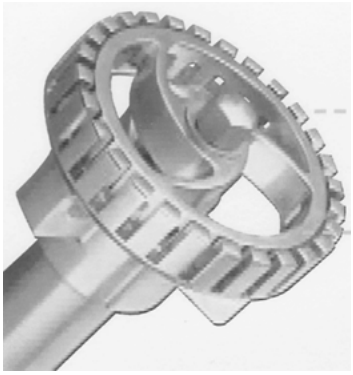

Fig. 1.7: Schematic representation of a toothed mixer (Ultra-Turrax).

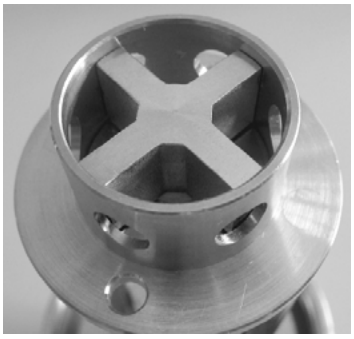

Fig. 1.8: Schematic representation of a batch radial discharge mixer (Silverson mixer).

The general purpose disintegrating stator (Fig. 1.9 (a)) is recommended for preparation of thick suspensions ("gels") whilst the slotted disintegrating stator (Fig. 1.9 (b)) is designed for suspensions containing elastic materials such as polymers. Square hole screens (Fig. 1.9 (c)) are recommended for the preparation of suspensions, whereas the standard screen (Fig. 1.9 (d)) is used for solid/liquid dispersion.

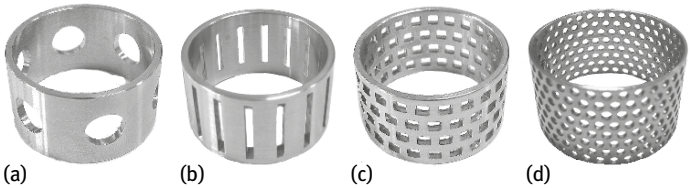

Fig. 1.9: Stators used in batch Silverson radial discharge mixers.

In all methods, there is liquid flow; unbounded and strongly confined flow. In unbounded flow any particle is surrounded by a large amount of flowing liquid (the confining walls of the apparatus are far away from most of the particles). The forces can be frictional (mostly viscous) or inertial. Viscous forces cause shear stresses to act on the interface between the particles and the continuous phase (primarily in the direction of the interface). The shear stresses can be generated by laminar flow (LV) or turbulent flow (TV); this depends on the dimensionless Reynolds numbers *Re*,

$$Re = \frac{\upsilon l \rho}{\eta}, \tag{1.53}$$

where υ is the linear liquid velocity, ρ is the liquid density and η is its viscosity. l is a characteristic length that is given by the diameter of flow through a cylindrical tube and by twice the slit width in a narrow slit.

For laminar flow $Re \lessapprox 1{,}000$, whereas for turbulent flow $Re \gtrapprox 2{,}000$. Thus whether the regime is linear or turbulent depends on the scale of the apparatus, the flow rate and the liquid viscosity [1–3].

Batch toothed and radial discharge rotor-stator mixers are manufactured in different sizes, ranging from the laboratory to the industrial scale. In lab applications mixing heads (assembly of rotor and stator) can be as small as 0.01 m (Ultra-Turrax, Silverson) and the volume of processed fluid can vary from several millilitres to few litres. In models used in industrial applications, mixing heads might have up to 0.5 m diameter enabling processing of several cubic meters of fluids in one batch.

In practical applications the selection of the rotor-stator mixer for a specific dispersion process depends on the required morphology of the product, frequently quantified in terms of average particle size or in terms of particle size distributions, and by the scale of the process. The selection of an appropriate mixer and processing conditions for a required formulation is frequently carried out by trial and error. Initially, one can carry out lab scale dispersion of given formulations testing different type/geometries of mixers they manufacture. Once the type of mixer and its operating parameters are determined at the lab scale the process needs to be scaled up. The majority of lab tests of dispersion is carried out in small batch vessels as it is easier and cheaper than running continuous processes. Therefore, prior to scaling up of the rotor-stator mixer it has to be decided whether industrial dispersion should be run as a batch or as a continuous process. Batch mixers are recommended for processes where formulation of a product requires long processing times typically associated with slow chemical reactions. They require simple control systems, but spatial homogeneity may be an issue in large vessels which could lead to a longer processing time. In processes where quality of the product is controlled by mechanical/hydrodynamic interactions between continuous and dispersed phases or by fast chemical reactions, but large amounts of energy are necessary to ensure adequate mixing, in-line rotor-stator mixers are recommended. In-line mixers are also recommended to efficiently process large volumes of fluid.

In the case of batch processing, rotor-stator devices immersed as top entry mixers is the simplest arrangement mechanically, but in some processes bottom entry mixers ensure better bulk mixing; however in this case sealing is more complex. In general, the efficiency of batch rotor-stator mixers decreases as the vessel size increases and as the viscosity of the processed fluid increases because of limited bulk mixing by rotor-stator mixers. Whilst the open structure of Ultra-Turrax mixers frequently enables sufficient bulk mixing even in relatively large vessels, if the suspension has a low apparent viscosity, processing of very viscous suspensions requires an additional impeller (typically anchor type) to induce bulk flow and to circulate the dispersion through the rotor-stator mixer. On the other hand, batch Silverson rotor-stator mixers have a very limited pumping capacity and even at the lab scale they are mounted off the centre of the vessel to improve bulk mixing. At the large scale there is always a need for at least one additional impeller and in the case of very large units more than one impeller is mounted on the same shaft.

Problems associated with the application of batch rotor-stator mixers for processing large volumes of fluid discussed above can be avoided by replacing batch mixers with in-line (continuous) mixers. There are many designs offered by different suppliers (Silverson, IKA, etc.) and the main differences are related to the geometry of the rotors and stators with stators and rotors designed for different applications. The main difference between batch and in-line rotor-stator mixers is that the latter have a strong pumping capacity, therefore they are mounted directly in the pipeline. One of the main advantages of in-line over batch mixers is that for the same power duty, a much smaller mixer is required, therefore they are better suited for processing of large volumes of fluid. When the scale of the processing vessel increases, a point is reached where it is more efficient to use an in-line rotor-stator mixer rather than a batch mixer of a large diameter. Because power consumption increases sharply with rotor diameter (to the fifth power) an excessively large motor is necessary at large scales. This transition point depends on the fluid rheology, but for a fluid with a viscosity similar to water, it is recommended to change from a batch to an in-line rotor-stator process at a volume of approximately 1 to 1.5 tonnes. The majority of manufacturers supply both single and multistage mixers for the emulsification of highly viscous liquids.

As mentioned above in all methods, there is liquid flow, unbounded and strongly confined flow. In unbounded flow any particle is surrounded by a large amount of flowing liquid (the confining walls of the apparatus are far away from most of the droplets); the forces can be frictional (mostly viscous) or inertial. Viscous forces cause shear stresses to act on the interface between the particles and the continuous phase (primarily in the direction of the interface). The shear stresses can be generated by laminar flow (LV) or turbulent flow (TV); this depends on the Reynolds number Re as given by equation (1.53). For laminar flow $Re \lessapprox 1{,}000$, whereas for turbulent flow $Re \gtrapprox 2{,}000$. Thus whether the regime is linear or turbulent depends on the scale of the apparatus, the flow rate and the liquid viscosity.

If the turbulent eddies are much larger than the particles, they exert shear stresses on the particles. If the turbulent eddies are much smaller than the particles, inertial forces will cause disruption (TI). In bounded flow other relations hold; if the smallest dimension of the part of the apparatus in which the particles are disrupted (say a slit) is comparable to particle size, other relations hold (the flow is always laminar).

Within each regime, an essential variable is the intensity of the forces acting; the viscous stress during laminar flow σ_{viscous} is given by,

$$\sigma_{\text{viscous}} = \eta G, \tag{1.54}$$

where G is the velocity gradient.

The intensity in turbulent flow is expressed by the power density ε (the amount of energy dissipated per unit volume per unit time); for turbulent flow,

$$\varepsilon = \eta G^2. \tag{1.55}$$

The most important regimes are:
- laminar/viscous (LV)
- turbulent/viscous (TV)
- turbulent/inertial (TI)

For water as the continuous phase, the regime is always TI. For higher viscosity of the continuous phase ($\eta_C = 0.1$ Pa s), the regime is TV. For still higher viscosity or a small apparatus (small l), the regime is LV. For very small apparatus (as is the case with most laboratory homogenizers), the regime is nearly always LV.

The mixing conditions have to be optimized: Heat generation at high stirring speeds must be avoided. This is particularly the case when the viscosity of the resulting dispersion increases during dispersion (note that the energy dissipation as heat is given by the product of the square of the shear rate and the viscosity of the suspension). One should avoid foam formation during dispersion; proper choice of the dispersing agent is essential and antifoams (silicones) may be applied during the dispersion process.

Rotor-stator mixers can be characterized as energy-intensive mixing devices. The main feature of these mixers is their ability to focus high energy/shear in a small volume of fluid. They consist of a high-speed rotor enclosed in a stator, with the gap between them ranging from 100 to 3,000 μm. Typically, the rotor speed is between 10 and 50 m s^{-1}, which, in combination with a small gap, generates very high shear rates. By operating at high speed, the rotor-stator mixers can significantly reduce processing time. In terms of energy consumption per unit mass of product, the rotor-stator mixers require high power input over a relatively short time. However, as the energy is uniformly delivered and dissipated in a relatively small volume, each element of the fluid is exposed to a similar intensity of processing. Frequently, the quality of the final product is strongly affected by its structure/morphology and it is essential that the key ingredients are uniformly distributed throughout the whole mixer volume.

The most common application of rotor-stator mixers is in dispersion of powders in liquids and they are used in manufacture of particle-based products with sizes between 1 and 20 μm, e.g. in pharmaceuticals, paints, agrochemicals and cosmetics.

As mentioned above, there are a wide range of designs of rotor-stator mixers, of which the Ultra-Turrax (IKA Works, Germany) and Silverson (UK) are the most commonly used. They are broadly classified according to their mode of operation such as batch or in-line (continuous) mixers. In-line radial-discharge mixers are characterized by high throughput and good pumping capacity at low energy consumption. The disperse phase can be injected directly into the high shear/turbulent zone, where mixing is much faster than by injection into the pipe or into the holding tank. They are used for manufacturing of very fine solid particles of relatively narrow dispersed size distribution. They are typically supplied with a range of interchangeable screens, making them reliable and versatile in different applications. Toothed devices are available as in-line as well as batch mixers. Due to their open structure they have a relatively good pumping capacity and they frequently do not need an additional impeller to induce bulk flow even in relatively large vessels.

In rotor-stator mixers, both shear rate in laminar flow and energy dissipate flow depend on the position inside the mixer. In laminar flow in stirred vessels, the average shear rate is proportional to the rotor speed N with the proportionality constant K dependent on the type of the impeller [1],

$$\dot{\gamma} = KN. \tag{1.56}$$

In stirred vessels the proportionality constant cannot be calculated and has to be determined experimentally. In rotor-stator mixers, the average shear rate in the gap between the rotor and stator can calculated if the rotor speed and geometry of the mixer are known,

$$\dot{\gamma} = \frac{\pi DN}{\delta} = K_1 N, \tag{1.57}$$

where D is the outer rotor diameter and δ is the rotor-stator gap width.

The average energy dissipation rate ε in turbulent flow in rotor-stator mixers can be calculated from [1],

$$\varepsilon = \frac{P}{\rho_c V}, \tag{1.58}$$

where P is the power draw, V is the swept rotor volume and ρ_c is the continuous phase density.

The power draw in batch rotor-stator mixers is calculated in the same way as in stirred vessels,

$$P = P_0 \rho_c N^3 D^5, \tag{1.59}$$

where P_0 is the power number constant for in-line rotor-stator mixers zero flow.

The power draw in in-line rotor-stator mixers in turbulent flow is given by,

$$P = P_{0z} \rho_c N^3 D^5 + k_1 M N^2 D^2 + P_L, \tag{1.60}$$

where M is the mass flow rate and P_L is the power loss term. The first term in equation (1.60) is analogous to power consumption in a batch rotor-stator mixer and the second term takes into account the effect of pumping action on total power consumption. The third term accounts for mechanical losses and is typically a few percent, and therefore can be ignored.

While in turbulent flow, P_{0z} in equation (1.60) is approximately independent of the Reynolds number Re, in laminar flow there is a strong dependency of power number on Re and in this case the power draw can be calculated from,

$$P = k_0 N^2 D^3 \eta_c + k_1 M N^2 D^2 + P_L, \tag{1.61}$$

where η_c is the viscosity of the continuous phase and k_0 is a constant that depends on the Reynolds number Re,

$$k_0 = P_{0z} Re. \tag{1.62}$$

From equations (1.59)–(1.62), the average energy dissipation rate in the rotor-stator mixer can be calculated.

1.3.3 Wet milling or comminution

The primary dispersion (sometimes referred to as the mill base) may then be subjected to a bead milling process to produce nanoparticles. Subdivision of the primary particles into much smaller units (< 1 µm) requires application of intense energy. In some cases high pressure homogenizers (such as the Microfluidizer, USA) may be sufficient to produce small particles. This is particularly the case with many drugs. In some cases, the high pressure homogenizer is combined with application of ultrasound to produce the small particles [1]. It has been shown that high pressure homogenization is a simple technique, well established on large scale for the production of fine suspensions and already available in the pharmaceutical industry. High pressure homogenization is also an efficient technique that has been utilized to prepare stable suspensions of several drugs such as carbazepin, bupravaquone, aphidicolin, cyclosporine, paclitaxel, prednisolone, etc. During homogenization, cavitation forces as well as collision and shear forces determine breakdown of the drug particles down to the nanometre range. Process conditions lead to an average particle size that remains constant as a result of continuous fragmentation and reaggregation processes. These high energetic forces can also induce a change of crystal structure and/or partial or total amorphization of the sample, which further enhances the solubility. For long-term storage stability of the nanosuspension formulation, the crystal structure modification must be maintained over the storage time.

Microfluidization is a milling technique that results in minimal product contamination. Besides minimal contamination, this technique can be easily scaled up. In this method a sample dispersion containing large particles is made to pass through

specially designed interaction chambers at high pressure. The specialized geometry of the chambers along with the high pressure causes the liquid stream to reach extremely high velocities and these streams then impinge against each other and against the walls of the chamber resulting in particle size reduction. The shear forces developed at high velocities due to attrition of particles against one another and against the chamber walls, as well as the cavitation fields generated inside the chamber are the main mechanisms of particle size reduction with this technique. In the interaction chambers the liquid feed is divided into two parts which are then made to impinge against each other and against the walls of the chambers. Particle size reduction occurs due to attrition between the particles and against the chamber walls at high velocities. Cavitation fields generated inside the chambers also contribute to particle size reduction [1].

The process of microfluidization for the preparation of suspensions varies in a complex way with the various critical processes and formulation parameters. Milling time, microfluidization pressure, stabilizer type, processing temperature and stabilizer concentration were identified as critical parameters affecting the formation of stable particles. Both ionic as well as steric stabilization were effective in stabilizing the suspensions. Microfluidization and precipitation under sonication can also be used for suspension preparation.

The extreme transient conditions generated in the vicinity and within the collapsing cavitational bubbles have been used for the size reduction of the material to the nanoscale. Particles synthesis techniques include sonochemical processing and cavitation processing. In sonochemistry, an acoustic cavitation process can generate a transient localized hot zone with extremely high temperature gradient and pressure. Such sudden changes in temperature and pressure assist the destruction of the sonochemical precursor and the formation of nanoparticles [1].

A dimensionless number known as the cavitation number (Cv) is used to relate the flow conditions with the cavitation intensity [1],

$$Cv = \frac{(P_2 - P_v)}{(0.5\rho V_0^2)}, \tag{1.63}$$

where P_2 is the recovered downstream pressure; P_v is the vapour pressure of the liquid, ρ is the density of dispersed media and V_0 is the liquid velocity at the orifice. The cavitation number at which the inception of cavitation occurs is known as the cavitation inception number Cv_i. Ideally speaking, the cavitation inception should occur at 1.0. It was also reported that, generally the inception of cavitation occurs from 1.0 to 2.5. This has been attributed to the presence of the dissolved gases in the flowing liquid. Cv is a function of the flow geometry and usually increases with an increase in the size of the opening in a constriction such as an orifice in a flow.

Cavitation can be used, for example, for the formation of the iron oxide particles. Iron precursor either as a neat liquid or in a decalin solution was sonicated and this

produced 10–20 nm size amorphous iron particles. Similar experiments have been reported for the synthesis of particles of many other inorganic materials using acoustic cavitation. To understand the mechanism of particle formation during the cavitation phenomenon, the hot spot theory has been successfully applied. It explains the adiabatic collapse of a bubble, producing the hot spots. This theory claims that very high temperatures (5,000–25,000 K) are obtained upon the collapse of the bubble. Since this collapse occurs in few microseconds, very high cooling rates have been obtained. These high cooling rates hinder the organization and crystallization of the products. While the explanation for the creation of amorphous products is well understood, the reason for the formation of nanostructured products under cavitation is not yet clear. The products are sometimes nanoamorphous particles, and in other cases, nanocrystalline. This depends on the temperature in the fluid ring region where the reaction takes place. The temperature in this liquid ring is lower than that inside the collapsing bubble, but higher than the temperature of the bulk liquid. In summary, in the sonochemical reactions leading to inorganic products, nanomaterials have been obtained. They vary in size, shape, structure, and in their solid phase (amorphous or crystalline), but they were always of nanometre size. Cavitation being a nuclei dominated (statistical in nature) phenomenon, such variations are expected.

In hydrodynamic cavitation, nanoparticles are generated through the creation and release of gas bubbles inside the sol–gel solution. By rapidly pressurizing in a supercritical drying chamber and exposing it to the cavitational disturbance and high temperature heating, the sol–gel solution is rapidly mixed. The erupting hydrodynamically generated cavitating bubbles are responsible for the nucleation, the growth of the nanoparticles, and also for their quenching to the bulk operating temperature. Particle size can be controlled by adjusting the pressure and the solution retention time in the cavitation chamber. Cavitation methods can be used to reduce the size of the rubber latex particles (styrene butadiene rubber, SBR), present in the form of aqueous suspension with micrometre particle initial size, to the nanoscale [1].

An alternative method of size reduction to produce nanoparticles, that is commonly used in many industrial applications, is through wet milling. This is referred to as comminution (the generic term for size reduction) and is a complex process. There is little fundamental information on its mechanism. For the breakdown of single crystals or particles into smaller units, mechanical energy is required. This energy in a bead mill is supplied by impaction of the glass or ceramic beads with the particles. Permanent deformation of the particles and crack initiation result. This will eventually lead to the fracture of particles into smaller units. Since the milling conditions are random, some particles receive impacts far in excess of those required for fracture whereas others receive impacts that are insufficient for the fracture process. This makes the milling operation grossly inefficient and only a small fraction of the applied energy is used in comminution. The rest of the energy is dissipated as heat, vibration, sound, interparticulate friction, etc.

The role of surfactants and dispersants on the grinding efficiency is far from being understood. In most cases the choice of surfactants and dispersant is made by trial and error until a system is found that gives the maximum grinding efficiency. Rehbinder and his collaborators [20] investigated the role of surfactants in the grinding process. As a result of surfactant adsorption at the solid/liquid interface, the surface energy at the boundary is reduced and this facilitates the process of deformation or destruction. The adsorption of surfactants at the solid/liquid interface in cracks facilitates their propagation. This mechanism is referred to as the Rehbinder effect.

Several factors affect the efficiency of dispersion and milling [1]:

(i) the volume concentration of dispersed particles (i.e. the volume fraction);
(ii) the nature of the wetting/dispersing agent;
(iii) the concentration of wetter/dispersant (which determines the adsorption characteristics).

For optimizing the dispersion/milling process the above parameters need to be systematically investigated. From the wetting performance of a surfactant, that can be evaluated using contact angle measurements, one can establish the nature and concentration of the wetting agent. The nature and concentration of dispersing agent required is determined by adsorption isotherm and rheological measurements.

Once the concentration of wetting/dispersing agent is established dispersions are prepared at various volume fractions keeping the ratio of wetting/dispersing agent to the solid content constant. Each system is then subjected to the dispersion/milling process keeping all parameters constant:

(i) speed of the stirrer (normally one starts at lower speed and gradually increases the speed in increments at fixed time);
(ii) volume and size of beads relative to the volume of the dispersion (an optimum value is required);
(iii) speed of the mill.

The change of average particle size with time of grinding is established using for example the Mastersizer (Malvern, UK). Fig. 1.10 shows a schematic representation of the reduction of particle size with grinding time in minutes using a typical bead mill (see below) at various volume fractions [21].

The representation in Fig. 1.10 is only schematic and is not based on experimental data. It shows the expected trend. When the volume fraction ϕ is below the optimum (in this case the relative viscosity of the dispersion is low) one requires a long time to achieve size reduction. In addition the final particle size may be large and outside the nanorange. When ϕ is above the optimum value the dispersion time is prolonged (due to the relatively high relative viscosity of the system) and the grinding time is also longer. In addition, the final particle size is larger than that obtained at the optimum ϕ. At the optimum volume fraction both the dispersion and grinding time are shorter and also the final particle size is smaller [1].

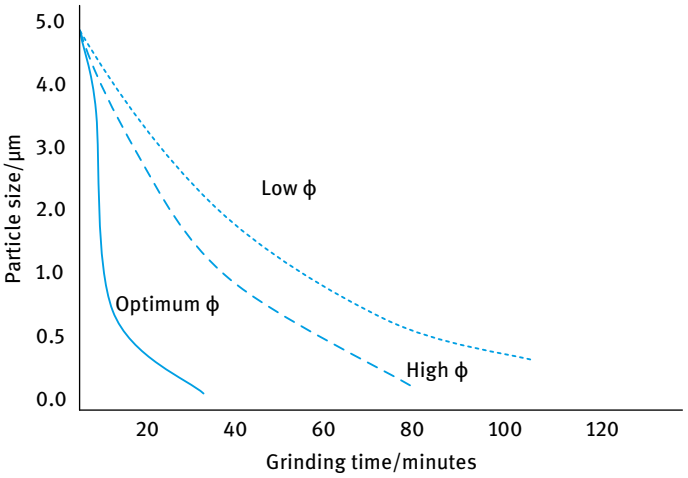

Fig. 1.10: Variation of particle size with grinding time in a typical bead mill.

For the preparation of suspensions bead mills are most commonly used. The beads are mostly made of glass or ceramics (which are preferred due to minimum contamination). The operating principle is to pump the premixed, preferably predispersed (using a high-speed mixer) mill base through a cylinder containing a specified volume of say ceramic beads (normally 0.5–1 mm diameter to achieve nanosize particles). The dispersion is agitated by a single or multi-disc rotor. The disc may be flat or perforated. The mill base passing through the shear zone is then separated from the beads by a suitable screen located at the opposite end of the feedport [1].

Generally speaking, bead mills may be classified to two types:

(i) vertical mills with open or closed top;
(ii) horizontal mills with closed chambers.

The horizontal mills are more efficient and the most commonly used one are: Netzsch (Germany) and Dyno Mill (Switzerland). These bead mills are available in various sizes from 0.5 to 500 litres. The factors affecting the general dispersion efficiency are known reasonably well (from the manufacturer). The selection of the right diameter of the beads is important for maximum utilization. In general, the smaller the size of the beads and the higher their density, the more efficient the milling process [1].

To understand the principle of operation of the bead mill, one must consider the centrifugal force transmitted to the grinding beads at the tip of the rotating disc which increases considerably with its weight. This applies greater shear to the mill base. This explains why the more dense beads are more efficient in grinding. The speed transmitted to the individual chambers of the beads at the tip of the disc assumes that speed and the force can be calculated [1].

The centrifugal force F is simply given by,

$$F = \frac{\upsilon^2}{rg}, \tag{1.64}$$

where υ is the velocity, r is the radius of the disc and g is the acceleration due to gravity.

1.3.4 Stabilization of the suspension during dispersion and milling and the resulting suspension

In order to maintain the particles as individual units during dispersion and milling, it is essential to use a dispersing agent that provides an effective repulsive barrier preventing aggregation of the particles by van der Waals forces. This dispersing agent must be strongly adsorbed on the particle surface and should not be displaced by the wetting agent. As was discussed in detail in Chapter 7 of Vol. 1, the repulsive barrier can be electrostatic in nature, whereby electrical double layers are formed at the solid/liquid interface [10, 11]. These double layers must be extended (by maintaining low electrolyte concentration) and strong repulsion occurs on double layer overlap. Alternatively, the repulsion can be produced by the use of nonionic surfactant or polymer layers which remain strongly hydrated (or solvated) by the molecules of the continuous medium [12, 13] as discussed in Chapter 8 of Vol. 1. On approach of the particles to a surface-to-surface separation distance that is lower than twice the adsorbed layer thickness strong repulsion occurs as a result of two main effects:

(i) unfavourable mixing of the layers when these are in good solvent conditions;
(ii) loss of configurational entropy on significant overlap of the adsorbed layers.

This process is referred to as steric repulsion [12, 13]. A third repulsive mechanism is that when both electrostatic and steric repulsion are combined, for example when using polyelectrolyte dispersants.

The particles of the resulting suspension may undergo aggregation (flocculation) on standing as a result of the universal van der Waals attraction. This was discussed in detail in Chapter 9 of Vol. 1. This attractive energy G_A becomes very large at short distances of separation between the particles.

As mentioned in Chapter 7 of Vol. 1, to overcome the everlasting van der Waals attraction energy, it is essential to have a repulsive energy between the particles. The first mechanism is electrostatic repulsive energy G_{elec} produced by the presence of electrical double layers around the particles produced by charge separation at the solid/liquid interface. The dispersant should be strongly adsorbed to the particles, produce high charge (high surface or zeta potential) and form an extended double layer (that can be achieved at low electrolyte concentration and low valency) [1–3].

When charged colloidal particles in a dispersion approach each other such that the double layers begin to overlap (particle separation becomes less than twice the

double layer extension), repulsion occurs. The individual double layers can no longer develop unrestrictedly, since the limited space does not allow complete potential decay [1–3]. The potential $\psi_{H/2}$ half way between the particles is no longer zero (as would be the case for isolated particles at $x \to \infty$).

Combining G_{elec} and G_A results in the well-known theory of stability of colloids (DLVO Theory) [10, 11],

$$G_T = G_{el} + G_A. \tag{1.65}$$

A plot of G_T versus h is shown in Fig. 1.11, which represents the case at low electrolyte concentrations, i.e. strong electrostatic repulsion between the particles. G_{elec} decays exponentially with h, i.e. $G_{elec} \to 0$ as h becomes large. $G_A \propto 1/h$, i.e. G_A does not decay to 0 at large h.

At long distances of separation, $G_A > G_{elec}$ resulting in a shallow minimum (secondary minimum), which for nanosuspensions is very low ($< kT$). At very short distances, $G_A \gg G_{elec}$ resulting in a deep primary minimum. At intermediate distances, $G_{elec} > G_A$ resulting in an energy maximum, G_{max}, whose height depends on ψ_0 (or ψ_d or zeta potential) and the electrolyte concentration and valency. At low electrolyte concentrations ($< 10^{-2}$ mol dm^{-3} for a 1 : 1 electrolyte), G_{max} is high ($> 25kT$) and this prevents particle aggregation into the primary minimum. The higher the electrolyte concentration (and the higher the valency of the ions), the lower the energy maximum.

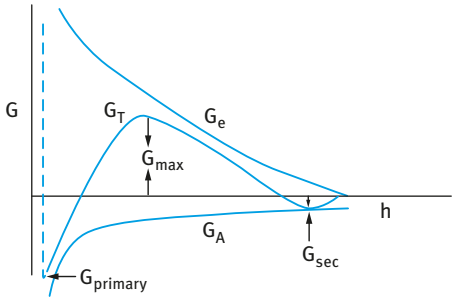

Fig. 1.11: Schematic representation of the variation of G_T with h according to the DLVO theory.

The second stabilization mechanism is referred to as steric repulsive energy produced by the presence of adsorbed (or grafted) layers of surfactant or polymer molecules [12, 13] as was discussed in detail in Chapter 8 of Vol. 1. In this case the nonionic surfactant or polymer (referred to as polymeric surfactant) should be strongly adsorbed to the particle surface and the stabilizing chain should be strongly solvated (hydrated in the case of aqueous suspensions) by the molecules of the medium [12, 13]. The most effective polymeric surfactants are those of A–B, A–B–A block or BA_n graft copolymers. The "anchor" chain B is chosen to be highly insoluble in the medium and has strong affinity to the surface. The A stabilizing chain is chosen to be highly soluble in the medium and strongly solvated by the molecules of the medium. For

nanosuspensions of hydrophobic solids in aqueous media, the B chain can be polystyrene, poly(methylmethacrylate) or poly(propylene oxide). The A chain could be poly(ethylene oxide) which is strongly hydrated by the medium.

When two particles each with a radius R and containing an adsorbed polymer layer with a hydrodynamic thickness δ_h, approach each other to a surface–surface separation distance h that is smaller than $2\delta_h$, the polymer layers interact with each other resulting in two main situations [12, 13]:

(i) the polymer chains may overlap with each other;
(ii) the polymer layer may undergo some compression.

In both cases, there will be an increase in the local segment density of the polymer chains in the interaction region. The real situation is perhaps in between the above two cases, i.e. the polymer chains may undergo some interpenetration and some compression.

Provided the dangling chains (the A chains in A–B, A–B–A block or BA_n graft copolymers) are in a good solvent, this local increase in segment density in the interaction zone will result in strong repulsion as a result of two main effects [12, 13]:

(i) An increase in the osmotic pressure in the overlap region as a result of the unfavourable mixing of the polymer chains, when these are in good solvent conditions. This is referred to as osmotic repulsion or mixing interaction and it is described by a free energy of interaction G_{mix}.
(ii) A reduction of the configurational entropy of the chains in the interaction zone; this entropy reduction results from the decrease in the volume available for the chains when these are either overlapped or compressed. This is referred to as volume restriction interaction, entropic or elastic interaction and it is described by a free energy of interaction G_{el}.

The combination of G_{mix} and G_{el} is usually referred to as the steric interaction free energy, G_s, i.e.,

$$G_s = G_{mix} + G_{el}. \tag{1.66}$$

The sign of G_{mix} depends on the solvency of the medium for the chains. If in a good solvent, i.e. the Flory–Huggins interaction parameter χ is less than 0.5, then G_{mix} is positive and the mixing interaction leads to repulsion (see below). In contrast if $\chi > 0.5$ (i.e. the chains are in a poor solvent condition), G_{mix} is negative and the mixing interaction becomes attractive. G_{el} is always positive and hence in some cases one can produce stable nanosuspensions in a relatively poor solvent (enhanced steric stabilization).

Combining G_{mix} and G_{el} with G_A gives the total energy of interaction G_T (assuming there is no contribution from any residual electrostatic interaction), i.e.,

$$G_T = G_{mix} + G_{el} + G_A. \tag{1.67}$$

A schematic representation of the variation of G_{mix}, G_{el}, G_A and G_T with surface–surface separation distance h is shown in Fig. 1.12. G_{mix} increases very sharply with decreasing h, when $h < 2\delta$. G_{el} increases very sharply with decreasing h, when $h < \delta$. G_T versus h shows a minimum, G_{min}, at separation distances comparable to 2δ. When $h < 2\delta$, G_T shows a rapid increase with decreasing h. The depth of the minimum depends on the Hamaker constant A, the particle radius R and adsorbed layer thickness δ. G_{min} decreases with decreasing A and R. At a given A and R, G_{min} decreases with increasing δ (i.e. with increasing molecular weight, M_w) of the stabilizer. This is illustrated in Fig. 1.13, which shows the energy–distance curves as a function of δ/R. The larger the value of δ/R, the smaller the value of G_{min}. In this case the system may approach thermodynamic stability as is the case with nanosuspensions.

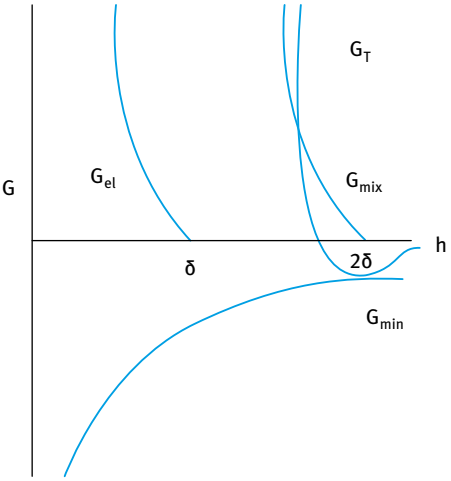

Fig. 1.12: Energy–distance curves for sterically stabilized systems.

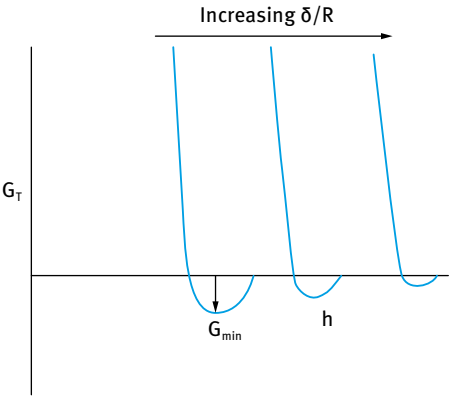

Fig. 1.13: Variation of G_{min} with δ/R.

1.4 Prevention of Ostwald ripening (crystal growth)

As discussed in Chapter 10 of Vol. 1, the driving force for Ostwald ripening is the difference in solubility between small and large particles (smaller particles have higher solubility than larger ones) [17].

A schematic representation of the enhancement the solubility $c(r)/c(0)$ with decreasing particle size according to the Kelvin equation is shown in Fig. 1.14. The solubility of suspension particles increases very rapidly with decreasing radius, particularly when $r < 100$ nm. This means that a particle with a radius of, say, 4 nm will have about 10 times solubility enhancement compared with a particle with, say, 10 nm radius, which has a solubility enhancement of only 2 times. Thus with time molecular diffusion will occur between the smaller and larger particle or droplet, with the ultimate disappearance of most of the small particles. This results in a shift in the particle size distribution to larger values on storage of the suspension. This could lead to the formation of a suspension with average particle size > 2 µm. This instability can cause severe problems, such sedimentation, flocculation and even flocculation of the suspension.

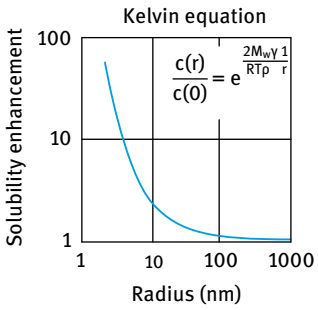

Fig. 1.14: Solubility enhancement with decreasing particle or droplet radius.

A second driving force for Ostwald ripening in suspensions is due to polymorphic changes. If, for example, a drug has two polymorphs A and B, the more soluble polymorph, say A (which may be more amorphous) will have higher solubility than the less soluble (more stable) polymorph B. During storage, polymorph A will dissolve and recrystallize as polymorph B. This can have a detrimental effect on bioefficacy, since the more soluble polymorph may be more active.

The kinetics of Ostwald ripening is described in terms of the theory developed by Lifshitz and Slesov [18] and by Wagner [19] (referred to as LSW theory). The LSW theory assumes that:

(i) the mass transport is due to molecular diffusion through the continuous phase;
(ii) the dispersed phase particles are spherical and fixed in space;
(iii) there is no interaction between neighbouring particles (the particles are separated by a distance much larger than the diameter of the particles);

(iv) the concentration of the molecularly dissolved species is constant except adjacent to the particle boundaries.

The rate of Ostwald ripening ω is given by:

$$\omega = \frac{\mathrm{d}}{\mathrm{d}r}(r_c^3) = \left(\frac{8\sigma DS(\infty)V_m}{9RT}\right)f(\phi) = \left(\frac{4DS(\infty)\alpha}{9}\right)f(\phi), \tag{1.68}$$

where r_c is the radius of a particle that is neither growing nor decreasing in size, D is the diffusion coefficient of the disperse phase in the continuous phase, $f(\phi)$ is a factor that reflects the dependence of ω on the disperse volume fraction and α is the characteristic length scale ($= 2\gamma V_m/RT$).

Particles with $r > r_c$ grow at the expense of smaller ones, while particles with $r < r_c$ tend to disappear. The validity of the LSW theory was tested by Kabalnov et al. [22, 23] using emulsions of 1,2 dichloroethane-in-water whereby the droplets were fixed to the surface of a microscope slide to prevent their coalescence. The evolution of the droplet size distribution was followed as a function of time by microscopic investigations. LSW theory predicts that the droplet growth over time is proportional to r_c^3.

LSW theory assumes that there are no interactions between the particles and it is limited to low particle volume fractions. At higher volume fractions the rate of ripening depends on the interaction between diffusion spheres of neighbouring particles. It is expected that suspensions with higher volume fractions of solid will have broader particle size distribution and faster absolute growth rates than those predicted by LSW theory. However, experimental results using high surfactant concentrations (5 %) showed the rate to be independent of the volume fraction in the range $0.01 \leq \phi \leq 0.3$. It has been suggested that the particles may have been screened from one another by surfactant micelles [24].

It has been suggested that micelles play a role in facilitating the mass transfer between particles by acting as carriers of solute molecules [25–28]. Three mechanisms were suggested:

(i) molecules are transferred via direct particle/micelle collisions;
(ii) molecules exit the particle and are trapped by micelles in the immediate vicinity of the particle;
(iii) molecules exit the particles collectively with a large number of surfactant molecules to form a micelle.

Numerous studies indicate, however, that the presence of micelles affects mass transfer to only a small extent [29]. The results showed only a two-fold increase in ω above the cmc. This result is consistent with many other studies which showed an increase in mass transfer of only 2–5 times with increasing micelle concentration. The lack of strong dependency of mass transfer on micelle concentration for ionic surfactants may result from electrostatic repulsion between the particles and micelles, which provides a high energy barrier preventing droplet/micelle collision.

When using nonionic surfactant micelles, larger increases in the Ostwald ripening rate might be expected due to the larger solubilization capacities of the nonionic surfactant micelles and absence of electrostatic repulsion between the particles and the uncharged micelles [30].

According to the above analysis, the growth of crystals can take place only under conditions of appreciable supersaturation, mostly > 1.5 %, which ensures the necessary work of formation of two-dimensional nuclei. However, experiments on the growth of various crystals have shown that crystal growth can take place at extremely low supersaturation. The existence of a critical finite supersaturation for the growth of crystals has only been established for a few materials and then for individual faces of crystals being different from case to case; at the most it is about 1 %. However, this discrepancy is not too surprising [31] since the crystals do not have a completely perfect surface needing fresh two-dimensional nucleation in order to grow. This discrepancy may be attributed to crystal dislocations and structural defects. The latter include cracks, surface kinks and surface roughness. According to Cabrera and Burton [32] and Frank [31], such defects result in the formation of steps at which crystals can grow without the need for the formation of nuclei. Screw dislocations are of special importance in the growth of real crystals. If just one dislocation of this type emerges at the centre of the face, that crystal face can grow perpetually up a "spiral staircase". The general importance of dislocations for crystal growth accounts for many observations, such as the individual behaviour of each crystal face, particularly on the microscopic scale.

It has long been known that trace concentrations of certain additives can have pronounced effects on crystal growth and habit. These effects are of great importance in many fields of science and technology, but the mechanism by which these additives affect crystal growth is not clear. It is generally agreed that additives must adsorb on a crystal surface in order to affect the growth on that face.

Sufficient effects on growth behaviour with very small impurity additives are usually produced by large organic molecules on colloidal materials. One part in 10^4 or 10^5 of such materials may be sufficient to completely alter the growth. The effects of large molecules are usually nonspecific, presumably due to their adsorption on almost any point of the crystal.

Assuming growth to be governed by creation and subsequent lateral motion of steps in the crystal surface [31, 32], it is possible to derive an expression for the effect of impurities on the flow of these steps [33].

As mentioned above, when the compound used for formulation of suspensions exists in two polymorphs, crystal growth may take place as a result of reversion of the thermodynamically less stable form to the more stable form. If this is the case, crystal growth is virtually unaffected by temperature, i.e. it is an isothermal process, which is solvent mediated. Crystal growth involving such polymorphic changes has been carried out by various investigators [34–36]. A thermodynamic analysis based on Gibbs' theory to account for the polymorphic changes, can be made. If a crystal exists

in two polymorphic forms, α and β, the Gibbs free energy is given by the expressions,

$$\Delta G^{\alpha} = \Delta G_{\mathrm{v}}^{\alpha} + \sum_{i}^{N} A_i \Delta G_{\mathrm{s}}^{\alpha}, \tag{1.69}$$

$$\Delta G^{\beta} = \Delta G_{\mathrm{v}}^{\beta} + \sum_{i}^{N} A_i \Delta G_{\mathrm{s}}^{\beta}, \tag{1.70}$$

where V is the crystal volume and A_i is the area. If $\Delta G^{\alpha} \neq \Delta G^{\beta}$, there exists a thermodynamic potential (driving force) to establish equilibrium by an appropriate change of phase or crystal habit. By this mechanism the less soluble phase grows at the expense of the more soluble phase. The different polymorphs can be characterized by X-ray diffraction.

It is clear from the above discussion that crystal growth in suspensions where the solid particles have substantial solubility or exist in various polymorphs, is the rule rather than the exception. The task of the formulation scientist is to reduce crystal growth to an acceptable level depending on the application. This is particularly the case with pharmaceutical and agrochemical suspensions, where crystal growth leads to a shift of the particle size distribution to larger values. Apart from reducing the physical stability of the suspension, e.g. increased sedimentation, the increase in particle size of the active ingredient reduces its bioavailability (reduction of disease control). Unfortunately, crystal growth inhibition is still an "art", rather than a "science", in view of the lack of adequate fundamental understanding of the process at a molecular level.

Since suspensions are prepared by using a wetting/dispersing agent, it is important to discuss how these agents can affect the growth rate. Firstly, the presence of wetting/dispersing agents influences the process of diffusion of the molecules from the surface of the crystal to the bulk solution. The wetting/dispersing agent may affect the rate of dissolution by affecting the rate of transport away from the boundary layer [1–3], although their addition is not likely to affect the rate of dissolution proper (passage from the solid to the dissolved state in the immediate adjacent layer). If the wetting/dispersing agent forms micelles that can solubilize the solute, the diffusion coefficient of the solute in the micelles is greatly reduced. However, as a result of solubilization, the concentration gradient of the solute is increased to an extent depending on the extent of solubilization. The overall effect may be an increase in crystal growth rate as a result of solubilization. In contrast, if the diffusion rate of the molecules of the wetting/dispersing agent is sufficiently rapid their presence will lower the flux of the solute molecules compared to that in the absence of the wetting/dispersing agent. In this case, the wetting/dispersing agent will lower the rate of crystal growth.

Secondly, wetting/dispersing agents are expected to influence growth when the rate is controlled by surface nucleation [1–3]. Adsorption of wetting/dispersing agents on the surface of the crystal can drastically change the specific surface energy and makes it inaccessible to the solute molecules. In addition, if the wetting/dispersing

agent is preferentially adsorbed at one or more of the faces of the crystal (for example by electrostatic attraction between a highly negative face of the crystal and cationic surfactant), surface nucleation is no longer possible at this particular face (or faces). Growth will then take place at the remaining faces, which are either bare or incompletely covered by the wetting/dispersing agent. This will result in a change in crystal habit.

The role of surfactants in modifying the crystal habit of adipic acid has been systematically studied by Michaels and collaborators [37–39]. These authors investigated the effect of various surfactants of the anionic and cationic type on the growth of adipic acid crystals from aqueous solution. Microscopic measurements of the crystals permitted calculation of the individual growth rates of the (001), (010) and (110) faces. The growth rate is governed by the rate at which solute is supplied to the individual steps on the crystal faces and the spacing between them. In other words, the growth rate is proportional to the step velocity and the distance between steps. Surfactants may alter the growth rate by changing either of these. At constant step velocity, the spacing between steps may be altered, with a corresponding modification in the growth rate, by a variation in the rate of step generation. With constant step spacing, an alteration of step velocity will likewise modify the growth rate. Sodium dodecylbenzene sulphonate (NaDBS) retards the growth on the (010) and (110) faces more than on the (001) face, thus favouring the formation of prismatic or needle crystals. Cationic surfactants such as cetyltrimethyl ammonium chloride have the opposite effect, thus favouring growth of the micaceous faces. Michaels et al. [37–39] concluded that the anionic surfactants are physically adsorbed on the faces of adipic acid crystals, while the cationics appear to be chemisorbed. In all cases, the surfactants retarded crystal growth by adsorption on the crystal faces, thus reducing the area on which nucleation would occur. In fact with relatively large crystals, the influence of surfactants on crystal growth can be correlated satisfactorily with Langmuir adsorption isotherm. Surfactants, in general, exhibit a far greater retarding influence on the crystal growth of very small crystals than on the growth of larger ones.

From the above discussion, it can be seen that surfactants (wetting/dispersing agents), if properly chosen, may be used for crystal growth inhibition and control of habit formation. Inhibition of crystal growth can also be achieved by polymeric surfactants and other additives. For example, Simonelli et al. [40] found that the crystal growth of the drug sulphathiazole can be inhibited by the addition of poly(vinylpyrrolidone) (PVP). The inhibition effect depends on the concentration and molecular weight of PVP. A minimum concentration (expressed as grams PVP/100 ml) of polymer is required for inhibition, which increases with increasing molecular weight of the polymer. However, if the concentration is expressed in mol dm^{-3}, the reverse is true, i.e. the higher the molar mass of PVP the lower the number of moles required for inhibition. This led Simonelli et al. [40] to conclude that inhibition must involve kinetic effects, i.e. the rate of diffusion of PVP to the surfaces. If the rate of deposition of PVP is relatively slow as compared to that of sulphathiazole molecules,

it is buried by the "avalanche" of the precipitating sulphathiazole molecules. If, on the other hand, its rate is rapid, it in turn can bury the precipitating sulphathiazole molecules and sufficiently cover the crystal surface to cause inhibition of crystal growth. Clearly, a higher PVP concentration would be needed at higher supersaturation rates to cause inhibition. This is due to the increase in diffusion rate at higher supersaturation [40].

Carless et al. [41] reported that the crystal growth of cortisone acetate in aqueous suspensions can be inhibited by addition of cortisone alcohol. Crystal growth in this system is mainly inhibited by polymorphic transformation [41]. The authors assumed that cortisone alcohol is adsorbed onto the particles of the stable form and this prevents the arrival of new cortisone acetate molecules which would result in crystal growth. The authors also noticed that the particles change their shape, growing to long needles. This means that the cortisone alcohol fits into the most dense lattice plane of the cortisone acetate crystal, thus preventing preferential growth on that face.

Many block A–B–A and graft BA_n copolymers (with B being the "anchor" part and A the stabilizing chain) are very effective in inhibiting crystal growth. The B chain adsorbs very strongly on the surface of the crystal and these sites become unavailable for deposition. This has the effect of reducing the rate of crystal growth. Apart from their influence on crystal growth, the above copolymers also provide excellent steric stabilization, providing the A chain is chosen to be strongly solvated by the molecules of the medium.

1.5 Sedimentation of suspensions and prevention of formation of hard sediments

As discussed in Chapter 13 of Vol. 1, most suspensions undergo separation on standing as a result of the density difference between the particles and the medium, unless the particles are small enough for Brownian motion to overcome gravity [1–4].

For a very dilute suspension of rigid non-interacting particles ($\phi \leq 0.01$), the rate of sedimentation v_0 can be calculated by application of Stokes' law, whereby the hydrodynamic force is balanced by the gravitational force,

$$v_0 = \frac{2}{9}\frac{R^2 \Delta\rho g}{\eta}, \tag{1.71}$$

where η is the viscosity of the medium (water).

v_0 calculated for three particle sizes (0.1, 1 and 10 μm) for a suspension with density difference $\Delta\rho = 0.2$ is 4.4×10^{-9}, 4.4×10^{-7} and 4.4×10^{-5} m s^{-1} respectively. The time needed for complete sedimentation in a 0.1 m container is 250 days, 60 hours and 40 minutes respectively.

For moderately concentrated suspensions, $0.2 > \phi > 0.01$, sedimentation is reduced as a result of hydrodynamic interaction between the particles, which no longer

sediment independently of each other [1]. Several contributions to the change in sedimentation rate, as a result of increasing particle number concentration, were considered by Bachelor [1], who derived the following equation relating the rate of sedimentation of a moderately concentrated suspension v to that of the Stokes' rate v_0,

$$v = v_0(1 - 6.55\phi). \tag{1.72}$$

This means that for a suspension with $\phi = 0.1$, $v = 0.345v_0$, i.e. the rate is reduced by a factor of ≈ 3.

For more concentrated suspensions ($\phi > 0.2$), the sedimentation velocity becomes a complex function of ϕ. An increase in the concentration of the suspension leads to a considerable increase in the complexity of the dependency of sedimentation rate on particle size. This is because there is a decrease in the distance between the particles in the disperse phase and also interactions between them occur (either directly or indirectly through the dispersion medium). In addition, an increase in the concentration of the solid phase in the suspension brings an increase in the density and viscosity of the whole disperse system. At high values of the volume fraction of the solid phase ($\phi > 0.1$) displacement of the dispersion medium occurs and of small particles sedimenting out originally by larger particles. At even higher volume fraction ($\phi > 0.4$), the particles tend to sediment in what is known as "hindered sedimentation" mode, whereby all particles sediment at the same rate independent of their size. The closeness of packing prevents differential movement of any large particles through the suspension and the observed sedimentation rate becomes very much less than the Stokes' sedimentation rate for any single particle. For a suspension sedimenting in this way the solid appears to "condense" slowly to a larger volume fraction leaving a clear supernatant liquid separated from the solid sediment by a sharp interface.

The above phenomenon of "hindered sedimentation" was theoretically analysed by Kynch [42] who considered the case of sedimentation of monodisperse particles. He assumed that the velocity v of any particle is a function only of the local concentration n of the particles in its immediate vicinity. The particle flux S, i.e. the number of particles passing a horizontal section, per unit area, per unit time, is given by,

$$S = nv. \tag{1.73}$$

It is assumed everywhere that the concentration is the same across any horizontal layer. The concentration n varies from zero at the top of the sedimentation vessel to some maximum value n_m at the bottom and presumably the velocity v of fall decreases from a finite value u to zero. By considering the flux of particles at various levels in a sedimenting suspension, Kynch [42] derived expressions for the decrease of the height of the suspension with time, when the initial concentration n remains constant and when the initial concentration increases towards the bottom with increasing n in the concentration n range covered during sedimentation. The x versus t diagram obtained by Kynch [42] is shown in Fig. 1.15.

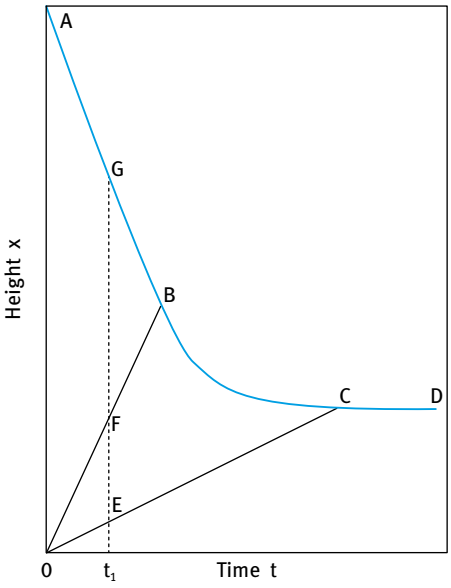

Fig. 1.15: Fall of surface of a suspension according to Kynch [42].

The curve in Fig. 1.15 is characterized by three sections: A0B, where the concentration n is the same as the initial concentration; 0CD, where the concentration is a maximum n_m; and 0BC, where there is a continuous but extremely rapid increase in concentration from n_B to the maximum concentration n_m. Thus the suspension falls like a "plug" which has the initial density of the suspension (section A0B), depositing a "plug" of maximum density at the bottom (section 0CD). At time t_1, there would be a suspension having the initial density above F, and a "plug" of maximum density below E. Between E and F, the density would decrease (in the upward direction) from the maximum to the initial density. Thus, for a suspension which is not flocculated, the sedimentation is constant with time in the first stage, becoming logarithmic in the third stage and the second stage is transition between the two. Unfortunately, Kynch's analysis [42] did not take into account the obvious change of sedimentation velocity with concentration, arising from hydrodynamic interactions [1, 8].

As discussed in Chapter 13 of Vol. 1, Buscall et al. [43] attempted to relate the decrease in sedimentation velocity with increasing particle volume fraction ϕ to the reduction in relative viscosity with increasing ϕ and they arrived at the following semi-empirical equation [44],

$$\frac{v}{v_0} = \left(1 - \frac{\phi}{\phi_p}\right)^{\alpha[\eta]\phi_p} = \left(1 - \frac{\phi}{\phi_p}\right)^{k\phi_p}. \tag{1.74}$$

The empirical relationship in equation (1.74) was tested for sedimentation of polystyrene latex suspensions with $R = 1.55\,\mu m$ in 10^{-3} mol dm^{-3} NaCl [43].

Michaels and Bolger [45] used a different model to describe the sedimentation of flocculated kaolin suspensions. Three types of sedimentation curves were consid-

ered, depending on the concentration range of the suspension. These are illustrated in Fig. 1.16. Curve a is the case of a dilute suspension, in which the aggregates are considered to be spherical, sedimenting individually thus producing a sharp interface. The sedimentation curve starts with a linear part, with the rate v_0 being a function of ϕ_A (the volume fraction of the aggregates). Michaels and Bolger [45] used Richardson and Zaki's formula [46] for v_0 and they obtained the following equation,

$$v_0 = \frac{g(\rho - \rho_0)d_A^2}{18\eta C_A}(1 - C_A\phi)^{4.56}, \tag{1.75}$$

where d_A is the mean diameter of aggregates, $\phi = (1 - \varepsilon)$ is the volume fraction of the solids with ε being a measure of porosity, i.e. $(1 - \varepsilon)$ is the volumetric density, ρ is the density of the particles and ρ_0 that of the medium. $C_A(= \phi_A/\phi)$ is a factor that characterizes the "looseness" of the aggregates (the ratio of immobilized liquid to the total volume).

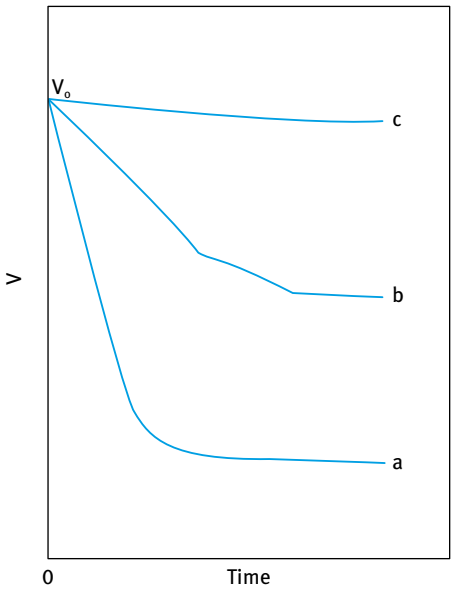

Fig. 1.16: Three types of sedimentation curves according to Michaels and Bolger [43].

In the intermediate concentration range (curve b) the sedimentation curve was accounted for by Michaels and Bolger [45] by considering a network model for the aggregates. The maximum sedimentation rate is given by,

$$v_1' = \frac{g(\rho - \rho_0)d_p^2}{32\eta}(1 - C_{AF}\phi_F), \tag{1.76}$$

where d_p is the mean pore diameter in the network, $C_{AF}(= \phi_A/\phi_F)$, where ϕ_F is the ratio of the volume of the flocs forming the aggregates and the volume of suspension.

The characteristics of the flocs can be determined by studying the sediment volume in detail.

The sedimentation of highly concentrated flocculated suspension (curve c) shows a slow decrease in the sediment volume with time and in some cases a clear liquid layer is "squeezed out" of the liquid bound to the particle surfaces to the top of the container. This process is sometimes referred to as syneresis and the compaction of the solid aggregates is referred to as consolidation

The sedimentation of particles in non-Newtonian fluids, such as aqueous solutions containing high molecular weight compounds (e.g. hydroxyethyl cellulose or xanthan gum) usually referred to as "thickeners", is not simple since these non-Newtonian solutions are shear thinning with the viscosity decreasing with increasing shear rate [9]. These solutions show a Newtonian region at low shear rates or shear stresses, usually referred to as the residual or zero shear viscosity $\eta(0)$, as shown in Chapter 14 of Vol. 1.

The viscosity of a polymer solution increases gradually with as its concentration increases and at a critical concentration, C^*, the polymer coils with a radius of gyration R_G and a hydrodynamic radius R_h (which is higher than R_G due to solvation of the polymer chains) begin to overlap and this shows a rapid increase in viscosity as shown in Chapter 14 of Vol. 1.

C^* is related to R_G and the polymer molecular weight M by,

$$C^* = \frac{3M}{4\pi R_G^3 N_{av}}. \tag{1.77}$$

N_{av} is Avogadro's number. As M increases, C^* becomes progressively lower. This shows that to produce physical gels at low concentrations by simple polymer coil overlap, one has to use high molecular weight polymers.

Another method to reduce the polymer concentration at which chain overlap occurs is to use polymers that form extended chains, such as xanthan gum that produces conformation in the form of a helical structure with a large axial ratio. These polymers give much higher intrinsic viscosities and they show both rotational and translational diffusion. The relaxation time for the polymer chain is much higher than a corresponding polymer with the same molecular weight but produces random coil conformation.

The above polymers interact at very low concentrations and the overlap concentration can be very low (< 0.01 %). These polysaccharides are used in many formulations to produce physical gels at very low concentrations thus reducing sedimentation.

The shear stress, σ_p, exerted by a particle (force/area) can be simply calculated [9],

$$\sigma_p = \frac{(4/3)\pi R^3 \Delta\rho g}{4\pi R^2} = \frac{\Delta\rho R g}{3}. \tag{1.78}$$

For a 10 μm radius particle with a density difference $\Delta\rho$ of 0.2 g cm^{-3}, the stress is equal to,

$$\sigma_p = \frac{0.2 \times 10^3 \times 10 \times 10^{-6} \times 9.8}{3} \approx 6 \times 10^{-3} \text{ Pa.} \quad (1.79)$$

For smaller particles smaller stresses are exerted.

Thus, to predict sedimentation, one has to measure the viscosity at very low stresses (or shear rates). These measurements can be carried out using a constant stress rheometer (Carrimed, Bohlin, Rheometrics, Haake or Physica) as described in Chapter 14 of Vol. 1.

Usually one obtains good correlation between the rate of sedimentation v and the residual viscosity $\eta(0)$. Above a certain value of $\eta(0)$, υ becomes equal to 0. Clearly, to minimize sedimentation one has to increase $\eta(0)$; an acceptable level for the high shear viscosity η_∞ must be achieved, depending on the application. In some cases, a high $\eta(0)$ may be accompanied by a high η_∞ (which may not be acceptable for the application).

The situation with more practical dispersions is more complex due to the interaction between the thickener and the particles. Most practical suspensions show some weak flocculation and the "gel" produced between the particles and thickener may undergo some contraction as a result of the gravity force exerted on the whole network. A useful method to describe separation in these concentrated suspensions is to follow the relative sediment volume V_t/V_0 or relative sediment height h_t/h_0 (where the subscripts t and 0 refer to time t and zero time respectively) with storage time. For good physical stability the values of V_t/V_0 or h_t/h_0 should be as close as possible to unity (i.e. minimum separation). This can be achieved by balancing the gravitational force exerted by the gel network with the bulk "elastic" modulus of the suspension. The latter is related to the high frequency modulus G' (Chapter 14 of Vol. 1 on rheology).

As mentioned before, dilatant sediments are produced with suspensions which are colloidally stable. These dilatant sediments are difficult to redisperse and hence they must be prevented from forming on standing. Several methods may be applied to prevent sedimentation and formation of clays or cakes in a suspension and these were described in Chapter 13 of Vol. 1.

References

[1] Tadros T. Suspension concentrates. Berlin: De Gruyter; 2017.
[2] Tadros T. Dispersion of powders in liquids and stabilisation of suspensions. Weinheim: Wiley-VCH; 2012.
[3] Tadros T. Formulation of disperse systems. Weinheim: Wiley-VCH; 2014.
[4] Tadros T. Suspensions. In: Tadros T, editor. Encyclopedia of colloid and interface science. Berlin: Springer; 2013.
[5] Tadros T. Nanodispersions. Berlin: De Gruyter; 2016.
[6] Tadros T. Applied surfactants. Weinheim: Wiley-VCH; 2005.

[7] Tadros T. Interfacial phenomena and colloid stability. Vol. 1. Berlin: De Gruyter; 2015.
[8] Tadros T (editor). Solid/liquid dispersions. London: Academic Press; 1987.
[9] Tadros T. Rheology of Dispersions. Weinheim: Wiley-VCH; 2010.
[10] Deryaguin BV, Landau L. Acta Physicochem USSR. 1941;14:633.
[11] Verwey EJW, Overbeek JTG. Theory of stability of lyophobic colloids. Amsterdam: Elsevier; 1948.
[12] Napper DH. Polymeric stabilisation of colloidal dispersions. London: Academic Press; 1983.
[13] Tadros T. Polymeric surfactants. Berlin: De Gruyter; 2017.
[14] Asakura A, Oosawa F. J Chem Phys. 1954;22:1255.
[15] Asakura A, Oosawa F. J Polymer Sci. 1958;33:183.
[16] Philipse A. Particulate Colloids: Aspects of Preparation and Characterisation. In: Lyklema J, editor. Fundamentals of Interface and Colloid Science. Vol. IV. Amsterdam: Elsevier; 2005.
[17] Thompson W (Lord Kelvin). Phil Mag. 1871;42:448.
[18] Lifshitz EM, Slesov VV. Soviet Physics JETP. 1959;35:331.
[19] Wagner C. Z Electrochem. 1961;35:581.
[20] Rehbinder PA. Colloid J USSR. 1958;20:493.
[21] Tadros T. Colloids in paints. Weinheim: Wiley-VCH; 2010.
[22] Kabalnov AS, Schukin ED. Adv Colloid Interface Sci. 1992;38:69.
[23] Kabalnov AS, Makarov KN, Pertsov AV, Shchukin ED. J Colloid Interface Sci. 1990;138:98.
[24] Taylor P. Colloids and Surfaces A. 1995;99:175.
[25] Ni Y, Pelura TJ, Sklenar TA, Kinner RA, Song D. Art Cells Blood Subs Immob Biorech. 1994;22:1307.
[26] Karaboni S, van Os NM, Esselink K, Hilbers PAJ. Langmuir. 1993;9:1175.
[27] Soma J, Papadadopoulos KD. J Colloid Interface Sci. 1996;181:225.
[28] Kabalanov AS. Langmuir. 1994;10:680.
[29] Taylor P, Ottewill RH. Colloids and Surfaces A. 1994;88:303.
[30] Anainsson EAG, Wall SN, Almagren M, Hoffmann H, Kielmann I, Ulbricht W, Zana R, Lang J, Tondre C. J Phys Chem. 1976;80:905.
[31] Frank FC. Disc Faraday Soc. 1949;5:48, 67.
[32] Cabrera N, Burton W. Disc Faraday Soc. 1949;5:33, 40.
[33] Cabrera N, Vermilyea DA. Proceedings International Conference on Crystal Growth. London: John Wiley and Sons; 1958. p. 393.
[34] Pearson JT, Varney G. J Pharm Pharmac Suppl. 1969;21:60.
[35] Pearson JT, Varney G. J Pharm Pharmac Suppl. 1973;25:62.
[36] Pfeiffer PR. J Pharm Pharmac. 1971;23:75.
[37] Michaels AS, Golville A Jr. J Phys Chem. 1960;64:13.
[38] Michaels AS, Tausch FW Jr. J Phys Chem. 1961;65:1730.
[39] Michaels AS, Brian PLT, Bech WF. Chem Phys Appl Surface Active Substances. Proceedings 4th Int. Congress, 2. 1967, 1053.
[40] Simonelli PA, Mehta SC, Higuchi WI. J Pharm Sci. 1970;59:633.
[41] Carless JE, Moustafa MA, Rapson HDC. J Pharm Pharmac. 1968;20:630.
[42] Kynch GJ. Trans Faraday Soc. 1952;48:166.
[43] Buscall R, Goodwin JW, Ottewill RH, Tadros TF. J Colloid Interface Sci. 1982;85:78.
[44] Krieger IM, Advances Colloid and Interface Sci. 1971;3:45.
[45] Michaels AS, Bolger JC. Ind Eng Chem. 1962;1:24.
[46] Richardson JF, Zaki WN. Trans Inst Chem Engrs. 1954;32:35.

2 Formulation of liquid/liquid dispersions (emulsions)

2.1 Introduction

Emulsions are a class of disperse systems consisting of two immiscible liquids [1–4]. The liquid droplets (the disperse phase) are dispersed in a liquid medium (the continuous phase). Several classes may be distinguished:

- oil-in-water (O/W);
- water-in-oil (W/O);
- oil-in-oil (O/O).

The latter class may be exemplified by an emulsion consisting of a polar oil (e.g. propylene glycol) dispersed in a nonpolar oil (paraffinic oil) and vice versa. To disperse two immiscible liquids one needs a third component, namely the emulsifier. The choice of the emulsifier is crucial in the formation of the emulsion and its long-term stability [1–4]. Many chemicals are formulated as emulsions, particularly those consisting of an oil that is immiscible in aqueous media. The oil can be emulsified in aqueous media using an appropriate surfactant. Several other components are added to the formulation, e.g. "thickeners" (rheology modifiers) to prevent creaming or sedimentation of the emulsion.

There are many examples one could quote of naturally occurring emulsions: milk and the O/W and W/O emulsions associated with oil-bearing rocks are just two examples. Industrial emulsion formulations include pharmaceuticals, cosmetics and personal care (such as lotions and hand creams), paints (e.g. latexes), agrochemicals and many food products (such as mayonnaise, salad cream and many desserts). Emulsion types can be classified on the basis of the nature of the emulsifier or the structure of the system as shown in Tab. 2.1.

Tab. 2.1: Classification of emulsions.

Nature of emulsifier	Structure of the system
– Simple molecules and ions	– Nature of internal and external phase: O/W, W/O
– Nonionic surfactants	– Nanoemulsions
– Ionic surfactants	– Micellar emulsions (microemulsions)
– Surfactant mixtures	– Macroemulsions
– Nonionic polymers	– Bilayer droplets
– Polyelectrolytes	– Double and multiple emulsions
– Mixed polymers and surfactants	– Mixed emulsions
– Liquid crystalline phases	
– Solid particles	

https://doi.org/10.1515/9783110587968-003

Several types of emulsifiers can be distinguished. The simplest type is ions such as OH^- which can be specifically adsorbed on the emulsion droplet thus producing a charge. An electrical double layer can be produced which provides electrostatic repulsion. This has been demonstrated with very dilute O/W emulsions by removing any acidity. Clearly that process is not practical. The most effective emulsifiers are nonionic surfactants, such as alcohol ethoxylates with the general formula $C_xH_{2x+1}–O–(CH_2–CH_2–O)_nH$, which can be used to emulsify oil in water or water in oil. In addition they can stabilize the emulsion against flocculation and coalescence. Ionic surfactants such as sodium dodecyl sulphate can also be used as emulsifiers (for O/W) but the system is sensitive to the presence of electrolytes.

Surfactant mixtures, e.g. ionic and nonionic or mixtures of nonionic surfactants can be more effective in emulsification and stabilization of the emulsion. Nonionic polymers, sometimes referred to as polymeric surfactants, e.g. Pluronics with the general formula $HO–(CH_2–CH_2–O)_n–(CH_2–CH(CH_3)–O)_m–(CH_2–CH_2–O)_n–OH$ or PEO–PPO–PEO are more effective in stabilizing the emulsion but they may suffer from being difficult to emulsify (to produce small droplets) unless high energy is applied to the process. Polyelectrolytes such as poly(methacrylic acid) can also be applied as emulsifiers. Mixtures of polymers and surfactants are ideal in achieving ease of emulsification and stabilization of the emulsion. Lamellar liquid crystalline phases that can be produced using surfactant mixtures are very effective in emulsion stabilization. Solid particles that can accumulate at the O/W interface can also be used for emulsion stabilization. These are referred to as Pickering emulsions, whereby particles are made partially wetted by the oil phase and partially wetted by the aqueous phase.

Emulsions can also be classified on the basis of the structure of the system. Emulsions (O/W or W/O) having a size range of 0.1–5 μm with an average of 1–2 μm are generally termed macroemulsions. These systems are usually opaque or milky due to the large size of the droplets and the significant difference in refractive index between the oil and water phases. Those usually with a size range 20–100 nm are classified as nanoemulsions. Like macroemulsions they are only kinetically stable. They can be transparent, translucent or opaque depending on the droplet size, the refractive index difference between the two phases and the volume fraction of the disperse phase. Another class are double and multiple emulsions that are emulsions-of-emulsions, W/O/W and O/W/O systems. They are usually prepared using a two-stage process. For example a W/O/W multiple emulsion is prepared by forming a W/O emulsion which is then emulsified in water to form the final multiple emulsion. Mixed emulsions are systems consisting of two different disperse droplets that do not mix in a continuous medium. A special class are micellar emulsions or microemulsions which will be described in Chapter 6. These usually have the size range 5–50 nm. They are thermodynamically stable and strictly speaking they should not be described as emulsions. A better description is “swollen micelles” or “micellar systems”.

The present chapter will only deal with macroemulsions, their formation and stability. Several breakdown processes may occur on storage depending on droplet size distribution and density difference between the droplets and the medium, magnitude of the attractive versus repulsive forces which determines flocculation, solubility of the disperse droplets and the particle size distribution which determines Ostwald ripening, stability of the liquid film between the droplets that determines coalescence, phase inversion, where the two phases exchange, e.g. an O/W emulsion inverting to W/O and vice versa. Phase inversion can be catastrophic as is the case when the oil phase in an O/W emulsion exceeds a critical value. The inversion can be transient when for example the emulsion is subjected to a temperature increase.

The various breakdown processes are illustrated in Fig. 2.1. The physical phenomena involved in each breakdown process are not simple and analysis of the various surface forces involved is required. In addition, the above processes may take place simultaneously rather than consecutively and this complicates the analysis. Model emulsions with monodisperse droplets cannot be easily produced and hence any theoretical treatment must take into account the effect of droplet size distribution. Theories that take into account the polydispersity of the system are complex and in many cases only numerical solutions are possible. In addition, measurement of surfactant and polymer adsorption in an emulsion is not easy and one has to extract such information from measurements at a planer interface.

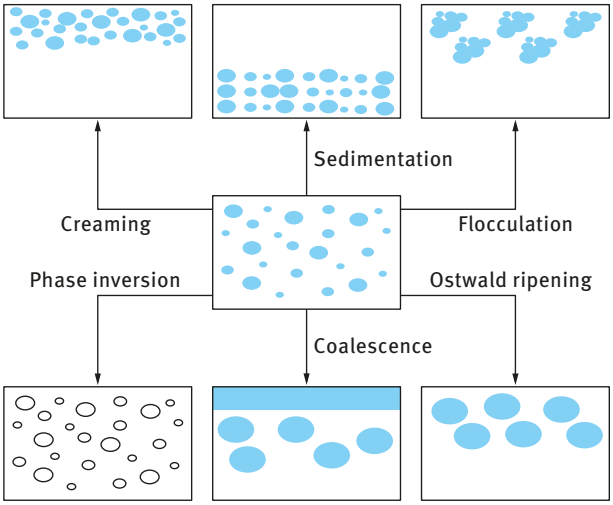

Fig. 2.1: Schematic representation of the various breakdown processes in emulsions.

A summary of each of the above breakdown processes is given below and details of each process and methods for its prevention is given separate chapters.

As discussed in Chapter 13 of Vol. 1, creaming and sedimentation with no change in droplet size result from external forces, usually gravitational or centrifugal. When such forces exceed the thermal motion of the droplets (Brownian motion), a concentration gradient builds up in the system with the larger droplets moving faster to the top (if their density is lower than that of the medium) or to the bottom (if their density is larger than that of the medium) of the container. In the limiting cases, the droplets may form a close-packed (random or ordered) array at the top or bottom of the system with the remainder of the volume occupied by the continuous liquid phase.

Flocculation refers to aggregation of the droplets (without any change in primary droplet size) into larger units. As discussed in Chapter 7 of Vol. 1, it is the result of van der Waals attraction which is universal with all disperse systems. The main force of attraction arises from the London dispersion force that results from charge fluctuations of the atoms or molecules in the disperse droplets. Van der Waals attraction increases with decreasing separation distance between the droplets and at small separation distances the attraction becomes very strong, resulting in droplet aggregation or flocculation. The latter occurs when there is not sufficient repulsion to keep the droplets apart to distances where van der Waals attraction is weak. Flocculation may be "strong" or "weak", depending on the magnitude of the attractive energy involved. In cases where the net attractive forces are relatively weak, an equilibrium degree of flocculation may be achieved (so-called weak flocculation), associated with the reversible nature of the aggregation process. The exact nature of the equilibrium state depends on the characteristics of the system. One can envisage the build-up of aggregate size distribution and an equilibrium may be established between single droplets and large aggregates. With a strongly flocculated system, one refers to a system in which all the droplets are present in aggregates due to strong van der Waals attraction between the droplets.

As discussed in Chapter 10 of Vol. 1, Ostwald ripening (disproportionation) results from the finite solubility of the liquid phases. Liquids which are referred to as being immiscible often have mutual solubilities which are not negligible. With emulsions which are usually polydisperse, the smaller droplets will have larger solubility when compared with the larger ones (due to curvature effects). With time, the smaller droplets disappear and their molecules diffuse to the bulk and become deposited on the larger droplets. With time the droplet size distribution shifts to larger values.

Coalescence (Chapter 11 of Vol. 1) refers to the process of thinning and disruption of the liquid film between the droplets which may be present in a creamed or sedimented layer, in a floc or simply during droplet collision, with the result of fusion of two or more droplets into larger ones. This process of coalescence results in a considerable change in the droplet size distribution, which shifts to larger sizes. The limiting case for coalescence is the complete separation of the emulsion into two distinct liquid phases. The thinning and disruption of the liquid film between the droplets is determined by the relative magnitudes of the attractive versus repulsive forces. To prevent coalescence, the repulsive forces must exceed the van der Waals attraction, thus preventing film rupture.

Phase inversion (Chapter 12 of Vol. 1) refers to the process where there will be an exchange between the disperse phase and the medium. For example an O/W emulsion may with time or change of conditions invert to a W/O emulsion. In many case, phase inversion passes through a transition state in which multiple emulsions are produced. For example with an O/W emulsion, the aqueous continuous phase may become emulsified in the oil droplets forming a W/O/W multiple emulsion. This process may continue until all the continuous phase is emulsified into the oil phase thus producing a W/O emulsion.

2.2 Thermodynamics of emulsion formation and breakdown

When two immiscible phases α and β (oil and water) come into contact, an interfacial region develops as described in detail in Chapter 4 of Vol. 1. The interfacial region is not a layer that is one molecule thick; it is a region with thickness δ with properties different from the two bulk phases α and β. Using Gibbs' model, it is possible to obtain a definition of the interfacial tension γ,

$$\gamma = \left(\frac{\partial G^{\sigma}}{\partial A} \right)_{T,n_i}. \tag{2.1}$$

For a stable interface γ is positive, i.e. if the interfacial area increases, G^{σ} increases. Note that γ is energy per unit area (mJ m^{-2}) which is dimensionally equivalent to force per unit length (mN m^{-1}), the unit usually used to define surface or interfacial tension.

For a curved interface, one should consider the effect of the radius of curvature. Fortunately, γ for a curved interface is estimated to be very close to that of a planer surface, unless the droplets are very small (< 10 nm).

Curved interfaces produce some other important physical phenomena which affect emulsion properties, e.g. the Laplace pressure Δp which is determined by the radii of curvature of the droplets,

$$\Delta p = \gamma \left(\frac{1}{r_1} + \frac{1}{r_2} \right), \tag{2.2}$$

where r_1 and r_2 are the two principal radii of curvature.

For a perfectly spherical droplet $r_1 = r_2 = r$ and,

$$\Delta p = \frac{2\gamma}{r}. \tag{2.3}$$

For a hydrocarbon droplet with radius 100 nm, and $\gamma_{O/W} = 50$ mN m^{-1}, $\Delta p \approx 10^6$ Pa ($\approx$ 10 atm).

Consider a system in which an oil is represented by a large drop 2 of area A_1 immersed in a liquid 2, which is now subdivided into a large number of smaller droplets with total area A_2 ($A_2 \gg A_1$) as shown in Fig. 2.2. The interfacial tension γ_{12} is the same for the large and smaller droplets since the latter are generally in the region of 0.1 to few μm.

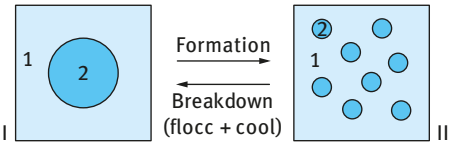

Fig. 2.2: Schematic representation of emulsion formation and breakdown.

The change in free energy in going from state I to state II is made up of two contributions: A surface energy term (that is positive) that is equal to $\Delta A\gamma_{12}$ (where $\Delta A = A_2 - A_1$). An entropy of dispersion term which is also positive (since producing a large number of droplets is accompanied by an increase in configurational entropy) which is equal to $T\Delta S^{\text{conf}}$.

From the second law of thermodynamics,

$$\Delta G^{\text{form}} = \Delta A\gamma_{12} - T\Delta S^{\text{conf}}. \tag{2.4}$$

In most cases $\Delta A\gamma_{12} \gg T\Delta S^{\text{conf}}$, which means that ΔG^{form} is positive, i.e. the formation of emulsions is nonspontaneous and the system is thermodynamically unstable. In the absence of any stabilization mechanism, the emulsion will break up by flocculation and coalescence as illustrated in Fig. 2.3 by the full line. In this case there are no free energy barriers either to flocculation or coalescence.

The kinetics of both breakdown processes is diffusion controlled: in the case of flocculation, by the diffusion of the droplets, and in the case of coalescence, by diffusion of molecules of liquid 1 out of the thin liquid film formed between two contacting droplets of liquid 2. The dashed line in Fig. 2.3 corresponds to the case where sedimentation or creaming is superimposed upon the flocculation and coalescence. The final state of the system (state III) is now the more familiar one of two liquid phases separated by a flat interface. The dotted line in Fig. 2.3 represents the situation if, in addition to the above effects, Ostwald ripening has to be taken into account. This occurs if the initial state IV is polydisperse and the liquids have a finite mutual solubility.

In the presence of a stabilizer (surfactant and/or polymer), an energy barrier is created between the droplets and therefore the reversal from state II to state I becomes noncontinuous as a result of the presence of these energy barriers. This is illustrated

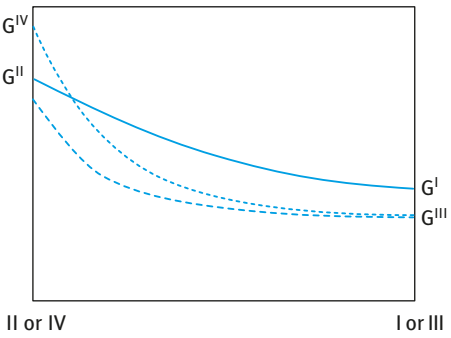

Fig. 2.3: Free energy path in emulsion breakdown; —, flocc. + coal., ---, flocc. + coal. + sed., ···, flocc. + coal. + sed. + Ostwald ripening.

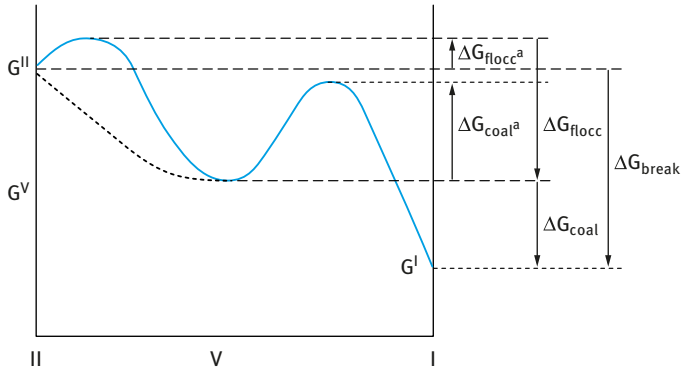

Fig. 2.4: Schematic representation of free energy path for breakdown (flocculation and coalescence) for systems containing an energy barrier.

in Fig. 2.4. In the presence of the above energy barriers, the system becomes kinetically stable. Strictly speaking, the ΔG_{flocc} and ΔG_{coal} are activation free energies. The intermediate state V is a metastable state and represents a flocculated emulsion that has undergone no coalescence. If ΔG_{coal} is sufficiently high, it may stay in this state indefinitely.

Similarly state II is also an unstable state, and if ΔG_{flocc} is sufficiently high, the stable, dispersed state may persist indefinitely. However, states II and V in these cases represent states of kinetic stability, rather than true thermodynamic stability. The dashed curve in Fig. 2.4 represents the situation if there is no free energy barrier to flocculation, but there is a large barrier to coalescence. Such a situation would arise for droplets stabilized, for example, by an adsorbed (neutral) polymer. In this case only the long-range van der Waals forces and the short-range steric repulsion forces (Chapter 13 of Vol. 1) are operating. If ΔG_{flocc} is not too large (say $< 10kT$ per droplet), then the flocculation is reversible and an equilibrium is set up as will be discussed below.

From Fig. 2.4, it is seen that,

$$\Delta G_{\text{break}} = \Delta G_{\text{flocc}} + \Delta G_{\text{coal}}. \tag{2.5}$$

It is worth considering the individual contributions to ΔG_{flocc} and ΔG_{coal} in the light of equations (2.4) and (2.5). The excess interfacial free energy G^{σ} associated with the presence of an interface is given by,

$$G^{\sigma} = \Delta A \gamma_{12} + \sum_i \mu_i n_i^{\sigma}. \tag{2.6}$$

If an interface disappears due to coalescence, the change in free energy ΔG_{coal} is simply given by,

$$\Delta G_{\text{coal}} = -\Delta(\gamma_{12} \Delta A). \tag{2.7}$$

The term $\sum_i \mu_i n_i^{\sigma}$ disappears since the chemical potential of species i is the same in either bulk phase and in the interface.

Considering equations (2.4), (2.5) and (2.7) leads to the conclusion that,

$$\Delta G_{\text{flocc}} = \Delta A \Delta \gamma_{12} - T\Delta S^{\text{conf}}. \tag{2.8}$$

Since,

$$\Delta(\Delta A \gamma_{12}) = \gamma_{12}\Delta\Delta A + \Delta A \Delta \gamma_{12}, \tag{2.9}$$

then ΔG_{flocc} is made up of two terms: the $\Delta A \Delta \gamma_{12}$ associated with the change in interfacial tension in the contact region of two droplets (i.e. for the two surfaces in the film separating the droplets) and the $T\Delta S^{\text{conf}}$ term associated with the change in configurational entropy. Both terms are negative and in most cases the $\Delta A \Delta \gamma_{12}$ term dominates, so that ΔG_{flocc} is negative, i.e. flocculation is thermodynamically spontaneous. However, if $(\Delta A \Delta \gamma_{12})$ is less than $(T\Delta S^{\text{conf}})$, then ΔG_{flocc} is positive and the emulsion is then thermodynamically stable against flocculation. This means that flocculation will not occur and the emulsion has to be concentrated by creaming/sedimentation or centrifugation before coalescence can occur. The condition $|\Delta A \Delta \gamma_{12}| < |T\Delta S^{\text{conf}}|$ may be realized if $\Delta \gamma_{12}$ is small, i.e. the secondary minimum in the energy–distance curve is small. Since $|T\Delta S^{\text{conf}}|$ decreases as the droplet number concentration increases, one can envisage that at some initial droplet concentration $\Delta G_{\text{flocc}} = 0$, i.e. below this concentration the emulsion is thermodynamically stable (ΔG_{flocc} positive), but that beyond this concentration the emulsion becomes thermodynamically unstable (ΔG_{flocc} negative) and reversible flocculation occurs.

2.3 Interaction forces between emulsion droplets and factors affecting their stability

As discussed in Chapters 7 and 8 of Vol. 1, there are three main interaction forces between emulsion droplets, namely van der Waals attraction, electrostatic (double layer) repulsion and steric repulsion. These interaction forces were described in detail in Chapters 7 and 8 of Vol. 1 respectively. As discussed in Chapter 7 of Vol. 1, the combination of van der Waals attraction with double layer repulsion forms the basis of the theory of colloid stability due to Deryaguin–Landau–Verwey–Overbeek (DLVO theory) [6, 7]. The combination of van der Waals attraction with steric repulsion leads to the theory of steric stabilization described in Chapter 8 of Vol. 1.

The energy–distance curves due to DLVO theory are shown in Fig. 2.5 for emulsions at low electrolyte concentration ($< 10^{-2}$ mol dm^{-3} 1 : 1 electrolyte, e.g. NaCl). G_{elec} decays exponentially with h, i.e. $G_{\text{elec}} \to 0$ as h becomes large. $G_{\text{A}} \propto 1/h$, i.e. G_{A} does not decay to 0 at large h. At long distances of separation, $G_{\text{A}} > G_{\text{elec}}$ resulting in a shallow minimum (secondary minimum). At very short distances, $G_{\text{A}} \gg G_{\text{elec}}$ resulting in a deep primary minimum. At intermediate distances, $G_{\text{elec}} > G_{\text{A}}$ resulting in

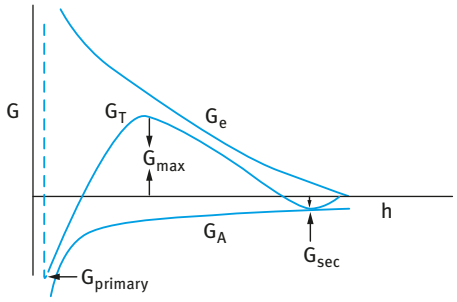

Fig. 2.5: Energy–distance curves according to the DLVO theory.

an energy maximum, G_{max}, whose height depends on ψ_0 (or ψ_d) and the electrolyte concentration and valency.

At low electrolyte concentrations ($< 10^{-2}$ mol dm^{-3} for a 1 : 1 electrolyte), G_{max} is high ($> 25kT$) and this prevents particle aggregation into the primary minimum. The higher the electrolyte concentration (and the higher the valency of the ions), the lower the energy maximum. Under some conditions (depending on electrolyte concentration and particle size), flocculation into the secondary minimum may occur. This flocculation is weak and reversible. By increasing the electrolyte concentration, G_{max} decreases until at a given concentration it vanishes and particle coagulation occurs.

Emulsions stabilized with nonionic surfactants and polymeric surfactants show steric repulsion that consists of two terms, a mixing term, G_{mix} (that results from the unfavourable mixing of the chains when these are in good solvent conditions) and an elastic term G_{el} (resulting from the loss of configurational entropy on chain overlap). Combining G_{mix} and G_{el} with the van der Waals attraction results in the energy–distance curve shown in Fig. 2.6.

G_{mix} increases very sharply with decreasing h, when $h < 2\delta$. G_{el} increases very sharply with decreasing h, when $h < \delta$. G_T versus h shows a minimum, G_{min}, at separation distances comparable to 2δ. When $h < 2\delta$, G_T shows a rapid increase with

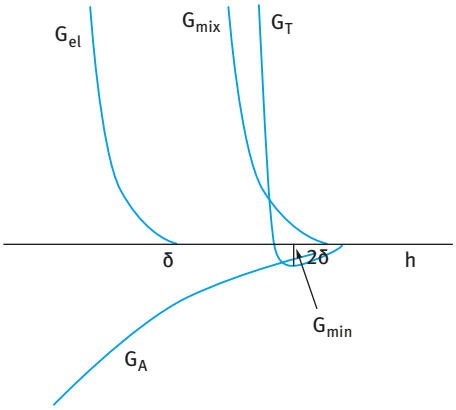

Fig. 2.6: Schematic representation of the energy–distance curve for a sterically stabilized emulsion.

decreasing h. The depth of the minimum depends on the Hamaker constant A, the particle radius R and adsorbed layer thickness δ. G_{min} increases with increasing A and R. At a given A and R, G_{min} decreases with increasing δ (i.e. with increasing molecular weight, M_w, of the stabilizer). This is illustrated in Fig. 2.7 which shows the energy–distance curves as a function of δ/R. The larger the value of δ/R, the smaller the value of G_{min}. In this case the system may approach thermodynamic stability as is the case with nanoemulsions.

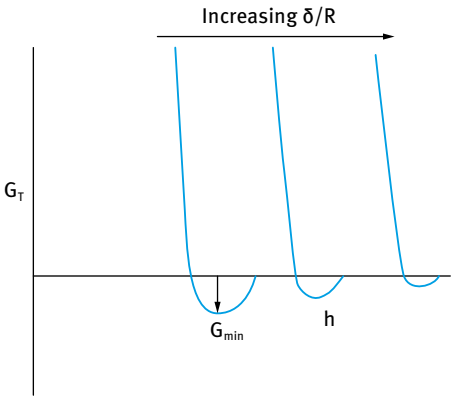

Fig. 2.7: Variation of G_T with h at various δ/R values.

2.4 Mechanism of emulsification and the role of the emulsifier

As mentioned above, to prepare an emulsion oil, water, surfactant and energy are needed. The composition of the system and its nature (oil-in-water, O/W, or water-in-oil, W/O) is determined by the nature of the emulsifier and the process applied [1–4]. Parameters such as the volume fraction of the disperse phase, ϕ, and the droplet size distribution are determined by the composition of the emulsifier layer around the droplets as well as the process of emulsification. In addition, the emulsifier composition and its nature determine the physical stability of the emulsion such as its flocculation behaviour, Ostwald ripening and coalescence. As mentioned above, emulsion formation is nonspontaneous and the system is thermodynamically unstable. The kinetic stability of the emulsion is determined by the balance of attractive and repulsive forces. It is important to know the process of emulsion formation and the mechanism of emulsification. The role of the emulsifier in droplet deformation and break-up must be considered at a fundamental level.

The mechanism of emulsification can be considered from a consideration of the energy required to expand the interface, $\Delta A\gamma$ (where ΔA is the increase in interfacial area when the bulk oil with area A_1 produces a large number of droplets with area A_2; $A_2 \gg A_1$ and γ is the interfacial tension). Since γ is positive, the energy to expand the interface is large and positive; this energy term cannot be compensated by the

small entropy of dispersion $T\Delta S^{\text{conf}}$ (which is also positive) and the total free energy of formation of an emulsion, ΔG^{form} given by equation (2.4) is positive. Thus, emulsion formation is nonspontaneous and energy is required to produce the droplets.

The formation of large droplets (few μm) as is the case for macroemulsions is fairly easy and hence high-speed stirrers such as the Ultra-Turrax or Silverson Mixer are sufficient to produce the emulsion. In contrast, the formation of small drops (submicron as is the case with nanoemulsions) is difficult and this requires a large amount of surfactant and/or energy. The high energy required for formation of nanoemulsions can be understood from a consideration of the Laplace pressure Δp (the difference in pressure between inside and outside the droplet) as given by equations (2.3) and (2.4). To break up a drop into smaller ones, it must be strongly deformed and this deformation increases Δp.

Surfactants play major roles in the formation of emulsions: By lowering the interfacial tension, Δp is reduced and hence the stress needed to break up a drop is reduced. Surfactants also prevent coalescence of newly formed drops (see below).

To assess emulsion formation, one usually measures the droplet size distribution using for example laser diffraction techniques. If the number frequency of droplets as a function of droplet diameter d is given by $f(d)$, the n-th moment of the distribution is,

$$S_n = \int_0^\infty d^n f(d)\, \partial d. \tag{2.10}$$

The mean droplet size is defined as the ratio of selected moments of the size distribution,

$$d_{nm} = \left[\frac{\int_0^\infty d^n f(d)\, \partial d}{\int_0^\infty d^m f(d)\, \partial d} \right]^{1/(n-m)}, \tag{2.11}$$

where n and m are integers and $n > m$ and typically n does not exceed 4.

Using equation (2.11) one can define several mean average diameters:

– The Sauter mean diameter with $n = 3$ and $m = 2$,

$$d_{32} = \left[\frac{\int_0^\infty d^3 f(d)\, \partial d}{\int_0^\infty d^2 f(d)\, \partial d} \right]. \tag{2.12}$$

– The mass mean diameter,

$$d_{43} = \left[\frac{\int_0^\infty d^4 f(d)\, \partial d}{\int_0^\infty d^3 f(d)\, \partial d} \right]. \tag{2.13}$$

– The number mean diameter,

$$d_{10} = \left[\frac{\int_0^\infty d^1 f(d)\, \partial d}{\int_0^\infty f(d)\, \partial d} \right]. \tag{2.14}$$

In most cases d_{32} (the volume/surface average or Sauter mean) is used. The width of the size distribution can be given as the variation coefficient c_m which is the standard deviation of the distribution weighted with d_m divided by the corresponding average d. Generally C_2 will be used, which corresponds to d_{32}.

Another is the specific surface area A (surface area of all emulsion droplets per unit volume of emulsion),

$$A = \pi S_2 = \frac{6\phi}{d_{32}}. \tag{2.15}$$

A typical droplet size distribution of an emulsion measured using the light diffraction technique (Malvern Mastersizer) is shown in Fig. 2.8.

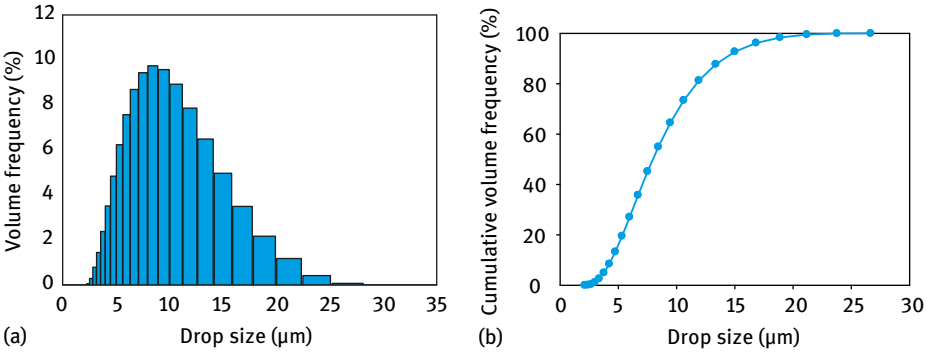

Fig. 2.8: Droplet size distribution of an emulsion: (a) volume frequency in discrete classes; (b) cumulative volume distribution.

Surfactants lower the interfacial tension γ and this causes a reduction in droplet size. Droplet size decreases with decreasing γ. For laminar flow the droplet diameter is proportional to γ; for turbulent inertial regime, the droplet diameter is proportional to $\gamma^{3/5}$.

The surfactant can lower the interfacial tension γ_0 of a clean oil–water interface to a value γ and,

$$\pi = \gamma_0 - \gamma, \tag{2.16}$$

where π is the surface pressure. The dependency of π on the surfactant activity a or concentration C is given by the Gibbs equation, as discussed in Chapter 4 of Vol. 1,

$$\mathrm{d}\pi = -\mathrm{d}\gamma = RT\Gamma\,\mathrm{d}\ln a = RT\Gamma\,\mathrm{d}\ln C, \tag{2.17}$$

where R is the gas constant, T is the absolute temperature and Γ is the surface excess (number of moles adsorbed per unit area of the interface).

At high a, the surface excess Γ reaches a plateau value; for many surfactants it is of the order of 3 mg m^{-2}. Γ increases with increasing surfactant concentration and eventually it reaches a plateau value (saturation adsorption). This is illustrated in Fig. 2.9 for various emulsifiers.

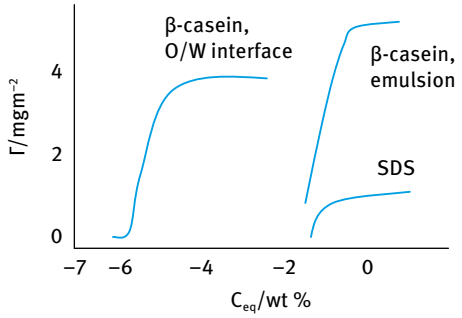

Fig. 2.9: Variation of Γ (mg m^{-2}) with log C_{eq} (wt%). The oils are β-casein (O/W interface) toluene, β-casein (emulsions) soybean, SDS benzene.

It can be seen from Fig. 2.9 that the polymer (β-casein) is more surface active than the surfactant (SDS). The value of C needed to obtain the same Γ is much smaller for the polymer when compared with the surfactant. In contrast, the value of γ reached at full saturation of the interface is lower for a surfactant (mostly in the region of 1–3 mN m^{-1} depending on the nature of the surfactant and the oil) when compared with a polymer (with γ values in the region of 10–20 mN m^{-1} depending on the nature of the polymer and the oil). This is due to the much closer packing of the small surfactant molecules at the interface when compared with the much larger polymer molecule that adopts tail–train–loop–tail conformation.

The effect of reducing γ on droplet size is illustrated in Fig. 2.10, which shows a plot of the droplet surface area A and mean drop size d_{32} as a function of surfactant concentration m for various systems. The amount of surfactant required to produce the smallest drop size will depend on its activity a (concentration) in the bulk which determines the reduction in γ, as discussed above.

Another important role of the surfactant is its effect on the interfacial dilational modulus ε,

$$\varepsilon = \frac{d\gamma}{d \ln A}. \tag{2.18}$$

ε is the absolute value of a complex quantity, composed of an elastic and a viscous term.

During emulsification an increase in the interfacial area A takes place and this causes a reduction in Γ. The equilibrium is restored by adsorption of surfactant from the bulk, but this takes time (shorter times occur at higher surfactant activity). Thus ε is small at small a and also at large a. Because of the lack or slowness of equilibrium with polymeric surfactants, ε will not be the same for expansion and compression of the interface.

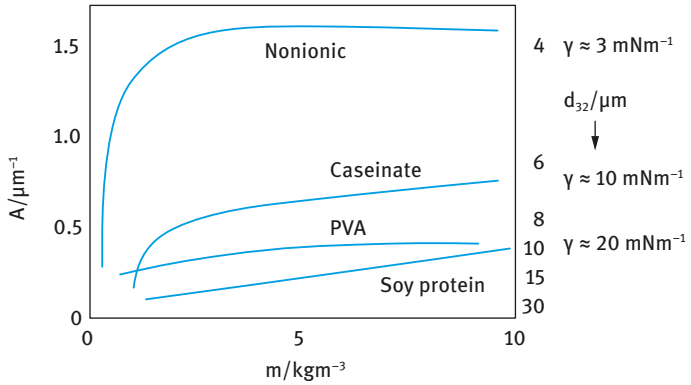

Fig. 2.10: Variation of A and d_{32} with m for various surfactant systems.

In practice emulsifiers are generally made of surfactant mixtures, often containing different components and these have pronounced effects on γ and ε. Some specific surfactant mixtures give lower γ values than either of the two individual components. The presence of more than one surfactant molecule at the interface tends to increase ε at high surfactant concentrations. The various components vary in surface activity. Those with the lowest γ tend to predominate at the interface, but if present at low concentrations, it may take a long time before reaching the lowest value. Polymer–surfactant mixtures may show some synergetic surface activity.

During emulsification, surfactant molecules are transferred from the solution to the interface and this leaves an ever lower surfactant activity [2]. Consider for example an O/W emulsion with a volume fraction $\phi = 0.4$ and a Sauter diameter $d_{32} = 1\,\mu m$. According to equation (2.15), the specific surface area is $2.4\,m^2\,ml^{-1}$ and for a surface excess Γ of $3\,mg\,m^{-2}$, the amount of surfactant at the interface is $7.2\,mg\,ml^{-1}$ emulsion, corresponding to $12\,mg\,ml^{-1}$ aqueous phase (or 1.2 %). Assuming that the concentration of surfactant, C_{eq} (the concentration left after emulsification), leading to a plateau value of Γ equals $0.3\,mg\,ml^{-1}$ then the surfactant concentration decreases from 12.3 to $0.3\,mg\,ml^{-1}$ during emulsification. This implies that the effective γ value increases during the process. If insufficient surfactant is present to leave a concentration C_{eq} after emulsification, even the equilibrium γ value would increase.

Another aspect is that the composition of surfactant mixture in solution may alter during emulsification [1, 2]. If some minor components are present that give a relatively small γ value, this will predominate at a macroscopic interface, but during emulsification, as the interfacial area increases, the solution will soon become depleted of these components. Consequently, the equilibrium value of γ will increase during the process and the final value may be markedly larger than what is expected on the basis of the macroscopic measurement.

During droplet deformation, its interfacial area is increased [2]. The drop will commonly have acquired some surfactant, and it may even have a Γ value close to the

equilibrium at the prevailing (local) surface activity. The surfactant molecules may distribute themselves evenly over the enlarged interface by surface diffusion or by spreading. The rate of surface diffusion is determined by the surface diffusion coefficient D_s that is inversely proportional to the molar mass of the surfactant molecule and also inversely proportional to the effective viscosity felt. D_s also decreases with increasing Γ. Sudden extension of the interface or sudden application of a surfactant to an interface, can produce a large interfacial tension gradient and in such a case spreading of the surfactant can occur.

Surfactants allow the existence of interfacial tension gradients that are crucial for formation of stable droplets. In the absence of surfactants (clean interface), the interface cannot withstand a tangential stress; the liquid motion will be continuous across a liquid interface (Fig. 2.11 (a)).

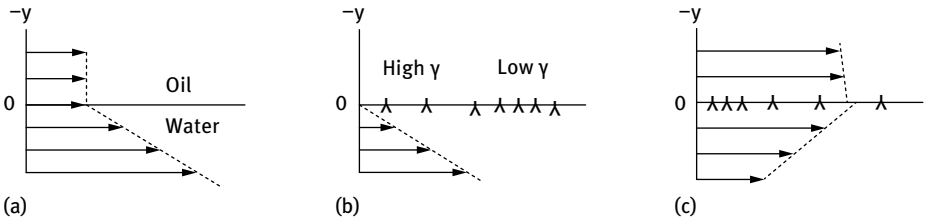

Fig. 2.11: Interfacial tension gradients and flow near an oil/water interface: (a) no surfactant; (b) velocity gradient causes an interfacial tension gradient; (c) interfacial tension gradient causes flow (Marangoni effect).

If a liquid flows along the interface with surfactants, the latter will be swept downstream causing an interfacial tension gradient (Fig. 2.11 (b)). A balance of forces will be established,

$$\eta\left[\frac{\mathrm{d}V_x}{\mathrm{d}y}\right]_{y=0} = -\frac{\mathrm{d}\gamma}{\mathrm{d}x}. \tag{2.19}$$

If the γ-gradient can become large enough, it will arrest the interface. The largest value attainable for dγ equals about π_{eq}, i.e. $\gamma_0 - \gamma_{eq}$. If it acts over a small distance, a considerable stress can develop, of the order of 10 kPa.

If the surfactant is applied at one site of the interface, a γ-gradient is formed that will cause the interface to move roughly at a velocity given by,

$$v = 1.2[\eta\rho z]^{-1/3}|\Delta\gamma|^{2/3}. \tag{2.20}$$

The interface will then drag some of the bordering liquid with it (Fig. 2.11 (c)). This is called the Marangoni effect [8–10].

Interfacial tension gradients are very important in stabilizing the thin liquid film between the droplets which is very important during the beginning of emulsification, when films of the continuous phase may be drawn through the disperse phase or when

collision of the still large deformable drops causes the film to form between them. The magnitude of the γ-gradients and of the Marangoni effect depends on the surface dilational modulus ε, which for a plane interface with one surfactant-containing phase, is given by the expressions,

$$\varepsilon = \frac{-\mathrm{d}\gamma/\mathrm{d}\ln\Gamma}{(1+2\xi+2\xi^2)^{1/2}}, \tag{2.21}$$

$$\xi = \frac{\mathrm{d}m_C}{\mathrm{d}\Gamma}\left(\frac{D}{2\omega}\right)^{1/2}, \tag{2.22}$$

$$\omega = \frac{\mathrm{d}\ln A}{\mathrm{d}t}, \tag{2.23}$$

where D is the diffusion coefficient of the surfactant and ω represents a timescale (time needed for doubling the surface area) that is roughly equal to τ_{def}.

During emulsification, ε is dominated by the magnitude of the numerator in equation (2.21) because ξ remains small. The value of $\mathrm{d}m_C/\mathrm{d}\Gamma$ tends to go to very high values when Γ reaches its plateau value; ε goes to a maximum when m_C is increased. However, during droplet deformation, Γ will always remain smaller. Taking reasonable values for the variables; $\mathrm{d}m_C/\mathrm{d}\Gamma = 10^2$–$10^4\ \mathrm{m}^{-1}$, $D = 10^{-9}$–$10^{-11}\ \mathrm{m}^2\,\mathrm{s}^{-1}$ and $\tau_{\mathrm{def}} = 10^{-2}$–$10^{-6}\ \mathrm{s}$, $\xi < 0.1$ at all conditions. The same conclusion can be drawn for values of ε in thin films, e.g. between closely approaching drops. It may be concluded that for conditions that prevail during emulsification, ε increases with m_C and follows the relation,

$$\varepsilon \approx \frac{\mathrm{d}\pi}{\mathrm{d}\ln\Gamma}, \tag{2.24}$$

except for very high surfactant concentration, where π is the surface pressure ($\pi = \gamma_0 - \gamma$). Fig. 2.12 shows the variation of π with $\ln\Gamma$; ε is given by the slope of the line.

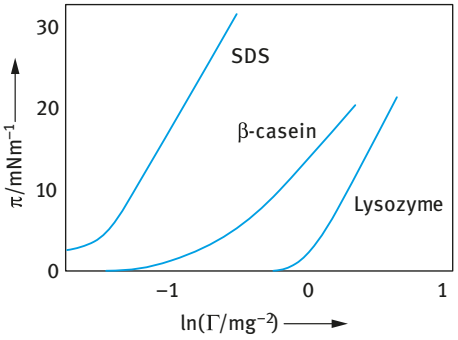

Fig. 2.12: π versus $\ln\Gamma$ for various emulsifiers.

SDS shows a much higher ε value during emulsification, when compared with the polymers β-casein and lysozome. This is because the value of Γ is higher for SDS. The two proteins show a difference in their ε values which may be attributed to the conformational change that occurs upon adsorption.

The presence of a surfactant means that during emulsification the interfacial tension need not be the same everywhere (Fig. 2.8). This has two consequences:

(i) the equilibrium shape of the drop is affected;
(ii) any γ-gradient formed will slow down the motion of the liquid inside the drop (this diminishes the amount of energy needed to deform and break up the drop).

Another important role of the emulsifier is to prevent coalescence during emulsification. This is certainly not due to the strong repulsion between the droplets, since the pressure at which two drops are pressed together is much greater than the repulsive stresses. The counteracting stress must be due to the formation of γ-gradients. When two drops are pushed together, liquid will flow out from the thin layer between them, and the flow will induce a γ-gradient. This was shown in Fig. 2.11 (c) This produces a counteracting stress given by,

$$\tau_{\Delta\gamma} \approx \frac{2|\Delta\gamma|}{(1/2)d}. \tag{2.25}$$

The factor 2 follows from the fact that two interfaces are involved. Taking a value of $\Delta\gamma = 10\,\mathrm{mN\,m^{-1}}$, the stress amounts to 40 kPa (which is of the same order of magnitude as the external stress). The stress due to the γ-gradient cannot as such prevent coalescence, since it only acts for a short time, but it will greatly slow down the mutual approach of the droplets. The external stress will also act for a short time, and it may well be that the drops move apart before coalescence can occur. The effective γ-gradient will depend on the value of ε as given by equation (2.24).

Closely related to the above mechanism, is the Gibbs–Marangoni effect [8–10], schematically represented in Fig. 2.13. The depletion of surfactant in the thin film between approaching drops results in a γ-gradient without liquid flow being involved. This results in an inward flow of liquid that tends to drive the drops apart. Such a mechanism would only act if the drops were insufficiently covered with surfactant (Γ below the plateau value) as occurs during emulsification.

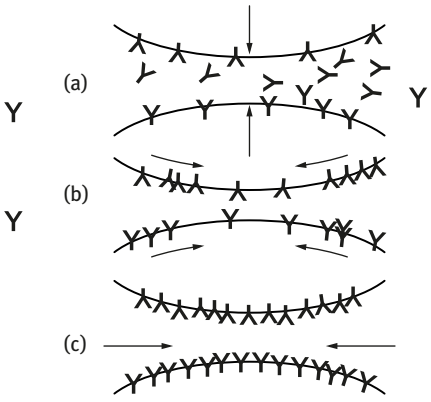

Fig. 2.13: Schematic representation of the Gibbs–Marangoni effect for two approaching drops.

The Gibbs–Marangoni effect also explains the Bancroft rule which states that the phase in which the surfactant is most soluble forms the continuous phase. If the surfactant is in the droplets, a γ-gradient cannot develop and the drops would be prone to coalescence. Thus, surfactants with HLB > 7 tend to form O/W emulsions and those with HLB < 7 tend to form W/O emulsions.

The Gibbs–Marangoni effect also explains the difference between surfactants and polymers for emulsification. Polymers give larger drops when compared with surfactants. Polymers give a smaller value of ε at small concentrations when compared to surfactants (Fig. 2.12).

Various other factors should also be considered for emulsification, such as the disperse phase volume fraction ϕ. An increase in ϕ leads to an increase in droplet collision and hence coalescence during emulsification. With increasing ϕ, the viscosity of the emulsion increases and could change the flow from being turbulent to being laminar. The presence of many particles results in a local increase in velocity gradients. In turbulent flow, an increase in ϕ will induce turbulence depression.

This will result in larger droplets. Turbulence depression by adding polymers tends to remove the small eddies, resulting in the formation of larger droplets.

If the mass ratio of surfactant to continuous phase is kept constant, an increase in ϕ results in a decrease in surfactant concentration and hence an increase in γ_{eq}, resulting in larger droplets. If the mass ratio of surfactant to disperse phase is kept constant, the above changes are reversed.

2.5 Methods of emulsification

Several procedures may be applied for emulsion preparation, these range from simple pipe flow (low agitation energy, L), static mixers (toothed devices such as the Ultra-Turrax and batch radial discharge mixers such as the Silverson mixers) and general stirrers (low to medium energy, L–M), colloid mills and high pressure homogenizers (high energy, H), ultrasound generators (M–H) and membrane emulsification methods. The method of preparation can be continuous (C) or batch-wise (B): pipe flow – C; static mixers and general stirrers and – B, C; colloid mill and high pressure homogenizers – C; ultrasound – B, C.

In all methods, there is liquid flow; unbounded and strongly confined flow. In unbounded flow any droplet is surrounded by a large amount of flowing liquid (the confining walls of the apparatus are far away from most of the droplets). The forces can be frictional (mostly viscous) or inertial. Viscous forces cause shear stresses to act on the interface between the droplets and the continuous phase (primarily in the direction of the interface). The shear stresses can be generated by laminar flow (LV) or turbulent flow (TV); this depends on the dimensionless Reynolds number *Re*,

$$Re = \frac{\upsilon l \rho}{\eta}, \tag{2.26}$$

where υ is the linear liquid velocity, ρ is the liquid density and η is its viscosity. l is a characteristic length that is given by the diameter of flow through a cylindrical tube and by twice the slit width in a narrow slit.

For laminar flow $Re \lessapprox 1{,}000$, whereas for turbulent flow $Re \gtrapprox 2{,}000$. Thus whether the regime is linear or turbulent depends on the scale of the apparatus, the flow rate and the liquid viscosity [1–4].

Rotor-stator mixers are the most commonly used mixers for emulsification. Two main types are available. Toothed devices such as the Ultra-Turrax (IKA Works, Germany) are the most commonly used device (schematically illustrated in Fig. 2.14).

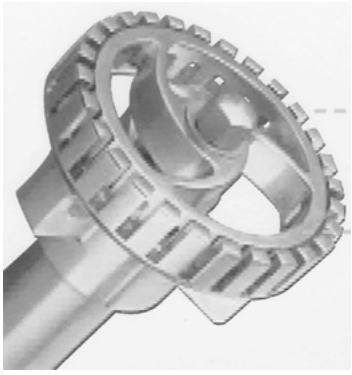

Fig. 2.14: Schematic representation of a toothed mixer (Ultra-Turrax).

Toothed devices are available both as in-line as well as batch mixers, and because of their open structure they have a relatively good pumping capacity. Therefore, in batch applications they frequently do not need an additional impeller to induce bulk flow even in relatively large mixing vessels. These mixers are used in the food industry to manufacture ice cream, margarine and salad dressings, in cosmetic and personal care products to manufacture creams and lotions as well as in manufacturing of speciality chemicals for micro-encapsulation of waxes and paraffin. They are also popular in the paper industry to process highly viscous and non-Newtonian paper pulp and in the manufacturing of paints and coatings. Ultra-Turrax mixers have been used to manufacture emulsion-based lipid carriers with drops below 1 µm and in emulsion polymerization to produce drops of the order of 300 nm. Batch radial discharge mixers such as Silverson mixers (Fig. 2.15) have a relatively simple design with a rotor equipped with four blades pumping the fluid through a stationary stator perforated with differently shaped/sized holes or slots.

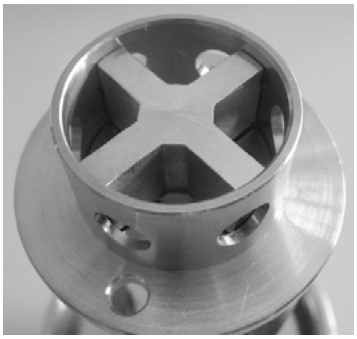

Fig. 2.15: Schematic representation of batch radial discharge mixer (Silverson mixer).

They are frequently supplied with a set of easily interchangeable stators enabling the same machine to be used for a range of operations such as emulsification, homogenization, blending, particle size reduction and de-agglomeration. Changing from one screen to another is quick and simple. Different stators/screens used in batch Silverson mixers are shown in Fig. 2.16. The general purpose disintegrating stator (Fig. 2.16 (a)) is recommended for preparation of thick emulsions (gels) whilst the slotted disintegrating stator (Fig. 2.16 (b)) is designed for emulsions containing elastic materials such as polymers. Square hole screens (Fig. 2.16 (c)) are recommended for the preparation of emulsions whereas the standard emulsor screen (Fig. 2.16 (d)) is used for liquid/liquid emulsification. Radial discharge high shear mixers are used in a wide range of industries ranging from foods through to chemicals, cosmetics and pharmaceuticals. Silverson rotor-stator mixers are used in the cosmetic and pharmaceutical industries to manufacture both concentrated liquid–liquid and liquid–solid emulsions such as creams, lotions, mascaras and deodorants to name the most common applications.

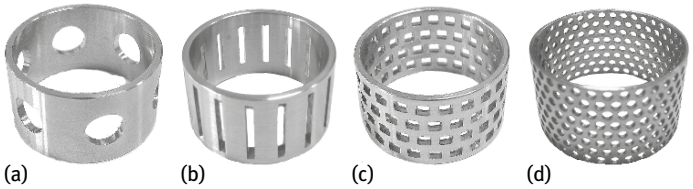

Fig. 2.16: Stators used in batch Silverson radial discharge mixers.

As mentioned above in all methods, there is liquid flow, unbounded and strongly confined flow. In the unbounded flow any droplet is surrounded by a large amount of flowing liquid (the confining walls of the apparatus are far away from most of the droplets); the forces can be frictional (mostly viscous) or inertial. Viscous forces cause shear stresses to act on the interface between the droplets and the continuous phase (primarily in the direction of the interface). The shear stresses can be generated by laminar flow (LV) or turbulent flow (TV); this depends on the Reynolds number *Re*

as given by equation (2.26). For laminar flow $Re \lessapprox 1{,}000$, whereas for turbulent flow $Re \gtrapprox 2{,}000$. Thus whether the regime is linear or turbulent depends on the scale of the apparatus, the flow rate and the liquid viscosity. If the turbulent eddies are much larger than the droplets, they exert shear stresses on the droplets. If the turbulent eddies are much smaller than the droplets, inertial forces will cause disruption (TI). In bounded flow other relations hold; if the smallest dimension of the part of the apparatus in which the droplets are disrupted (say a slit) is comparable to droplet size, other relations hold (the flow is always laminar). If the turbulent eddies are much larger than the droplets, they exert shear stresses on the droplets. If the turbulent eddies are much smaller than the droplets, inertial forces will cause disruption (TI). A different regime prevails if the droplets are directly injected through a narrow capillary into the continuous phase (injection regime), i.e. membrane emulsification. Within each regime, an essential variable is the intensity of the forces acting; the viscous stress during laminar flow σ_{viscous} is given by,

$$\sigma_{\text{viscous}} = \eta G, \tag{2.27}$$

where G is the velocity gradient.

The intensity in turbulent flow is expressed by the power density ε (the amount of energy dissipated per unit volume per unit time); for turbulent flow,

$$\varepsilon = \eta G^2. \tag{2.28}$$

The most important regimes are:
- laminar/viscous (LV)
- turbulent/viscous (TV)
- turbulent/inertial (TI)

For water as the continuous phase, the regime is always TI. For higher viscosity of the continuous phase ($\eta_C = 0.1$ Pa s), the regime is TV. For still higher viscosity or a small apparatus (small l), the regime is LV. For very small apparatus (as is the case with most laboratory homogenizers), the regime is nearly always LV.

For the above regimes, a semi-quantitative theory is available that can give the timescale and magnitude of the local stress σ_{ext}, the droplet diameter d, timescale of droplets deformation τ_{def}, timescale of surfactant adsorption, τ_{ads} and mutual collision of droplets.

Laminar flow can be of a variety of types from purely rotational to purely extensional. For simple shear the flow consists of equal parts of rotation and elongation. The velocity gradient G (in reciprocal seconds) is equal to the shear rate γ. For hyperbolic flow G is equal to the elongation rate. The strength of a flow is generally expressed by the stress it exerts on any plane in the direction of flow; it is simply equal to $G\eta$ (η is simply the shear viscosity).

For elongational flow, the elongational viscosity η_{el} is given by,

$$\eta_{\text{el}} = Tr\,\eta, \tag{2.29}$$

where Tr is the dimensionless Trouton number which is equal to 2 for Newtonian liquids in two-dimensional uneasily elongation flow. $Tr = 3$ for axisymmetric uniaxial flow and it is equal to 4 for biaxial flows. Elongational flows exert higher stresses for the same value of G than simple shear. For non-Newtonian liquids, the relationships are more complicated and the values of Tr tends to be much higher.

An important parameter that describes droplet deformation is the Weber number We (which gives the ratio of the external stress over the Laplace pressure),

$$We = \frac{G\eta_C R}{2\gamma}. \tag{2.30}$$

The deformation of the drop increases with increasing We and above a critical value We_{cr} the drop bursts forming smaller droplets. We_{cr} depends on two parameters:
(i) the velocity vector α ($\alpha = 0$ for simple shear and $\alpha = 1$ for hyperbolic flow);
(ii) the viscosity ratio λ of the oil η_D and the external continuous phase η_C,

$$\lambda = \frac{\eta_D}{\eta_C}. \tag{2.31}$$

The variation of critical Weber number with λ at various α values is shown in Fig. 2.17.

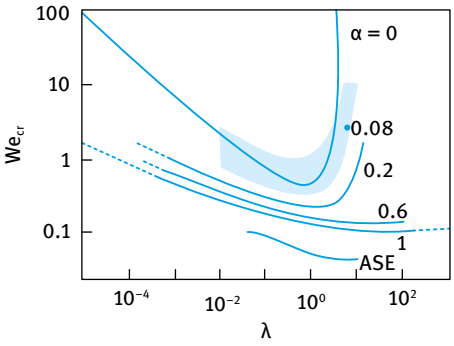

Fig. 2.17: Critical Weber number for break-up of drops in various types of flow. The hatched area represents the apparent We_{cr} in a colloid mill.

The viscosity of the oil plays an important role in the break-up of droplets; the higher the viscosity, the longer it will take to deform a drop. The deformation time τ_{def} is given by the ratio of oil viscosity to the external stress acting on the drop,

$$\tau_{def} = \frac{\eta_D}{\sigma_{ext}}. \tag{2.32}$$

The above ideas for simple laminar flow were tested using emulsions containing 80 % oil in water stabilized with egg yolk. A colloid mill and static mixers were used to prepare the emulsion. The results are shown in Fig. 2.18, which gives the number of droplets n in which a parent drop is broken down when it is suddenly extended into a long thread, corresponding to We_b which is larger than We_{cr}. The number of drops

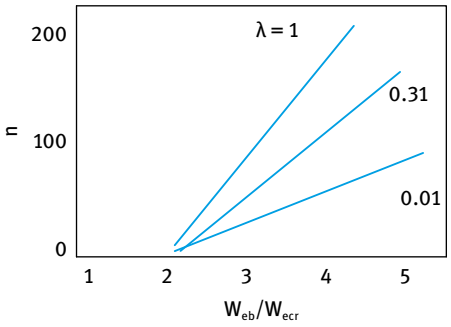

Fig. 2.18: Variation of n with We_b/We_{cr}.

increases with increasing We_b/We_{cr}. The largest number of drops, i.e. the smallest droplet size is obtained when $\lambda = 1$, i.e. when the viscosity of the oil phase is closer to that of the continuous phase. In practice, the resulting drop size distribution is of greater importance than the critical drop size for break-up.

Turbulent flow is characterized by the presence of eddies, which means that the average local flow velocity u generally differs from the time average value $\bar{u}$. The velocity fluctuates in a chaotic way and the average difference between u and u' equals zero; however, the root mean square average u' is finite [5–8],

$$u' = \langle (u - \bar{u})^2 \rangle^{1/2}. \tag{2.33}$$

The value of u' generally depends on direction, but for very high Re (> 50,000) and at small length scales the turbulent flow can be isotropic, and u' does not depend on direction. Turbulent flow shows a spectrum of eddy sizes (l); the largest eddies have the highest u', they transfer their kinetic energy to smaller eddies, which have a smaller u' but larger velocity gradient u'/l.

The viscosity of the oil plays an important role in the break-up of droplets; the higher the viscosity, the longer it will take to deform a drop. The deformation time τ_{def} is given by the ratio of oil viscosity to the external stress acting on the drop,

$$\tau_{def} = \frac{\eta_D}{\eta_C}. \tag{2.34}$$

The viscosity of the continuous phase η_C plays an important role in some regimes: For turbulent inertial regime, η_C has no effect on droplets size. For turbulent viscous regime, larger η_C leads to smaller droplets. For laminar viscous the effect is even stronger.

The value of η_C and the size of the apparatus determine which regime prevails, via the effect on Re. In a large machine and low η_C, Re is always very large and the resulting average droplet diameter d is proportional to $P_H^{-0.6}$ (where P_H is the homogenization pressure). If η_C is higher and $Re_{dr} < 1$, the regime is TV and $d \propto P_H^{-0.75}$. For a smaller machine, as used in the lab, where the slit width of the valve may be of the order of µm, Re is small and the regime is LV; $d \propto P_H^{-1.0}$. If the slit is made very small (of the order of droplet diameter), the regime can become TV.

Fig. 2.19 shows the variation of average droplet diameter d_{43} with P_H at low and high *Re* for 20 % soybean oil/water emulsion stabilized with sodium caseinate (30 mg/ml). Fig. 2.20 shows the variation of width of distribution with number of passages at low and high R. Addition of high molecular weight polymers in the continuous phase increases η_C resulting in turbulence depression increasing d_{32} while decreasing c_2.

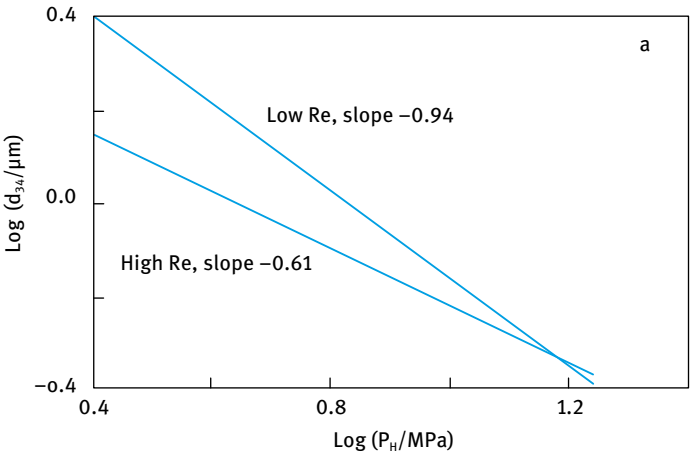

Fig. 2.19: Comparison of droplet size distribution obtained with two-high pressure homogenizers; a very small one (low *Re*) and a large one (high *Re*).

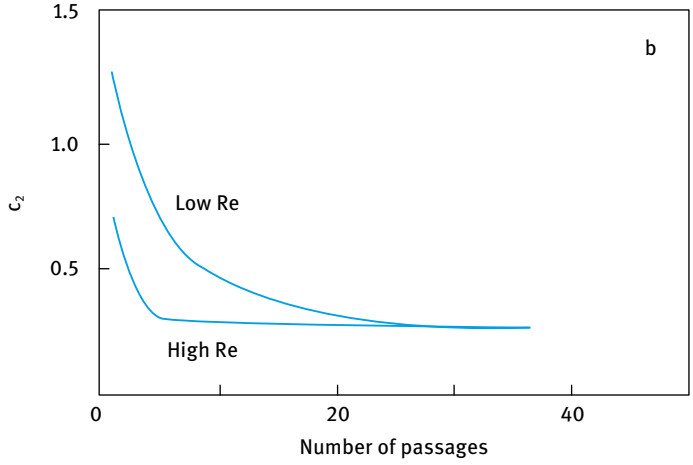

Fig. 2.20: Relative distribution width c_2 as a function of number of passes through the homogenizers.

In membrane emulsification, the disperse phase is passed through a membrane and droplets leaving the pores are immediately taken up by the continuous phase. The membrane is commonly made of porous glass or of ceramic materials. The general configuration is a membrane in the shape of a hollow cylinder; the disperse phase is pressed through it from outside, and the continuous phase pumped through the cylinder (cross flow). The flow also causes detachment of the protruding droplets from the membrane [1].

Several requirements are necessary for the process:

(i) For a hydrophobic disperse phase (O/W emulsion) the membrane should be hydrophilic, whereas for a hydrophilic disperse phase (W/O emulsion) the membrane should be hydrophobic, since otherwise the droplets cannot be detached.

(ii) The pores must be sufficiently far apart to prevent the droplets coming out from touching each other and coalescing.

(iii) The pressure over the membrane should be sufficiently high to achieve drop formation. This pressure should be at least of the order of Laplace pressure of a drop with diameter equal to the pore diameter. For example, for pores of 0.4 µm and $\gamma = 5\,\mathrm{mN\,m^{-1}}$, the pressure should be of the order of 10^5 Pa, but larger pressures are needed in practice, this would amount to 3×10^5 Pa, also to obtain a significant flow rate of the disperse phase through the membrane.

The smallest drop size obtained by membrane emulsification is about three times the pore diameter. The main disadvantage is its slow process, which can be of the order of 10^{-3} m^3 per m^2 per second. This implies that very long circulation times are needed to produce even small volume fractions.

The most important variables that affect the emulsification process are the nature of the oil and the emulsifier, the volume fraction of the disperse phase ϕ and the emulsification process. The effect of the nature of the oil and the emulsifier were discussed before. The method of emulsification and the regime (laminar or turbulent) have a pronounced effect on the process and the final droplet size distribution. The effect of the volume fraction of the disperse phase requires special attention. It affects the rate of collision between droplets during emulsification, and thereby the rate of coalescence. As a first approximation, this would depend on the relation between τ_{ads} and τ_{coal} (where τ_{ads} is the average time it takes for surfactant adsorption and τ_{coal} is the average time it takes until a droplet collides with another one). In the various regimes, the hydrodynamic constraints are the same for τ_{ads}. For example, in regime LV, $\tau_{\mathrm{coal}} = \pi/8\phi G$. Thus for all regimes, the ratio of $\tau_{\mathrm{ads}}/\tau_{\mathrm{coal}}$ is given by [1, 2],

$$\kappa \equiv \frac{\tau_{\mathrm{ads}}}{\tau_{\mathrm{coal}}} \propto \frac{\phi\Gamma}{m_{\mathrm{C}} d}, \tag{2.35}$$

where the proportionality factor would be at least of order 10. For example, for $\phi = 0.1$, $\Gamma/m_{\mathrm{C}} = 10^{-6}$ m and $d = 10^{-6}$ m (total surfactant concentration of the emulsion should then be about 0.5 %), κ would be of the order of 1. For $\kappa \gg 1$, considerable

coalescence is likely to occur, particularly at high ϕ. The coalescence rate would then markedly increase during emulsification, since both m_C and d become smaller during the process. If emulsification proceeds long enough, the droplet size distribution may then be the result of a steady state of simultaneous break-up and coalescence.

The effect of increasing ϕ can be summarized as follows [1, 2]:

(i) τ_{coal} is shorter and coalescence will be faster unless κ remains small.

(ii) Emulsion viscosity η_{em} increases, hence Re decreases. This implies a change of flow from turbulent to laminar (LV).

(iii) In laminar flow, the effective η_C becomes higher. The presence of many droplets means that the local velocity gradients near a droplet will generally be higher than the overall value of G. Consequently, the local shear stress ηG does increase with increasing ϕ, which is as if η_C increases.

(iv) In turbulent flow, increasing ϕ will induce turbulence depression leading to larger d.

(v) If the mass ratio of surfactant to continuous phase is constant, an increase in ϕ gives a decrease in surfactant concentration; hence an increase in γ_{eq}, an increase in κ, and an increase in d are produced by an increase in coalescence rate. If the mass ratio of surfactant to disperse phase is kept constant, the above mentioned changes are reversed, unless $\kappa \ll 1$.

It is clear from the above discussion that general conclusions cannot be drawn, since several of the above mentioned mechanisms may come into play. Using a high pressure homogenizer, Walstra [11] compared the values of d with various ϕ values up to 0.4 at constant initial m_C, regime TI probably changing to TV at higher ϕ. With increasing ϕ (> 0.1), the resulting d increased and dependency on homogenizer pressure p_H (Fig. 2.21). This points to increased coalescence (effects (i) and (v)).

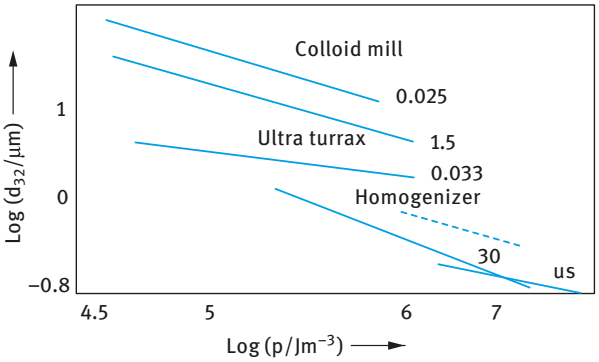

Fig. 2.21: Average droplet diameters obtained in various emulsifying machines as a function of energy consumption p. The number near the curves denotes the viscosity ratio λ; the results for the homogenizer are for $\phi = 0.04$ (solid line) and $\phi = 0.3$ (broken line); us means ultrasonic generator.

Fig. 2.21 shows a comparison of the average droplet diameter versus power consumption using different emulsifying machines. It can be seen that the smallest droplet diameters were obtained when using the high pressure homogenizers.

2.6 Selection of emulsifiers

Several surfactants and their mixtures are used for the preparation and stabilization of oil-in-water (O/W) and water-in-oil (W/O) emulsions. A summary of the most commonly used surfactants was given in Chapter 2 of Vol. 1. Two general methods can be applied for selecting emulsifiers, namely the hydrophilic–lipophilic balance (HLB) and the phase inversion temperature (PIT) concepts. The hydrophilic–lipophilic balance (HLB number) is a semi-empirical scale for selecting surfactants developed by Griffin [12]. This scale is based on the relative percentage of hydrophilic to lipophilic (hydrophobic) groups in the surfactant molecule(s). For an O/W emulsion droplet the hydrophobic chain resides in the oil phase whereas the hydrophilic head group resides in the aqueous phase. For a W/O emulsion droplet, the hydrophilic group(s) reside in the water droplet, whereas the lipophilic groups reside in the hydrocarbon phase. Tab. 2.2 gives a guide to the selection of surfactants for a particular application. The HLB number depends on the nature of the oil. As an illustration, Tab. 2.3 gives the required HLB numbers to emulsify various oils. Examples of the HLB numbers of a list of surfactants are given in Tab. 2.4.

The relative importance of the hydrophilic and lipophilic groups was first recognized when using mixtures of surfactants containing varying proportions of a low and high HLB number. The efficiency of any combination (as judged by phase separation) was found to pass a maximum when the blend contained a particular proportion of the surfactant with the higher HLB number. This is illustrated in Fig. 2.22 which shows the variation of emulsion stability, droplet size and interfacial tension with percentage surfactant with high HLB number.

The average HLB number may be calculated from additivity,

$$\mathrm{HLB} = x_1\mathrm{HLB}_1 + x_2\mathrm{HLB}_2. \tag{2.36}$$

x_1 and x_2 are the weight fractions of the two surfactants with HLB_1 and HLB_2.

Tab. 2.2: Summary of HLB ranges and their applications.

HLB range	Application
3–6	W/O emulsifier
7–9	Wetting agent
8–18	O/W emulsifier
13–15	Detergent
15–18	Solubilizer

Tab. 2.3: Required HLB numbers to emulsify various oils.

Oil	W/O emulsion	O/W emulsion
Paraffin oil	4	10
Beeswax	5	9
Linolin, anhydrous	8	12
Cyclohexane	—	15
Toluene	—	15
Silicone oil (volatile)	—	7–8
Isopropyl myristate	—	11–12
Isohexadecyl alcohol	11–12	
Castor oil		14

Tab. 2.4: HLB numbers of some surfactants.

Surfactant	Chemical name	HLB
Span 85	Sorbitan trioleate	1.8
Span 80	Sorbitan monooleate	4.3
Brij 72	Ethoxylated (2 mol ethylene oxide) stearyl alcohol	4.9
Triton X-35	Ethoxylated octylphenol	7.8
Tween 85	Ethoxylated (20 mol ethylene oxide) sorbitan trioleate	11.0
Tween 80	Ethoxylated (20 mol ethylene oxide) sorbitan monooleate	15.0

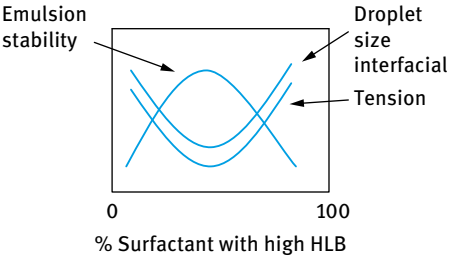

Fig. 2.22: Variation of emulsion stability, droplet size and interfacial tension with percentage surfactant with high HLB number.

Griffin [12] developed simple equations for calculating the HLB number of relatively simple nonionic surfactants. For a polyhydroxy fatty acid ester,

$$\mathrm{HLB} = 20\left(1 - \frac{S}{A}\right). \tag{2.37}$$

S is the saponification number of the ester and A is the acid number. For a glyceryl monostearate, $S = 161$ and $A = 198$; the HLB is 3.8 (suitable for a W/O emulsion).

For a simple alcohol ethoxylate, the HLB number can be calculated from the weight percent of ethylene oxide (E) and polyhydric alcohol (P),

$$\mathrm{HLB} = \frac{E + P}{5}. \tag{2.38}$$

If the surfactant contains PEO as the only hydrophilic group, the contribution from one OH group is neglected,

$$\mathrm{HLB} = \frac{E}{5}. \tag{2.39}$$

For a nonionic surfactant $C_{12}H_{25}-O-(CH_2-CH_2-O)_6$, the HLB is 12 (suitable for an O/W emulsion).

The above simple equations cannot be used for surfactants containing propylene oxide or butylene oxide. Nor can they be applied for ionic surfactants. Davies [13, 14] devised a method for calculating the HLB number for surfactants from their chemical formulae, using empirically determined group numbers. A group number is assigned to various component groups. A summary of the group numbers for some surfactants is given in Tab. 2.5.

Tab. 2.5: HLB group numbers.

	Group number
Hydrophilic	
$-SO_4Na^+$	38.7
–COOK	21.2
–COONa	19.1
N(tertiary amine)	9.4
Ester (sorbitan ring)	6.8
–O–	1.3
CH–(sorbitan ring)	0.5
Lipophilic	
$(-CH-)$, $(-CH_2-)$, CH_3	0.475
Derived	
$-CH_2-CH_2-O$	0.33
$-CH_2-CHCH_3-O-$	0.11

The HLB is given by the following empirical equation,

$$\mathrm{HLB} = 7 + \sum(\text{hydrophilic group numbers}) - \sum(\text{lipohilic group numbers}). \tag{2.40}$$

Davies has shown that the agreement between HLB numbers calculated from the above equation and those determined experimentally is quite satisfactory.

Various other procedures have been developed to obtain a rough estimate of the HLB number. Griffin found good correlation between the cloud point of 5 % solution of various ethoxylated surfactants and their HLB number.

Davies [13, 14] attempted to relate the HLB values to the selective coalescence rates of emulsions. Such correlations were not realized since it was found that the emulsion's stability and even its type depend to a large extent on the method of dispersing

the oil into the water and vice versa. At best the HLB number can only be used as a guide for selecting optimum compositions of emulsifying agents.

One may take any pair of emulsifying agents that fall at opposite ends of the HLB scale, e.g. Tween 80 (sorbitan monooleate with 20 mol EO, HLB = 15) and Span 80 (sorbitan monooleate, HLB = 5) and use them in various proportions to cover a wide range of HLB numbers. The emulsions should be prepared in the same way, with a few percent of the emulsifying blend. For example, a 20 % O/W emulsion is prepared by using 4 % emulsifier blend (20 % with respect to oil) and 76 % water. The stability of the emulsion is then assessed at each HLB number from the rate of coalescence or qualitatively by measuring the rate of oil separation. In this way one may be able to find the optimum HLB number for a given oil. For example with a given oil, the optimum HLB number is found to be 10.3. The latter can be determined more exactly by using mixtures of surfactants with narrower HLB range, say between 9.5 and 11. Having found the most effective HLB value, various other surfactant pairs are compared at this HLB value, to find the most effective pair. This is illustrated in Fig. 2.23 which schematically shows the difference between three chemical classes of surfactants. Although the different classes give a stable emulsion at HLB = 12, mixture A gives the best emulsion stability.

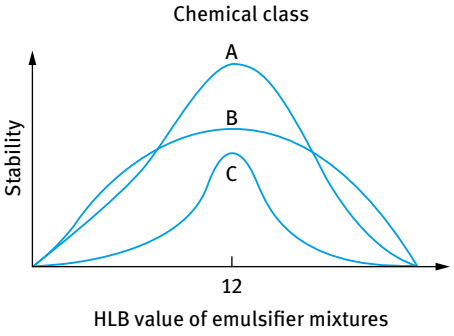

Fig. 2.23: Stabilization of emulsion by different classes of surfactants as a function of HLB.

The HLB value of a given magnitude can be obtained by mixing emulsifiers of different chemical types. The "correct" chemical type is as important as the "correct" HLB number. This is illustrated in Fig. 2.24, which shows that an emulsifier with unsaturated alkyl chain such as oleate (ethoxylated sorbitan monooleate, Tween 80) is more suitable for emulsifying an unsaturated oil [15]. An emulsifier with saturated alkyl chain (stearate in Tween 60) is better for emulsifying a saturated oil.

Various procedures have been developed to determine the HLB of different surfactants. Griffin [12] found a correlation between the HLB and the cloud points of 5 % aqueous solution of ethoxylated surfactants as illustrated in Fig. 2.25. A titration procedure was developed [16] for estimating the HLB number. In this method, a 1 % solution of surfactant in benzene plus dioxane is titrated with distilled water at constant

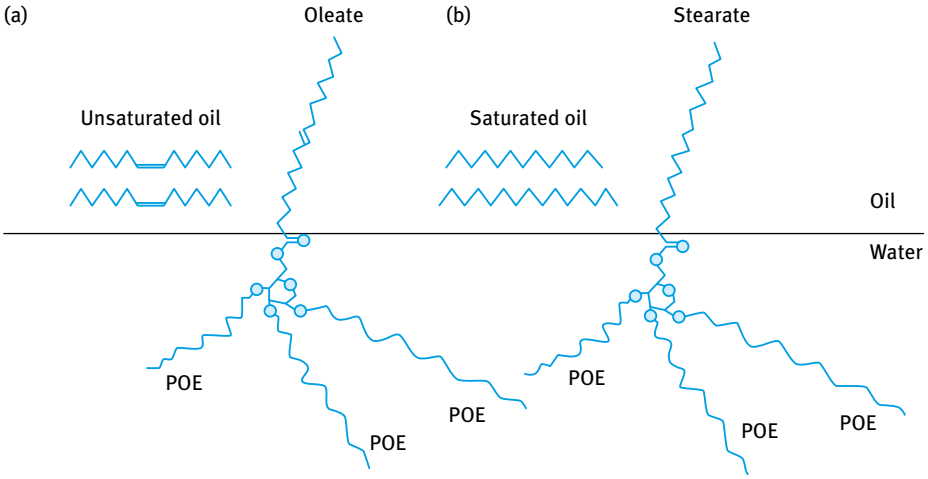

Fig. 2.24: Selection of Tween type to correspond to the type of the oil to be emulsified.

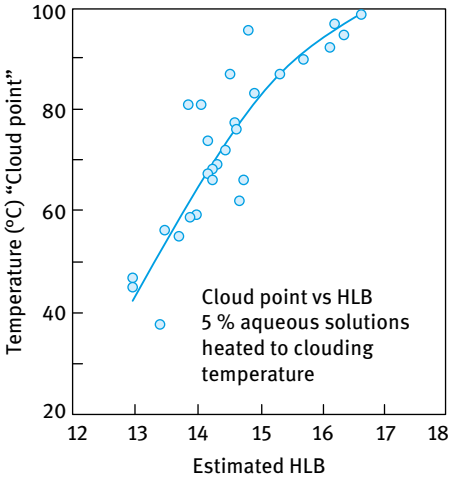

Fig. 2.25: Relationship between cloud point and HLB.

temperature until a permanent turbidity appears. He found a good linear relationship between the HLB number and the water titration value for polyhydric alcohol esters as shown in Fig. 2.26. However, the slope of the line depends on the class of material used.

Gas liquid chromatography (GLC) can also be used to determine the HLB number [16]. Since in GLC the efficiency of separation depends on the polarity of the substrate with respect to the components of the mixture, it should be possible to determine the HLB directly by using the surfactant as the substrate and passing an oil phase down the column. Thus, when a 50 : 50 mixture of ethanol and hexane is passed down a column of a simple nonionic surfactant, such as sorbitan fatty acid esters and

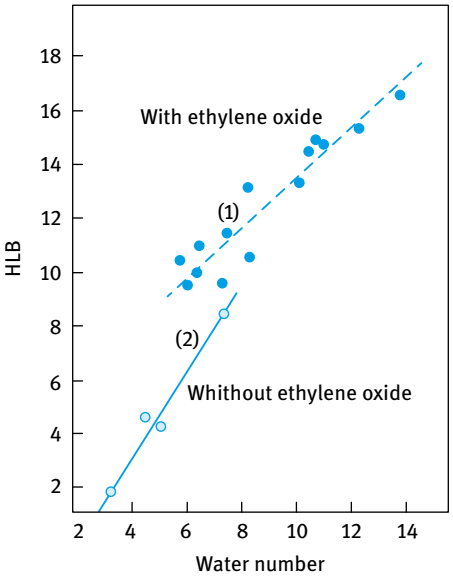

Fig. 2.26: Correlation of HLB with water number.

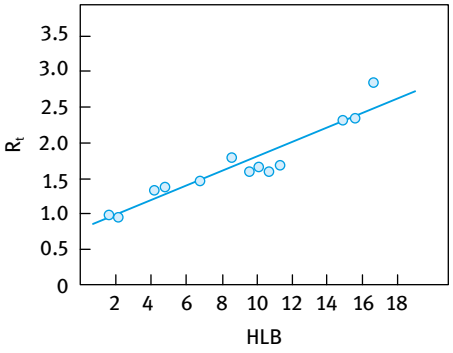

Fig. 2.27: Correlation between retention time and HLB of sorbitan fatty acid esters and polyoxyethylated fatty acid esters.

polyoxyethylated sorbitan fatty acid esters, two well-defined peaks, corresponding to hexane (which appears first) and ethanol appears on the chromatograms. A good correlation was found between the retention time ratio R_t (ethanol/hexane) and the HLB value. This is illustrated in Fig. 2.27. Statistical analysis of the data gave the following empirical relationship between R_t and HLB,

$$\mathrm{HLB} = 8.55R_t - 6.36, \tag{2.41}$$

where,

$$R_t = \frac{R_t^{\mathrm{ETOH}}}{R_t^{\mathrm{hexane}}}. \tag{2.42}$$

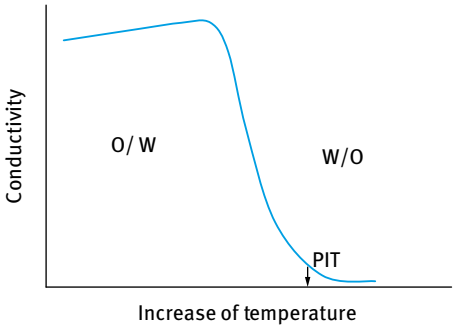

Fig. 2.28: Variation of conductivity with temperature for an O/W emulsion.

The phase inversion temperature (PIT) concept was developed by Shinoda and co-workers [17, 18] who found that many O/W emulsions stabilized with nonionic surfactants undergo a process of inversion at a critical temperature (PIT). The PIT can be determined by following the emulsion conductivity (small amount of electrolyte is added to increase the sensitivity) as a function of temperature as illustrated in Fig. 2.28. The conductivity of the O/W emulsion increases with increasing temperature until the PIT is reached, above which there will be a rapid reduction in conductivity (W/O emulsion is formed). Shinoda and co-workers [17, 18] found that the PIT is influenced by the HLB number of the surfactant [19] as shown in Fig. 2.29. For any given oil, the PIT increases with increasing HLB number. The size of the emulsion droplets was found to depend on the temperature and HLB number of the emulsifiers. The droplets are less stable towards coalescence close to the PIT. However, by rapid cooling of the emulsion a stable system may be produced. Relatively stable O/W emulsions were obtained when the PIT of the system was 20–65 °C higher than the storage temperature. Emulsions prepared at a temperature just below the PIT followed by rapid cooling generally have smaller droplet sizes. This can be understood if one considers the change of interfacial tension with temperature as is illustrated in Fig. 2.30. The interfacial tension decreases with increasing temperature reaching a minimum close to the PIT, after which it increases.

Thus, the droplets prepared close to the PIT are smaller than those prepared at lower temperatures. These droplets are relatively unstable towards coalescence near the PIT, but by rapid cooling of the emulsion one can retain the smaller size. This procedure may be applied to prepare mini-(nano-)emulsions.

The optimum stability of the emulsion was found to be relatively insensitive to changes in the HLB value or the PIT of the emulsifier, but instability was very sensitive to the PIT of the system. It is essential, therefore to measure the PIT of the emulsion as a whole (with all other ingredients).

At a given HLB value, stability of the emulsions against coalescence increases markedly as the molar mass of both the hydrophilic and lipophilic components increases. The enhanced stability using high molecular weight surfactants (polymeric surfactants) can be understood from a consideration of the steric repulsion which produces more stable films. Films produced using macromolecular surfactants resist

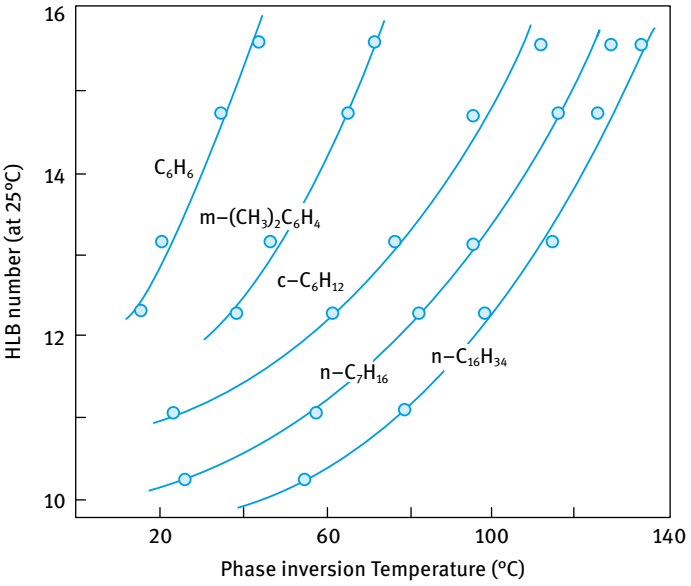

Fig. 2.29: Correlation between HLB number and PIT for various O/W (1 : 1) emulsions stabilized with nonionic surfactants (1.5 wt%).

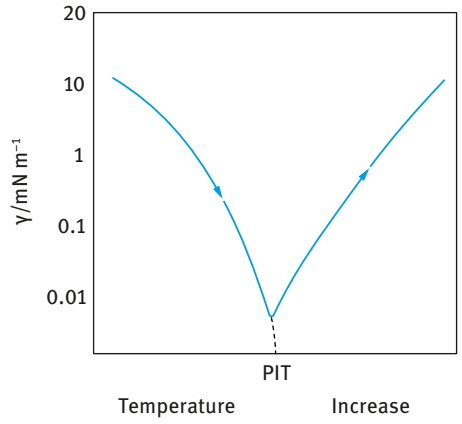

Fig. 2.30: Variation of interfacial tension with temperature increase for an O/W emulsion.

thinning and disruption, thus reducing the possibility of coalescence. The emulsions showed maximum stability when the distribution of the PEO chains was broad. The cloud point is lower but the PIT is higher than in the corresponding case for narrow size distributions. The PIT and HLB number are directly related parameters.

Addition of electrolytes reduces the PIT and hence an emulsifier with a higher PIT value is required when preparing emulsions in the presence of electrolytes. Electrolytes cause dehydration of the PEO chains and in effect this reduces the cloud point of the nonionic surfactant. One needs to compensate for this effect by using a sur-

factant with higher HLB. The optimum PIT of the emulsifier is fixed if the storage temperature is fixed.

In view of the above correlation between PIT and HLB and the possible dependence of the kinetics of droplet coalescence on the HLB number, Sherman and coworkers suggested the use of PIT measurements as a rapid method for assessing emulsion stability [16]. However, one should be careful in using such methods for assessing long-term stability since the correlations were based on a very limited number of surfactants and oils.

Measurement of the PIT can at best be used as a guide for the preparation of stable emulsions. Assessments of the stability should be evaluated by following the droplet size distribution as a function of time using a Coulter Counter or light diffraction techniques. Following the rheology of the emulsion as a function of time and temperature may also be used to assess the stability against coalescence [20]. Care should be taken in analysing the rheological results. Coalescence results in an increase in the droplet size and this is usually followed by a reduction in the viscosity of the emulsion. This trend is only observed if the coalescence is not accompanied by flocculation of the emulsion droplets (which results in an increase in the viscosity). Ostwald ripening can also complicate the analysis of the rheological data.

2.7 Creaming/sedimentation of emulsions and its prevention

As discussed in Chapter 13 of Vol. 1, the process of creaming or sedimentation of emulsions is the result of gravity, when the density of the droplets and the medium are not equal. When the density of the disperse phase is lower than that of the medium (as with most oil-in-water O/W emulsions), creaming occurs, whereas if the density of the disperse phase is higher than that of the medium (as with most W/O emulsions), sedimentation occurs.

The rate of creaming or sedimentation can be calculated by equating the hydrodynamic force with the gravity force. For very dilute non-interacting emulsion droplets with radius R and density difference from the medium $\Delta\rho$, the rate can be calculated using Stokes' law,

$$v_0 = \frac{2}{9}\frac{\Delta\rho g R^2}{\eta_0}. \tag{2.43}$$

v_0 is the Stokes velocity and η_0 is the viscosity of the medium.

For an O/W emulsion with $\Delta\rho = 0.2$ in water ($\eta_0 \approx 10^{-3}$ Pa s), the rate of creaming or sedimentation is $\approx 4.4 \times 10^{-5}$ m s^{-1} for 10 µm droplets and $\approx 4.4 \times 10^{-7}$ m s^{-1} for 1 µm droplets. This means that in a 0.1 m container creaming or sedimentation of the 10 µm droplets is complete in ≈ 0.6 hour and for the 1 µm droplets this takes ≈ 60 hours.

If the droplets are deformable, a liquid drop moving within a second liquid phase has an internal circulation imparted to it. As a result of this, the motion through the continuous phase has a "rolling" as well as a "sliding" component. This situation has

been treated theoretically resulting in the following equation [1],

$$\upsilon = \frac{2}{3}\frac{\Delta\rho g R^2}{\eta_0}\frac{\eta_0 + \eta}{3\eta_0 + 2\eta}, \tag{2.44}$$

where η is the viscosity of the internal phase. For the case $\eta \gg \eta_0$, equation (2.44) predicts υ to be 50 % higher than υ_0, whereas for two liquids having similar viscosities ($\eta \approx \eta_0$), υ is only 20 % greater than υ_0. However, these theoretical predictions do not agree well with the experimental data for υ. This could be due to the neglect of the interfacial viscosity contribution.

With large droplets, shape distortion may occur due to changes in pressure with the "vertical height" of the droplet. The difference in pressure between "top" and "bottom" of the droplet is $\Delta\rho g d$, where d is the distorted vertical diameter. Any deviation from spherical geometry leads to an increase in surface area ΔA. Thus the distorting force due to gravity is opposed by the work necessary to increase the surface area ($\gamma\Delta A$). For small deformities, $d \approx 2R$ and the fractional change in the radius is $\Delta\rho g R^2/\gamma$. For $\Delta\rho = 0.1$ g cm^3 and $\gamma = 2$ mN m^{-1}, a 2 µm diameter droplet would undergo a distortion in radius of $\approx 5 \times 10^{-5}$ %, whereas for a 200 µm diameter droplet the distortion would be ≈ 0.5 %. Thus, this effect is really only significant for large droplets.

For moderately concentrated emulsions ($0.2 > \phi > 0.1$), one has to take into account the hydrodynamic interaction between the droplets and the Stokes' rate is reduced to v,

$$\upsilon = \upsilon_0(1 - 6.55\phi). \tag{2.45}$$

Equation (2.45) is referred to as the Bachelor equation [19], which shows that for $\phi = 0.1$, the rate of creaming or sedimentation is reduced by about 65 %.

For more concentrated emulsions ($\phi > 0.2$), the rate of creaming or sedimentation becomes a complex function of ϕ as was illustrated in Chapter 13 of Vol. 1. υ decreases with increasing ϕ and ultimately it approaches zero when ϕ exceeds a critical value, ϕ_p, which is the so-called "maximum packing fraction". The value of ϕ_p for monodisperse "hard spheres" ranges from 0.64 (for random packing) to 0.74 for hexagonal packing. The value of ϕ_p exceeds 0.74 for polydisperse systems. Also for emulsions which are deformable, ϕ_p can be much larger than 0.74. When ϕ approaches ϕ_p, η_r approaches ∞. In practice most emulsions are prepared at ϕ values well below ϕ_p, usually in the range 0.2–0.5, and under these conditions creaming or sedimentation is the rule rather than the exception. Several procedures may be applied to reduce or eliminate creaming or sedimentation and these were discussed in Chapter 13 of Vol. 1.

The structure of the creamed layer represents the equilibrium volume where the mutual distances between the droplets are determined by the balance between the external gravitational field and the mutual interdroplet forces (electrostatic and/or steric forces associated with an interfacial polymer layer). Due to the polydispersity of the emulsion and deformation from spherical geometry, the maximum packing in the creamed layer can exceed that for monodisperse spheres ($\phi = 0.74$ for hexagonal

packing and 0.64 for random packing). The effects of polydispersity are important in that the smaller droplets may fit into the voids between the larger droplets in a packed cream. Packings of greater than 0.90 can be achieved in this way. If the droplets are deformable, the volume of the packed cream layer is reduced and ϕ values in the range 0.95–0.99 can be reached. The greater the size of the droplets and density difference between the two liquid phases, the greater the tendency for deformation to occur. In many cases, the droplets distort to polyhedral cells resembling a foam in structure, with a corresponding network of more-or-less planer thin liquid films of one liquid separating cells of the other liquid. The stability of the system to coalescence then depends on the stability to rupture of these films.

If flocculation occurs in the emulsion, the overall rate of creaming will be faster since the flocs are larger in size. However, the final cream volume will be greater due to the more open structure.

The methods that can be applied for preventing creaming or sedimentation were described in Chapter 13 of Vol. 1. The first method is to match the density of oil and aqueous phases. Clearly if $\Delta\rho = 0$, $\upsilon = 0$ as shown by equation (2.43). Consider for example an O/W emulsion where the oil density is 0.9 g cm^{-3}. To match the density of the aqueous phase (≈ 1 g cm^{-3}), the density of the oil must be increased; this can be achieved by replacing 20 % of the oil with another oil with density 1.4 g cm^{-3}. However, this method is seldom practical, since if density matching is possible, it only occurs at one temperature.

The second method for reducing creaming or sedimentation is to reduce the droplet size to values well below 1 μm. Since the gravity force is proportional to R^3, then if R is reduced by a factor of 10, the gravity force is reduced by 1,000. Below a certain droplet size (which also depends on the density difference between oil and water), Brownian diffusion may exceed gravity and creaming or sedimentation is prevented. This is the principle of formulation of nanoemulsions (with size range 20–200 nm) which may show very little or no creaming or sedimentation.

The most practical method for reducing creaming or sedimentation of macroemulsions (with size > 1 μm) is to use "thickeners" as described in Chapter 13 of Vol. 1. These are high molecular weight polymers, natural or synthetic such as xanthan gum, hydroxyethyl cellulose, alginates, carrageenans, etc. These "thickeners" give a very high residual (or zero shear) viscosity that can prevent any creaming or sedimentation. The residual viscosity $\eta(0)$ can be used to predict creaming or sedimentation of emulsions.

An effective method for reducing creaming/sedimentation of emulsions is to use associative thickeners. These are hydrophobically modified polymer molecules in which alkyl chains (C_{12}–C_{16}) are either randomly grafted on a hydrophilic polymer molecule such as hydroxyethyl cellulose (HEC), or simply grafted at both ends of the hydrophilic chain. An example of hydrophobically modified HEC is Natrosol plus (Hercules) which contains 3–4 C_{16} randomly grafted onto hydroxyethyl cellulose. Another example of a polymer that contains two alkyl chains at both ends of the

molecule is HEUR (Rohm and Haas) that is made of polyethylene oxide (PEO) that is capped at both ends with linear C_{18} hydrocarbon chains.

The above hydrophobically modified polymers form gels when dissolved in water. Gel formation can occur at relatively lower polymer concentrations when compared with the unmodified molecule. The most likely explanation of gel formation is due to hydrophobic bonding (association) between the alkyl chains in the molecule. This effectively causes an apparent increase in the molecular weight. These associative structures are similar to micelles, except the aggregation numbers are much smaller. The viscosity of hydrophobically modified polymers shows a rapid increase at critical concentration, which may be defined as the critical aggregation concentration (CAC). At and above the CAC, the polymer solution shows non-Newtonian flow (shear thinning behaviour) and its shows a high viscosity at low shear rates. These hydrophobically modified polymers are also viscoelastic (Chapter 14 of Vol. 1) and at high frequency the elastic modulus becomes much higher than the viscous modulus and this can prevent any separation of the emulsion. These hydrophobically modified polymers can also interact with hydrophobic oil droplets in an emulsion forming several other associative structures.

Another method for reducing creaming or sedimentation of emulsions is to apply the principle of controlled flocculation as discussed in Chapter 13 of Vol. 1. As discussed before, the total energy–distance of separation curve for an electrostatically stabilized emulsion shows a shallow minimum (secondary minimum) at relatively long distance of separation between the droplets. By addition of small amounts of electrolyte such a minimum can be made sufficiently deep for weak flocculation to occur. The same applies for sterically stabilized emulsions which show only one minimum, whose depth can be controlled by reducing the thickness of the adsorbed layer. This can be obtained by reducing the molecular weight of the stabilizer and/or addition of a nonsolvent for the chains (e.g. electrolyte).

The above phenomenon of weak flocculation may be applied to reduce creaming or sedimentation, in particular for concentrated emulsions. In the latter case, the attractive energy required for inducing weak flocculation can be small (of the order of few kT units).

A useful method for reducing creaming or sedimentation is to apply the phenomenon of depletion flocculation that was described in detail in Chapter 13 of Vol. 1. Many thickeners such as HEC or xanthan gum may not adsorb on the droplets. This is described as "free" (nonadsorbing) polymer in the continuous phase [21]. At a critical concentration, or volume fraction of free polymer, ϕ_p^+, weak flocculation occurs, since the free polymer coils become "squeezed out" from between the droplets. Since the polymer coils do not adsorb on the droplet surface, a "polymer-free" zone with thickness Δ (that is proportional to the radius of gyration R_G of the free polymer) is produced. When two droplets approach each other such that the interdroplet distance $h \leq 2\Delta$, the polymer coils become "squeezed out" from between the droplets. The osmotic pressure outside the droplets is higher than in between the droplets and

this results in attraction whose magnitude depends on the concentration of the free polymer and its molecular weight, as well as the droplet size and ϕ. The value of ϕ_p^+ decreases with increasing molecular weight of the free polymer. It also decreases as the volume fraction of the emulsion increases.

Initial addition of "free polymer" produces weak flocs that show an increase in the rate of creaming. With a further increase in the "free polymer" concentration, the rate of creaming increases and the emulsion separates into two layers: a cream layer at the top and a clear liquid layer at the bottom of the container. However, above a critical concentration of "free polymer", the emulsion shows no creaming. This behaviour was recently demonstrated by Abend et al. [22] who investigated the effect of adding xanthan gum to an O/W emulsion (the oil being Isopar V, a hydrocarbon oil) with a volume fraction $\phi = 0.5$, that was stabilized using an A–B–A block copolymer (with A being polyethylene oxide, PEO, and B is polypropylene oxide, PPO, containing 26.5 EO units and 29.7 PO units). The xanthan gum concentration was varied between 0.01 and 0.67 %. Fig. 2.31 shows the visual observation of the emulsions after 8 months of storage.

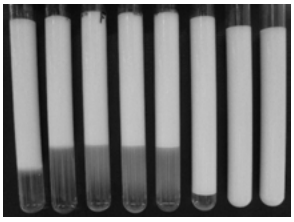

Fig. 2.31: Visual observation (after 8 months storage) of O/W emulsions ($\phi = 0.5$) stabilized with an A–B–A block copolymer (PEO–PPO–PEO) at various xanthan gum concentrations; from left to right: 0.0, 0.01, 0.05, 0.1, 0.25, 0.50, 0.67 % xanthan gum.

It can be seen from Fig. 2.31 that initial addition of xanthan gum up to 0.1 % enhances the creaming of the emulsion as a result of depletion flocculation. The emulsion containing 0.25 % xanthan gum shows less creaming, but phase separation did occur. However, at 0.5 and 0.67 % xanthan gum no creaming occurs after storage for 8 months. At a concentration of 0.5 and 0.67 % xanthan gum, the arrested network formed by the droplets appears now to be strong enough to withstand the gravitational stress (creaming) and no clear water phase is visible at the bottom of the vessel even after eight months of storage.

As discussed in Chapter 13 of Vol. 1, sedimentation or creaming of emulsions can be reduced by the addition of "inert" fine particles to the continuous phase. Several fine particulate inorganic materials produce "gels" when dispersed in aqueous media, e.g. sodium montmorillonite or silica. These particulate materials produce three-dimensional structures in the continuous phase as a result of interparticle interaction. For example, sodium montmorillonite (referred to as swellable clay) forms gels at low and intermediate electrolyte concentrations. Van Olphen [23] suggested a mechanism of gel formation of montmorillonite involving interaction of the oppositely charged

double layers at the faces and edges of the clay particles. This structure, which is usually referred to as a "card-house" structure, was considered to be the reason for the formation of the voluminous clay gel. However, Norrish [24] suggested that the voluminous gel is the result of the extended double layers, particularly at low electrolyte concentrations.

Finely divided silica such as Aerosil 200 (produced by Degussa) produces gel structures by simple association (by van der Waals attraction) of the particles into chains and cross chains. When incorporated into the continuous phase of an emulsion, these gels prevent creaming or sedimentation.

By combining thickeners such as hydroxyethyl cellulose or xanthan gum with particulate solids such as sodium montmorillonite, a more robust gel structure can be produced. By using such mixtures, the concentration of the polymer can be reduced, thus overcoming the problem of dispersion on dilution. This gel structure may be less temperature dependent and could be optimized by controlling the ratio of the polymer and the particles. If these combinations of say sodium montmorillonite and a polymer such as hydroxyethyl cellulose, polyvinyl alcohol (PVA) or xanthan gum, are balanced properly, they can provide a "three-dimensional structure", which entraps all the droplets and stops creaming or sedimentation of the emulsion. The mechanism of gelation of such combined systems depends to a large extent on the nature of the droplets, the polymer and the conditions. If the polymer adsorbs on the particle surface (e.g. PVA on sodium montmorillonite or silica) a three-dimensional network may be formed by polymer bridging. Under conditions of incomplete coverage of the particles by the polymer, the latter becomes simultaneously adsorbed on two or more particles. In other words the polymer chains act as "bridges" or "links" between the particles.

Another method for reducing creaming or sedimentation of emulsions is to use liquid crystalline phases. As discussed in Chapter 13 of Vol. 1, surfactants produce liquid crystalline phases at high concentrations [3]. Three main types of liquid crystals can be identified: hexagonal phase (sometimes referred to as middle phase), cubic phase and lamellar (neat phase). All these structures are highly viscous and they also show elastic response. If produced in the continuous phase of emulsions, they can eliminate creaming or sedimentation of the droplets. These liquid crystalline phases are particularly useful for applications in hand creams which contain high surfactant concentrations

2.8 Flocculation of emulsions

Flocculation is the process in which the emulsion drops aggregate, without rupture of the stabilizing layer at the interface, if the pair interaction free energy becomes appreciably negative at a certain separation. This negative interaction is the result of van der Waals attraction G_A that is universal for all disperse systems. As shown in Chapter 7 of

Vol. 1, G_A is inversely proportional to the droplet-droplet distance of separation h and it depends on the effective Hamaker constant A of the emulsion system. Flocculation may be weak (reversible) or strong (not easily reversible) depending on the strength of the interdroplet forces. Flocculation usually leads to enhanced creaming because the flocs rise faster than individual drops due to their larger effective radius. Exceptions occur in concentrated emulsions where the formation of a gel-like network structure can have a stabilizing influence. Flocculation is enhanced by polydispersity since the differential creaming speeds of small and large drops cause them to come into close proximity more often than would occur in a monodisperse system [1]. The cream layer formed towards the end of the creaming process is actually a concentrated floc. The rate of flocculation can be estimated from the product of a frequency factor (how often drops encounter each other) and a probability factor (how long they stay together). The former can be calculated for the case of Brownian motion (perikinetic flocculation) or under shear flow (orthokinetic flocculation) as will be discussed below. Orthokinetic flocculation depends on the interaction energy, i.e. the free energy required to bring drops from infinity to a specified distance apart.

In calculating the interaction energy as a function of interdroplet distance, three terms are normally considered: van der Waals attraction (which depends on droplet radius and the effective Hamaker constant), electrostatic repulsion, produced for example by adsorption of ionic surfactants (which depends on the surface or zeta potential, drop radius and ionic strength of the medium) and steric repulsion, produced by adsorption of nonionic surfactants or polymers (which depends on the adsorption density, conformation of the chain at the O/W interface and solvent quality).

Flocculation can occur if the energy barrier is small or absent (for electrostatically stabilized emulsions) or when the stabilizing chains reach poor solvency (for sterically stabilized emulsions, i.e. the Flory–Huggins interaction parameter $\chi > 0.5$).

As mentioned in Chapter 7 of Vol. 1, the condition for kinetic stability described by the Deryaguin–Landau–Verwey–Overbeek (DLVO) theory [6, 7] is the magnitude of the energy maximum, G_{max}, at intermediate separation of droplets. For an emulsion to remain kinetically stable (with no flocculation), $G_{max} > 25kT$. When $G_{max} < 5kT$, or is completely absent, flocculation occurs. Two types of flocculation kinetics may be distinguished: Fast flocculation with no energy barrier and slow flocculation when an energy barrier exists. The fast flocculation kinetics was treated by Smoluchowki [25], who considered the case where there is no interaction between the two colliding droplets until they come into contact, whereupon they adhere irreversibly. The process is simply represented by second-order kinetics and it is simply diffusion controlled.

Smoluchowski [25] originally accounted for the effect of an energy barrier G_{max}, arising from interparticle interaction, on the kinetics of flocculation by introducing a correction parameter α, where α is the fraction of collisions which are "effective", i.e. leading to irreversible flocculation.

Fuchs [26] showed that when particle interactions are present the flux is made up of two contributions, one due to the Brownian diffusion of the particles, the other due

to the interactions. In this way, the rate constant k of slow flocculation is related to the Smoluchowski rate k_0 by the stability constant W,

$$W = \frac{k_0}{k}. \tag{2.46}$$

W is related to G_{max} [27] and for charge-stabilized emulsions, W is given by the following expression [27],

$$W = \frac{1}{2\kappa R} \exp\left(\frac{G_{max}}{kT}\right), \tag{2.47}$$

where κ is the Debye–Hückel parameter that is given by,

$$\kappa = \left(\frac{2Z^2e^2C}{\varepsilon_r\varepsilon_0 kT}\right)^{1/2}, \tag{2.48}$$

where Z is the valency of counterions, e is the electronic charge, C is the electrolyte concentration in bulk solution, ε_r is the relative permittivity of the medium, ε_0 is the permittivity of free space, k is the Boltzmann constant and T is the absolute temperature.

Since G_{max} is determined by the electrolyte concentration C and valency, one can derive an expression relating W to C and Z,

$$\log W = \text{const} - 2.06 \times 10^9 \left(\frac{R\gamma^2}{Z^2}\right) \log C, \tag{2.49}$$

where γ is a function that is determined by the surface potential ψ_0,

$$\gamma = \left[\frac{\exp(Ze\psi_0/kT) - 1}{\exp(ZE\psi_0/kT) + 1}\right]. \tag{2.50}$$

Plots of $\log W$ versus $\log C$ are shown in Fig. 2.32, which shows a linear relationship in the slow flocculation regime. In the fast flocculation regime $G_{max} = 0$ and $d(\log W)/d(\log C) = 0$. The condition $\log W = 0$ ($W = 1$) is the onset of fast flocculation. The electrolyte concentration at this point defines the critical flocculation concentration CFC. Above the CFC, $W < 1$ (due to the contribution of van der Waals attraction which accelerates the rate above the Smoluchowski value). Below the CFC, $W > 1$ and it increases with decreasing electrolyte concentration. The figure also shows that the CFC decreases with increasing valency in accordance to the Schulze–Hardy rule.

As described in Chapter 7 of Vol. 1, the energy–distance curve described by DLVO theory [6, 7] shows the presence of a shallow energy well, namely the secondary minimum (G_{min}) which is few kT units. In this case flocculation is weak and reversible and hence one must consider both the rate of flocculation (forward rate k_f) and deflocculation (backward rate k_b). The rate of decrease of the number of particles with time is given by the expression,

$$-\frac{dn}{dt} = -k_f n^2 + k_b n. \tag{2.51}$$

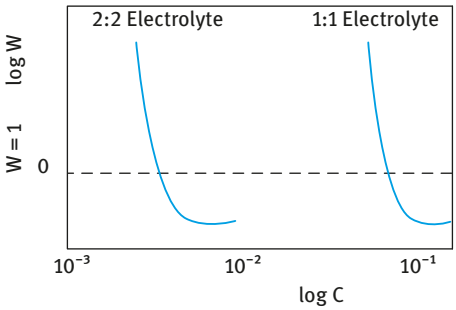

Fig. 2.32: log W–log C curves for electrostatically stabilized emulsions.

The backward reaction (break-up of weak flocs) reduces the overall rate of flocculation. k_b may depend on the floc size and the exact way in which the flocs break down. Another complication in the analysis of weak (reversible) flocculation is the effect of droplet number concentration. Flocculation of this type is a critical phenomenon rather than a chain (or sequential) process. Thus, a critical droplet number concentration, n_{crit} has to be exceeded before flocculation occurs.

The process of flocculation occurs under shearing conditions and is referred to as orthokinetic (to distinguish it from the diffusion-controlled perikinetic process). The simplest analysis is for laminar flow, since for turbulent flow with chaotic vortices (as is the case in a high-speed mixer) the particles are subjected to a wide and unpredictable range of hydrodynamic forces [28].

The rate of orthokinetic flocculation is given by,

$$-\frac{dn}{dt} = \alpha\frac{16}{3}n_p^2R^3\dot{\gamma}. \tag{2.52}$$

A comparison can be made between the collision frequency or rate of orthokinetic and perikinetic flocculation, c_f and c_B respectively,

$$\frac{c_f}{c_B} = \frac{2\alpha\eta_0R^3\dot{\gamma}}{kT}. \tag{2.53}$$

If the particles are dispersed in water at a temperature of 25 °C, the ratio in equation (2.53) becomes,

$$\frac{c_f}{c_B} \approx 4 \times 10^{17}R^3\dot{\gamma}. \tag{2.54}$$

When a liquid is stirred in a beaker using a rod the velocity gradient r shear rate is in the range 1–10 s^{-1}, with a mechanical stirrer it is about 100 s^{-1} and at the tip of a turbine in a large reactor it can reach values as high as 1,000–10,000 s^{-1}. This means that the particle radius R must be less than 1 µm if even slow mixing can be disregarded. This shows how the effect of shear can increase the rate of aggregation.

It should be mentioned that the above analysis is for the case where there is no energy barrier, i.e. the Smoluchowski case [25]. In the presence of an energy barrier, i.e. potential limited aggregation, one must consider the contribution due to the hydrodynamic forces acting on the colliding pair [28].

The flocculation of sterically stabilized emulsions occurs when the solvency of the medium for the stabilizing chain becomes worse than a θ-solvent or the Flory–Huggins interaction parameter $\chi > 0$ (Chapter 9 of Vol. 1). The Flory–Huggins interaction parameter χ may be conveniently changed by varying the temperature, adding a nonsolvent or increasing the electrolyte concentration in the external phase.

As an illustration, Fig. 2.33 shows the variation of G_{mix}, G_{el}, G_A and G_T with h as χ is increased from < 0.5 to > 0.5.

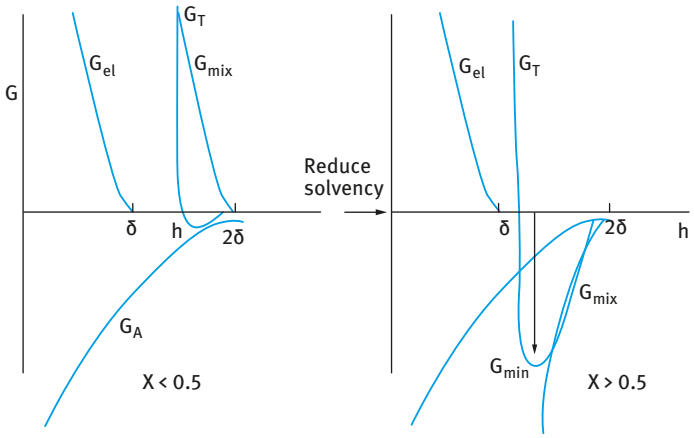

Fig. 2.33: Schematic representation of the interaction free energy-separation curves for two droplets stabilized by high molar mass polymer.

It can be seen that when $\chi > 0.5$ (i.e. the medium for the A chains becomes worse than a θ-solvent), a significant value of G_{min} is attained, resulting in catastrophic flocculation (sometimes referred to as incipient flocculation). With many systems good correlation between the flocculation point and the θ point is obtained. For example, the emulsion will flocculate at a temperature (referred to as the critical flocculation temperature, CFT) that is equal to the θ-temperature of the stabilizing chain. The emulsion may flocculate at a critical volume fraction of a nonsolvent (CFV) which is equal to the volume of nonsolvent that brings it to a θ-solvent.

It should be mentioned, however, that some emulsions flocculate on cooling and others on heating. Generally speaking (but not always), the former occurs when a non-aqueous solvent is the external phase (e.g. W/O emulsions), while the latter occurs when water is the external phase (O/W emulsions).

As discussed in Chapter 8 of Vol. 1, the energy–distance curve of sterically stabilized emulsions shows a shallow minimum G_{min}, at separation distances $h \approx 2\delta$, whose depth can be of the order of few kT units. The minimum depth depends on droplet radius R, Hamaker constant A and adsorbed layer thickness δ (i.e. with decreasing molecular weight of the stabilizer). For a given R and A, G_{min} increases with

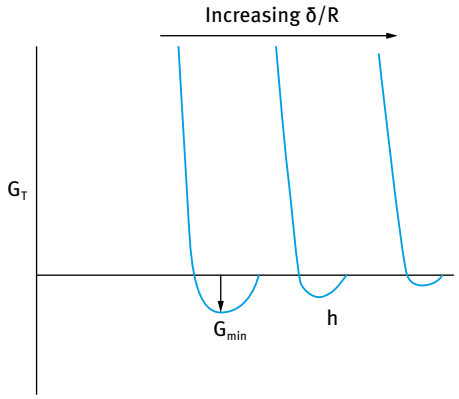

Fig. 2.34: Variation of G_{min} with δ/R.

decreasing δ. This is illustrated in Fig. 2.34 which shows the energy–distance curves as a function of δ/R. The smaller the value of δ/R, the larger the value of G_{min}.

The minimum depth required for causing weak flocculation depends on the volume fraction of the emulsion. The higher the volume fraction, the lower the minimum depth required for weak flocculation. This can be understood if one considers the free energy of flocculation that consists of two terms, an energy term determined by the depth of the minimum (G_{min}) and an entropy term that is determined by a reduction in configurational entropy on aggregation of droplets,

$$\Delta G_{flocc} = \Delta H_{flocc} - T\Delta S_{flocc}. \tag{2.55}$$

With dilute emulsions, the entropy loss on flocculation is larger than with concentrated emulsions. Hence for flocculation of dilute emulsions, a higher energy minimum is required when compared with the case with concentrated emulsions. This flocculation is weak and reversible, i.e. on shaking the container redispersion of the emulsion occurs. On standing, the dispersed droplets aggregate to form a weak "gel". This process (referred to as sol–gel transformation) leads to reversible time dependency of viscosity (thixotropy). On shearing the emulsion, the viscosity decreases and when the shear is removed the viscosity is recovered.

As mentioned above, depletion flocculation is produced by addition of "free" nonadsorbing polymer [21]. In this case, the polymer coils cannot approach the droplets to a distance Δ (that is determined by the radius of gyration of free polymer R_G), since the reduction of entropy on close approach of the polymer coils is not compensated by an adsorption energy. The emulsion droplets will be surrounded by a depletion zone with thickness Δ. Above a critical volume fraction of the free polymer, ϕ_p^+, the polymer coils are "squeezed out" from between the droplets and the depletion zones begin to interact. The interstices between the droplets are now free from polymer coils and hence an osmotic pressure is exerted outside the droplet surface (the osmotic pressure outside is higher than in-between the particles) resulting in weak flocculation [21].

The magnitude of the depletion attraction free energy, G_{dep}, is proportional to the osmotic pressure of the polymer solution, which in turn is determined by ϕ_p and molecular weight M. The range of depletion attraction is proportional to the thickness of the depletion zone, Δ, which is roughly equal to the radius of gyration, R_G, of the free polymer. A simple expression for G_{dep} is [21],

$$G_{dep} = \frac{2\pi R\Delta^2}{V_1}(\mu_1 - \mu_1^0)\left(1 + \frac{2\Delta}{R}\right), \tag{2.56}$$

where V_1 is the molar volume of the solvent, μ_1 is the chemical potential of the solvent in the presence of free polymer with volume fraction ϕ_p and μ_1^0 is the chemical potential of the solvent in the absence of free polymer. $(\mu_1 - \mu_1^0)$ is proportional to the osmotic pressure of the polymer solution.

Certain long chain polymers may adsorb in such a way that different segments of the same polymer chain are adsorbed on different droplets, thus binding or "bridging" the droplets together, despite the electrical repulsion [29]. With polyelectrolytes of opposite charge to the droplets, another possibility exists; the droplet charge may be partly or completely neutralized by the adsorbed polyelectrolyte, thus reducing or eliminating the electrical repulsion and destabilizing the droplets.

Effective flocculants are usually linear polymers, often of high molecular weight, which may be nonionic, anionic or cationic in character. Ionic polymers should be strictly referred to as polyelectrolytes. The most important properties are molecular weight and charge density. There are several polymeric flocculants that are based on natural products, e.g. starch and alginates, but the most commonly used flocculants are synthetic polymers and polyelectrolytes, e.g. polyacrylamide and copolymers of acrylamide and a suitable cationic monomer such as dimethylaminoethyl acrylate or methacrylate. Other synthetic polymeric flocculants are poly(vinyl alcohol), poly(ethylene oxide) (nonionic), sodium polystyrene sulphonate (anionic) and polyethyleneimine (cationic).

As mentioned above, bridging flocculation occurs because segments of a polymer chain adsorb simultaneously on different droplets thus linking them together. Adsorption is an essential step and this requires favourable interaction between the polymer segments and the droplets. Several types of interactions are responsible for adsorption that is irreversible in nature:

(i) Electrostatic interaction when a polyelectrolyte adsorbs on a surface bearing oppositely charged ionic groups, e.g. adsorption of a cationic polyelectrolyte on a negative emulsion surface.
(ii) Hydrophobic bonding that is responsible for adsorption of nonpolar segments on a hydrophobic surface, e.g. partially hydrolyzed poly(vinyl acetate) (PVA) on a hydrophobic surface such as hydrocarbon oil.
(iii) Hydrogen bonding as for example interaction of the amide group of polyacrylamide with hydroxyl groups on an emulsion surface.

(iv) Ion binding, as is the case of adsorption of anionic polyacrylamide on a negatively charged surface in the presence of Ca_2^+.

Effective bridging flocculation requires the adsorbed polymer extends far enough from the droplet surface to attach to other droplets and that there is sufficient free surface available for adsorption of these segments of extended chains. When excess polymer is adsorbed, the droplets can be restabilized, either because of surface saturation or by steric stabilization as discussed before. This is one explanation of the fact that an "optimum dosage" of flocculant is often found; at low concentration there is insufficient polymer to provide adequate links and with larger amounts restabilization may occur. A schematic picture of bridging flocculation and restabilization by adsorbed polymer is given in Fig. 2.35.

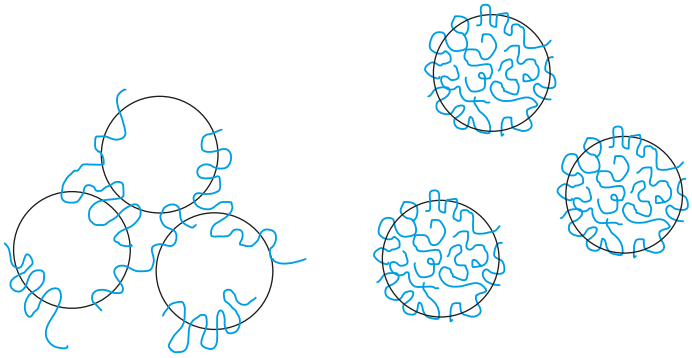

Fig. 2.35: Schematic illustration of bridging flocculation (left) and restabilization (right) by adsorbed polymer.

If the fraction of droplet surface covered by polymer is θ then the fraction of uncovered surface is $(1 - \theta)$ and the successful bridging encounters between the droplets should be proportional to $\theta(1 - \theta)$, which has its maximum when $\theta = 0.5$. This is the well-known condition of "half-surface coverage" that has been suggested as giving the optimum flocculation.

An important condition for bridging flocculation with charged droplets is the role of electrolyte concentration. This determines the extension ("thickness") of the double layer which can reach values as high as 100 nm (in 10^{-5} mol dm^{-5} 1 : 1 electrolyte such as NaCl). For bridging flocculation to occur, the adsorbed polymer must extend far enough from the surface to a distance over which electrostatic repulsion occurs (> 100 nm in the above example). This means that at low electrolyte concentrations quite high molecular weight polymers are needed for bridging to occur. As the ionic strength is increased, the range of electrical repulsion is reduced and lower molecular weight polymers should be effective.

In many practical applications, it has been found that the most effective flocculants are polyelectrolytes with a charge opposite to that of the droplets. In aqueous media most droplets are negatively charged, and cationic polyelectrolytes such as polyethyleneimine are often necessary. With oppositely charged polyelectrolytes it is likely that adsorption occurs to give a rather flat configuration of the adsorbed chain, due to the strong electrostatic attraction between the positive ionic groups on the polymer and the negative charged sites on the droplet surface. This would probably reduce the probability of bridging contacts with other particles, especially with fairly low molecular weight polyelectrolytes with high charge density. However, the adsorption of a cationic polyelectrolyte on a negatively charged droplet will reduce the surface charge of the latter, and this charge neutralization could be an important factor in destabilizing the particles.

Another mechanism for destabilization has been suggested by Gregory [10] who proposed an "electrostatic patch" model. This applied to cases where the droplets have a fairly low density of immobile charges and the polyelectrolyte has a fairly high charge density. Under these conditions, it is not physically possible for each surface site to be neutralized by a charged segment on the polymer chain, even though the droplet may have sufficient adsorbed polyelectrolyte to achieve overall neutrality. There are then "patches" of excess positive charge, corresponding to the adsorbed polyelectrolyte chains (probably in a rather flat configuration), surrounded by areas of negative charge, representing the original particle surface. Droplets which have this "patchy" or "mosaic" type of surface charge distribution may interact in such a way that the positive and negative "patches" come into contact, giving quite strong attraction (although not as strong as in the case of bridging flocculation). A schematic illustration of this type of interaction is given in Fig. 2.36. The electrostatic patch concept (which can be regarded as another form of "bridging") can explain a number of features of flocculation of negatively charged droplets with positive polyelectrolytes.

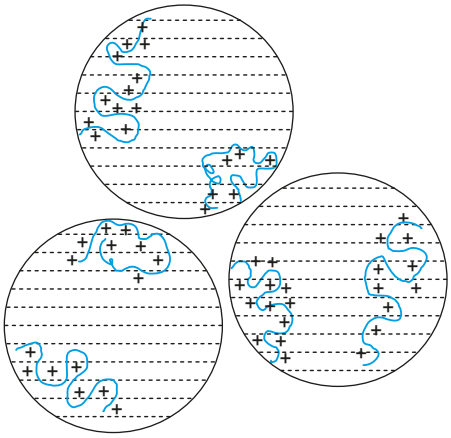

Fig. 2.36: "Electrostatic patch" model for the interaction of negatively charged droplets with adsorbed cationic polyelectrolytes.

These include the rather small effect of increasing the molecular weight and the effect of ionic strength on the breadth of the flocculation dosage range and the rate of flocculation at optimum dosage.

Flocculation of emulsions can be reduced by controlling the parameters that affect its stabilization. For charge stabilized emulsions, e.g. using ionic surfactants, the most important criterion is to make G_{max} as high as possible; this is achieved by three main conditions, namely high surface or zeta potential, low electrolyte concentration and low valency of ions. For sterically stabilized emulsions, four main criteria are necessary:

(i) Complete coverage of the droplets by the stabilizing chains.
(ii) Firm attachment (strong anchoring) of the chains to the droplets. This requires the chains to be insoluble in the medium and soluble in the oil. However, this is incompatible with stabilization which requires a chain that is soluble in the medium and strongly solvated by its molecules. These conflicting requirements are solved by the use of A–B, A–B–A block or BA_n graft copolymers (B is the "anchor" chain and A is the stabilizing chain(s)). Examples for the B chains for O/W emulsions are polystyrene, polymethylmethacrylate, polypropylene oxide and alkyl polypropylene oxide. For the A chain(s), polyethylene oxide (PEO) or polyvinyl alcohol are good examples. For W/O emulsions, PEO can form the B chain, whereas the A chain(s) could be polyhydroxy stearic acid (PHS) which is strongly solvated by most oils.
(iii) Thick adsorbed layers; the adsorbed layer thickness should be in the region of 5–10 nm. This means that the molecular weight of the stabilizing chains could be in the region of 1,000–5,000.
(iv) The stabilizing chain should be maintained in good solvent conditions ($\chi < 0.5$) under all conditions of temperature changes on storage.

2.9 Ostwald ripening in emulsions and its prevention

As mentioned in Chapter 10 of Vol. 1, the driving force of Ostwald ripening is the difference in solubility between smaller and larger droplets [1]. Small droplets with radius r_1 will have higher solubility than larger droplet with radius r_2. The solubility of droplets increases very rapidly with decreasing radius, particularly when $r < 100$ nm. This means that a droplet with a radius of say 4 nm will have about 10 times solubility enhancement compared say with a droplet with 10 nm radius which has a solubility enhancement of only 2 times. Thus, with time, molecular diffusion will occur between smaller and larger droplets, with the ultimate disappearance of most of the small droplets. This results in a shift in the droplet size distribution to larger values on storage of the emulsion. This could lead to the formation of a dispersion droplet size > μm. This instability can cause severe problems, such as creaming or sedimentation, flocculation and even coalescence of the emulsion.

The kinetics of Ostwald ripening is described in terms of the theory developed by Lifshitz and Slesov [31] and by Wagner [32] (referred to as LSW theory). The LSW theory assumes that:

(i) the mass transport is due to molecular diffusion through the continuous phase;
(ii) the dispersed phase droplets are spherical and fixed in space;
(iii) there are no interactions between neighbouring droplets (the droplets are separated by a distance much larger than the diameter of the droplets);
(iv) the concentration of the molecularly dissolved species is constant except adjacent to the droplet boundaries.

The rate of Ostwald ripening ω is given by:

$$\omega = \frac{\mathrm{d}}{\mathrm{d}r}(r_c^3) = \left(\frac{8\gamma DS(\infty)V_m}{9RT}\right)f(\phi) = \left(\frac{4DS(\infty)\alpha}{9}\right)f(\phi), \tag{2.57}$$

where r_c is the radius of a particle or droplet that is neither growing nor decreasing in size, D is the diffusion coefficient of the disperse phase in the continuous phase, $f(\phi)$ is a factor that reflects the dependency of ω on the disperse volume fraction and α is the characteristic length scale ($= 2\gamma V_m/RT$).

Droplets with $r > r_c$ grow at the expense of smaller ones, while droplets with $r < r_c$ tend to disappear. The validity of the LSW theory was tested by Kabalnov et al. [5] who used 1,2 dichloroethane-in-water emulsions whereby the droplets were fixed to the surface of a microscope slide to prevent their coalescence. The evolution of the droplet size distribution was followed as a function of time by microscopic investigations. The LSW theory predicts that the droplet growth over time will be proportional to r_c^3.

The influence of the alkyl chain length of the hydrocarbon on the Ostwald ripening rate of nanoemulsions was systematically investigated by Kabalanov et al. [33, 34]. An increase in the alkyl chain length of the hydrocarbon used for the emulsion results in a decrease of the oil solubility. According to LSW theory this reduction in solubility should result in a decrease of the Ostwald ripening rate. This was confirmed by the results of Kabalnov et al. [33, 34] who showed that the Ostwald ripening rate decreases with increasing the alkyl chain length from C_9–C_{16}.

Although the results showed the linear dependency of the cube of the droplet radius with time in accordance with LSW theory, the experimental rates were ≈ 2–3 times higher than the theoretical values. The deviation between theory and experiment has been ascribed to the effect of Brownian motion [33, 34]. LSW theory assumes that the droplets are fixed in space and the molecular diffusion is the only mechanism of mass transfer. For droplets undergoing Brownian motion, one must take into account the contributions of molecular and convective diffusion.

LSW theory assumes that there are no interactions between the droplets and it is limited to low oil volume fractions. At higher volume fractions the rate of ripening depends on the interaction between diffusion spheres of neighbouring droplets. It is expected that emulsions with higher volume fractions of oil will have broader droplet

size distribution and faster absolute growth rates than those predicted by LSW theory. However, experimental results using high surfactant concentrations (5 %) showed the rate to be independent of the volume fraction in the range $0.01 \leq \phi \leq 0.3$. It has been suggested that the emulsion droplets may have been screened from one another by surfactant micelles [33, 34]. A strong dependency on volume fraction has been observed for fluorocarbon-in-water emulsions [33, 34]. A threefold increase in ω was found when ϕ was increased from 0.08 to 0.52.

It has been suggested that micelles play a role in facilitating the mass transfer between emulsion droplets by acting as carriers of oil molecules [33, 34]. Three mechanisms were suggested:

(i) oil molecules are transferred via direct droplet/micelle collisions;
(ii) oil molecules exit the oil droplet and are trapped by micelles in the immediate vicinity of the droplet;
(iii) oil molecules exit the oil droplet collectively with a large number of surfactant molecules to form a micelle.

Numerous studies indicate, however, that the presence of micelles affects mass transfer to only a small extent [35]. Results were obtained for decane-in-water emulsions using sodium dodecyl sulphate (SDS) as emulsifier at concentrations above the critical micelle concentration (cmc). The results showed only a two-fold increase in ω above the cmc. This result is consistent with many other studies which showed an increase in mass transfer of only 2–5 times with increasing micelle concentration. The lack of strong dependence of mass transfer on micelle concentration for ionic surfactants may result from electrostatic repulsion between the emulsion droplets and micelles, which provides a high energy barrier preventing droplet/micelle collision.

To account for the discrepancy between theory and experiment in the presence of surfactant micelles, Kabalanov [36] considered the kinetics of micellar solubilization and he proposed that the rate of oil monomer exchange between the oil droplets and the micelles is slow, and rate determining. Thus at low micellar concentration, only a small proportion of the micelles are able to rapidly solubilize the oil. This leads to a small, but measurable increase in the Ostwald ripening rate with micellar concentration. Taylor and Ottewill [37] proposed that micellar dynamics may also be important. According to Anainsson et al. [38], micellar growth occurs in a stepwise fashion and is characterized by two relaxation times τ_1 and τ_2. The short relaxation time τ_1 is related to the transfer of monomers in and out of the micelles, while the long relaxation time τ_2 is the time required for break-up and reformation of the micelle. At low SDS ($0.05\,\mathrm{mol\,dm^{-3}}$) concentration $\tau_2 \approx 0.01$ s, whereas at higher SDS concentration ($0.2\,\mathrm{mol\,dm^{-3}}$) $\tau_2 \approx 6$ s. Taylor and Ottewill [37] suggested that, at low SDS concentration, τ_2 may be fast enough to have an effect on the Ostwald ripening rate, but at 5 % SDS τ_2 may be as long as 1,000 s (taking into account the effect of solubilization on τ_2), which is too long to have a significant effect on the Ostwald ripening rate.

When using nonionic surfactant micelles, larger increases in the Ostwald ripening rate might be expected due to the larger solubilization capacities of the nonionic surfactant micelles and absence of electrostatic repulsion between the nanoemulsion droplets and the uncharged micelles. This was confirmed by Weiss et al. [39] who found a large increase in the Ostwald ripening rate in tetradecane-in-water emulsions in the presence of Tween 20 micelles.

Several methods have been suggested for reducing Ostwald ripening. Huguchi and Misra [40] suggested that adding a second disperse phase that is virtually insoluble in the continuous phase, such as squalane, can significantly reduce the Ostwald ripening rate. In this case, significant partitioning between different droplets is predicted, with the component having the low solubility in the continuous phase (e.g. squalane) being expected to be concentrated in the smaller droplets. During Ostwald ripening in a two-component disperse system, equilibrium is established when the difference in chemical potential between different sized droplets, which results from curvature effects, is balanced by the difference in chemical potential resulting from partitioning of the two components. Huguchi and Misra [40] derived the following expression for the equilibrium condition, wherein the excess chemical potential of the medium soluble component, $\Delta\mu_1$, is equal for all of the droplets in a polydisperse medium,

$$\frac{\Delta\mu_i}{RT} = \left(\frac{a_1}{r_{eq}}\right) + \ln(1 - X_{eq2}) = \left(\frac{a_1}{r_{eq}}\right) - X_{02}\left(\frac{r_0}{r_{eq}}\right)^3 = \text{const}, \tag{2.58}$$

where $\Delta\mu_1 = \mu_1 - \mu_1^*$ is the excess chemical potential of the first component with respect to the state μ_1^* when the radius $r = \infty$ and $X_{02} = 0$, r_0 and r_{eq} are the radii of an arbitrary drop under initial and equilibrium conditions respectively, X_{02} and X_{eq2} are the initial and equilibrium mole fractions of the medium insoluble component 2, a_1 is the characteristic length scale of the medium soluble component 1.

The equilibrium determined by equation (2.58) is stable if the derivative $\partial\Delta\mu_1/\partial r_{eq}$ is greater than zero for all the droplets in a polydisperse system. Based on this analysis, Kabalanov et al. [41] derived the following criterion,

$$X_{02} > \frac{2a_1}{3d_0}, \tag{2.59}$$

where d_0 is the initial droplet diameter. If the stability criterion is met for all droplets, two patterns of growth will result, depending on the solubility characteristic of the secondary component. If the secondary component has zero solubility in the continuous phase, then the size distribution will not deviate significantly from the initial one, and the growth rate will be equal to zero. In the case of limited solubility of the secondary component, the distribution is governed by rules similar to LSW theory, i.e. the distribution function is time variant. In this case, the Ostwald ripening rate ω_{mix} will be a mixture growth rate that is approximately given by the following equation [41],

$$\omega_{\text{mix}} = \left(\frac{\phi_1}{\omega_1} + \frac{\phi_2}{\omega_2} \right)^{-1}, \tag{2.60}$$

where ϕ_1 is the volume fraction of the medium soluble component and ϕ_2 is the volume fraction of the medium insoluble component respectively.

If the stability criterion is not met, a bimodal size distribution is predicted to emerge from the initially monomodal one. Since the chemical potential of the soluble component is predicted to be constant for all the droplets, it is also possible to derive the following equation for the quasi-equilibrium component 1,

$$X_{02} + \frac{2a_1}{d} = \text{const}, \tag{2.61}$$

where d is the diameter at time t.

Kabalanov et al. [42] studied the effect of addition of hexadecane to a hexane-in-water nanoemulsion. Hexadecane, which is less soluble than hexane, was studied at three levels $X_{02} = 0.001$, 0.01 and 0.1. For the higher mole fraction of hexadecane, namely 0.01 and 0.1, the emulsion had a physical appearance similar to that of an emulsion containing only hexadecane and the Ostwald ripening rate was reliably predicted by equation (2.60). However, the emulsion with $X_{02} = 0.001$ quickly separated into two layers, a sedimented layer with a droplet size of ca. 5 µm and a dispersed population of submicron droplets (i.e. a bimodal distribution). Since the stability criterion was not met for this low volume fraction of hexadecane, the observed bimodal distribution of droplets is predictable.

The second method that can be applied to reduce Ostwald ripening is to modify the interfacial layer. According to LSW theory, the Ostwald ripening rate ω is directly proportional to the interfacial tension γ. Thus by reducing γ, ω is reduced. This could be confirmed by measuring ω as a function of SDS concentration for decane-in-water emulsion below the critical micelle concentration (cmc). Below the cmc, γ shows a linear decrease with increasing log[SDS] concentration.

Several other mechanisms have been suggested to account for a reduction in the Ostwald ripening rate by modification of the interfacial layer. For example, Walstra [43] suggested that emulsions could be effectively stabilized against Ostwald ripening by the use of surfactants that are strongly adsorbed at the interface and which do not desorb during the Ostwald ripening process. In this case the increase in interfacial dilational modulus ε and decreases in interfacial tension γ would be observed for the shrinking droplets. Eventually the difference in ε and γ between droplets would balance the difference in capillary pressure (i.e. curvature effects) leading to a quasi-equilibrium state. In this case, emulsifiers with low solubilities in the continuous phase such as proteins would be preferred. Long chain phospholipids with a very low solubility (cmc $\approx 10^{-10}$ mol dm^{-3} are also effective in reducing Ostwald ripening of some emulsions. The phospholipid would have to have a solubility in water about three orders of magnitude lower than the oil [19].

2.10 Emulsion coalescence and its prevention

As discussed in Chapter 11 of Vol. 1, when two emulsion droplets come into close contact in a floc or creamed layer or during Brownian diffusion, a thin liquid film or lamella forms between them [1]. Coalescence results from the rupture of this film. If the film cannot be ruptured, adhesion or engulfment may occur. Film rupture usually commences at a specified "spot" in the lamella, arising from thinning in that region. The liquid surfaces undergo some fluctuations forming surface waves. The surface waves may grow in amplitude and the apices may join as a result of the strong van der Waals attraction (at the apex, the film thickness is the smallest). The same applies if the film thins to a small value (critical thickness for coalescence). In order to understand the behaviour of these films, one has to consider two aspects of their physics:

(i) the nature of the forces acting across the film; these determine whether the film is thermodynamically stable, metastable or unstable;
(ii) the kinetic aspects associated with local (thermal or mechanical) fluctuations in film thickness.

Several approaches have been considered to analyse the stability of thin films between emulsion droplets in terms of the relevant interactions. Deryaguin [44] introduced the concept of disjoining pressure to account for the stability of the liquid film. Deryaguin [44] suggested that a "disjoining pressure" $\pi(h)$ is produced in the film which balances the excess normal pressure,

$$\pi(h) = P(b) - P_0, \tag{2.62}$$

where $P(h)$ is the pressure of a film with thickness b and P_0 is the pressure of a sufficiently thick film such that the net interaction free energy is zero.

$\pi(h)$ may be equated to the net force (or energy) per unit area acting across the film,

$$\pi(h) = -\frac{\mathrm{d}G_\mathrm{T}}{\mathrm{d}b}, \tag{2.63}$$

where G_T is the total interaction energy in the film.

$\pi(h)$ is made up of three contributions due to electrostatic repulsion (π_E), steric repulsion (π_s) and van der Waals attraction (π_A),

$$\pi(h) = \pi_\mathrm{E} + \pi_\mathrm{s} + \pi_\mathrm{A}. \tag{2.64}$$

To produce a stable film $\pi_\mathrm{E} + \pi_\mathrm{s} > \pi_\mathrm{A}$ and this is the driving force for preventing coalescence which can be achieved by two mechanisms and their combination:

(i) increased repulsion, both electrostatic and steric;
(ii) dampening the fluctuation by enhancing the Gibbs elasticity.

In general smaller droplets are less susceptible to surface fluctuations and hence coalescence is reduced.

Van den Tempel [45] derived an expression for the coalescence rate of emulsion droplets by assuming the rate to be proportional to the number of contact points between the droplets in an aggregate. Both flocculation and coalescence are taken into account simultaneously. The number of droplets n at time t is related to the number n_0 at $t = 0$ by,

$$n = \frac{n_0}{Kt}[1 - \exp(-kt)], \tag{2.65}$$

where K is the rate of coalescence and k is the rate of flocculation.

This means that the rate of coalescence no longer depends on the rate of flocculation for concentrated emulsions. Van den Tempel calculated the change in droplet number concentration with time for concentrated ($n_0 > 10^{10}$ cm^{-3}) and dilute emulsion ($n_0 = 10^9$ cm^{-3}) and for values of $k = 5 \times 10^{-11}$ cm^3 s^{-1} and $K = 10^3$ s^{-1}.

Davies and Rideal [14] discussed the problem of coalescence, incorporating an energy barrier term into the Smoluchowski equation, in order to account for the slow coalescence for emulsions stabilized by sodium oleate. The Smoluchowski equation may be written in terms of the mean volume V of emulsion droplets,

$$V = \frac{\phi}{n_0} + 4\pi DR\phi t, \tag{2.66}$$

where ϕ is the volume fraction of the dispersed phase, D is the diffusion coefficient of the droplets and R is the collision radius. D can be calculated using the Stokes–Einstein equation,

$$D = \frac{kT}{6\pi\eta R}. \tag{2.67}$$

k is the Boltzmann constant, T is the absolute temperature, η is the viscosity of the medium and R is the droplet radius.

Equation (2.66) predicts that the mean volume of the droplets should be doubled in about 43 seconds, whereas experiments show that in the presence of sodium oleate, this takes about 50 days. To account for this an energy barrier (ΔG_{coal}) was introduced in equation (2.66),

$$V = V_0 + 4\pi DR\phi t \exp\left(-\frac{\Delta G_{\text{coal}}}{kT}\right). \tag{2.68}$$

Substituting for D from equation (2.67) and differentiating with respect to t, the rate of coalescence for an O/W emulsion is given by,

$$\frac{\mathrm{d}V}{\mathrm{d}t} = \frac{4\phi kT}{3\eta_{\text{w}}} \exp\left(-\frac{\Delta G_{\text{coal}}}{kT}\right) = C_1 \exp\left(-\frac{\Delta G_{\text{coal}}}{kT}\right), \tag{2.69}$$

where η_{w} is the viscosity of the continuous phase (water for O/W emulsion) and C_1 is the collision factor.

For a W/O emulsion, the corresponding relation would be,

$$\frac{\mathrm{d}V}{\mathrm{d}t} = \frac{4(1-\phi)kT}{3\eta_0} \exp\left(-\frac{\Delta G_{\text{coal}}}{kT}\right) = C_2 \exp\left(-\frac{\Delta G_{\text{coal}}}{kT}\right), \tag{2.70}$$

where η_0 is the viscosity of the oil continuous phase and C_2 is the corresponding collision factor.

Davies and Rideal considered the energy barrier in terms of the electrical potential ψ_0 at the surface of the oil droplets, arising from drops stabilized by ionic surfactants. The energy barrier preventing coalescence is proportional to ψ_0^2 according to DLVO theory [6, 7] as described above,

$$\Delta G_{\text{coal}} = B\psi_0^2, \tag{2.71}$$

where B is a constant that depends on the radius of curvature of the droplets. When two approaching droplets tend to flatten in the region of contact in a lamella, the radius of curvature to be used for emulsion droplets may be considerably different from the actual droplet radius. However, the degree of flattening is negligible for small emulsion droplets (< 1 μm in diameter). If there is specific adsorption of counterions, the electric potential to be used in evaluating the electrical double repulsion will be less than ψ_0. In this case one has to use the Stern potential ψ_{d} at the plane of specifically adsorbed ions, i.e.,

$$\Delta G_{\text{coal}} = B\psi_{\text{d}}^2. \tag{2.72}$$

Several methods can be applied to reduce coalescence. It has long been known that mixed surfactants can have a synergistic effect on emulsion stability, with respect to coalescence rates. For example, Schulman and Cockbain [46] found that the stability of Nujol/water emulsions increases markedly on addition of cetyl alcohol or cholesterol to an emulsion prepared using sodium cetyl sulphate. The enhanced stability was assumed to be associated with the formation of a densely packed interfacial layer. The maximum effect is obtained when a water-soluble surfactant (cetyl sulphate) and an oil-soluble surfactant (cetyl alcohol), sometimes referred to as cosurfactant, are used in combination. Suitable combinations lead to enhanced stability as compared to the individual components. These mixed surfactant films also produce a low interfacial tension, in the region of 0.1 mN m^{-1} or lower. This reduction in interfacial tension may be due to the cooperative adsorption of the two surfactant molecules, as predicted by the Gibbs adsorption equation for multicomponent systems. The two surfactant molecules should adsorb simultaneously and they should not interact with each other, otherwise they lower their respective activities. Thus, the surfactant and cosurfactant molecules should vary in nature, one predominantly water-soluble (such as an anionic surfactant) and the other predominantly oil-soluble (such as a long chain alcohol).

The synergistic effect of surfactant mixtures can be accounted for by the enhanced lowering of interfacial tension of the mixture when compared with individual components. For example, addition of cetyl alcohol to an O/W emulsion stabilized by cetyl trimethyl ammonium bromide results in lowering of the interfacial tension, and a shift of the critical micelle concentration (cmc) to lower values, probably due to the increased packing of the molecules at the O/W interface [1]. Another effect of using surfactant mixtures is due to the enhanced Gibbs dilational elasticity, ε.

Prins and van den Tempel [47] showed that the surfactant mixture sodium laurate plus lauric acid gives a very high Gibbs elasticity (of the order of 10^3 mN m^{-1})

when compared with that of sodium laurate alone. In the presence of laurate ions, lauric acid has an extremely high surface activity. At half coverage, the interface contains 1.3 mol dm^{-3} laurate ions and 4.8×10^{-7} mol dm^{-3} lauric acid. Thus, under these conditions, the minor constituent can contribute more to the Gibbs elasticity than the major constituent. Similar results were obtained by Prins et al. [48] who showed that ε increases markedly in the presence of lauryl alcohol for O/W emulsions stabilized by sodium lauryl sulphate. A correlation between film elasticity and coalescence rate has been observed for O/W emulsions stabilized with proteins [49].

It has long been assumed that a high interfacial viscosity could account for the stability of liquid films. This must play a role under dynamic conditions, i.e. when two droplets approach each other. Under static conditions, the interfacial viscosity does not play a direct role. However, a high interfacial viscosity is often accompanied by a high interfacial elasticity and this may be an indirect contribution to the increased stability of the emulsion. Prins and van den Tempel [47] argued against there being any role played by the interfacial viscosity due to two main observations, namely the small changes in film stability with changes in temperature (which should have a significant effect on the interfacial viscosity) and the sudden decrease of the interfacial viscosity with a slight increase in the concentration of the major component. Thus, Prins and van den Tempel [47] attributed the enhanced emulsion stability resulting from the presence of a minor component to be solely due to an increase in interfacial elasticity.

Another possible explanation for enhanced stability in the presence of mixed surfactants could be connected to the hindered diffusion of the surfactant molecules in the condensed film. This would imply that the desorption of surfactant molecules is hindered on the approach of two emulsion droplets, and hence thinning of the film is prevented.

Another effect of using surfactant mixtures is to produce liquid crystalline phase formation. Friberg and co-workers [50] attributed the enhanced stability of emulsions formed with mixtures of surfactants to the formation of three-dimensional structures, namely, liquid crystals. These structures can form, for example, in a three-component system of surfactant, alcohol and water. The lamellar liquid crystalline phase is particularly important for stabilizing the emulsion against coalescence. In this case the liquid crystals "wrap" around the droplets in several layers. These multilayers form a barrier against coalescence. Friberg et al. [50] have given an explanation in terms of the reduced attractive potential energy between two emulsion droplets, each surrounded by a layer of liquid crystalline phase. They have also considered changes in the hydrodynamic interactions in the interdroplet region; this affects the aggregation kinetics. Friberg et al. [50] have calculated the effect on the van der Waals attraction of the presence of a liquid crystalline phase surrounding the droplets. A schematic representation of the flocculation and coalescence of droplets with and without a liquid crystalline layer is shown in Fig. 2.37.

The upper part of Fig. 2.37 (A to F) represents the flocculation process when the emulsifier is adsorbed as a monomolecular layer. The distance d between the water

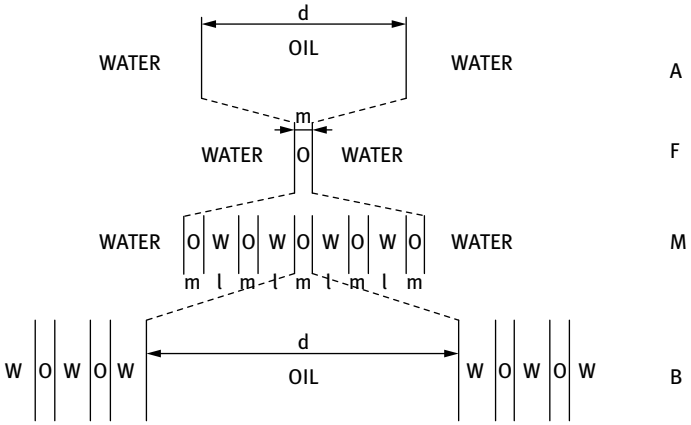

Fig. 2.37: Schematic representation of flocculation and coalescence in the presence and absence of liquid crystalline phases.

droplets decreases to a distance m at which the film ruptures and the droplets coalesce; *m* is chosen to correspond to the thickness of the hydrophilic layers in the liquid crystalline phase. This simplifies the calculations and facilitates comparison with the case in which the liquid crystalline layer is adsorbed around the droplets.

The flocculation process for the case of droplets covered with liquid crystalline layers is illustrated in the lower part of Fig. 2.37 (B to M). The oil layer between the droplets thins to thickness m. The coalescence process that follows involves the removal of successive layers between the droplets until a thickness of one layer is reached (F); the final coalescence step occurs in a similar manner to the case for a monomolecular layer of adsorbed surfactant.

An effective method to reduce coalescence is to use polymeric surfactants. The most convenient polymeric surfactants are those of the block and graft copolymer type. A block copolymer is a linear arrangement of blocks of variable monomer composition. The nomenclature for a diblock is poly-A-block–poly-B and for a triblock is poly-A-block–poly-B–poly-A. One of the most widely used triblock polymeric surfactants are the "Pluronics" (BASF, Germany) which consists of two poly-A blocks of poly (ethylene oxide) (PEO) and one block of poly (propylene oxide) (PPO). Several chain lengths of PEO and PPO are available.

The above polymeric triblocks can be applied as emulsifiers, whereby the assumption is made that the hydrophobic PPO chain resides at the hydrophobic surface, leaving the two PEO chains dangling in aqueous solution and hence providing steric repulsion, and this reduces or eliminates the coalescence of emulsions. A graft copolymer based on polysaccharides of inulin, namely INUTEC® SP1, a linear polyfructose chain with a glucose end, has been developed for stabilizing emulsions [1]. The main advantages of INUTEC® SP1 as a stabilizer for emulsions are: Strong adsorption to the droplet by multipoint attachment with several alkyl chains, which ensures lack of

desorption and displacement of the molecule from the interface; strong hydration of the linear polyfructose chains both in water and in the presence of high electrolyte concentrations and high temperatures, which ensures effective steric stabilization. Evidence for the high stability of the liquid film between emulsion droplets when using INUTEC® SP1 was obtained by Exerowa et al. [51] using disjoining pressure measurements.

2.11 Phase inversion and its prevention

As mentioned in Chapter 12 of Vol. 1, phase inversion is the process whereby the internal and external phase of an emulsion suddenly invert, e.g. O/W to W/O or vice versa [1–4]. Catastrophic inversion is induced by increasing the volume fraction of the disperse phase. This type of inversion is not reversible [1]; the value of the water: oil ratio at the transition when oil is added to water is not the same as that when water is added to oil. The inversion point depends on the intensity of agitation and the rate of liquid addition to the emulsion.

Phase inversion can also be transitional, induced by changing factors which affect the HLB of the system, e.g. temperature and/or electrolyte concentration. The average droplet size decreases and the emulsification rate (defined as the time required to achieve a stable droplet size) increases as inversion is approached. Both trends are consistent with O/W interfacial tension reaching a minimum near the inversion point.

In the early theories of phase inversion, it was postulated that the inversion takes place as a result of the difficulty in packing the emulsion droplets above a certain volume fraction. For example, according to Ostwald [52] an assembly of spheres of equal radii should occupy 74 % of the total volume. Thus, at phase volume $\phi > 0.74$, the emulsion droplets have to be packed more densely than is possible. This means that any attempt to increase the phase volume beyond that point should result in distortion, breaking or inversion. However, several investigations showed the invalidity of this argument, inversion being found to take place at phase volumes much greater or smaller than this critical value. For example, Shinoda and Saito [53] showed that inversion of olive oil/water emulsions takes place at $\phi = 0.25$. Moreover, Sherman [54] showed that the volume fraction at which inversion takes place depends to a large extent on the nature of the emulsifier. It should be mentioned that Ostwald's theory [52] applies only to the packing of rigid, non-deformable spheres of equal size. Emulsion droplets are nether resistant to deformation, nor are they, in general, of equal size. The wide distribution of droplet sizes makes it possible to achieve a higher internal phase volume fraction by virtue of the fact that the smaller droplets can be fitted into the interstices between the larger ones. If one adds to this the possibility that the droplets may be deformed into polyhedra, even denser packing is possible. This is the principle of preparing high internal phase emulsions (HIPE) reaching $\phi > 0.95$.

References

[1] Tadros T. Emulsions. Berlin: De Gruyter; 2016.
[2] Binks BP, editor. Modern aspects of emulsion science. Cambridge: The Royal Society of Chemistry Publication; 1998.
[3] Tadros T. Applied surfactants. Weinheim: Wiley-VCH; 2005.
[4] Tadros T. Emulsion Formation Stability and Rheology. In: Tadros T, editor. Emulsion formation and stability. Weinheim: Wiley-VCH; 2013. Chapter 1.
[5] Gibbs JW. Collected papers. Vol. 1. Thermodynamics. New York: Dover; 1961.
[6] Deryaguin BV, Landau L. Acta Physicochem USSR. 1941;14:633.
[7] Verwey EJW, Overbeek JTG. Theory of stability of lyophobic colloids. Amsterdam: Elsevier; 1948.
[8] Lucassen-Reynders EH. Colloids and Surfaces. 1994;A91:79.
[9] Lucassen J. In: Lucassen-Reynders EH, editor. Anionic surfactants. New York: Marcel Dekker; 1981.
[10] van den Tempel M. Proc Int Congr Surf Act. 1960;2:573.
[11] Walstra P, Smolders PEA. In: Binks BP, editor. Modern aspects of emulsions. Cambridge: The Royal Society of Chemistry; 1998.
[12] Griffin WC. J Cosmet Chemists. 1949;1:311; 1954;5:249.
[13] Davies JT. Proc Int Congr Surface Activity. Vol. 1. 1959. p. 426.
[14] Davies JT, Rideal EK. Interfacial phenomena. New York: Academic Press; 1969.
[15] Mollet H, Grubenmann A. Formulation Technology. Weinheim: Wiley-VCH; 2001.
[16] Tadros TF, Vincent B. In: Becher P, editor. Encyclopedia of Emulsion Technology. New York: Marcel Dekker; 1983.
[17] Shinoda K. J Colloid Interface Sci. 1967;25:396.
[18] Shinoda K, Saito H. J Colloid Interface Sci. 1969;30:258.
[19] Bachelor GK. J Fluid Mech. 1972;52:245.
[20] Tadros T. Rheology of Dispersions. Weinheim: Wiley-VCH; 2010.
[21] Asakura A, Oosawa F. J Chem Phys. 1954;22:1235; J Polymer Sci. 1958;33:183.
[22] Abend S, Holtze C, Tadros T, Schutenberger P. Langmuir. 2012;28:7967.
[23] van Olphen H. Clay colloid chemistry. New York: Wiley; 1963.
[24] Norrish K. Discussion Faraday Soc. 1954;18:120.
[25] Smoluchowski MV. Z Phys Chem. 1927;92:129.
[26] Fuchs N. Z Physik. 1936;89:736.
[27] Reerink H, Overbeek JTG. Discussion Faraday Soc. 1954;18:74.
[28] Tadros T. Interfacial phenomena and colloid stability. Vol. 1. Berlin: De Gruyter; 2015.
[29] Gregory J. In: Tadros T, editor. Solid/liquid dispersions. London: Academic Press; 1987.
[30] Thompson W (Lord Kelvin). Phil Mag. 1871;42:448.
[31] Lifshitz EM, Slesov VV. Soviet Physics JETP. 1959;35:331.
[32] Wagner C. Z Electrochem. 1961;35:581.
[33] Kabalnov AS, Schukin ED. Adv Colloid Interface Sci. 1992;38:69.
[34] Kabalnov AS, Makarov KN, Pertsov AV, Shchukin ED. J Colloid Interface Sci. 1990;138:98.
[35] Taylor P. Colloids and Surfaces A. 1995;99:175.
[36] Kabalanov AS. Langmuir. 1994;10:680.
[37] Taylor P, Ottewill RH. Colloids and Surfaces A. 1994;88:303.
[38] Anainsson EAG, Wall SN, Almagren M, Hoffmann H, Kielmann I, Ulbricht W, Zana R, Lang J, Tondre C. J Phys Chem. 1976;80:905.
[39] Weiss J, Coupland JN, Brathwaite D, McClemments DJ. Colloids and Surfaces A. 1997;121:53.
[40] Higuchi WI, Misra J. J Pharm Sci. 1962;51:459.

[41] Kabalnov AS, Pertsov AV, Shchukin ED. Colloids and Surfaces. 1987;24:19.
[42] Kabalnov AS, Pertsov AV, Aprosin YD, Shchukin ED. Kolloid Zh. 1995;47:1048.
[43] Walstra P. In: Binks BP, editor. Encyclopedia of emulsion technology. Vol. 4. New York: Marcel Dekker; 1996.
[44] Deryaguin BV, Scherbaker RL. Kolloid Zh. 1961;23:33.
[45] van den Tempel M. Rec Trav Chim. 1953;72:433, 442.
[46] Schulman JH, Cockbain EG. Transaction Faraday Soc. 1940;36:661.
[47] Prins A, van den Tempel M. Proc Int Congr Surface Activity (4th). Vol. II. London: Gordon and Breach; 1967. p. 1119.
[48] Prins A, Arcuri C, van den Tempel M. J Colloid and Interface Sci. 1967;24:811.
[49] Biswas B, Haydon DA. Proc Roy Soc. 1963;A271:296; 1963;A2:317.
[50] Friberg S, Jansson PO, Cederberg E. J Colloid Interface Sci. 1976;55:614.
[51] Exerowa D, Gotchev G, Kolarev T, Khristov K, Levecke B, Tadros T. Langmuir. 2007;23:1711.
[52] Ostwald WO. Kolloid Z. 1910;6:103; 1910;7:64.
[53] Shinoda K, Saito H. J Colloid Interface Sci. 1969;30:258.
[54] Sherman P. J Oc Chem Inc (London). 1950;69(Suppl. 2):570.
[55] Brooks BW, Richmond HN, Zefra M. Phase inversion and drop formation in agitated liquid-liquid dispersions. In: Binks BP, editor. Modern aspects of emulsion science. Cambridge: The Royal Society of Chemistry Publication; 1998.
[56] Marzall L. In: Schick MJ, editor. Nonionic surfactants: Physical chemistry. Surfactant Science Series, Vol. 23. New York: Marcel Dekker; 1967.
[57] Winsor PA. Trans Faraday Soc. 1948;44:376.
[58] Kabalnov AS. Coalescence in emulsions. In: Binks BP, editor. Modern aspects of emulsion science. Cambridge: The Royal Society of Chemistry Publication; 1998.

3 Formulation of foams

3.1 Introduction

A gas/liquid dispersion or foam consists of gas bubbles separated by liquid layers [1]. Because of the significant density difference between the gas bubbles and the medium, the system quickly separates into two layers with the gas bubbles rising to the top, which may undergo deformation to form polyhedral structures as will be discussed below.

Many examples can be given where a stable foam is required, e.g. foam produced at the top of beer, foam produced in shaving creams, firefighting foam, foam produced in many cakes and deserts, etc. However, with many industrial systems foam formation is undesirable, e.g. in dispersion of powders in liquids. In this case, foam inhibitors (antifoam) agents are required as will be discussed below.

Pure liquids cannot foam unless a surface active material, mostly a surfactant, is present. When a gas bubble is introduced below the surface of a liquid, it burst almost immediately as a soon as the liquid has drained away. With dilute surfactant solutions, as the liquid/air interface expands and the equilibrium at the surface is disturbed, a resorting force is set up which tries to establish the equilibrium. The restoring force arises from the Gibbs–Marangoni effect which was discussed in Chapter 2. As a result of the presence of surface tension gradients $d\gamma$ (due to incomplete coverage of the film by surfactant), a dilational elasticity ε is produced (Gibbs elasticity). This surface tension gradient induces flow of surfactant molecules from the bulk to the interface and these molecules carry liquid with them (the Marangoni effect). The Gibbs–Marangoni effect prevents thinning and disruption of the liquid film between the air bubbles and this stabilizes the foam.

Several surface active foaming materials may be distinguished, e.g. ionic, nonionic and zwitterionic surfactants, polymers (polymeric surfactants). Particles that accumulate at the air/solution interface can also stabilize the foam. In some cases, specifically adsorbed cations or anions from inorganic salts may also stabilize the foam bubbles. Many of the surfactants can cause foaming at extremely low concentrations (as low as 10^{-9} mol dm^{-3})

In kinetic terms foams may be classified into two main types, namely unstable, transient foams (lifetime of seconds) and metastable or permanent foams (lifetimes of hours or days).

https://doi.org/10.1515/9783110587968-004

3.2 Foam preparation

Like most disperse systems, foams can be obtained by condensation (top-down) and dispersion (bottom-up) methods. The condensation methods for generating foam involve creating gas bubbles in the solution by decreasing the external pressure, by increasing temperature or as a result of chemical reaction. Thus, bubble formation may occur through homogeneous nucleation that occurs at high supersaturation or heterogeneous nucleation (e.g. from catalytic sites) that occurs at low supersaturation. The most frequently applied technique for generating foam is by a simple dispersion technique (mechanical shaking or whipping). This method is not satisfactory since accurate control of the amount of air incorporated is difficult to achieve. The most convenient method is to pass a flow of gas (sparging) through an orifice with well-defined radius r_0.

The size of the bubbles (produced at an orifice) r may be roughly estimated from the balance of the buoyancy force F_b with the surface tension force F_s [1],

$$F_b = (4/3)\pi r^3 \rho g, \tag{3.1}$$

$$F_s = 2\pi r_0 \gamma, \tag{3.2}$$

$$r = \left(\frac{3\gamma r_0}{2\rho g}\right)^{1/3}. \tag{3.3}$$

r and r_0 are the radii of the bubble and orifice, ρ is the specific gravity of liquid, g is the acceleration due to gravity and γ is the gas/liquid surface tension.

Since the dynamic surface tension of the growing bubble is greater than the equilibrium tension, the contact base may spread, depending on the wetting conditions. Thus, the main problem is the value of γ to be used in equation (3.3). Another important factor that controls bubble size is the adhesion tension $\gamma \cos\theta$, where θ is the dynamic contact angle of the liquid on the solid of the orifice. With a hydrophobic surface, a bubble develops with a greater size than the hole. One should always distinguish between the equilibrium contact angle θ and the dynamic contact angle, θ_{dyn}, during bubble growth. As the bubble detaches from the orifice, the dimensions of the bubble will determine the velocity of the rise. The rise of the bubble through the liquid causes a redistribution of surfactant on the bubble surface, with the top having a reduced concentration and the polar base having a higher concentration than the equilibrium value. This unequal distribution of surfactant on the bubble surface has an important role in foam stabilization (due to the surface tension gradients). When the bubble reaches the interface, a thin liquid film is produced on its top. The lifetime of this thin film depends on many factors, e.g. surfactant concentration, rate of drainage, surface tension gradient, surface diffusion and external disturbances.

3.3 Foam structure

Two main types of foams may be distinguished [1]:

(i) Spherical foam ("Kugelschaum") consisting of gas bubbles separated by thick films of viscous liquid produced in freshly prepared systems. This may be considered a temporary dilute dispersion of bubbles in the liquid.

(ii) Polyhedral gas cells produced on aging; thin flat "walls" are produced with junction points of the interconnecting channels (Plateau borders). Due to the interfacial curvature, the pressure is lower and the film is thicker in the plateau border. A capillary suction effect of the liquid occurs from the centre of the film to its periphery.

The pressure difference between neighbouring cells, Δp, is related to the radius of curvature (r) of the Plateau border by,

$$\Delta p = \frac{2\gamma}{r}. \tag{3.4}$$

In a foam column, several transitional structures may be distinguished as illustrated in Fig. 3.1. Near the surface, a high gas content (polyhedral foam) is formed, with a much lower gas content structure near the base of the column (bubble zone). A transition state may be distinguished between the upper and bottom layers. The drainage of excess liquid from the foam column to the underlying solution is initially driven by hydrostatic pressure, which causes the bubble to become distorted. Foam collapse usually occurs from the top to the bottom of the column. The films in the polyhedral foam are more susceptible to rupture by shock, temperature gradient or vibration.

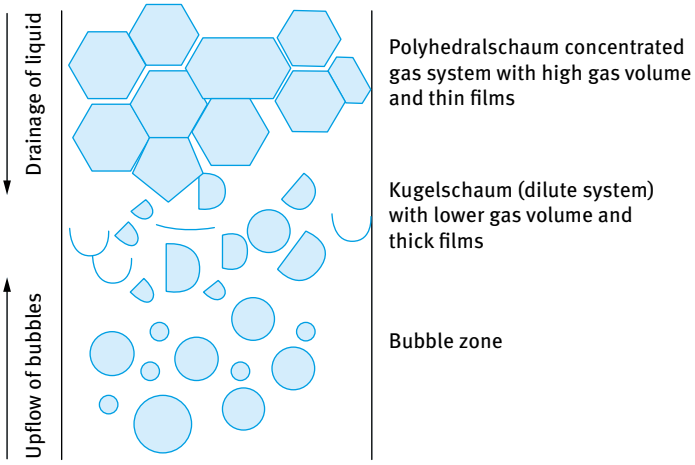

Fig. 3.1: Schematic representation of a foam structure in a column.

Another mechanism of foam instability is due to Ostwald ripening (disproportionation). The driving force for this process is the difference in Laplace pressure between the small and the larger foam bubbles. The smaller bubbles have higher Laplace pressure than the larger ones. The gas solubility increases with pressure and hence gas molecules will diffuse from the smaller to the larger bubbles. This process only occurs with spherical foam bubbles. This process may be opposed by the Gibbs elasticity effect. Alternatively rigid films produced using polymers may resist Ostwald ripening as a result of the high surface viscosity.

With polyhedral foam with planer liquid lamella, the pressure difference between the bubbles is not large and hence Ostwald ripening is not the mechanism for foam instability in this case. With polyhedral foam, the main driving force for foam collapse is the surface forces that act across the liquid lamella.

To keep the foam stable (i.e. to prevent complete rupture of the film), this capillary suction effect must be prevented by an opposing "disjoining pressure" that acts between the parallel layers of the central flat film (see below). The generalized model for drainage involves the Plateau borders forming a "network" through which the liquid flows due to gravity.

3.4 Classification of foam stability

As with most disperse systems, all foams are thermodynamically unstable [1]. This is due to the high interfacial free energy $\Delta A\gamma$ (where ΔA is the increase in interfacial area when producing the foam bubbles and γ is the surface tension) that exceeds the entropy of dispersion $T\Delta S$ (where T is the absolute temperature and ΔS is the increase in entropy in forming a large number of air bubbles. Thus, the free energy of formation of a foam ΔG,

$$\Delta G = \Delta A\gamma - T\Delta S \tag{3.5}$$

is positive and foam formation is nonspontaneous and the resulting foam is thermodynamically unstable.

For convenience foams, are classified according to the kinetics of their breakdown:

(i) Unstable (transient) foams, with a lifetime of seconds. These are generally produced using "mild" surfactants, e.g. short chain alcohols, aniline, phenol, pine oil, short chain undissociated fatty acid. Most of these compounds are sparingly soluble and may produce a low degree of elasticity.

(ii) Metastable ("permanent") foams, with a lifetime of hours or days. These metastable foams are capable of withstanding ordinary disturbances (thermal or Brownian fluctuations). They can collapse from abnormal disturbances (evaporation, temperature gradients, etc.).

The above metastable foams are produced from surfactant solutions near or above the critical micelle concentration (cmc). The stability is governed by the balance of surface forces (see below). The film thickness is comparable to the range of intermolecular forces. In the absence of external disturbances, these foams may stay stable indefinitely. They are produced using proteins, long chain fatty acids or solid particles. Gravity is the main driving force for foam collapse, directly or indirectly through the Plateau border. Thinning and disruption may be opposed by surface tension gradients at the air/water interface. Alternatively the drainage rate may be decreased by increasing the bulk viscosity of the liquid (e.g. addition of glycerol or polymers). Stability may be increased in some cases by the addition of electrolytes that produce a "gel network" in the surfactant film. Foam stability may also be enhanced by increasing the surface viscosity and/or surface elasticity. High packing of surfactant films (high cohesive forces) may also be produced using mixed surfactant films or surfactant/polymer mixtures.

For investigating foam stability one must consider the role of the Plateau border under dynamic and static conditions. One should also consider foam films with intermediate lifetimes, i.e. between unstable and metastable foams.

3.5 Drainage and thinning of foam films

As mentioned above, gravity is the main driving force for film drainage. Gravity can act directly on the film or through capillary suction in the Plateau borders. As a general rule, the rate of drainage of foam films may be decreased by increasing the bulk viscosity of the liquid from which the foam is prepared. This can be achieved by adding glycerol or high molecular weight poly(ethylene oxide). Alternatively, the viscosity of the aqueous surfactant phase can be increased by addition of electrolytes that form a "gel" network (liquid crystalline phases may be produced). Film drainage can also be decreased by increasing the surface viscosity and surface elasticity. This can be achieved, for example, by addition of proteins, polysaccharides and even particles. These systems are applied in many food foams.

Most quantitative studies on film drainage have been carried out by Scheludko and co-workers [2–5] who studied the drainage of small horizontal films using a specially designed measuring system, illustrated in Fig. 3.2.

The foam film c is formed in the middle of a biconcave drop b, situated in a glass tube of radius R, by withdrawing liquid from it (A and B) and in the hole of a porous plate g (C). A suitable tube diameter in A and B is 0.2–0.6 mm and the film radius ranges from 100 to 500 nm. In C, the hole radius can be considerably smaller, in the range of 120 μm and the film radius is 10 μm. The film can be observed under the microscope and when it thins to form the so-called "black" film, black spots are observed under the microscope.

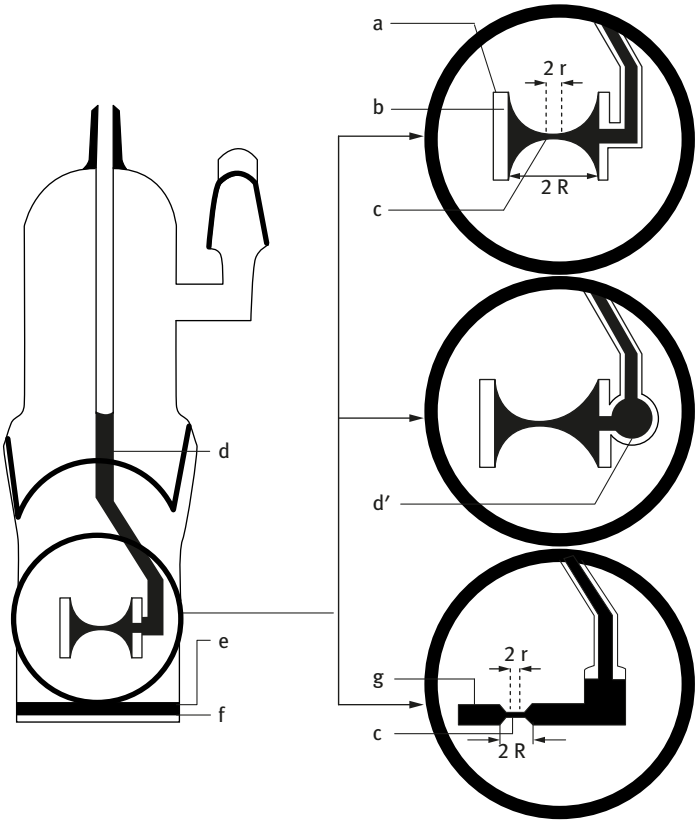

Fig. 3.2: Cell used for studying macroscopic foam films: (A) in a glass tube; (B) with a reservoir of surfactant solution d'; (C) in a porous plate. (a) glass tube film holder; (b) biconcave drop; (c) macroscopic foam film; (d) glass capillary; (e) surfactant solution; (f) optically flat glass; (g) porous plate.

The film thickness is determined by interferometry, which is based on comparison between the intensities of the light falling on the film and that reflected from it [4].

The drainage time T is determined and compared to the theoretical value for a flat film calculated from the Reynolds equation [6],

$$T = \int_{h_t}^{h_0} \frac{\mathrm{d}h}{V}. \tag{3.6}$$

h_0 is the initial film thickness and h_t is the value after time t. V is the velocity of thinning $V = -\mathrm{d}h/\mathrm{d}t$.

For horizontal, fairly thick films (> 100 nm), Scheludko [3] derived an expression for the thinning between two disc surfaces under the influence of a uniform external pressure. The change in film thickness with drainage time, V_{re}, is given by the expression,

$$V_{re} = -\frac{dh}{dt} = \frac{2h^3\Delta P}{3\eta R^2}, \tag{3.7}$$

where R is the radius of the disc, η is the viscosity of the liquid and ΔP is the difference in pressure between the film and bulk solution. ΔP was taken to be equal to the capillary pressure in the Plateau border. For very thin films, the pressure gradient also includes the disjoining pressure (see below).

Equation (3.7) applies for the following conditions:

(i) the liquid flows between parallel plane surfaces;
(ii) the film surfaces are tangentially immobile;
(iii) the rate of thinning due to evaporation is negligible compared to the thinning due to drainage.

Experimental results obtained by Scheludko and co-workers [2–4] with comparatively thick rigid films produced from dilute solutions of sodium oleate and isoamyl alcohol, gave reasonably good agreement with the drainage equation. However, deviation from the Reynolds equation was observed in many cases due to tangential surface mobility. Surface viscosity can also slow down the drainage. A schematic representation of film drainage is given in Fig. 3.3 [5].

Fig. 3.3 (a) represents the case for thick film (> 100 nm), where the drainage velocity can be determined from the Reynolds equation. Fig. 3.3 (b) represents the case for most surfactant films, where the surfaces are not rigid and the tangential velocity at the surface is not zero. Fig. 3.3 (c) represents the case where surface mobility during drainage causes interfacial tension gradients. Fig. 3.3 (d) represents the case where surface diffusion along the surface and from the bulk solution occurs with both adsorption and convective flow. For thinner films, large electrostatic repulsive interactions can reduce the driving force for film drainage and may lead to stable films. For thick films that contain high surfactant concentrations (> cmc), the micelles present in the film can produce a repulsive structural mechanism.

The drainage of vertical films was investigated by pulling a frame out of a reservoir containing a surfactant solution. Three stages could be identified:

(i) initial formation of the film that is determined by the withdrawal velocity;
(ii) drainage of the film within the lamella which causes thinning with time;
(iii) aging of the film, which may result in the formation of a metastable film.

Assuming that the monolayer of the surfactant film at the boundaries of the film is rigid, film drainage may be described by the viscous flow of the liquid under gravity between two parallel plates. As the process proceeds, thinning can also occur by a horizontal mechanism, known as marginal regeneration [7–9], in which the liquid is

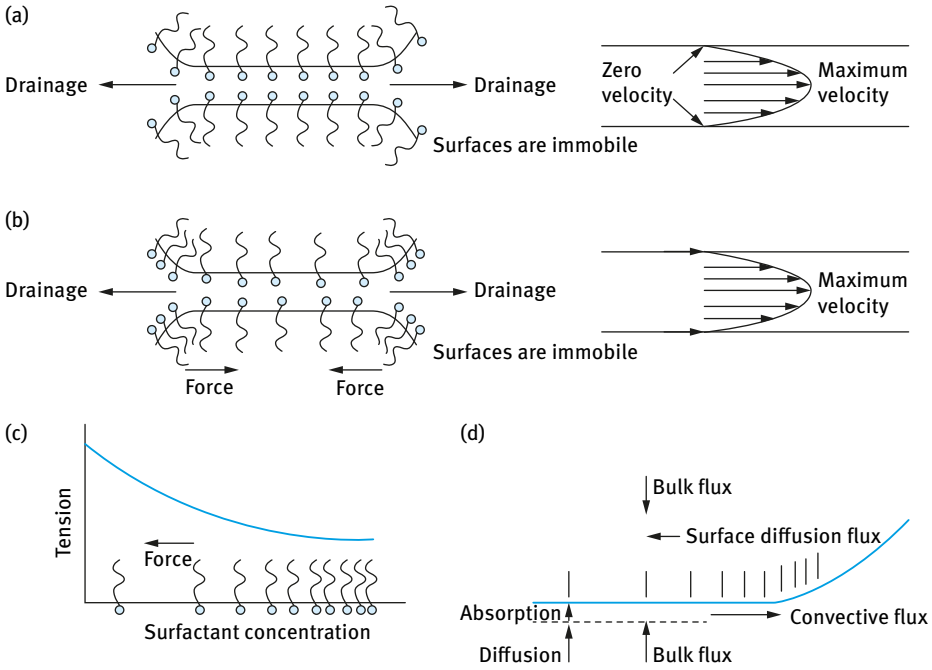

Fig. 3.3: Schematic representation of film drainage: (a) thick rigid films; (b) mobile surfactant films; (c) interfacial tension gradients; (d) diffusion along the surface and from bulk solution [5].

drained from the film near the border region and exchanged within the low pressure plateau border. Marginal regeneration is probably the most important cause of film drainage in films with mobile surfaces, i.e. at surfactant concentrations above the cmc.

3.6 Theories of foam stability

3.6.1 Surface viscosity and elasticity theory

The adsorbed surfactant film is assumed to control the mechanical-dynamical properties of the surface layers by virtue of its surface viscosity and elasticity. This concept may be true for thick films (> 100 nm) whereby intermolecular forces are less dominant (i.e. foam stability under dynamic conditions). Surface viscosity reflects the speed of the relaxation process which restores the equilibrium in the system after imposing a stress on it. Surface elasticity is a measure of the energy stored in the surface layer as a result of an external stress.

The viscoelastic properties of the surface layer are important parameters. The most useful techniques to study the viscoelastic properties of surfactant monolayers are the surface scattering methods. When transversal ripples occur, periodic dilation

and compression of the monolayer occurs and this can be accurately measured. This enables one to obtain the viscoelastic behaviour of monolayers under equilibrium and non-equilibrium conditions, without disturbing the original sate of the adsorbed layer. Some correlations have been found between surface viscosity and elasticity and foam stability, e.g. when adding lauryl alcohol to sodium lauryl sulphate which tends to increase the surface viscosity and elasticity [10].

3.6.2 The Gibbs–Marangoni effect theory

The Gibbs coefficient of elasticity, ε, was introduced as a variable resistance to surface deformation during thinning:

$$\varepsilon = 2\left(\frac{\mathrm{d}\gamma}{\mathrm{d}\ln A}\right) = -2\left(\frac{\mathrm{d}\gamma}{\mathrm{d}\ln h}\right). \tag{3.8}$$

$\mathrm{d}\ln h$ is the relative change in lamella thickness. ε is the "film elasticity of compression modulus" or "surface dilational modulus". ε is a measure of the ability of the film to adjust its surface tension to an instant stress. In general, the higher the value of ε the more stable the film is. ε depends on surface concentration and film thickness. For a freshly produced film to survive, a minimum ε is required [8].

The main deficiency of early studies on Gibbs elasticity was that it was applied to thin films and the diffusion from the bulk solution was neglected. In other words, the Gibbs theory applies to the case where there are insufficient surfactant molecules in the film to diffuse to the surface and lower the surface tension. This is clearly not the case with most surfactant films. For thick lamella under dynamic conditions, one should consider diffusion from the bulk solution, i.e. the Marangoni effect. The Marangoni effect tends to oppose any rapid displacement of the surface (Gibbs effect) and may provide a temporary restoring force to "dangerously" thin films. In fact, the Marangoni effect is superimposed on the Gibbs elasticity, so that the effective restoring force is a function of the rate of extension, as well as the thickness. When the surface layers behave as insoluble monolayers, then the surface elasticity has its greatest value and is referred to as the Marangoni dilational modulus, ε_{m}.

The Gibbs–Marangoni effect explains the maximum foaming behaviour at intermediate surfactant concentration [5]. At low surfactant concentrations (well below the cmc), the greatest possible differential surface tension will only be relatively small (Fig. 3.4 (a)) and little foaming will occur. At very high surfactant concentration (well above the cmc), the differential tension relaxes too rapidly because of the supply of surfactant which diffuses to the surface (Fig. 3.4 (c)). This causes the restoring force to have time to counteract the disturbing forces and produces a dangerously thinner film and foaming is poor. It is the intermediate surfactant concentration range that produces maximum foaming (Fig. 3.4 (b)).

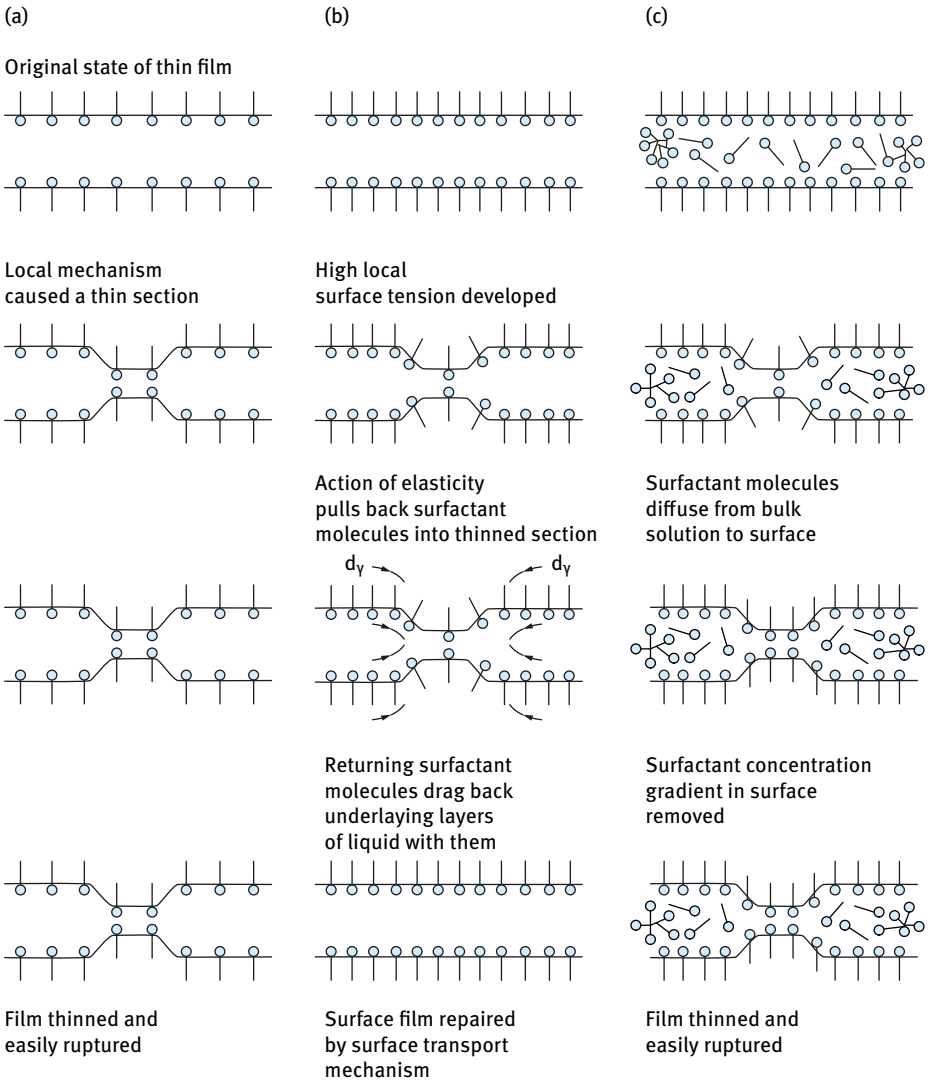

Fig. 3.4: Schematic representation of the Gibbs–Marangoni effect: (a) low surfactant concentration (< cmc); (b) intermediate surfactant concentration; (c) high surfactant concentration (> cmc).

3.6.3 Surface forces theory (disjoining pressure π)

This theory operates under static (equilibrium) conditions in relatively dilute surfactant solutions ($h < 100$ nm). In the early stages of formation, foam films drain under the action of gravitation or capillary forces. Provided the films remain stable during this drainage stage, they may approach a thickness in the range of 100 nm. At this stage, surface forces come into play, i.e. the range of the surface forces now becomes

comparable to the film thickness. Deryaguin and co-workers [11, 12] introduced the concept of disjoining pressure which should remain positive to slow down further drainage and film collapse. This is the principle of formation of thin metastable (equilibrium) films.

In addition to the Laplace capillary pressure, three additional forces can operate at surfactant concentration below the cmc: electrostatic double layer repulsion π_{el}, van der Waals attraction π_{vdW} and steric (short-range) forces π_{st},

$$\pi = \pi_{el} + \pi_{vdw} + \pi_{st}. \tag{3.9}$$

In the original definition of disjoining pressure by Deryaguin [11, 12], he only considered the first two terms on the right-hand side of equation (3.9). At low electrolyte concentrations, double layer repulsion predominates and π_{el} can compensate the capillary pressure, i.e. $\pi_{el} = P_c$. This results in the formation of an equilibrium-free film which is usually referred to as the thick common film CF (≈ 50 nm thickness). This equilibrium metastable film persists until thermal or mechanical fluctuations cause rupture. The stability of the CF can be described in terms of the theory of colloid stability due to Deryaguin, Landau [13] and Verwey and Overbeek [14] (DLVO theory).

The critical thickness value at which the CF ruptures (due to thickness perturbations) fluctuates and an average value h_{cr} may be defined. However, an alternative situation may occur as h_{cr} is reached and instead of rupturing a metastable film (high stability) may be formed with a thickness $h < h_{cr}$. The formation of this metastable film can be experimentally observed through the formation of "islands of spots" which appear black in light reflected from the surface. This film is often referred to a "first black" or "common black" film. The surfactant concentration at which this "first black" film is produced can be 1–2 orders of magnitude lower than the cmc.

Further thinning can cause an additional transformation into a thinner stable region (a stepwise transformation). This usually occurs at high electrolyte concentrations which leads to a second, very stable, thin black film usually referred to as Newton secondary black film, with a thickness in the region of 4 nm. Under these conditions, the short range steric or hydration forces control the stability and this provided the third contribution to the disjoining press, π_{st} described in equation (3.9).

Fig. 3.5 shows a schematic representation of the variation of disjoining pressure π with film thickness h, which shows the transition from the common film to the common black film and to the Newton black film. The common black film has a thickness in the region of 30 nm, whereas the Newton black film has a thickness in the region of 4–5 nm, depending on electrolyte concentration.

Several investigations have been carried out to study the above transitions from common film to common black film and finally to Newton black film. For sodium dodecyl sulphate, the common black films have thicknesses ranging from 200 nm in very dilute system to about 5.4 nm. The thickness depends strongly on electrolyte concentration and their stability may be considered to be caused by the secondary minimum in the energy–distance curve. In cases where the film thins further and overcomes

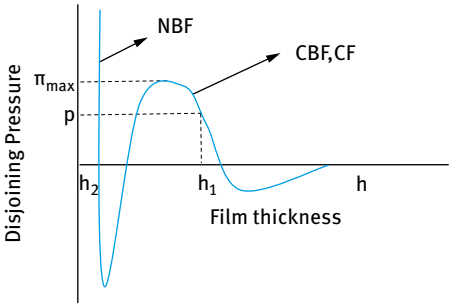

Fig. 3.5: Variation of disjoining pressure with film thickness.

the primary energy maximum, it will fall into the primary minimum potential energy sink, where very thin Newton black films are produced. The transition from common black films to Newton black films occurs at a critical electrolyte concentration which depends on the type of surfactant.

The rupture mechanisms of thin liquid films were considered by de Vries [15] and by Vrij and Overbeek [16]. It was assumed that thermal and mechanical disturbances (having a wave-like nature) cause film thickness fluctuations (in thin films) leading to rupture or coalescence of bubbles at a critical thickness. Vrij and Overbeek [16] carried out a theoretical analysis of the hydrodynamic interfacial force balance, and expressed the critical thickness of rupture in terms of the attractive van der Waals interaction (characterized by the Hamaker constant A), the surface or interfacial tension γ and disjoining pressure. The critical wavelength, λ_{crit}, for the perturbation to grow (assuming the disjoining pressure just exceeds the capillary pressure) was determined. Film collapse occurs when the amplitude of the fast growing perturbation was equal to the thickness of the film. The critical thickness of rupture, h_{cr}, was defined by the following equation,

$$h_{crit} = 0.267\left(\frac{a_f A^2}{6\pi\gamma\Delta p}\right)^{1/7}, \tag{3.10}$$

where a_f is the area of the film.

Many poorly foaming liquids with thick film lamella are easily ruptured, e.g. pure water and ethanol films (with thickness between 110 and 453 nm). Under these conditions, rupture occurs by growth of disturbances which may lead to thinner sections [17]. Rupture can also be caused by spontaneous nucleation of vapour bubbles (forming gas cavities) in the structured liquid lamella [18]. An alternative explanation for rupture of relatively thick aqueous films containing low level of surfactants is the hydrophobic attractive interaction between the surfaces that may be caused by bubble cavities [19, 20].

3.6.4 Stabilization by micelles (high surfactant concentrations > cmc)

At high surfactant concentrations (above the cmc), micelles of ionic or nonionic surfactants can produce organized molecular structures within the liquid film [21, 22]. This will provide an additional contribution to the disjoining pressure. Thinning of the film occurs through a stepwise drainage mechanism, referred to as stratification [23]. The ordering of surfactant micelles (or colloidal particles) in the liquid film due to the repulsive interaction provides an additional contribution to the disjoining pressure and this prevents the thinning of the liquid film.

3.6.5 Stabilization by lamellar liquid crystalline phases

This is particularly the case with nonionic surfactants that produce lamellar liquid crystalline structure in the film between the bubbles [24, 25]. These liquid crystals reduce film drainage as a result of the increase in viscosity of the film. In addition, the liquid crystals act as a reservoir of surfactant of the optimal composition to stabilize the foam.

3.6.6 Stabilization of foam films by mixed surfactants

It has been found that a combination of surfactants gives slower drainage and improved foam stability. For example, mixtures of anionic and nonionic surfactants or anionic surfactant and long chain alcohol produce much more stable films than the single components. This could be attributed to several factors. For example, addition of a nonionic surfactant to an anionic surfactant causes a reduction in the cmc of the anionic. The mixture can also produce lower surface tension compared to the individual components. The combined surfactant system also has a high surface elasticity and viscosity when compared with the single components.

3.7 Foam inhibitors

Two main types of inhibition may be distinguished, namely antifoamers that are added to prevent foam formation and deformers that are added to eliminate an existing foam. For example, alcohols such as octanol are effective as defoamers but ineffective as antifoamers. Since the drainage and stability of liquid films is far from being fully understood, it is very difficult at present to explain the antifoaming and foam breaking action obtained by addition of substances. This is also complicated by the fact that in many industrial processes foams are produced by unknown impurities. For these reasons, the mechanism of action of antifoamers and defoamers is far from

being understood [26]. A summary of the various methods that can be applied for foam inhibition and foam breaking is given below.

3.7.1 Chemical inhibitors that lower viscosity and increase drainage

Chemicals that reduce the bulk viscosity and increase drainage can cause a decrease in foam stability. The same applies for materials that reduce surface viscosity and elasticity (swamping the surface layer with excess compound of lower viscosity).

It has been suggested that a spreading film of antifoam may simply displace the stabilizing surfactant monolayer. As the oil lens spreads and expands on the surface, the tension will be gradually reduced to a lower uniform value. This will eliminate the stabilizing effect of the interfacial tension gradients, i.e. elimination of surface elasticity.

Reduction of surface viscosity and elasticity may be achieved by low molecular weight surfactants. This will reduce the coherence of the layer, e.g. by addition of small amounts of nonionic surfactants. These effects depend on the molecular structure of the added surfactant. Other materials which are not surface active can also destabilize the film by acting as cosolvents and reduce the surfactant concentration in the liquid layer. Unfortunately, these nonsurface-active materials, such as methanol or ethanol, need to be added in large quantities (> 10 %).

3.7.2 Solubilized chemicals which cause antifoaming

It has been demonstrated that solubilized antifoamers such as tributyl phosphate and methyl isobutyl carbinol when added to surfactant solutions such as sodium dodecyl sulphate and sodium oleate may reduce foam formation [27]. In cases where the oils exceed the solubility limit, the emulsifier droplets of oil can have a great influence on the antifoam action. It has been claimed [27] that the oil solubilized in the micelle causes a weak defoaming action. Mixed micelle formation with extremely low concentrations of surfactant may explain the actions of insoluble fatty acid esters, alkyl phosphate esters and alkyl amines.

3.7.3 Droplets and oil lenses which cause antifoaming and defoaming

Undissolved oil droplets form in the surface of the film and this can lead to film rupture. Several examples of oils may be used: Alkyl phosphates, diols, fatty acid esters and silicone oils (polydimethyl siloxane).

A widely accepted mechanism for the antifoaming action of oils considers two steps: the oil drops enter the air/water interface; the oil spreads over the film causing rupture.

The antifoaming action can be rationalized [28] in terms of the balance between the entering coefficient E and the Harkins [29] spreading coefficient S which are given by the following equations,

$$E = \gamma_{W/A} + \gamma_{W/O} - \gamma_{O/A}, \tag{3.11}$$

$$S = \gamma_{W/A} - \gamma_{W/O} - \gamma_{O/A}, \tag{3.12}$$

where $\gamma_{W/A}$, $\gamma_{O/A}$ and $\gamma_{W/O}$ are the macroscopic interfacial tensions of the aqueous phase, oil phase and interfacial tension of the oil/water interface respectively.

Ross and McBain [30] suggested that for efficient defoaming, the oil drop must enter the air/water interface and spreads to form a duplex film at both sides of the original film. This leads to displacement of the original film, leaving an oil film which is unstable and can easily break. Ross [28] used the spreading coefficient (equation (3.12)) as a defoaming criteria.

For antifoaming both E and S should be > 0 for entry and spreading. A schematic representation of oil entry and the balance of the relevant tensions is given in Fig. 3.6 [5].

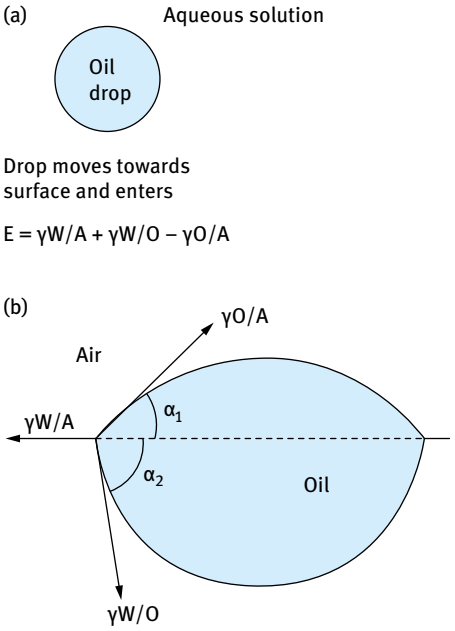

Fig. 3.6: Schematic representation of entry of oil droplet into the air/water interface (a) and its further spreading (b).

A typical example of this type of spreading/breaking is illustrated for a hydrocarbon surfactant stabilized film. For most surfactant systems, $\gamma_{AW} = 35–45\ mN\ m^{-1}$ and $\gamma_{OW} = 5–10\ mN\ m^{-1}$ and hence for an oil to act as an antifoaming agent γ_{OA} should be less than $25\ mN\ m^{-1}$. This shows why low surface tension silicone oils which have surface tensions as low as $10\ mN\ m^{-1}$ are effective.

3.7.4 Surface tension gradients (induced by antifoamers)

It has been suggested that some antifoamers act by eliminating the structure tension gradient effect in foam films by reducing the Marangoni effect. Since spreading is driven by a surface tension gradient between the spreading front and the leading edge of the spreading front, then thinning and foam rupture can occur by this surface tension gradient acting as a shear force (dragging the underlying liquid away from the source). This could be achieved by solids or liquids containing surfactant other than that stabilizing the foam. Alternatively, liquids that contain foam stabilizers at higher concentrations than that present in the foam may also act by this mechanism. A third possibility is the use of adsorbed vapours of surface active liquids.

3.7.5 Hydrophobic particles as antifoamers

Many solid particles with some degree of hydrophobicity have been shown to cause destabilization of foams, e.g. hydrophobic silica, PTFE particles. These particles exhibit a finite contact angle when adhering to the aqueous interface. It has been suggested that many of these hydrophobic particles can deplete the stabilizing surfactant film by rapid adsorption and can cause weak spots in the film.

A further mechanism was suggested based on the degree of wetting of the hydrophobic particles [31] and this led to the idea of particle bridging. For large smooth particles (large enough to touch both surfaces and with a contact angle $\theta > 90°$) dewetting can occur. Initially the Laplace pressure in the film adjacent to the particle becomes positive and causes liquid to flow away from the particle, leading to enhanced drainage and formation of a "hole". In the case of $\theta < 90°$, then initially the situation is the same as for $\theta > 90°$, but as the film drains it attains a critical thickness where the film is planar and the capillary pressure becomes zero. At this point, further drainage reverses the sign of the radii of curvature causing unbalanced capillary forces which prevent drainage occurring. This can cause a stabilizing effect for certain types of particles. This means that a critical receding contact angle is required for efficient foam breaking.

With particles containing rough edges, the situation is more complex, as demonstrated by Johansson and Pugh [32], using finely ground quartz particles of different size fractions. The particle surfaces were hydrophobized by methylation. These studies and others reported in the literature confirmed the importance of size, shape and hydrophobicity of the particles on foam stability.

3.7.6 Mixtures of hydrophobic particles and oils as antifoamers

The synergetic antifoaming effect of mixtures of insoluble hydrophobic particles and hydrophobic oils when dispersed in aqueous medium has been well established in the patent literature. These mixed antifoamers are very effective at very low concentrations (10–100 ppm). The hydrophobic particles could be hydrophobized silica and the oil is polydimethyl siloxane (PDMS).

One possible explanation for the synergetic effect is that the spreading coefficient of PDMS oil is modified by the addition of hydrophobic particles. It has been suggested that the oil–particle mixtures form composite entities where the particles can adhere to the oil–water interface. The presence of particles adhering to the oil–water interface may facilitate the emergence of oil droplets into the air–water interface to form lenses leading to rupture of the oil–water–air film.

3.8 Physical properties of foams

3.8.1 Mechanical properties

The compressibility of a foam is determined by the ability of the gas to compress, its wetting power that is determined by the properties of the foaming solution [4]. As with any disperse system, a foam may acquire the properties of a solid body, i.e. it can maintain its shape and it possesses a shear modulus (see below).

One of the basic mechanical properties of foams is its compressibility [4] (elasticity) and a bulk modulus E_v may be defined by the following expression,

$$E_v = -\frac{dp_0}{d\ln V}, \tag{3.13}$$

where p_0 is the external pressure, causing deformation and V is the volume of the deforming system.

By taking into account the liquid volume V_L, the modulus of bulk elasticity of the "wet" foam E'_v is given by the expression,

$$E_v = \frac{dp_0}{d\ln V_F} = \frac{V_F\, dp_0}{d(V_L + V_G)} = E_v\left(1 + \frac{V_L}{V_G}\right). \tag{3.14}$$

Thus, the real modulus of bulk elasticity ("wet" foam) is higher than E_v ("dry" foam).

3.8.2 Rheological properties

Like any disperse system, foams produce non-Newtonian systems and to characterize their rheological properties one needs to obtain information on the elasticity modulus (modulus of compressibility and expansion), the shear modulus, yield stress and effective viscosity, elastic recovery, etc.

It is difficult to study the rheological properties of a foam since on deformation its properties change. The most convenient geometry to measure foam rheology is to use a parallel plate. The rheological properties could be characterized by a variable viscosity [4],

$$\eta = \eta^*(\dot{\gamma}) + \frac{\tau_\beta}{\dot{\gamma}}, \tag{3.15}$$

where γ is the shear rate.

The shear modulus of a foam is given by,

$$G = \frac{\tau_\beta \Delta l}{H}, \tag{3.16}$$

where Δl is the shear deformation and H is the distance between parallel plates in the rheometer.

Deryaguin [33] obtained the following expression for the shear modulus,

$$G = \frac{2}{5}p_\gamma = \frac{2}{5}\left(\frac{2}{3}\gamma\varepsilon\right) \approx \frac{4\gamma}{3R_\mathrm{v}}, \tag{3.17}$$

where R_v is the average volume of the bubble and ε is the specific surface area.

Bikerman [34] obtained the following equation for the yield stress of a foam,

$$\tau_\beta = 0.5\frac{N_\mathrm{f}}{N_\mathrm{F} - 1}p_\gamma \cos\theta \approx \frac{\gamma}{R}\cos\theta, \tag{3.18}$$

where N_f is the number of films contacting the plate per unit area and θ is the average angle between the plate and the film.

Princen [35] used a two-dimensional hexagonal package model to derive an expression for the shear modulus and yield stress of a foam, taking into account the foam expansion ratio and the contact angles,

$$G = 0.525\frac{\gamma\cos\theta}{R}\phi^{1/2}, \tag{3.19}$$

$$\tau_\beta = 1.05\frac{\gamma\cos\theta}{R}\phi^{1/2}F_\mathrm{max}, \tag{3.20}$$

where F_max is a coefficient that is equal to 0.1–0.5, depending on the gas volume fraction ϕ.

For a "dry" foam ($\phi \to 1$), the yield stress can be calculated from the expression,

$$\tau_\beta = 0.525\gamma\cos\frac{\theta}{R}. \tag{3.21}$$

For real foams, the value of τ_β can be expressed by the general expression,

$$\tau_\beta = C\frac{\gamma \cos\theta}{R}\phi^{1/3}F_{\max}, \tag{3.22}$$

where C is a coefficient that is approximately equal to 1.

3.8.3 Electrical properties

Only the liquid phase in a foam possesses electrical conductivity. The specific conductivity of a foam, κ_F, depends on the liquid content and its specific conductivity κ_L,

$$\kappa_F = \frac{\kappa_L}{nB}, \tag{3.23}$$

where n is the foam expansion ratio and B is a structural coefficient that depends on the foam expansion ratio and the liquid phase distribution between the Plateau borders. B changes monotonically from 1.5 to 3 with increasing foam expansion factor.

3.8.4 Electrokinetic properties

In foams with charged gas/liquid interface, one can obtain various electrokinetic parameters, such as streaming potential and zeta potential ζ. For example, the relation between the volumetric flow of a liquid Q flowing through a capillary or membrane, the electric current I and ζ is given by,

$$Q = \frac{\varepsilon\varepsilon_0\zeta I}{\eta\kappa} = \frac{\varepsilon\varepsilon_0\zeta r^2}{\eta}\frac{\Delta V}{L}, \tag{3.24}$$

where ε is the permittivity of the liquid and ε_0 is the permittivity of free space, I is the value of the electric current, η is the viscosity of the liquid, r is the capillary radius, L is its length and ΔV is the potential distance between the electrodes placed at the capillary ends.

The interpretation of electrokinetic results is complicated because of surface mobility and border and film elasticity, which causes large non-homogeneities in density and border radii at hydrostatic equilibrium and liquid motion.

3.8.5 Optical properties

The extinction of the luminous flux passing through a foam layer occurs as a result of light scattering (reflection, refraction, interference and diffraction from the foam elements) and light absorption by the solution [4]. In polyhedral foam, there are three

structural elements that can be clearly distinguished by their optical properties: films, Plateau border and vertexes.

The optical properties of single foam films have been extensively studied, but those of the foam as disperse system are poorly considered. It has been concluded that the extinction of luminous flux (I/I_0, where I is the intensity of the light passing through the foam and I_0 is the intensity of the incident light) is a linear function of the specific foam area. This can be used to determine the specific surface area of a foam.

3.9 Experimental techniques for studying foams

3.9.1 Techniques for studying foam films

Most quantitative studies on foams have been carried out using foam films. As discussed above, microscopic horizontal films were studied by Scheludko and co-workers [2–4]. The foam thickness was determined by interferometry. Studies on vertical films were carried out by Mysels and collaborators [5–7].

One of the most important characteristics of foam films is the contact angle θ appearing at the contact of the film with the bulk phase (solution) from which it is formed. This can be obtained by a topographic technique (that is suitable for small contact angles) that is based on determination of the radii of the interference Newton rings when the film is observed in a reflected monochromatic light.

Another technique for studying foam films is to use α-particle irradiation, which can destroy the film. Depending on the intensity of the α-source, the film either ruptures instantaneously or lives for a much shorter time than required for its spontaneous rupture. The lifetime τ_a of a black film subjected to irradiation is considered as a parameter characterizing the destructive effect of α-particles.

A third technique for studying foam films is fluorescence recovery after photobleaching (FRAP). This technique was applied by Clark et al. [36] for lateral diffusion in foam films. The technique involves irreversible photobleaching of fluorophore molecules in the sample by intense laser light. The time for redistribution of probe molecules (assumed to be randomly distributed within the constitutive membrane lipids in the film) is monitored. The lateral diffusion coefficient, D, is calculated from the rate of recovery of fluorescence in the bleaching region due to the entry of unbleaching fluoroprobes of adjacent parts of the membranes.

Deryaguin and Titijevskaya [37] measured the isotherms of disjoining pressure of microscopic foam films (common thin films) in a narrow range of pressures. At equilibrium, the capillary p_σ pressure in the flat horizontal foam film is equal to the disjoining pressure π in it,

$$p_\sigma = \pi = p_g - p_L, \tag{3.25}$$

where p_g is the pressure in the gas phase and p_L is the pressure in the liquid phase.

Several other techniques have been applied for measuring foam films, e.g. ellipsometry, FT-IR spectroscopy, X-ray reflection and measurement of gas permeability through the film. These techniques are described in detail in the text by Exerowa and Kruglyakov [4] to which the reader should refer.

3.9.2 Techniques for studying structural parameters of foams

Polyhedral foam consists of gas bubbles with polyhedral shape whose faces are flat or slightly bent liquid films, their edges are the Plateau borders and the edge cross points are the vortexes. Several techniques can be applied to obtain the analytical dependency of these characteristics and the structural parameters of the foam [4].

The foam expansion ratio can be characterized by the liquid volume fraction in the foam, which is the sum of the volume fractions of the films, Plateau borders and vertexes. Alternatively, one can use the foam density as a measure of the foam expansion ratio. The reduced pressure in the foam Plateau border can be measured using a capillary manometer [4]. The bubble size and shape distribution in a foam can be determined by microphotography of the foam. Information about the liquid distribution between films and Plateau borders is obtained from the data on the border radius of curvature, the film thickness and the film to Plateau border number ratio obtained in an elementary foam cell.

3.9.3 Measuring foam drainage

After foam formation the liquid starts to drain out of the foam. The "excess" liquid in the foam film drains into the Plateau borders, then through them flows down from the upper to the lower foam layers following the direction of gravity until the gradient of the capillary pressure equalizes the gravity force,

$$\frac{\mathrm{d}p_\sigma}{\mathrm{d}l} = \rho g, \tag{3.26}$$

where l is a coordinate in opposite direction to gravity.

Simultaneously with drainage from films into borders, the liquid begins to flow out from the foam when the pressure in the lower foam film outweighs the external pressure. This process is similar to gel syneresis and it is sometimes referred to as "foam syneresis" and "foam drainage".

The rate of foam drainage is determined by the hydrodynamic characteristics of the foam as well as the rate of internal foam collapse and breakdown of the foam column. Foam drainage is determined by measuring the quantity of liquid that drains from the foam per unit time. Various types of vessels and graduated tubes can be used

for measuring the liquid quantity draining from a foam. Alternatively, one can measure the change in electrical conductivity of the layer at the vessel mouth compared to the electrical conductivity of the foaming solution [4].

3.9.4 Measuring foam collapse

This can be followed by measuring the bubble size distribution as function of time. This can be done for example by microphotography or by counting the number of bubbles. Alternatively one can measure the specific surface area or average bubble size as a function of time. Other techniques such as light scattering or ultrasound can also be applied.

References

[1] Tadros T. Formulation of disperse systems. Weinheim: Wiley-VCH; 2014.
[2] Scheludko A. Colloid Science. Amsterdam: Elsevier; 1966.
[3] Scheludko A. Advances Colloid Interface Sci. 1971;1:391.
[4] Exerowa D, Kruglyakov PM. Foam and Foam Films. Amsterdam: Elsevier; 1997.
[5] Pugh RJ. Advances Colloid and Interface Sci. 1995.
[6] Reynolds O. Phil Trans Royal Soc London Ser. A. 1886;177:157.
[7] Mysels KJ. J Phys Chem. 1964;68:3441.
[8] Lucassen J. In: Lucassen-Reynders EH, editor. Anionic surfactants. New York: Marcel Dekker; 1981. p. 217
[9] Stein HN. Advances Colloid Interface Sci. 1991;34:175.
[10] Davies JT. In: Schulman JH, editor. Proceedings of the second International Congress of Surface Activity. Vol. 1. London: Butterworth; 1957.
[11] Deryaguin BV, Scherbaker RL. Kolloid Zh. 1976;38:438.
[12] Deryaguin BV. Theory of stability of colloids and thin films. New York: Consultant Bureau; 1989.
[13] Deryaguin BV, Landau L. Acta Physicochem USSR. 1941;14:633.
[14] Verwey EJW, Overbeek JTG. Theory of stability of lyophobic colloids. Amsterdam: Elsevier; 1948.
[15] de Vries AJ. Disc Faraday Soc. 1966;42:23.
[16] Vrij A, Overbeek JTG. J Amer Chem Soc. 1968;90:3074.
[17] Radoev B, Scheludko A, Manev E. J Colloid Interface Sci. 1983;95:254.
[18] Gleim VG, Shelomov IV, Shidlovskii BR. J Appl Chem USSR. 1959;32:1069.
[19] Pugh RJ, Yoon RH. J Colloid Interface Sci. 1994;163:169.
[20] Claesson PM, Christensen HK. J Phys Chem. 1988;92:1650.
[21] Johnott ES. Philos Mag. 1906;11:746.
[22] Perrin J. Ann Phys. 1918;10:160.
[23] Loeb L, Wasan DT. Langmuir. 1993;9:1668.
[24] Frieberg S. Mol Cryst Liq Cryst. 1977;40:49.
[25] Perez JE, Proust JE Saraga TM. In: Ivanov IB, editor. Thin liquid films. New York: Marcel Dekker; 1988. p. 70.
[26] Garrett PR, editor. Defoaming. Surfactant Science Series, Vol. 45. New York: Marcel Dekker; 1993.

[27] Ross S, Haak RM. J Phys Chem. 1958;62:1260.
[28] Robinson JV, Woods WW. J Soc Chem Ind. 1948;67:361.
[29] Harkins WD. J Phys Chem. 1941;9:552.
[30] Ross S, Mc Bain JW. Ind Chem Eng. 1944;36:570.
[31] Garett PR. J Colloid Interface Sci. 1979;69:107.
[32] Johansson G, Pugh RG. Int J Mineral Process. 1992;34:1.
[33] Deryaguin BV. Kolloid Z. 1933;64:1.
[34] Bikermann JJ. Foams. New York: Springer-Verlag; 1973.
[35] Princen H. J Colloid Interface Sci. 1983;91:160.
[36] Clark D, Dann R, Mackie A, Mingins J, Pinder A, Purdy P, Russel E, Smith L, Wilson D. J Colloid Interface Sci. 1990;138:195.
[37] Deryaguin BV, Titijevskaya AS. Kolloid Z. 1953;15:416.

4 Formulation of gels

4.1 Introduction

A gel is a "semi-solid" consisting of a "network" in which the solvent is "entrapped". It may be classified as a "liquid-in-solid" dispersion [1]. A gel shows some solid-like properties as well as liquid-like properties, i.e. it is a viscoelastic system (Chapter 14 of Vol. 1). Depending on the gel strength, the system may behave as a viscoelastic solid or a viscoelastic liquid depending on the stress applied on the gel. For "strong" gels (such as those produced by chemical crosslinking) the system may behave as a viscoelastic solid up to high stresses and the gel could also show a significant yield value. For "weaker" gels, e.g. those produced by associative thickeners, the system may show viscoelastic liquid-like behaviour at lower applied stresses when compared with chemical gels.

Gels are applied in many industries of which pharmaceuticals, cosmetics and food products are probably the most useful examples. In pharmaceuticals gels find use as delivery systems for oral administration, as gels proper or as capsule shells made from gelatin. For topical drugs, gels are applied directly to the skin, mucous membrane or eye and for long acting forms of drugs injected intramuscularly. Gelling agents are also useful as binders in tablet granulations, protective colloids in suspensions, thickeners in oral liquids and suppository bases. Cosmetically, gels have been used in hand creams, shampoos, fragrant products, dentifrices and skin and hair preparations. In the food industry various types of gels can be distinguished. The first type is gels by formation of liquid crystalline phases produced when food-grade surfactants such as monoglycerides are mixed with water above the Krafft temperature of the surfactant. Gels are also produced by interaction between proteins and polysaccharides or surfactant and polysaccharides. Gels are also produced in some food products by formation of a "three-dimensional" network of particles in the continuous phase, e.g. fat crystals in margarine.

4.2 Classification of gels

Several classes of gels can be identified [1]:

(i) Gels produced as a result of repulsive interaction, e.g. expanded double layers.
(ii) Self-structured systems in which one induces weak flocculation to produce a "gel" by the particles or droplets. This requires control of the particle size and shape, volume fraction of the dispersion and depth of the secondary minimum.
(iii) Thickeners consisting of high molecular weight polymers or finely divided particulate systems that interact in the continuous phase forming a "three-dimensional" structure.

https://doi.org/10.1515/9783110587968-005

(iv) Self-assembled structures such as associative thickeners.
(v) Crosslinked polymers (chemical gels).
(vi) Liquid crystalline structures of the hexagonal, cubic or lamellar phases.

4.3 Gel-forming materials

The most commonly used materials to produce a gel network are polymers, both natural and synthetic. However, many colloidal particulate solids can form gels by some specific interactions between the particles. High concentrations of nonionic surfactants can also produce clear gels in systems containing up to 15 % mineral oil.

Natural gums have been used for a long time as gelling agents. These gums are typically branched-chain polysaccharides, mostly anionic although some such as guar gum are uncharged. Unfortunately, these gums are subject to microbial degradation and they require the addition of a preservative. An important gum that is used to produce gels is xanthan gum that is produced from sugar by microbiological preparation.

Several other gums have been used to produce gels, of which alginates, carrageenan, tragacanth, pectin, gelatin and agar are probably the most important. Alginates are derived from brown seaweeds in the form of monovalent and divalent salts. Sodium alginate is the most widely used gum. Gelation occurs by reduction of pH or reaction with divalent cations. Carrageenan is produced by extraction from red seaweeds and it is a mixture of sodium, potassium, ammonium, calcium and magnesium sulphate esters of polymerized galactose and 3,6-anhydrogalactose. The main copolymer types are labelled kappa-, iota- and lambda-carrageenan. They are all anionic in nature. Alpha and iota fractions form thermally reversible gels in water. At high temperatures, the copolymers exist as random coils and on cooling they result in the formation of double helices which act as crosslinks.

Tragacanth is produced by extraction from special plants grown in the Middle East. It is a complex material composed chiefly of an acidic polysaccharide (tragacanthic acid) containing calcium, magnesium and potassium, as well as a smaller amount of neutral polysaccharide (tragacanthin). The gum swells in water and a concentration of 2 % or above of a "high quality" gum produces a gel. Hydration takes place over a period of time so that the development of maximum gel strength requires several hours.

Pectin is a polysaccharide extracted from the inner rind of citrus fruits or apple pomace. The gel is formed at an acid pH in aqueous solution containing calcium and possibly other agents that act to dehydrate the gum.

Gelatin is used as a bodying agent and gel-former in the food industry and occasionally in pharmaceutical products. Agar can be used to make firm gels; it is most frequently used in culture media. Gellan gum has been more recently used as a substitute for agar.

Several synthetic gel-forming materials have been developed for various applications. Cellulose derivatives (such as hydroxyethyl cellulose and carboxymethyl cellu-

lose) are frequently used as gelling agents in several disperse systems (such as suspensions and emulsions). Cellulose is a natural structural polymer found in plants. Treatment in the presence of various active substances results in breakdown of the cellulose backbone as well as substitution of a portion of its hydroxyl moieties. The major factors affecting the gel characteristics (and rheological properties) of the resulting material are the nature of the substituent, degree of substitution and average molecular weight of the resultant polymer. The cellulose derivatives are subject to enzymatic degradation, and sterilization of the aqueous system and/or addition of preservatives are employed to prevent viscosity reduction resulting from depolymerization due to enzyme production by microorganisms.

One of the most frequently used synthetic gelling agents in the cosmetic industry is carbomer (sold under trade name "Carbopol"). It is an acrylic polymer crosslinked with a polyalkenyl ether. The polymer can be easily dispersed in aqueous media and on neutralization with a suitable base (such as NaOH or ethylamine) a gel is produced. Carbomer can produce gels at concentrations as low as 0.5 %.

Various forms of polyethylene and its copolymers are used to gel hydrophobic liquids. Polyethylene is a suitable gelling agent for simple aliphatic hydrocarbon liquids but it may lack compatibility with many other oils found in personal care products. In this case copolymers with vinyl acetate and acrylic acid may be used, perhaps with the aid of a cosolvent. To produce the gel, it is necessary to disperse the polymer at high temperature (above 80 °C) and then shock cool to precipitate fine crystals that make up the matrix.

Several finely divided solids, such as sodium montmorillonite and silica, can also be used as gelling agents. The mechanisms by which these particulate solids form gels will be discussed in detail below.

4.4 Rheological behaviour of a gel

One of the most effective techniques to characterize a gel is to investigate its rheological (viscoelastic) behaviour, in particular under conditions of low deformation [1, 2]. The basic principles of these rheological techniques have been discussed in detail in Chapter 14 of Vol. 1 and a brief summary is given here. As discussed in Chapter 14 of Vol. 1, three methods can be applied to investigate the viscoelastic properties of a gel.

4.4.1 Stress relaxation (after sudden application of strain)

One of the most useful ways to describe a gel is to consider the relaxation time of the system. Consider a "gel" with the components in some sort of a "three-dimensional" structure. To deform it instantly, a stress is required and energy is stored in the system (high energy structure). To maintain the new shape (constant deformation) the stress

required becomes smaller since the components of the "gel" undergo some diffusion resulting in a lower energy structure to be approached (structural or stress relaxation). At long times, deformation becomes permanent with complete relaxation of the structure (new low energy structure) and viscous flow will occur.

The above exponential decay of the stress can be represented by the following equation,

$$\sigma(t) = \sigma_0 \exp\left(-\frac{t}{\tau}\right), \tag{4.1}$$

where τ is the stress relaxation time.

If the stress is divided by the strain, one obtains the modulus G

$$G(t) = G_0 \exp\left(\frac{t}{\tau}\right). \tag{4.2}$$

G_0 is the instantaneous modulus (the spring constant).

The above behaviour is schematically represented in Fig. 4.1 if the modulus (after sudden application of strain) is plotted as a function of time. This representation is for a viscoelastic liquid (Maxwell element represented by a spring and dashpot in series) with complete relaxation of the springs at infinite time (Chapter 14 of Vol. 1). In other words the modulus approaches zero at infinite time.

Many crosslinked gels behave like viscoelastic solids (Kelvin model) with another spring in parallel having an elasticity G_e. The modulus does not decay to zero.

The relaxation modulus is given by,

$$G(t) = G_0 \exp\left(\frac{t}{\tau}\right) + G_e. \tag{4.3}$$

Fig. 4.2 shows the variation of $G(t)$ with time for a viscoelastic solid.

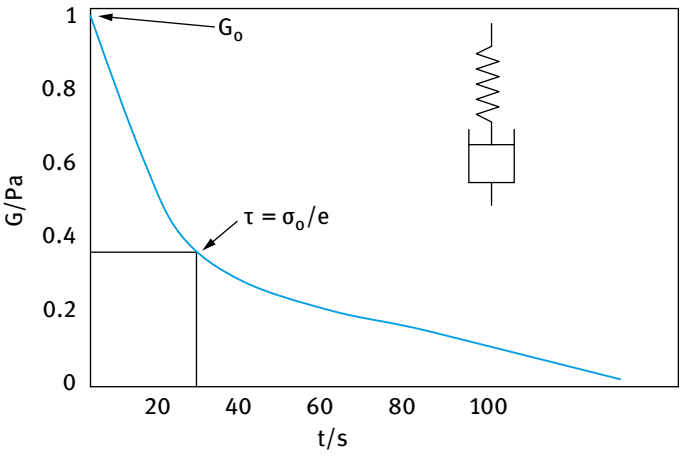

Fig. 4.1: Variation of modulus with time for a viscoelastic liquid.

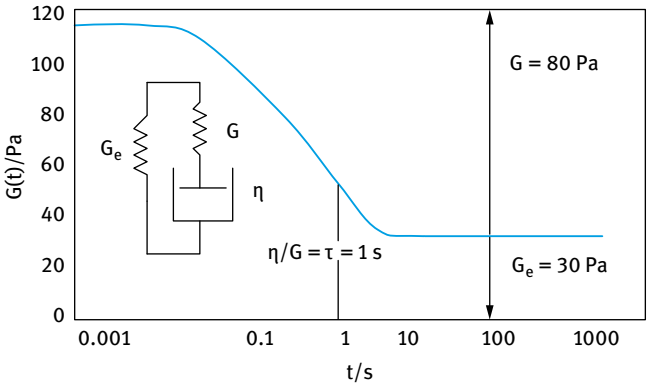

Fig. 4.2: Variation of $G(t)$ with t for a viscoelastic solid.

A useful way to distinguish between the various gels is to consider the Deborah number De,

$$De = \frac{\tau}{t_e}. \tag{4.4}$$

For a gel that shows "solid-like" behaviour ("three-dimensional structure") De is large when compared with a gel that behaves as a viscoelastic liquid.

4.4.2 Constant stress (creep) measurements

In this case a constant stress σ is applied and the strain (deformation) γ or compliance $J(= \gamma/\sigma, \text{Pa}^{-1})$ is followed as a function of time [1]. A gel that consists of a strong "three-dimensional" structure (e.g. crosslinked) behaves as a viscoelastic solid as illustrated in Fig. 4.3. This behaviour may occur up to high applied stresses. In other words the critical stress above which significant deformation occurs can be quite high. A weaker gel (produced for example by high molecular weight polymers that are physically attached) behaves as a viscoelastic liquid as shown in Fig. 4.3. In this case viscoelastic solid behaviour only occurs at much lower stresses than that observed with the crosslinked gels.

4.4.3 Dynamic (oscillatory) measurements

A sinusoidal strain (or stress) with amplitude γ_0 and frequency ω (rad s^{-1}) is applied on the system and the resulting stress (or strain) with amplitude σ_0 is simultaneously measured [1]. This is illustrated in Fig. 4.4.

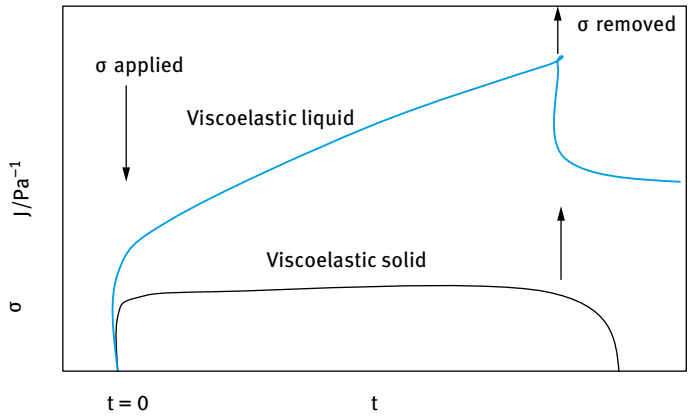

Fig. 4.3: Viscoelastic solid and viscoelastic liquid response for gels.

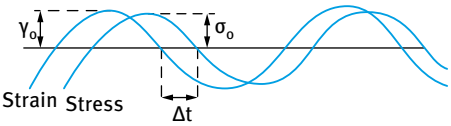

Δt = time shift for sine waves of stress and strain
Δt ω = δ, phase angle shift
ω = frequency in radian s^{-1}
ω = 2 π ν

Perfectly elasic solid	δ = 0
Perfectly viscous liquid	δ = 90°
Viscoelastic system	0 < δ < 90°

Fig. 4.4: Strain and stress sine waves for a viscoelastic system.

For any gel $\delta < 90°$ and the smaller the value of δ the stronger the gel. From the amplitudes of stress and strain (σ_0 and γ_0) and the phase angle shift δ one can obtain the various viscoelastic parameters.

$$|G^*| = \frac{\sigma_0}{\gamma_0} \tag{4.5}$$

$$\text{storage (elastic) modulus } G' = |G^*| \cos \delta \tag{4.6}$$

$$\text{loss (viscous) modulus } G'' = |G^*| \sin \delta \tag{4.7}$$

$$\tan \delta = \frac{G''}{G'} \tag{4.8}$$

For gels $\tan \delta < 1$ and the smaller the value the stronger the gel.

4.5 Polymer gels

4.5.1 Physical gels obtained by chain overlap

Flexible polymers that produce random coils in solution can produce "gels" at a critical concentration C^*, referred to as the polymer coil "overlap" concentration. This picture can be realized if one considers the coil dimensions in solution: Considering the polymer chain to be represented by a random walk in three dimensions, one may define two main parameters, namely the root mean square end-to-end length $\langle r^2 \rangle^{1/2}$ and the root mean square radius of gyration $\langle s^2 \rangle^{1/2}$ (sometimes denoted by R_G). The two are related by,

$$\langle r^2 \rangle^{1/2} = 6^{1/2} \langle s^2 \rangle^{1/2}. \tag{4.9}$$

The viscosity of a polymer solution increases gradually as its concentration increases and at a critical concentration, C^*, the polymer coils with a radius of gyration R_G and a hydrodynamic radius R_h (which is higher than R_G due to solvation of the polymer chains) begin to overlap and this shows a rapid increase in viscosity. This is illustrated in Fig. 4.5 which shows the variation of log η with log C.

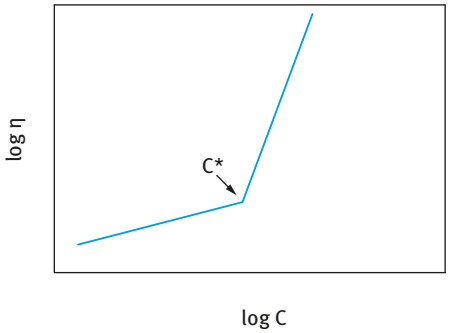

Fig. 4.5: Variation of log η with log C.

In the first part of the curve $\eta \propto C$, whereas in the second part (above C^*) $\eta \propto C^{3.4}$. A schematic representation of polymer coil overlap is shown in Fig. 4.6, which shows the effect of gradually increasing polymer concentration. Polymer concentration above C^* is referred to as the semi-dilute range [3].

C^* is related to R_G and the polymer molecular weight M by,

$$C^* = \left(\frac{4}{3}\right)\pi R_G^3 \left(\frac{N_{av}}{M}\right) \approx 1. \tag{4.10}$$

N_{av} is Avogadro's number. As M increases C^* becomes progressively lower. This shows that to produce physical gels at low concentrations by simple polymer coil overlap, one has to use high molecular weight polymers.

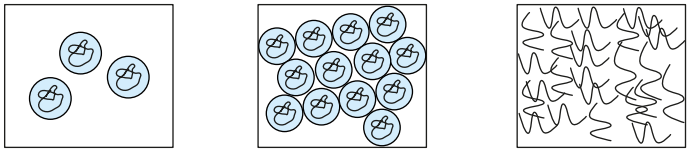

(a) Dilute

C < C*

(b) Onset of overlap

C = C*

(c) Semi-dilute

C > C*

Fig. 4.6: Crossover between dilute and semi-dilute solutions.

Another method to reduce the polymer concentration at which chain overlap occurs is to use polymers that form extended chains, such as xanthan gum which produces conformation in the form of a helical structure with a large axial ratio. These polymers give much higher intrinsic viscosities and they show both rotational and translational diffusion. The relaxation time for the polymer chain is much higher than a corresponding polymer with the same molecular weight but produces random coil conformation.

The above polymers interact at very low concentrations and the overlap concentration can be very low (< 0.01 %). These polysaccharides are used in many formulations to produce physical gels at very low concentrations.

4.5.2 Gels produced by associative thickeners

Associative thickeners are hydrophobically modified polymer molecules in which alkyl chains (C_{12}–C_{16}) are either randomly grafted onto a hydrophilic polymer molecule such as hydroxyethyl cellulose (HEC), or simply grafted at both ends of the hydrophilic chain [4]. An example of hydrophobically modified HEC is Natrosol plus (Hercules) which contains 3–4 C_{16} randomly grafted onto hydroxyethyl cellulose. Another example of a polymer that contains two alkyl chains at both ends of the molecule is HEUR (Rohm and Haas) that is made of polyethylene oxide (PEO) that is capped at both ends with linear C_{18} hydrocarbon chains.

The above hydrophobically modified polymers form gels when dissolved in water. Gel formation can occur at relatively lower polymer concentrations when compared with the unmodified molecule.

The most likely explanation of gel formation is due to hydrophobic bonding (association) between the alkyl chains in the molecule [4]. This effectively causes an apparent increase in the molecular weight. These associative structures are similar to micelles, except the aggregation numbers are much smaller.

Fig. 4.7 shows the variation of viscosity (measured using a Brookfield at 30 rpm) as a function of the alkyl content (C_8, C_{12} and C_{16}) for hydrophobically modified HEC (i.e. HMHEC). The viscosity reaches a maximum at a given alkyl group content that

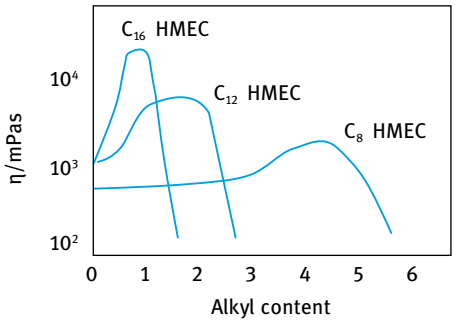

Fig. 4.7: Variation of viscosity of 1 % HMHEC versus alkyl group content of the polymer.

decreases with increasing alkyl chain length. The viscosity maximum increases with increasing alkyl chain length [4].

Associative thickeners also show interaction with surfactant micelles that are present in the formulation. The viscosity of the associative thickeners shows a maximum at a given surfactant concentration that depends on the nature of surfactant. This is shown schematically in Fig. 4.8.

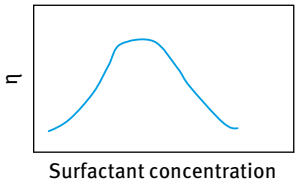

Fig. 4.8: Schematic plot of viscosity of HM polymer with surfactant concentration.

The increase in viscosity is attributed to the hydrophobic interaction between the alkyl chains on the backbone of the polymer with the surfactant micelles. A schematic picture showing the interaction between HM polymers and surfactant micelles is shown in Fig. 4.9. At higher surfactant concentration, the "bridges" between the HM polymer molecules and the micelles are broken (free micelles) and η decreases.

The viscosity of hydrophobically modified polymers shows a rapid increase at a critical concentration, which may be defined as the critical aggregation concentration (CAC), as illustrated in Fig. 4.10 for HMHEC (WSP-D45 from Hercules). The assumption is made that the CAC is equal to the coil overlap concentration C^*.

From a knowledge of C^* and the intrinsic viscosity $[\eta]$ one can obtain the number of chains in each aggregate. For the above example $[\eta] = 4.7$ and $C^*[\eta] = 1$, giving an aggregation number of ≈ 4.

At C^* the polymer solution shows non-Newtonian flow (shear thinning behaviour) and its shows a high viscosity at low shear rates. This is illustrated in Fig. 4.11 which shows the variation of apparent viscosity with shear rate (using a constant stress rheometer). Below $\approx 0.1\,s^{-1}$, a plateau viscosity value $\eta(0)$ (referred to as residual or zero shear viscosity) is reached (≈ 200 Pa s).

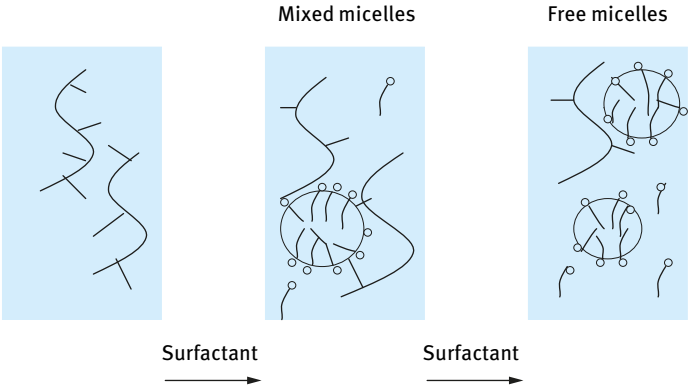

Fig. 4.9: Schematic representation of the interaction of polymers with surfactants.

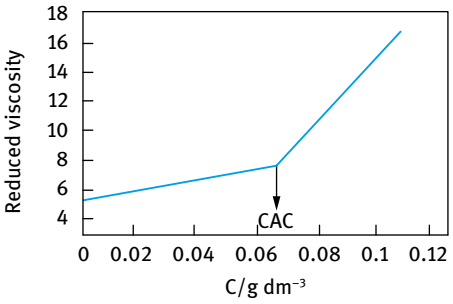

Fig. 4.10: Variation of reduced viscosity with HMHEC concentration.

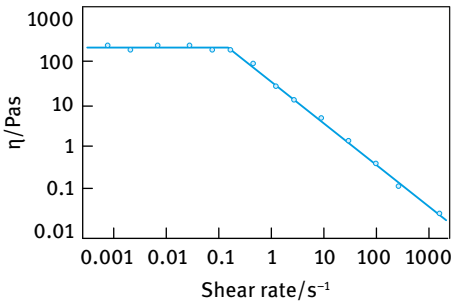

Fig. 4.11: Variation of viscosity with shear rate for HMEC WSP-47 at 0.75 g/100 cm^{-3}.

With an increase in polymer concentration above C^*, the zero shear viscosity increases with increasing polymer concentration. This is illustrated in Fig. 4.12.

The above hydrophobically modified polymers are viscoelastic. This is illustrated in Fig. 4.13 for a solution 5.25 % of C_{18} end-capped PEO with M = 35,000, which shows the variation of the storage modulus G' and loss modulus G'' with frequency ω (rad s^{-1}). G' increases with increasing frequency and ultimately it reaches a plateau value at high frequency. G'' (which is higher than G' in the low frequency regime) increases with increasing frequency, reaches a maximum at a characteristic fre-

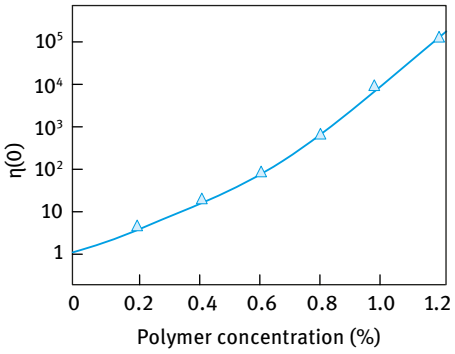

Fig. 4.12: Variation of $\eta(0)$ with polymer concentration.

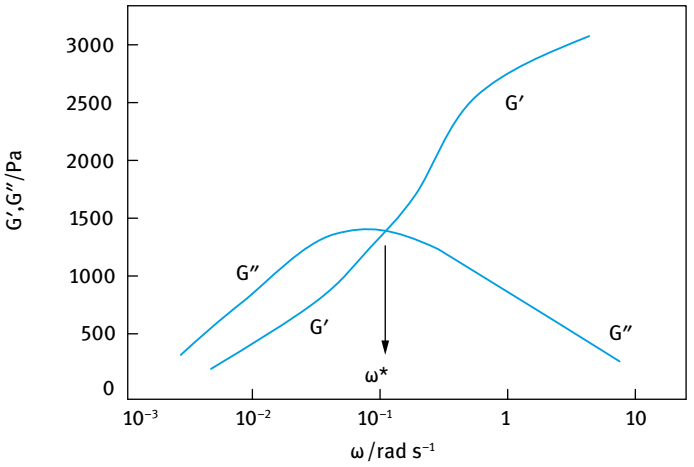

Fig. 4.13: Variation of G' and G'' with frequency for 5.24 HM PEO.

quency ω^* (at which $G' = G''$) and then decreases to near zero value in the high frequency regime.

The above variation of G' and G'' with ω is typical for a system that shows Maxwell behaviour.

From the crossover point ω^* (at which $G' = G''$) one can obtain the relaxation time τ of the polymer in solution,

$$\tau = \frac{1}{\omega^*}. \tag{4.11}$$

For the above polymer $\tau = 8$ s.

The above gels (sometimes referred to as rheology modifiers) are used in many formulations to produce the right consistency and also for reduction of sedimentation or creaming of suspensions and emulsions. These hydrophobically modified polymers can also interact with hydrophobic particles in a suspension forming several other associative structures.

The high frequency modulus, sometimes referred to as the network modulus, can be used to obtain the number of "links" in the gel-network structure. Using the theory of rubber elasticity, the network modulus G_N is related to the number of elastically effective links N and a factor A that depends on the junction functionality,

$$G_N = ANkT, \tag{4.12}$$

where k is the Boltzmann constant and T is the absolute temperature.

For an end-capped PEO (i.e. HEUR) the junctions should be multifunctional ($A = 1$); for tetra-functional junctions $A = 1/2$.

4.5.3 Crosslinked gels (chemical gels)

Many commercially available gels are made using crosslink agents to produce what is sometimes referred to as "microgels". These microgel particles are dispersed in the liquid and they undergo solvent swelling which may also be enhanced by some chemical modification, e.g. pH adjustment in aqueous systems [1].

As mentioned before, an acrylic polymer crosslinked with a polyalkenyl ether, namely carbomer, that is commercially sold under the trade name "Carbopol" (B. F. Goodrich) forms gels at concentrations as low as 0.5 %. The polymer can be easily dispersed in aqueous media and on neutralization with a suitable base (such as NaOH or ethylamine) a gel is produced. The polymer swells as a result of the ionization of the polyacrylic acid chains. The ionization of polyacrylic acid occurs when the pH is increased above ≈ 5 and these ionized chains form extended double layers forming gels at low microgel concentration (mostly less than 0.5 % of the microgel particles).

Another example of microgels is that based on N-isopropyl acrylamide crosslinked with NN′-methylene bisacrylamide (poly-NIPAM). These microgel particles are swollen by temperature changes. At temperatures > 35 °C, the crosslinked polymer is in a collapsed state. When the temperature is reduced, the crosslinked polymer swells absorbing water that reaches several orders of magnitudes its volume. These polymer gels are sometimes referred to as "smart" colloids and they have several applications in controlled release.

4.6 Particulate gels

Two main interactions can cause gel formation with particulate materials:

(i) Long-range repulsions between the particles, e.g. using extended electrical double layers or steric repulsion resulting from the presence of adsorbed or grafted surfactant or polymer chains.
(ii) Van der Waals attraction between the particles (flocculation), which can produce three-dimensional gel networks in the continuous phase.

All the above systems produce non-Newtonian systems that show a "yield value" and high viscosity at low shear stresses or shear rates. Several examples may be quoted to illustrate the above particulate gels:

(i) Swellable clays, e.g. sodium montmorillonite (sometimes referred to as Bentonite) at low electrolyte concentration. These produce gels as a result of the formation of extended double layers. At moderate electrolyte concentrations the clay particles may form association structures as a result of face-to-edge flocculation (see below). These clays can be modified by interaction with alkyl ammonium salts (cationic surfactants) to produce hydrophobically modified clays sometimes referred to as organo-clays or Bentones. These can be dispersed in nonaqueous media and swollen by addition of polar solvents.

(ii) Finely divided oxide, e.g. silica, which can produce gels by aggregation of the particles to form three-dimensional gel structures. In many cases, particulate solids are combined with high molecular weight polymers to enhance gel formation, e.g. as a result of "bridging" or "depletion flocculation".

4.6.1 Aqueous clay gels

Sodium montmorillonite (referred to as swellable clay) forms gels at low and intermediate electrolyte concentrations [5]. This can be understood from a knowledge of the structure of the clay particles. These consist of plate-like particles consisting of a octahedral alumina sheet sandwiched between two tetrahedral silica sheets. This is shown schematically in Fig. 4.14, which also shows the change in the spacing of these sheets. In the tetrahedral sheet tetravalent Si is sometimes replaced by trivalent Al. In the octahedral sheet there may be replacement of trivalent Al by divalent Mg, Fe, Cr or Zn. The small size of these atoms allows them to take the place of small Si and Al.

This replacement is usually referred to as isomorphic substitution whereby an atom of lower positive valence replaces one of higher valence, resulting in a deficit of positive charge or excess of negative charge. This excess of negative layer charge is compensated by adsorption at the layer surfaces of cations that are too big to be accommodated in the crystal. In aqueous solution, the compensation cations on the layer surfaces may be exchanged by other cations in solution, and hence may be referred to as exchangeable cations. With montmorillonite, the exchangeable cations are located on each side of the layer in the stack, i.e. they are present in the external surfaces as well as between the layers. This causes a slight increase of the local spacing from about 9.13 Å to about 9.6 Å; the difference depends on the nature of the counterion.

When montmorillonite clays are placed in contact with water or water vapour the water molecules penetrate between the layers, causing interlayer swelling or (intra)crystalline swelling. This leads to a further increase in the basal spacing to 12.5–20 Å, depending on the type of clay and cation. This interlayer swelling leads, at

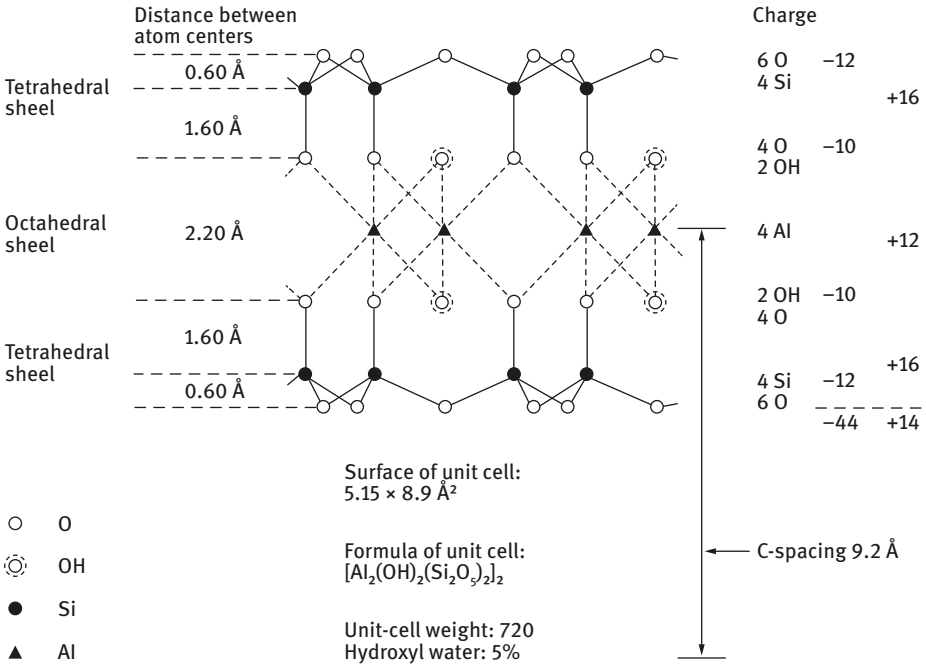

Fig. 4.14: Atom arrangement in one unit cell of 2 : 1 layer mineral.

most, to a doubling of the volume of dry clay when four layers of water are adsorbed. The much larger degree of swelling, which is the driving force for "gel" formation (at low electrolyte concentration), is due to osmotic swelling. It has been suggested that swelling of montmorillonite clays is due to the electrostatic double layers that are produced between the charge layers and cations. This is certainly the case at low electrolyte concentration where the double layer extension (thickness) is large (Fig. 4.15).

As discussed above, the clay particles carry a negative charge as a result of isomorphic substitution of certain electropositive elements by elements of lower valency. The negative charge is compensated by cations, which in aqueous solution form a diffuse

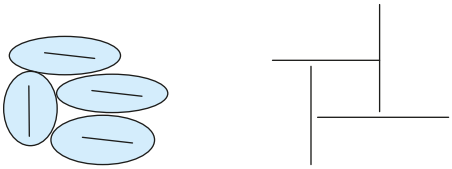

(a) Gels produced by Double layer overlap

(b) Gels produced by edge-to-face association

Fig. 4.15: Schematic representation of gel formation in aqueous clay dispersions.

layer, i.e. an electric double layer is formed at the clay plate/solution interface. This double layer has a constant charge, which is determined by the type and degree of isomorphic substitution. However, the flat surfaces are not the only surfaces of the plate-like clay particles, they also expose an edge surface. The atomic structure of the edge surfaces is entirely different from that of the flat-layer surfaces. At the edges, the tetrahedral silica sheets and the octahedral alumina sheets are disrupted, and the primary bonds are broken. The situation is analogous to that of the surface of silica and alumina particles in aqueous solution. On such edges, therefore, an electric double layer is created by adsorption of potential determining ions (H^+ and OH^-) and one may, therefore identify an isoelectric point (IEP) as the point of zero charge (pzc) for these edges. With broken octahedral sheets at the edge, the surface behaves as Al-OH with an IEP in the region of pH 7–9. Thus in most cases the edges become negatively charged above pH 9 and positively charged below pH 9.

Van Olphen [5] suggested a mechanism of gel formation of montmorillonite involving interaction of the oppositely charged double layers at the faces and edges of the clay particles. This structure, which is usually referred to as a "card-house" structure, was considered to be the reason for the formation of the voluminous clay gel. However, Norrish suggested that the voluminous gel is the result of the extended double layers, particularly at low electrolyte concentrations. A schematic picture of gel formation produced by double layer expansion and "card-house" structure is shown in Fig. 4.15.

Evidence for the above picture was obtained by Van Olphen [5] who measured the yield value of 3.22 % montmorillonite dispersions as a function of NaCl concentration as shown in Fig. 4.16. When $C = 0$, the double layers are extended and gel formation is due to double layer overlap (Fig. 4.15 (a)). First addition of NaCl causes compression of the double layers and hence the yield value decreases very rapidly. At intermediate NaCl concentrations, gel formation occurs as a result of face-to-edge association

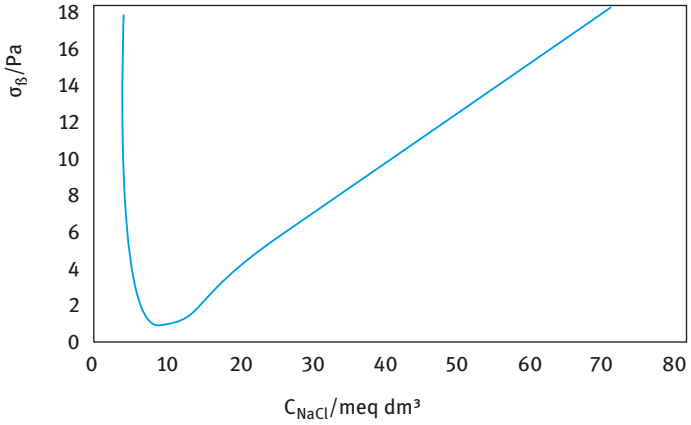

Fig. 4.16: Variation of yield value with NaCl concentration for 3.22 % sodium montmorillonite dispersions.

(house of card structure) (Fig. 4.15 (b)) and the yield value increases very rapidly with increasing NaCl concentration. If the NaCl concentration is increased further, face-to-face association may occur and the yield value decreases (the gel is destroyed).

4.6.2 Organo-clays (Bentones)

These are produced by exchanging the Na^+ ions with alkyl ammonium ions, e.g. dodecyl or cetyl trimethyl ammonium ions. In some cases dialkyl ammonium ions are also used. In this case the clay particle surface will be covered with hydrophobic alkyl groups and hence it can be dispersed in organic solvents, e.g. hydrocarbon or silicone oils. The exchange is not carried out completely, leaving a few hydrophilic groups on the surface. The dispersed organo-clays are then activated by addition of a polar solvent such as propylene carbonate, alcohols, glycols, etc.

The gel is produced by hydrogen bonding between the polar groups on the surface of the clay and the polar solvent added. Several types of organo-clays are commercially available depending on the application and the type of solvent in which a gel is required. In some cases, organo-clays, already activated can be supplied.

Organo-clays are applied to "thicken" many personal care products, e.g. foundations, nonaqueous creams, nail polish, lipsticks, etc. The procedure for dispersion of the organo-clay particles and their subsequent activation is crucial and it requires good process control.

4.6.3 Oxide gels

The most commonly used oxide gels are based on silica. Various forms of silicas can be produced, the most common are referred to as fumed and precipitated silicas. Fumed silicas, such as Aerosil 200, are produced by reaction of silicon tetrachloride with steam. The surface contains siloxane bonds and isolated silanol groups (referred to as vicinal). Precipitated silicas are produced from sodium silicate by acidification. The surface is more populated with silanol groups than fumed silica. It contains geminal OH groups (two attached to the same Si atom). Both fumed and precipitated silicas can produce gels, both in aqueous and nonaqueous systems. Gelation results from aggregation of silica particles thus producing three-dimensional gel networks with a yield value.

In aqueous media, the gel strength depends on the pH and electrolyte concentration [6]. As an illustration, Fig. 4.17 shows the variation of viscosity and yield value with Aerosil silica (which has been dispersed by sonication) concentration at three different pH values. In all cases, the viscosity and yield value show a rapid increase above a certain silica concentration that depends on the pH of the system.

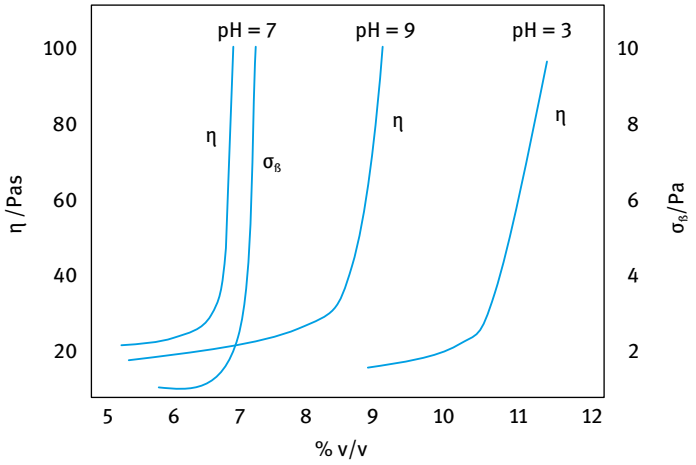

Fig. 4.17: Variation of viscosity η and yield value σ_β with Aerosil 200 concentration at three pH values.

At pH = 3 (near the isoelectric point of silica), the particles are aggregated (forming flocs) and the increase in viscosity occurs at relatively high silica concentration (> 11 % v/v). At pH = 7, the silica becomes negatively charged and the double layers stabilize the silica particles against aggregation. In this case the particles remain as small units and the viscosity and yield value increases sharply above 7 % v/v. At pH = 9, some aggregation occurs as a result of the electrolyte released on adjusting the pH; in this case the viscosity increases at higher concentration (> 9 % v/v) when compared with the results at pH = 7. These results clearly indicate the importance of pH and electrolyte concentration in gelation of silica. It seems that the optimum gel formation occurs at neutral pH.

4.7 Gels produced by mixtures of polymers and finely divided particulate solids

By combining thickeners such as hydroxyethyl cellulose or xanthan gum with particulate solids such as sodium montmorillonite, a more robust gel structure can be produced. By using such mixtures, the concentration of the polymer can be reduced, thus overcoming the problem of dispersion on dilution (e.g. with many agrochemical suspension concentrates). This gel structure may be less temperature dependent and could be optimized by controlling the ratio of the polymer and the particles. If these combinations of say sodium montmorillonite and a polymer such as hydroxyethyl cellulose, polyvinyl alcohol (PVA) or xanthan gum, are balanced properly, they can provide a “three-dimensional structure”, which entraps all the particles and stops

settling and formation of dilatant clays. The mechanism of gelation of such combined systems depends to a large extent on the nature of the solid particles, the polymer and the conditions. If the polymer adsorbs on the particle surface (e.g. PVA on sodium montmorillonite or silica) a three-dimensional network may be formed by polymer bridging. Under conditions of incomplete coverage of the particles by the polymer, the latter becomes simultaneously adsorbed on two or more particles. In other words, the polymer chains act as "bridges" or "links" between the particles.

The optimum composition of these particulate–polymer mixtures can be obtained using rheological measurements. By measuring the yield value as a function of polymer concentration at a fixed particulate concentration, one can obtain the optimum polymer concentration required. In most cases the yield value reaches a maximum at a given ratio of particulate solid to polymer. This trend may be due to bridging flocculation, which reaches an optimum at a given surface coverage of the particles (usually at 0.25–0.5 surface coverage).

All the above mentioned gels produce thixotropy, i.e. a reversible decrease of viscosity on application of shear (at constant shear rate) and recovery of the viscosity on standing. This thixotropic behaviour finds application in many systems in personal care, e.g. in creams, toothpastes, foundations, etc. One of the most useful techniques to study thixotropy is to follow the change of modulus with time after application of shear, i.e. after subjecting the dispersion to a constant shear rate oscillatory measurements are carried out at low strains and high frequency and the increase in modulus with time (which is exponential) can be used to characterize the recovery of the gel.

4.8 Gels based on surfactant systems

In dilute solutions surfactants tend to form spherical micelles with aggregation numbers in the range 50–100 units. These micellar solutions are isotropic with low viscosity. At much higher surfactant concentration (> 30 % depending on the surfactant nature) they produce liquid crystalline phases of the hexagonal (H_1) and lamellar (L_α) phases which are anisotropic with much higher viscosities [7]. A schematic representation of the hexagonal and lamellar phases is shown in Fig. 4.18 and 4.19.

These liquid crystalline phases, which are viscoelastic, can be used as rheology modifiers. However, for practical applications such as in shampoos, such very high surfactant concentrations are undesirable [8]. One way to increase the viscosity of a surfactant solution at lower concentrations is to add an electrolyte that causes a change from spherical to cylindrical micelles which can grow in length and above a critical surfactant volume fraction ϕ^* these worm-like micelles begin to overlap forming a "gel" as illustrated in Fig. 4.20.

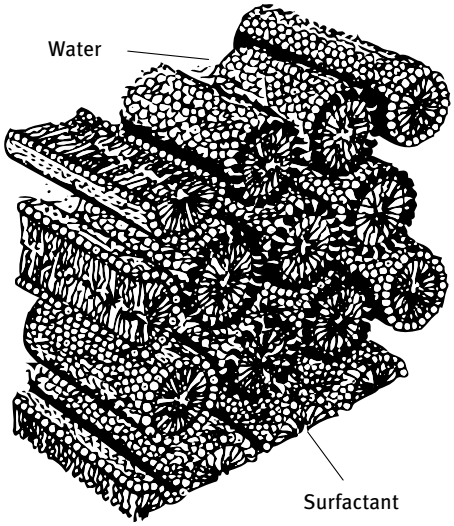

Fig. 4.18: Schematic representation of hexagonal phase.

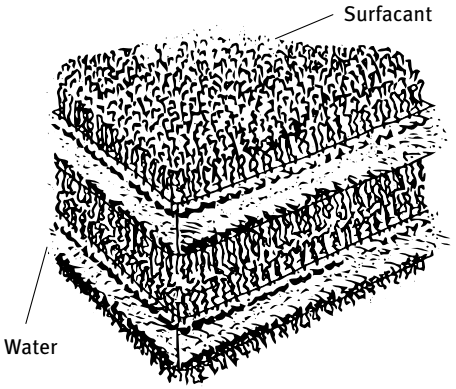

Fig. 4.19: Schematic representation of lamellar phase.

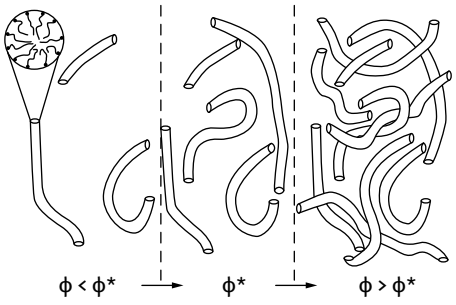

Fig. 4.20: Overlap of thread-like micelles.

An alternative method to produce gels in emulsions is to use mixtures of surfactants. By proper choice of the surfactant types (e.g. their hydrophilic–lipophilic balance, HLB) one can produce lamellar liquid crystalline structures that can "wrap" around the oil droplets and extend in solution to form gel networks [7, 8]. These structures (sometimes referred to as oleosomes) are schematically shown in Fig. 4.21. Alternatively, the liquid crystalline structures may produce a "three-dimensional" gel network and the oil droplets become entrapped in the "holes" of the network. These structures are sometimes referred to as hydrosomes and they are illustrated in Fig. 4.22.

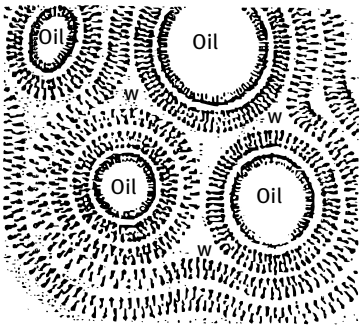

Fig. 4.21: Schematic representation of "oleosomes".

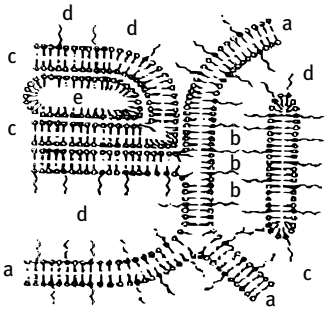

Fig. 4.22: Schematic representation of "hydrosomes".

The above mentioned surfactant systems are used in most personal care and cosmetic formulations [8]. Apart from giving the right consistency for application (e.g. good skin feel) they are also effective in stabilizing emulsions against creaming or sedimentation, flocculation and coalescence.

Liquid crystalline structures can also influence the delivery of active ingredients, both of the lipophilic and hydrophilic types. Since lamellar liquid crystals mimic the skin structure (in particular the stratum corneum) they can offer prolonged hydration potential.

References

[1] Tadros T. Rheology of Dispersions. Weinheim: Wiley-VCH; 2010.
[2] Ferry JD. Viscoelastic properties of polymers. New York: John Wiley & Sons; 1980.
[3] de Gennes PG. Scaling concepts of polymer physics. Ithaca: Cornell University Press; 1979.
[4] Goddard ED. In: Goddard ED, Gruber JV, editors. Polymer/surfactant interaction. New York: Marcel Dekker; 1999. Chapters 4 & 5.
[5] van Olphen H. Clay colloid chemistry. New York: Wiley; 1963.
[6] Heath D, Tadros TF. J Colloid Interface Sci. 1983;90:207, 320
[7] Tadros T. Applied surfactants. Weinheim: Wiley-VCH; 2005.
[8] Tadros T. Formulation of Cosmetics and Personal Care. Berlin: De Gruyter; 2016.

5 Formulation of polymer colloids (latexes)

5.1 Introduction

Polymers (latexes) are widely used in many industrial applications, e.g. in paints and coatings (film formers), as adhesives, as diagnostic markers for certain diseases, etc. In paints and coatings, latexes are used in aqueous emulsion paints that are used for home decoration. These aqueous emulsion paints are applied at room temperature and the latexes coalesce on the substrate forming a thermoplastic film. Sometimes functional polymers are used for crosslinking in the coating system. The polymer particles are typically submicron (0.1–0.5 μm).

Generally speaking, there are three methods for preparing polymer dispersions, namely emulsion, dispersion and suspension polymerization. In emulsion polymerization, monomer is emulsified in a nonsolvent, commonly water, usually in the presence of a surfactant [1]. A water-soluble initiator is added, and particles of polymer form and grow in the aqueous medium as the reservoir of the monomer in the emulsified droplets is gradually used up. In dispersion polymerization (which is usually applied for preparing nonaqueous polymer dispersions, commonly referred to as nonaqueous dispersion polymerization, NAD) monomer, initiator, stabilizer (referred to as protective agent) and solvent initially form a homogeneous solution. The polymer particles precipitate when the solubility limit of the polymer is exceeded. The particles continue to grow until the monomer is consumed. In suspension polymerization the monomer is emulsified in the continuous phase using a surfactant or polymeric suspending agent. The initiator (which is oil-soluble) is dissolved in the monomer droplets and the droplets are converted into insoluble particles, but no new particles are formed.

A description of both emulsion and dispersion polymerization is given below, with particular reference to the control of their particle size and colloid stability which is greatly influenced by the emulsifier or dispersant used. Particular emphasis will be given to the effect of polymeric surfactants that have been recently used for the preparation of emulsion polymers.

5.2 Emulsion polymerization

As mentioned above, in emulsion polymerization, the monomer, e.g. styrene or methyl methacrylate that is insoluble in the continuous phase, is emulsified using a surfactant that adsorbs at the monomer/water interface [1]. The surfactant micelles in bulk solution solubilize some of the monomer. A water-soluble initiator such as potassium persulphate $K_2S_2O_8$ is added and this decomposes in the aqueous phase forming free radicals that interact with the monomers forming oligomeric chains. It has long been

https://doi.org/10.1515/9783110587968-006

assumed that nucleation occurs in the "monomer swollen micelles". The reasoning behind this mechanism was the sharp increase in the rate of reaction above the critical micelle concentration and that the number of particles formed and their size depend to a large extent on the nature of the surfactant and its concentration (which determines the number of micelles formed). However, this mechanism was later disputed and it was suggested that the presence of micelles means that excess surfactant is available and molecules will readily diffuse to any interface.

The most accepted theory of emulsion polymerization is referred to as coagulative nucleation theory [2, 3]. A two-step coagulative nucleation model has been proposed by Napper and co-workers [2, 3]. In this process the oligomers grow by propagation and this is followed by a termination process in the continuous phase. A random coil is produced which is insoluble in the medium and this produces a precursor oligomer at the θ-point. The precursor particles subsequently grow primarily by coagulation to form true latex particles. Some growth may also occur by further polymerization. The colloidal instability of the precursor particles may arise from their small size, and the slow rate of polymerization can be due to reduced swelling of the particles by the hydrophilic monomer [2, 3]. The role of surfactants in these processes is crucial since they determine the stabilizing efficiency and the effectiveness of the surface active agent, ultimately determining the number of particles formed. This was confirmed by using surface active agents of different nature. The effectiveness of any surface active agent in stabilizing the particles was the dominant factor and the number of micelles formed was relatively unimportant.

A typical emulsion polymerization formulation contains water, 50 % monomer blended for the required glass transition temperature, T_g, surfactant (and often colloid), initiator, pH buffer and fungicide. Hard monomers with a high T_g used in emulsion polymerization may be vinyl acetate, methyl methacrylate and styrene. Soft monomers with a low T_g include butyl acrylate, 2-ethylhexyl acrylate, vinyl versatate and maleate esters. Most suitable monomers are those with low, but not too low, water solubility. Other monomers such as acrylic acid, methacrylic acid, or adhesion promoting monomers may be included in the formulation. It is important that the latex particles coalesce as the diluent evaporates. The minimum film forming temperature (MFFT) of the paint is a characteristic of the paint system. It is closely related to the T_g of the polymer but the latter can be affected by materials present such as surfactant and the inhomogeneity of the polymer composition at the surface. High T_g polymers will not coalesce at room temperature and in this case a plasticizer ("coalescing agent") such as benzyl alcohol is incorporated in the formulation to reduce the T_g of the polymer, thus reducing the MFFT of the paint. Clearly, for any paint system one must determine the MFFT since, as mentioned above, the T_g of the polymer is greatly affected by the ingredients in the paint formulation.

Several types of surfactants (anionic, cationic, zwitterionic and nonionic) can be used in emulsion polymerization; the various classes have been described in detail in Chapter 8 of Vol. 1.

The role of surfactants is two-fold, firstly to provide a locus for the monomer to polymerize and secondly to stabilize the polymer particles as they form. In addition, surfactants aggregate to form micelles (above the critical micelle concentration) and these can solubilize the monomers. In most cases a mixture of anionic and nonionic surfactant is used for optimum preparation of polymer latexes. Cationic surfactants are seldom used, except for some specific applications where a positive charge is required on the surface of the polymer particles.

In addition to surfactants, most latex preparations require the addition of a polymer (sometimes referred to as "protective colloid") such as partially hydrolyzed polyvinyl acetate (commercially referred to as polyvinyl alcohol, PVA), hydroxyethyl cellulose or a block copolymer of polyethylene oxide (PEO) and polypropylene oxide (PPO). These polymers can be supplied with various molecular weights or proportions of PEO and PPO. When used in emulsion polymerization, they can be grafted by the growing chain of the polymer being formed. They assist in controlling the particle size of the latex, enhancing the stability of the polymer dispersion and controlling the rheology of the final paint.

A typical emulsion polymerization process involves two stages known as the seed stage and the feed stage. In the seed stage, an aqueous charge of water, surfactant, and colloid is raised to the reaction temperature (85–90 °C) and 5–10 % of the monomer mixture is added along with a proportion of the initiator (a water-soluble persulphate). In this seed stage, the formulation contains monomer droplets stabilized by surfactant, a small amount of monomer in solution as well as surfactant monomers and micelles. Radicals are formed in solution from the breakdown of the initiator and these radicals polymerize the small amount of monomer in solution. These oligomeric chains will grow to some critical size, the length of which depends on the solubility of the monomer in water. The oligomers build up to a limiting concentration and this is followed by a precipitous formation of aggregates (seeds), a process similar to micelle formation, except in this case the aggregation process is irreversible (unlike surfactant micelles which are in dynamic equilibrium with monomers).

In the feed stage, the remaining monomer and initiator are fed together and the monomer droplets become emulsified by the surfactant remaining in solution (or by extra addition of surfactant). Polymerization proceeds as the monomer diffuses from the droplets, through the water phase, into the already forming growing particles. At the same time radicals enter the monomer-swollen particles causing both termination and re-initiation of polymerization. As the particles grow, the remaining surfactant from the water phase is adsorbed onto the surface of particles to stabilize the polymer particles. The stabilization mechanism involves both electrostatic and steric repulsion. The final stage of polymerization may include a further shot of initiator to complete the conversion.

According to the theory of Smith and Ewart [4] of the kinetics of emulsion polymerization, the rate of propagation R_p is related to the number of particles N formed in a reaction by the equation,

$$-\frac{d[M]}{dt} = R_p k_p N n_{av}[M], \tag{5.1}$$

where $[M]$ is the monomer concentration in the particles, k_p is the propagation rate constant and n_{av} is the average number of radicals per particle.

According to equation (5.1), the rate of polymerization and the number of particles are directly related to each other, i.e. an increase in the number of particles will increase the rate. This has been found for many polymerizations, although there are some exceptions. The number of particles is related to the surfactant concentration $[S]$ by the equation [4],

$$N \approx [S]^{3/5}. \tag{5.2}$$

Using the coagulative nucleation model, Napper et al. [2, 3] found that the final particle number increases with increasing surfactant concentration with a monotonically diminishing exponent. The slope of $d(\log N_c)/d(\log t)$ varies from 0.4 to 1.2. At high surfactant concentration, the nucleation time will be long in duration since the new precursor particles will be readily stabilized. As a result, more latex particles are formed and eventually will outnumber the very small precursor particles at long times. The precursor/particle collisions will become more frequent and fewer latex particles are produced. The dN_c/dt will approach zero and at long times the number of latex particles remain constant. This shows the inadequacy of the Smith–Ewart theory which predicts a constant exponent (3/5) at all surfactant concentrations. For this reason, the coagulative nucleation mechanism has now been accepted as the most probable theory for emulsion polymerization. In all cases, the nature and concentration of the surfactant used is very crucial and this is very important in the industrial preparation of latex systems.

Most reports on emulsion polymerization have been limited to commercially available surfactants, which in many cases are relatively simple molecules such as sodium dodecyl sulphate and simple nonionic surfactants. However, studies on the effect of surfactant structure on latex formation have revealed the importance of the structure of the molecule. Block and graft copolymers (polymeric surfactants) are expected to be better stabilizers when compared to simple surfactants. The use of these polymeric surfactants in emulsion polymerization and the stabilization of the resulting polymer particles is discussed below.

Most aqueous emulsion and dispersion polymerization reported in the literature is based on a few commercial block and graft copolymers, with a broad molecular weight distribution and varying block composition. The results obtained from these studies could not establish what effect the structural features of the block copolymer has on their stabilizing ability and effectiveness in polymerization. Fortunately, model block copolymers with well-defined structures could be synthesized and their role in

emulsion polymerization has been investigated out using model polymers and model latexes.

A series of well-defined A–B block copolymers of polystyrene-block-polyethylene oxide (PS–PEO) type were synthesized [5] and used for emulsion polymerization of styrene. These molecules are "ideal" since the polystyrene block is compatible with the polystyrene formed and thus it forms the best anchor chain. The PEO chain (the stabilizing chain) is strongly hydrated with water molecules and it extends into the aqueous phase forming the steric layer necessary for stabilization. However, the PEO chain can become dehydrated at high temperature (due to the breakage of hydrogen bonds) thus reducing the effective steric stabilization. Thus the emulsion polymerization should be carried out at temperatures well below the theta (θ)-temperature of PEO.

Five block copolymers were synthesized [5] with various molecular weights of the PS and PEO blocks. The molecular weight of the polystyrene block and the resulting PS–PEO polymer was determined using gel permeation chromatography. The mole percent of ethylene oxide and the percent of PEO in the block was determined using H^1 NMR spectroscopy. The molecular weight of the blocks varied from M_n = 1,000–7,000 for PS and M_w = 3,000–9,000 for PEO. These five block copolymers were used for emulsion polymerization of styrene at 50 °C (well below the θ-temperature of PEO). The results indicated that for efficient anchoring, the PS block need not be more than 10 monomer units. The PEO block should have an $M_w \geq 3{,}000$. However the ratio of the two blocks is very important; for example if the wt% of PEO is $\leq 3{,}000$ the molecule becomes insoluble in water (not sufficiently hydrophilic) and no polymerization could occur when using this block copolymer. In addition, the 50 % PEO block could produce a latex but it was unstable and coagulated at 35 % conversion. It became clear from these studies that the % PEO in the block copolymer plays an important role and this should exceed 75 %. However, the overall molecular weight of the block copolymer is also very important. For example if one uses a PS block with M_n = 7,000, the PEO molecular weight have to be 21,000, which is too high and may result in bridging flocculation, unless one prepares a very dilute latex.

Another systematic study of the effect of block copolymer on emulsion polymerization was carried out using blocks of poly(methylmethacrylate)-block–polyethylene oxide (PMMA–PEO) for the preparation of PMMA latexes [5]. The ratio and molecular weight of PMMA to PEO in the block copolymer was varied. Ten different PMMA–PEO blocks were synthesized [5] with M_n for PMMA varying between 400 and 2,500. The M_w of PEO was varied between 750 and 5,000. The recipe for MMA polymerization consisted of 100 monomer, 800 g water, 20 g PMMA–PEO block copolymer and 0.5 g potassium persulphate. Polymerization was carried out at 45 °C, which is well below the θ-temperature of PEO. The rate of polymerization R_p was calculating by using latex samples drawn from the reaction mixture at various time intervals (the amount of latex was determined gravimetrically). The particle size of each latex sample was determined by dynamic light scattering (photon correlation spectroscopy, PCS). The

number of particles, N, in each case was calculated from the weight of the latex and the z-average diameter. The results obtained were used to study the effect of the anchoring group PMMA, molecular weight, the effect of PEO molecular weight and the effect of the total molecular weight of the block copolymer. The results are summarized in Tab. 5.1 and 5.2.

Tab. 5.1: Effect of PMMA and PEO molecular weight in the diblock.

M_n PMMA	M_w PEO	wt% PEO	$R_p \times 10^4$ (mol/l s)	D (nm)	$N \times 10^{-13}$ (cm^{-3})
400	750	65	1.3	213	1.7
400	2000	83	1.5	103	14.7
400	5000	93	2.4	116	10.3
900	750	46	Unstable latex	—	—
800	2000	71	3.4	92	20.6
800	5000	86	3.2	106	13.5
1300	2000	61	2.4	116	10.3
1200	5000	81	4.6	99	16.6
1900	5000	72	3.4	110	11.4
2500	5000	67	2.2	322	0.4

Tab. 5.2: Effect of total molecular weight of the PMMA–PEO diblock.

M_w	wt% PEO	$R_p \times 10^4$ (mol/l s)	D (nm)	$N \times 10^{-13}$ (cm^{-3})
1150	65	1.3	213	1.7
2400	83	1.5	103	14.7
2800	71	3.4	92	20.6
3300	61	2.4	99	16.6
6200	81	4.6	99	16.6
6900	72	3.4	110	11.4
7500	67	2.2	322	0.4

These results of the systematic study (Tab. 5.1 and 5.2) of varying the PMMA and PEO block molecular weight, the % PEO in the chain as well as the overall molecular weight clearly show the effect of these factors on the resulting latex. For example, when using a block copolymer with 400 molecular weight of PMMA and 750 molecular weight of PEO (i.e. containing 65 wt% PEO) the resulting latex has fewer particles when compared with the other surfactants. The most dramatic effect was obtained when the PMMA molecular weight was increased to 900 while keeping the PEO molecular weight (750) the same. This block copolymer contains only 46 wt% PEO and it became insoluble in water due to the lack of hydrophilicity. The latex produced was unstable and it collapsed at the early stage of polymerization. A PEO molecular weight of 750 is insufficient to provide effective steric stabilization. By increasing the molecular

weight of PEO to 2,000 or 5,000 while keeping the PMMA molecular weight at 400 or 800 a stable latex was produced with a small particle diameter and large number of particles. The best results were obtained by keeping the molecular weight of PMMA at 800 and that of PEO at 2,000. This block copolymer gave the highest conversion rate, the smallest particle diameter and the largest number of particles (Tab. 5.2). It is interesting to note that by increasing the PEO molecular weight to 5,000 while keeping the PMMA molecular weight at 800, the rate of conversion decreased, the average diameter increased and the number of particles decreased when compared with the results obtained using 2,000 molecular weight for PEO. It seems that when the PEO molecular weight is increased the hydrophilicity of the molecule increased (86 wt% PEO) and this reduced the efficiency of the copolymer. It seems that by increasing hydrophilicity of the block copolymer and its overall molecular weight, the rate of adsorption of the polymer to the latex particles and its overall adsorption strength may have decreased. The effect of the overall molecular weight of the block copolymer and its overall hydrophilicity have a big effect on latex production (Tab. 5.2). Increasing the overall molecular weight of the block copolymer above 6,200 resulted in a reduction in the rate of conversion, an increase in the particle diameter and a reduction in the number of latex particles. The worst results were obtained with an overall molecular weight of 7,500 while reducing the PEO wt% in which case particles with 322 nm diameter were obtained and the number of latex particles is significantly reduced.

The importance of the affinity of the anchor chain (PMMA) to the latex particles was investigated by using different monomers [5]. For example, when using styrene as the monomer the resulting latex was unstable and it showed the presence of coagulum. This can be attributed to the lack of chemical compatibility of the anchor chain (PMMA) and the polymer to be stabilized, namely polystyrene. This clearly indicates that block copolymers of PMMA–PEO are not suitable for emulsion polymerization of styrene. However, when using vinyl acetate monomer, where the resulting poly(vinyl acetate) latex should have strong affinity to the PMMA anchor, no latex was produced when the reaction was carried out at 45 °C. It was speculated that the water solubility of the vinyl acetate monomer resulted in the formation of oligomeric chain radicals which could exist in solution without nucleation. Polymerization at 60 °C, which did nucleate particles, was found to be controlled by chain transfer of the vinyl acetate radical with the surfactant, resulting in broad molecular weight distributions

Emulsion polymerization of MMA using triblock copolymers was carried out using PMMA-block-PEO-PMMA with the same PMMA molecular weight (800 or 900) while varying the PEO molecular weight from 3,400 to 14,000 in order to vary the loop size. Although the rate of polymerization was not affected by the loop size, the particles with the smallest diameter were obtained with the 10,000 molecular weight PEO. Comparison of the results obtained using the triblock copolymer with those obtained using diblock copolymer (while keeping the PMMA block molecular weight the same) showed the same rate of polymerization. However, the average particle diameter was smaller and the total number of particles larger when using the diblock copolymer.

This clearly shows the higher efficacy of the diblock copolymer when compared with the triblock copolymer.

The first systematic study of the effect of graft copolymers were carried out by Piirma and Lenzotti [6] who synthesized well characterized graft copolymers with different backbone and side chain lengths. Several grafts of poly(p-methylstyrene)-graft–polyethylene oxide, (PMSt)–$(PEO)_n$, were synthesized and used in styrene emulsion polymerization. Three different PMSt chain length (with molecular weights of 750, 2,000 and 5,000) and three different PEO chain lengths were prepared. In this way the structure of the amphipathic graft copolymer could be changed in three different ways:

(i) three different PEO graft chain lengths;
(ii) three different backbone chain lengths with the same wt% PEO;
(iii) four different wt% PEO grafts.

Piirma and Lenzotti [6] first investigated the graft copolymer concentration required to produce the highest conversion rate, the smallest particle size and the largest number of latex particles. The monomer-to-water ratio was kept at 0.15 to avoid overcrowding of the resulting particles. They found that a concentration of 18 g/100 g monomer (2.7 % aqueous phase) was necessary to obtain the above results, after which a further increase in graft copolymer concentration did not have any significant effect on increasing the rate of polymerization or increasing the number of particles used. Using the graft copolymer concentration of 2.7 % aqueous phase, the results showed an increase in the number of particles with increasing conversion, reaching a steady value at about 35 % conversion. Obviously, before that conversion, new particles are still being stabilized from the oligomeric precursor particles, after which all precursor particles are assimilated by the existing particles. The small size of the latex produced, namely 30–40 nm, clearly indicates the efficiency with which this graft copolymer stabilizes the dispersion.

Three different backbone chain lengths with M_n of 1,140, 4,270 and 24,000 were used while the weight percent of PEO (82 %) was kept the same, that is equivalent to 3, 10 and 55 PEO chains per backbone respectively. The results showed that the rate of polymerization, particle diameter and number of particles was similar for the three cases. Since the graft copolymer concentration was the same in each case, it can be concluded that one molecule of the highest molecular graft is just as effective as 18 molecules of the lowest molecular weight graft in stabilizing the particles.

Four graft copolymers were synthesized with a PMSt backbone with M_w of 4,540 while increasing the wt% of PEO: 68, 73, 82 and 92 wt% (corresponding to 4.8, 6, 10 and 36 grafts per chain). The results showed a sharp decrease (by more than one order of magnitude) in the number of particles as the wt% of PEO is increased from 82 to 94 %. The reason for this reduction in the number of particles is the increased hydrophilicity of the graft copolymer which could result in desorption of the molecule from the surface of the particle. In addition, a graft with 36 side chains does not leave enough space for anchoring by the backbone.

The effect of PEO side chain length on emulsion polymerization using graft copolymers was systematically studied by keeping the backbone molecular weight the same (1,380) while gradually increasing the PEO molecular weight of the side chains from 750 to 5,000. For example by increasing M_w of PEO from 750 to 2,000 while keeping the wt% of PEO roughly the same (84 and 82 wt% respectively) the number of side chains in the graft decreases from 10 to 3. The results showed a decrease in the rate of polymerization as the number of side chains in the graft increases. This is followed by a sharp reduction in the number of particles produced. This clearly shows the importance of spacing of the side chains to ensure anchoring of the graft copolymer to the particle surface which is stronger with the graft containing a smaller number of side chains. If the number of side chains for the PEO with M_w of 2,000 is increased from 3 to 9 (93 wt% of PEO) the rate of polymerization and number of particles decrease. Using a PEO chain with M_w of 5,000 (92 wt% PEO) and 3 chains per graft gives the same result as the PEO 2,000 with 3 side chains. Any increase in the number of side chains in the graft results in a reduction in the rate of polymerization and the number of latex particles produced. This clearly shows the importance of spacing of the side chains of the graft copolymer.

Similar results were obtained using a graft copolymer of poly(methyl methacrylate-co-2-hydroxypropyl methacrylate)-graft–polyethylene oxide, PMMA(PEO)$_n$, for emulsion polymerization of methyl methacrylate. As with PMSt(PEO)$_n$ graft, the backbone molecular weight had little effect on the rate of polymerization or the number of particles used. The molecular weight of the PEO side chains was varied at constant M_w of the backbone (10,000). Three PEO grafts with M_w of 750, 2,000 and 5,000 were used. Although the rate of polymerization was similar for the three graft copolymers, yet the number of particles was significantly lower with the graft containing PEO 750. This shows that this short PEO chain is not sufficient to stabilize the particles. The overall content of PEO in the graft has also a big effect. Using the same backbone chain length while changing the wt% of PEO 200, it was found that the molecule containing 67 wt% PEO is not sufficient to stabilize the particles when compared with a graft containing 82 wt% PEO. This shows that a high concentration of PEO in the adsorbed layer is required for effective steric stabilization.

The chemical nature of the monomer also plays an important role. For example, stable latexes could be produced using PMSt(PEO)$_n$ graft but not with PMMA(PEO)$_n$ graft.

A novel graft copolymer of hydrophobically modified inulin (INUTEC® SP1) has been used in emulsion polymerization of styrene, methyl methacrylate, butyl acrylate and several other monomers [7]. All latexes were prepared by emulsion polymerization using potassium persulphate as initiator. The z-average particle size was determined by photon correlation spectroscopy (PCS) and electron micrographs were also taken.

Emulsion polymerization of styrene or methylmethacrylate showed an optimum weight ratio of (INUTEC® SP1)/monomer of 0.0033 for PS and 0.001 for PMMA particles. The (initiator)/(monomer) ratio was kept constant at 0.00125. The monomer conversion was higher than 85 % in all cases. Latex dispersions of PS reaching 50 % and of PMMA reaching 40 % could be obtained using such low concentrations of INUTEC® SP1. Fig. 5.1 shows the variation of particle diameter with monomer concentration.

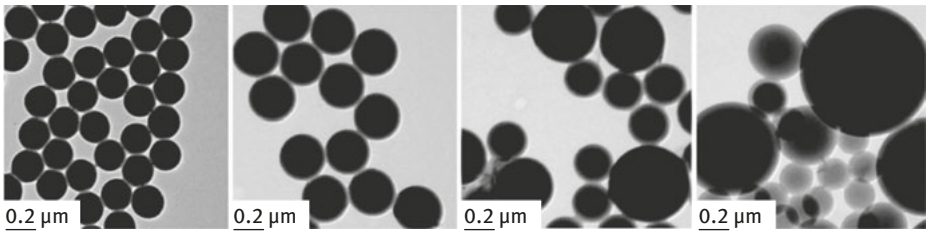

(5 wt%) (10 wt%) (30 wt%) (40 wt%)

(a) PS latexes

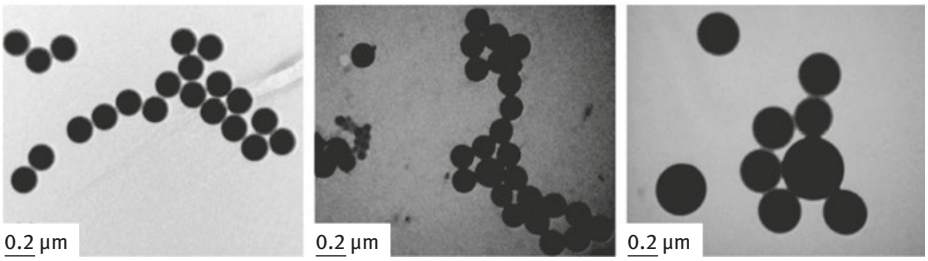

(10 wt%) (20 wt%) (30 wt%)

(b) PMMA latexes

Fig. 5.1: Electron micrographs of the latexes.

The stability of the latexes was determined by determining the critical coagulation concentration (CCC) using $CaCl_2$. The CCC was low (0.0175–0.05 mol dm^{-3}) but this was higher than that for the latex prepared without surfactant. Post addition of INUTEC® SP1 resulted in a large increase in the CCC as illustrated in Fig. 5.2 which shows log W–log C curves (where W is the ratio between the fast flocculation rate constant to the slow flocculation rate constant, referred to as the stability ratio) at various additions of INUTEC® SP1.

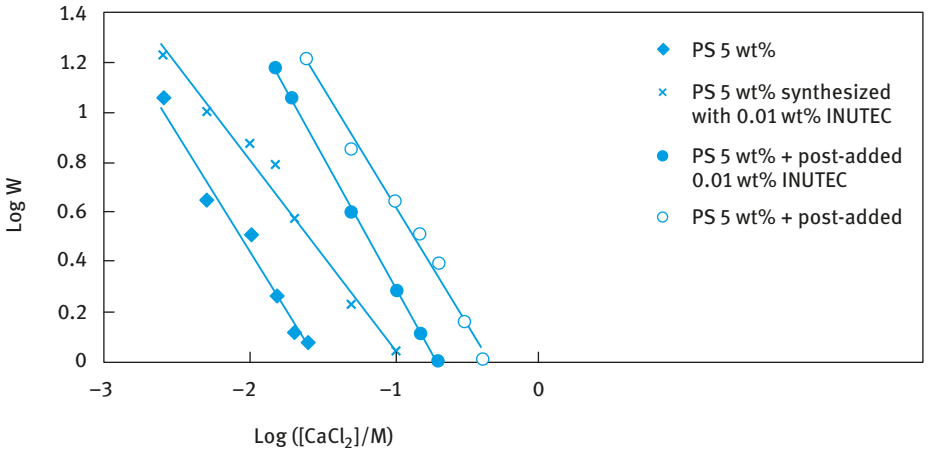

Fig. 5.2: Influence of post addition of INUTEC® SP1 on the latex stability.

As with the emulsions, the high stability of the latex when using INUTEC® SP1 is due to the strong adsorption of the polymeric surfactant on the latex particles and formation of strongly hydrated loops and tails of polyfructose that provide effective steric stabilization. Evidence for the strong repulsion produced when using INUTEC® SP1 was obtained from atomic force microscopy investigations [8] in which the force between hydrophobic glass spheres and hydrophobic glass plate, both containing an adsorbed layer of INUTEC® SP1, was measured as a function of distance of separation both in water and in the presence of various Na_2SO_4 concentrations. The results are shown in Fig. 5.3 and 5.4.

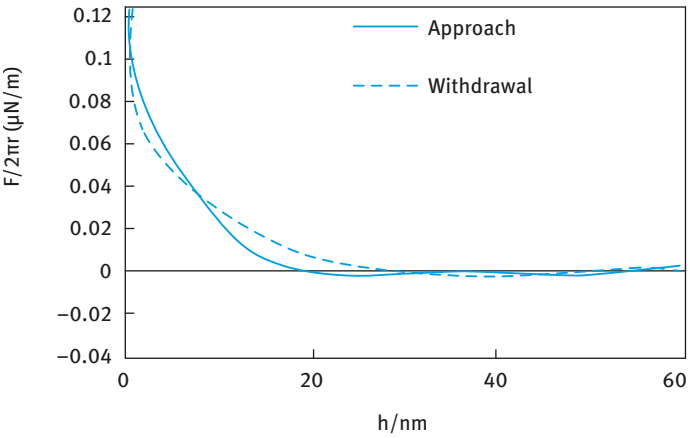

Fig. 5.3: Force–distance curves between hydrophobized glass surfaces containing adsorbed INUTEC® SP1 in water.

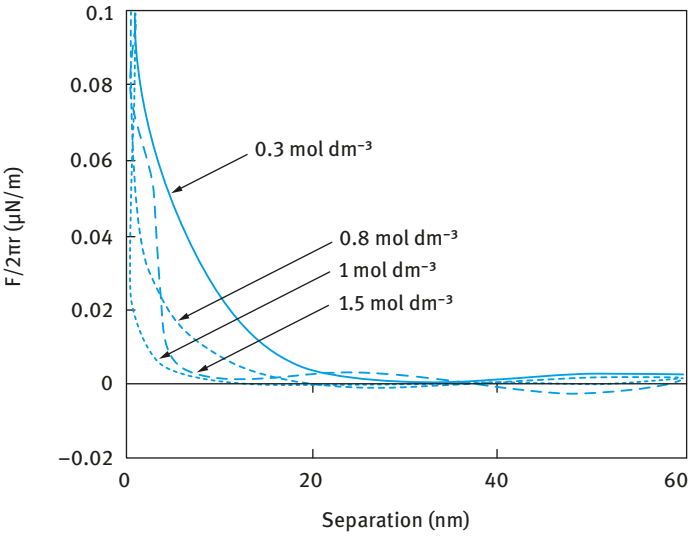

Fig. 5.4: Force–distance curves for hydrophobized glass surfaces containing adsorbed INUTEC® SP1 at various Na_2SO_4 concentrations.

5.3 Polymeric surfactants for stabilizing preformed latex dispersions

For this purpose polystyrene (PS) latexes were prepared using the surfactant-free emulsion polymerization [9]. Two latexes with *z*-average diameter of 427 and 867 (as measured using photon correlation spectroscopy, PCS) that are reasonably monodisperse were prepared. Two polymeric surfactants, namely Hypermer CG-6 and Atlox 4913 were used. Both are of the graft ("comb") type, consisting of polymethylmethacrylate/polymethacrylic acid (PMMA/PMA) backbone with methoxy-capped polyethylene oxide (PEO) side chains (M = 750 Daltons). Hypermer CG-6 is the same graft copolymer as Atlox 4913 but it contains a higher proportion of methacrylic acid in the backbone. The average molecular weight of the polymer is ≈ 5,000 Daltons. Fig. 5.5 shows a typical adsorption isotherm of Atlox 4913 on the two latexes. Similar results were obtained for Hypermer CG-6 but the plateau adsorption was lower (1.2 mg m^{-2} compared with 1.5 mg m^{-2} for Atlox 4913). It is likely that the backbone of Hypermer CG-6 that contains more PMA is more polar and hence less strongly adsorbed. The amount of adsorption was independent of particle size.

The influence of temperature on adsorption is shown in Fig. 5.6. The amount of adsorption increases with increasing temperature. This is due to the poorer solvency of the medium for the PEO chains. The PEO chains become less hydrated at higher temperature and the reduction of solubility of the polymer enhances adsorption.

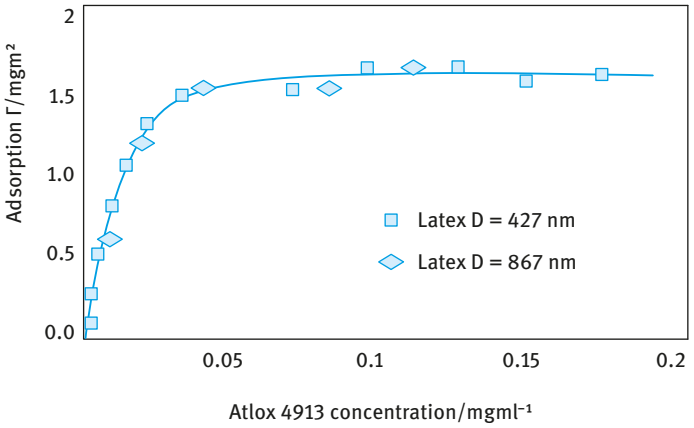

Fig. 5.5: Adsorption isotherms of Atlox 4913 on the two latexes at 25 °C.

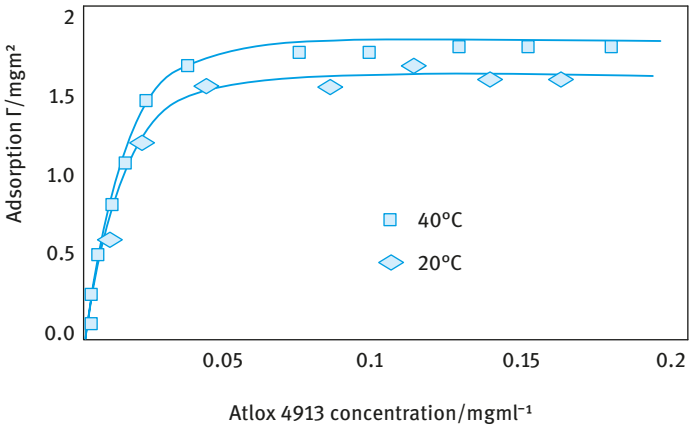

Fig. 5.6: Effect of temperature on adsorption of Atlox 4913 on PS.

The adsorbed layer thickness of the graft copolymer on the latexes was determined using rheological measurements (Chapter 14 of Vol. 1). Steady state (shear stress σ–shear rate $\dot{\gamma}$) measurements were carried out and the results were fitted to the Bingham equation to obtain the yield value σ_β and the high shear viscosity η of the suspension,

$$\sigma = \sigma_\beta + \eta\dot{\gamma}. \tag{5.3}$$

As an illustration Fig. 5.7 shows a plot of σ_β versus volume fraction ϕ of the latex for Atlox 4913. Similar results were obtained for latexes stabilized using Hypermer CG-6.

At any given volume fraction, the smaller latex has higher σ_β when compared to the larger latex. This is due to the higher ratio of adsorbed layer thickness to particle radius, Δ/R, for the smaller latex. The effective volume fraction of the latex ϕ_{eff} is

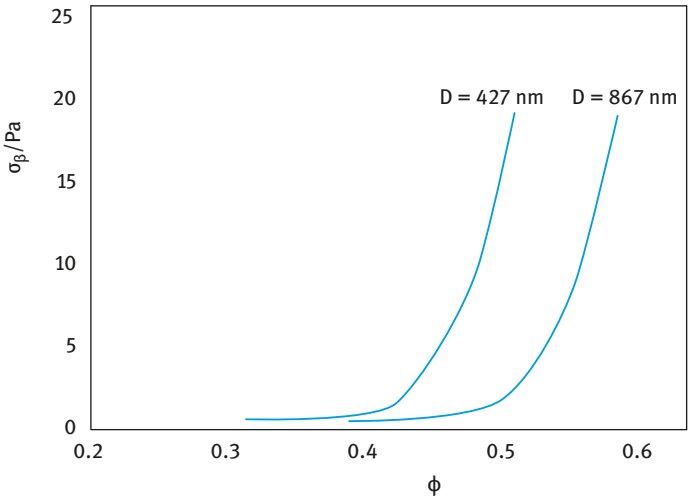

Fig. 5.7: Variation of yield stress with latex volume fraction for Atlox 4913.

related to the core volume fraction ϕ by the equation,

$$\phi_{\text{eff}} = \phi\left[1 + \frac{\Delta}{R}\right]^3. \tag{5.4}$$

ϕ_{eff} can be calculated from the relative viscosity η_r using the Dougherty–Krieger equation [10, 11],

$$\eta_r = \left[1 - \left(\frac{\phi_{\text{eff}}}{\phi_p}\right)\right]^{-[\eta]\phi_p}, \tag{5.5}$$

where ϕ_p is the maximum packing fraction.

The maximum packing fraction ϕ_p can be calculated using the following empirical equation [9],

$$\frac{(\eta_r^{1/2} - 1)}{\phi} = \left(\frac{1}{\phi_p}\right)(\eta^{1/2} - 1) + 1.25. \tag{5.6}$$

The results showed a gradual decrease of adsorbed layer thickness Δ with increasing volume fraction ϕ. For the latex with diameter D of 867 nm and Atlox 4913, Δ decreased from 17.5 nm at $\phi = 0.36$ to 6.5 at $\phi = 0.57$. For Hypermer CG-6 with the same latex, Δ decreased from 11.8 nm at $\phi = 0.49$ to 6.5 at $\phi = 0.57$. The reduction of Δ with increasing ϕ may be due to overlap and/or compression of the adsorbed layers as the particles come close to each other at higher volume fraction of the latex.

The stability of the latexes was determined using viscoelastic measurements, as discussed in Chapter 14 of Vol. 1. For this purpose, dynamic (oscillatory) measurements were used to obtain the storage modulus G^*, the elastic modulus G' and the viscous modulus G'' as a function of strain amplitude γ_0 and frequency ω (rad s^{-1}). The method relies on application of a sinusoidal strain or stress and the resulting

stress or strain is measured simultaneously. For a viscoelastic system the strain and stress sine waves oscillate with the same frequency but out of phase. From the time shift Δt and ω one can obtain the phase angle shift δ.

The ratio of the maximum stress σ_0 to the maximum strain γ_0 gives the complex modulus $|G^*|$

$$|G^*| = \frac{\sigma_0}{\gamma_0}. \tag{5.7}$$

$|G^*|$ can be resolved into two components: storage (elastic) modulus G', the real component of the complex modulus; loss (viscous) modulus G'', the imaginary component of the complex modulus. The complex modulus can be resolved into G' and G'' using vector analysis and the phase angle shift δ,

$$G' = |G^*| \cos \delta, \tag{5.8}$$

$$G'' = |G^*| \sin \delta. \tag{5.9}$$

G' is measured as a function of electrolyte concentration and/or temperature to assess the latex's stability. As an illustration Fig. 5.8 shows the variation of G' with temperature for latex stabilized with Atlox 4913 in the absence of any added electrolyte and in the presence of 0.1, 0.2 and 0.3 mol dm^{-3} Na_2SO_4. In the absence of electrolyte G' showed no change with temperature up to 65 °C.

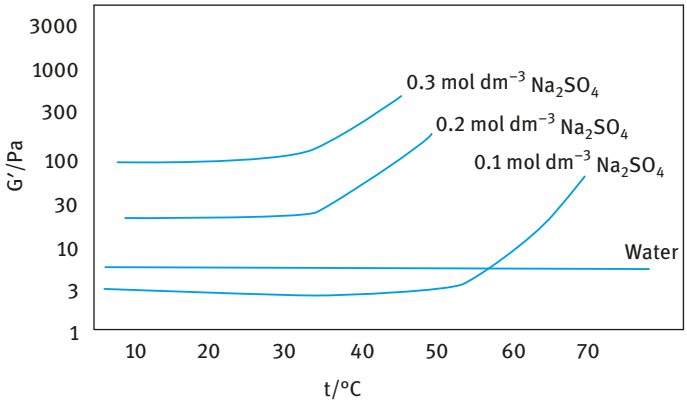

Fig. 5.8: Variation of G' with temperature in water and at various Na_2SO_4 concentrations.

In the presence of 0.1 mol dm^{-3} Na_2SO_4, G' remained constant up to 40 °C above which G' increased with any further increase of temperature. This temperature is denoted as the critical flocculation temperature (CFT). The CFT decreases with increasing electrolyte concentration reaching ≈ 30 °C in 0.2 and 0.3 mol dm^{-3} Na_2SO_4. This reduction in CFT with increasing electrolyte concentration is due to the reduction in solvency of the PEO chains with increasing electrolyte concentrations. The latex stabilized with

Hypermer CG-6 gave relatively higher CFT values when compared with that stabilized using Atlox 4913.

5.4 Dispersion polymerization

This method is usually applied for the preparation of nonaqueous latex dispersions and hence it is referred to as NAD [12]. The method has also been adapted to prepare aqueous latex dispersions by using an alcohol–water mixture.

In the NAD process the monomer, normally an acrylic, is dissolved in a nonaqueous solvent, normally an aliphatic hydrocarbon and an oil-soluble initiator and a stabilizer (to protect the resulting particles from flocculation, sometimes referred to as "protective colloid") are added to the reaction mixture. The most successful stabilizers used in NAD are block and graft copolymers. These block and graft copolymers are assembled in a variety of ways to provide the molecule with an "anchor chain" and a stabilizing chain. The anchor chain should be sufficiently insoluble in the medium and have a strong affinity to the polymer particles produced. In contrast, the stabilizing chain should be soluble in the medium and strongly solvated by its molecules to provide effective steric stabilization. The length of the anchor and stabilizing chains has to be carefully adjusted to ensure strong adsorption (by multipoint attachment of the anchor chain to the particle surface) and a sufficiently "thick" layer of the stabilizing chain that prevents close approach of the particles to a distance where the van der Waals attraction becomes strong. Several configurations of block and graft copolymers are possible, as is illustrated in Fig. 5.9.

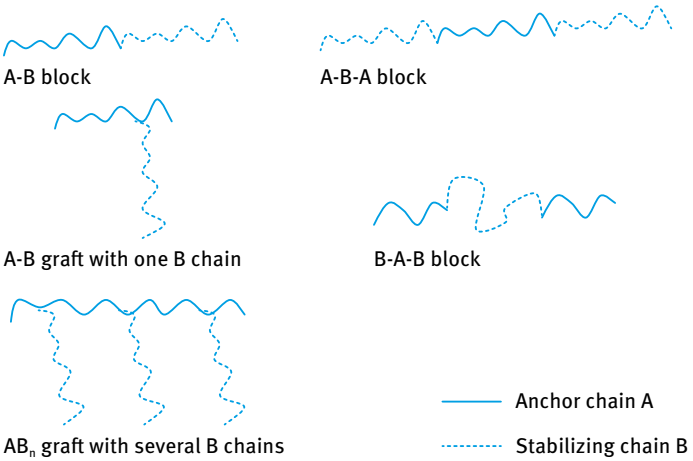

Fig. 5.9: Configurations of block and graft copolymers.

Typical preformed graft stabilizers based on poly(12-hydroxy stearic acid) (PHS) are simple to prepare and effective in NAD polymerization. Commercial 12-hydroxystearic acid contains 8–15 % palmitic and stearic acids which limits the molecular weight during polymerization to an average of 1,500–2,000. This oligomer may be converted to a "macromonomer" by reacting the carboxylic group with glycidyl methacrylate. The macromonomer is then copolymerized with an equal weight of methyl methacrylate (MMA) or similar monomer to give a "comb" graft copolymer with an average molecular weight of 10,000–20,000. The graft copolymer contains on average 5–10 PHS chains pendent from a polymeric anchor backbone of PMMA. This graft copolymer can stabilize latex particles of various monomers. The major limitation of the monomer composition is that the polymer produced should be insoluble in the medium used.

Several other examples of block and graft copolymers that are used in dispersion polymerization are given in Tab. 5.3 which also shows the continuous phase and disperse polymer that can be used with these polymers.

Tab. 5.3: Block and graft copolymers used in dispersion polymerization.

Polymeric surfactant	Continuous phase	Disperse polymer
Polystyrene-block–poly(dimethyl siloxane)	Hexane	Polystyrene
Polystyrene-block–poly(methacrylic acid)	Ethanol	Polystyrene
Polybutadiene-graft–poly(methacrylic acid)	Ethanol	Polystyrene
Poly(2-ethylhexyl acrylate)-graft–poly(vinyl acetate)	Aliphatic hydrocarbon	Poly(methyl methacrylate)
Polystyrene-block–poly(t-butylstyrene)	Aliphatic hydrocarbon	Polystyrene

Two main criteria must be considered in the process of dispersion polymerization:
(i) the insolubility of the formed polymer in the continuous phase;
(ii) the solubility of the monomer and initiator in the continuous phase.

Initially, dispersion polymerization starts as a homogeneous system but after sufficient polymerization, the insolubility of the resulting polymer in the medium forces it to precipitate. Initially, polymer nuclei are produced which then grow to polymer particles. The latter are stabilized against aggregation by the block or graft copolymer that is added to the continuous phase before the process of polymerization starts. It is essential to choose the right block or graft copolymer which should have a strong anchor chain A and good stabilizing chain B as schematically represented in Fig. 5.9.

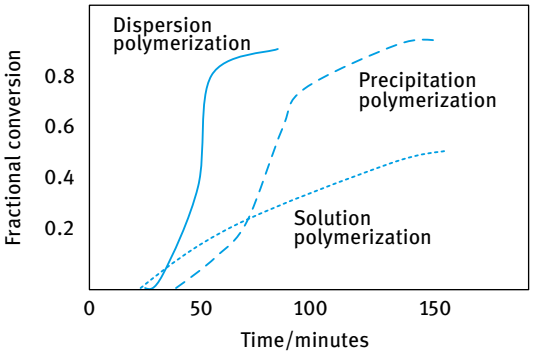

Fig. 5.10: Comparison of rates of polymerization.

Dispersion polymerization may be considered as a heterogeneous process which may include emulsion, suspension, precipitation and dispersion polymerization. In dispersion and precipitation polymerization, the initiator must be soluble in the continuous phase, whereas in emulsion and suspension polymerization the initiator is chosen to be soluble in the disperse phase of the monomer. A comparison of the rate of polymerization of methylmethacrylate at 80 °C for the three systems was given by Barrett and Thomas [13] as illustrated in Fig. 5.10. The rate of dispersion polymerization is much faster than that of precipitation or solution polymerization. The enhancement of the rate in precipitation polymerization over solution polymerization has been attributed to the hindered termination of the growing polymer radicals.

Several mechanisms have been proposed to explain the mechanism of emulsion polymerization; however, no single mechanism can explain all happenings in emulsion polymerization. Barrett and Thomas [13] suggested that particles are formed in emulsion polymerization by two main steps:

(i) Initiation of monomer in the continuous phase and subsequent growth of the polymer chains until the latter become insoluble. This process clearly depends on the nature of the polymer and medium.
(ii) The growing oligomeric chains associate with each other forming aggregates which below a certain size are unstable and they become stabilized by the block or graft copolymer added.

As mentioned before, this aggregative nucleation theory cannot explain all happenings in dispersion polymerization. An alternative mechanism based on Napper's theory [2, 3] for aqueous emulsion polymerization can be adapted to the process of dispersion polymerization. This theory includes coagulation of the nuclei formed and not just association of the oligomeric species. The precursor particles (nuclei) being unstable can undergo one of the following events to become colloidally stable:

(i) homocoagulation, i.e. collision with other precursor particles;
(ii) growth by propagation, adsorption of stabilizer;
(iii) swelling with monomer.

The nucleation terminating events are diffusional capture of oligomers and heterocoagulation.

The number of particles formed in the final latex does not depend on particle nucleation alone, since other steps are involved which determine how many precursor particles created are involved in the formation of a colloidally stable particle. This clearly depends on the effectiveness of the block or graft copolymer used in stabilizing the particles (see below).

In most cases an increase in polymeric surfactant concentration (at any given monomer amount) results in the production of larger number of particles with smaller size. This is to be expected since the larger number of particles with smaller size (i.e. larger total surface area of the disperse particles) requires more polymeric surfactant for their formation. The molecular weight of the polymeric surfactant can also influence the number of particles formed. For example Dawkins and Taylor [14] found that in dispersion polymerization of styrene in hexane, increasing the molecular weight of the block copolymer of polydimethyl siloxane-block–polystyrene resulted in the formation of smaller particles, which was attributed to the more effective steric stabilization by the higher molecular weight block.

A systematic study of the effect of monomer solubility and concentration in the continuous phase was carried out by Antl and co-workers [15]. Dispersion polymerization of methyl methacrylate in hexane mixed with a high boiling point aliphatic hydrocarbon was investigated using poly(12-hydoxystyearic acid)-glycidyl methacrylate block copolymer. They found that the methyl methacrylate concentration had a drastic effect on the size of the particles produced. When the monomer concentration was kept below 8.5 %, very small particles (80 nm) were produced and these remained very stable. However, between 8.5 and 35 % monomer the latex produced was initially stable but flocculated during polymerization. An increase in monomer concentration from 35 to 50 % results in the formation of a stable latex, but the particle size increased sharply from 180 nm to 2.6 μm as the monomer concentration increased. The authors suggested that the final particle size and stability of the latex are strongly affected by increased monomer concentration in the continuous phase. The presence of monomer in the continuous phase increases the solvency of the medium for the polymer formed. In a good solvent for the polymer, the growing chain is capable of reaching higher molecular weight before it is forced to phase separate and precipitate.

NAD polymerization is carried in two steps:

(i) Seed stage: the diluent, portion of the monomer, portion of dispersant and initiator (azo or peroxy type) are heated to form an initial low-concentration fine dispersion.
(ii) Growth stage: the remaining monomer together with more dispersant and initiator are then fed over the course of several hours to complete the growth of the particles.

A small amount of transfer agent is usually added to control the molecular weight. Excellent control of particle size is achieved by proper choice of the designed dispersant and correct distribution of dispersant between the seed and growth stages. NAD acrylic polymers are applied in automotive thermosetting polymers, and hydroxy monomers may be included in the monomer blend used.

Two main factors must be considered when considering the long-term stability of a nonaqueous polymer dispersion. The first and very important factor is the nature of the "anchor chain" A. As mentioned above, this should have a strong affinity to the produced latex and in most cases it can be designed to be "chemically" attached to the polymer surface. Once this criterion is satisfied, the second important factor in determining stability is the solvency of the medium for the stabilizing chain B. As will be discussed in detail, the solvency of the medium is characterized by the Flory–Huggins interaction parameter χ. Three main conditions can be identified:

- $\chi < 0.5$ (good solvent for the stabilizing chain);
- $\chi > 0.5$ (poor solvent for the stabilizing chain);
- $\chi = 0.5$ (referred to as the θ-solvent).

Clearly, to maintain stability of the latex dispersion, the solvent must be better than a θ-solvent. The solvency of the medium for the B chain is affected by addition of a nonsolvent and/or temperature changes. It is, therefore, essential to determine the critical volume fraction (CFV) of a nonsolvent above which flocculation (sometimes referred to as incipient flocculation) occurs. One should also determine the critical flocculation temperature at any given solvent composition, below which flocculation occurs. The correlation between CFV or CFT and the flocculation of the nonaqueous polymer dispersion has been demonstrated by Napper [16] who investigated the flocculation of poly(methyl methacrylate) dispersions stabilized by poly(12-hydroxy stearic acid) or poly(n-lauryl methacrylate-co-glycidyl methacrylate) in hexane by adding a nonsolvent such as ethanol or propanol and cooling the dispersion. The dispersions remained stable until the addition of ethanol transformed the medium to a θ-solvent for the stabilizing chains in solution. However, flocculation did occur under conditions of slightly better than θ-solvent for the chains. The same was found for the CFT which was 5–15 K above the θ-temperature. This difference was accounted for by the polydispersity of the polymer chains. The θ-condition is usually determined by cloud point measurements and the least soluble component will precipitate first, giving values that are lower than the CFV or higher than the CFT.

5.5 Particle formation in polar media

The process of dispersion polymerization has been applied in many cases using completely polar solvents such as alcohol or alcohol–water mixtures [17]. The results obtained showed completely different behaviour when compared with dispersion poly-

merization in nonpolar media. For example, results obtained by Lok and Ober [17] using styrene as monomer and hydroxypropyl cellulose as stabilizer showed a linear increase in particle diameter with increasing weight percent of the monomer. There was no region in monomer concentration where instability occurred (as has been observed for the dispersion polymerization of methyl methacrylate in aliphatic hydrocarbons). Replacing water in the continuous phase with 2-methoxyethanol, Lok and Ober were able to grow large, monodisperse particles up to 15 μm in diameter. They concluded from these results that the polarity of the medium is the controlling factor in the formation of particles and their final size. The authors suggested a mechanism in which the polymeric surfactant molecule grafts to the polystyrene chain, forming a physically anchored stabilizer (nuclei). These nuclei grow to form the polymer particles. Paine [18] carried out dispersion polymerization of styrene by systematically increasing the alcohol chain length from methanol to octadecanol and using hydroxypropyl cellulose as stabilizer. The results showed an increase in particle diameter with increasing number of carbon atoms in the alcohol, reaching a maximum when hexanol was used as the medium, after which there was a sharp decrease in the particle diameter with a further increase in the number of carbon atoms in the alcohol. Paine explained his results in terms of the solubility parameter of the dispersion medium. The largest particles are produced when the solubility parameter of the medium is closest to those of styrene and hydroxypropyl cellulose.

References

[1] Blakely DC. Emulsion polymerization. London; Elsevier Applied Science; 1975.
[2] Litchi G, Gilbert RG, Napper DH. J Polym Sci. 1983;21:269.
[3] Feeney PJ, Napper DH, Gilbert RG. Macromolecules. 1984;17:2520; 1987;20:2922.
[4] Smith WV, Ewart RH. J Chem Phys. 1948;16:592.
[5] Piirma I. Polymeric surfactants. Surfactant Science Series, No.42. New York: Marcel Dekker; 1992.
[6] Piirma I, Lenzotti JR. Br Polymer J. 1959;21:45.
[7] Nestor J, Esquena J, Solans C, Levecke B, Booten K, Tadros TF. Langmuir. 2005;21:4837.
[8] Nestor J, Esquena J, Solans C, Luckham PF, Levecke B, Tadros TF. J Colloid Interface Sci. 2007;311:430.
[9] Liang W, Bognolo G, Tadros TF. Langmuir. 1995;11:2899.
[10] Krieger IM, Dougherty TJ. Trans Soc Rheol. 1959;3:137.
[11] Krieger IM, Advances Colloid and Interface Sci. 1972;3:111.
[12] Barrett KEJ, editor. Dispersion polymerization in organic media. Chichester: John Wiley & Sons, Ltd; 1975.
[13] Barrett KEJ and Thomas HR. J Polym Sci Part A1. 1969;7:2627.
[14] Dawkins JV, Taylor G. Polymer. 1987;20:171.
[15] Antl I, Goodwin JW, Hill RD, Ottewill RH, Owen SM, Papworth S, Waters JA. Colloids Surf. 1986;1:67.
[16] Napper DH. Polymeric stabilisation of colloidal dispersions. London: Academic Press; 1983.
[17] Lok KP, Ober CK. Can J Chem. 1985;63:209.
[18] Paine AJ. J Polymer Sci Part A. 1990;28:2485.

6 Formulation of microemulsions

6.1 Introduction

Microemulsions, which are better described as swollen micelles, are a special class of nanodispersions (transparent or translucent) which actually have little in common with emulsions. The term microemulsion was first introduced by Hoar and Schulman [1, 2] who discovered that by titration of a milky emulsion (stabilized by soap such as potassium oleate) with a medium chain alcohol such as pentanol or hexanol, a transparent or translucent system was produced. A schematic representation of the titration method adopted by Schulman and co-workers is given below,

O/W emulsion stabilized by soap	→	Add cosurfactant, e.g. $C_5H_{11}OH$, $C_6H_{13}OH$	→	Transparent or translucent

Microemulsions are applied in many industrial formulations of which the following are worth mentioning: enhanced and tertiary oil recovery, for preparation of nanoparticles by mixing two microemulsions containing two or more chemicals that can interact on collision of two microemulsion droplets, in agrochemicals for enhancing biological performance, in dry cleaning formulations, in floor polishes, etc.

A convenient way to describe microemulsions is to compare them with micelles. Micelles are thermodynamically stable and may consist of spherical units with a radius that is usually less than 5 nm. Two types of micelles may be considered: normal micelles with the hydrocarbon tails forming the core and the polar head groups in contact with the aqueous medium; and reverse micelles (formed in nonpolar media) with a water core containing the polar head groups and the hydrocarbon tails now in contact with the oil. Normal micelles can solubilize oil in the hydrocarbon core forming O/W microemulsions, whereas reverse micelles can solubilize water forming a W/O microemulsion. A schematic representation of these systems is shown in Fig. 6.1.

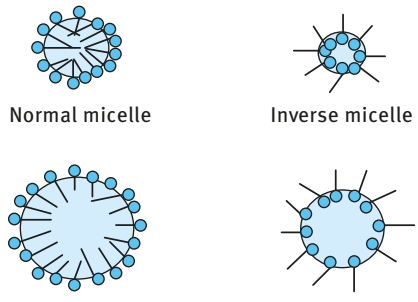

Fig. 6.1: Schematic representation of microemulsions.

https://doi.org/10.1515/9783110587968-007

A rough guide to the dimensions of micelles, micellar solutions and macroemulsions is as follows: micelles, $R < 5$ nm (they scatter little light and are transparent); macroemulsions, $R > 50$ nm (opaque and milky); micellar solutions or microemulsions, 5–50 nm (transparent, 5–10 nm, translucent 10–50 nm).

The classification of microemulsions based on size is not adequate. Whether a system is transparent or translucent depends not only on the size but also on the difference in refractive index between the oil and the water phases. A microemulsion with small size (in the region of 10 nm) may appear translucent if the difference in refractive index between the oil and the water is large. Relatively large sized microemulsion droplets (in the region of 50 nm) may appear transparent if the refractive index difference is very small. The best definition of microemulsions is based on the application of thermodynamics as is discussed below.

6.2 Thermodynamic definition of microemulsions

A thermodynamic definition of microemulsions can be obtained from a consideration of the energy and entropy terms for formation of microemulsions. This is represented in Fig. 6.2 which schematically shows the process of formation of a microemulsion from a bulk oil phase (for an O/W microemulsion) or bulk water phase (for a W/O microemulsion). A_1 is the surface area of the bulk oil phase and A_2 is the total surface area of all the microemulsion droplets. γ_{12} is the O/W interfacial tension.

The increase in surface area when going from state I to state II is $\Delta A (= A_2 - A_1)$ and the surface energy increase is equal to $\Delta A \gamma_{12}$. The increase in entropy when going from state I to state II is $T\Delta S^{\text{conf}}$ (note that state II has higher entropy since a large number of droplets can arrange themselves in several ways, whereas state I with one oil drop has much lower entropy).

According to the second law of thermodynamics, the free energy of formation of microemulsions ΔG_{m} is given by the following expression,

$$\Delta G_{\text{m}} = \Delta A \gamma_{12} - T\Delta S^{\text{conf}}. \tag{6.1}$$

With macroemulsions $\Delta A \gamma_{12} \gg T\Delta S^{\text{conf}}$ and $\Delta G_{\text{m}} > 0$. The system is nonspontaneous (it requires energy for formation of the emulsion drops) and it is thermodynamically unstable. With microemulsions $\Delta A \gamma_{12} \leq T\Delta S^{\text{conf}}$ (this is due to the ultra-low interfacial tension accompanying microemulsion formation) and $\Delta G_{\text{m}} \leq 0$. The system is produced spontaneously and it is thermodynamically stable.

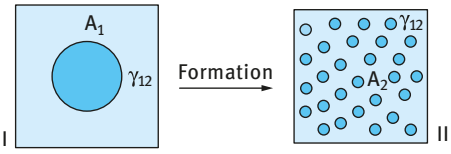

Fig. 6.2: Schematic representation of microemulsion formation.

The above analysis shows the contrast between emulsions and microemulsion: With emulsions, an increase in mechanical energy and an increase in surfactant concentration usually result in the formation of smaller droplets which become kinetically more stable. With microemulsions, neither increasing mechanical energy nor increasing surfactant concentration can result in its formation. Formation of microemulsions is based on a specific combination of surfactants and specific interaction with the oil and the water phases and the system is produced at optimum composition.

Thus, microemulsions have nothing in common with macroemulsions and in many cases it is better to describe the system as "swollen micelles". The best definition of microemulsions is as follows [3]: "system of water + oil + amphiphile that is a single optically isotropic and thermodynamically stable liquid solution". Amphiphiles refer to any molecule that consists of hydrophobic and hydrophilic portions, e.g. surfactants, alcohols, etc.

The driving force for microemulsion formation is the low interfacial energy which is overcompensated by the negative entropy of dispersion term. The low (ultra-low) interfacial tension is produced in most cases by the combination of two molecules, referred to as the surfactant and cosurfactant (e.g. medium chain alcohol).

6.3 Mixed film and solubilization theories of microemulsions

6.3.1 Mixed film theories [4]

The film (which may consist of surfactant and cosurfactant molecules) is considered a liquid "two-dimensional" third phase in equilibrium with both oil and water. Such a monolayer could be a duplex film, i.e. giving different properties on the water side and on the oil side. The initial "flat" duplex film (Fig. 6.3) has different tensions at the oil and water sides. This is due to the different packing of the hydrophobic and hydrophilic groups (these groups have different sizes and cross-sectional areas).

It is convenient to define a two-dimensional surface pressure π,

$$\pi = \gamma_0 - \gamma. \tag{6.2}$$

γ_0 is the interfacial tension of the clean interface, whereas γ is the interfacial tension with adsorbed surfactant.

One can define two values for π at the oil and water phases, π_o and π_w which for a flat film are not equal, i.e. $\pi'_o \neq \pi'_w$. As a result of the difference in tensions, the film will bend until $\pi_o = \pi_w$. If $\pi'_o > \pi'_w$, the area at the oil side has to expand (resulting in reduction of π'_o) until $\pi_o = \pi_w$. In this case a W/O microemulsion is produced. If $\pi'_w > \pi'_o$, the area at the water side expands until $\pi_w = \pi_o$. In this case an O/W microemulsion is produced. A schematic representation of film bending for the production of W/O or W/O microemulsions is illustrated in Fig. 6.3.

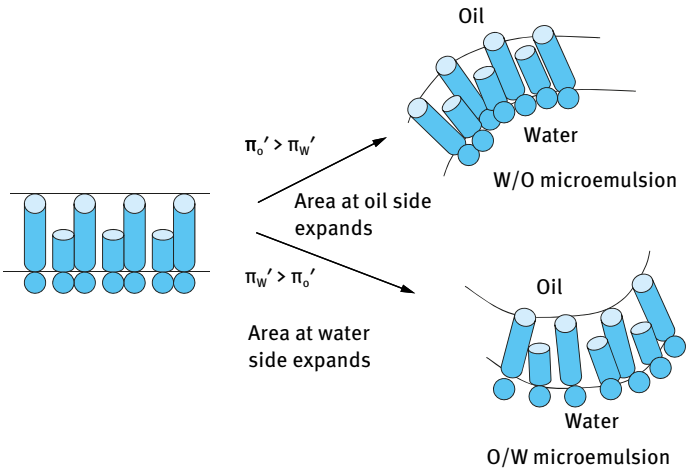

Fig. 6.3: Schematic representation of film bending.

According to the duplex film theory, the interfacial tension γ_T is given by the following expression [5],

$$\gamma_T = \gamma_{(o/w)} - \pi, \tag{6.3}$$

where $(\gamma_{o/w})_a$ is the interfacial tension that is reduced by the presence of the alcohol.

The value of $(\gamma_{o/w})_a$ is significantly lower than $\gamma_{o/w}$ in the absence of the alcohol (for example, for hydrocarbon/water $\gamma_{o/w}$ is reduced from 50 to 15–20 mN m^{-1} on the addition of a significant amount of a medium chain alcohol like pentanol or hexanol). Contributions to π are considered to be due to crowding of the surfactant and cosurfactant molecules and penetration of the oil phase into the hydrocarbon chains of the interface. According to equation (6.3) if $\pi > (\gamma_{o/w})_a$, γ_T becomes negative and this leads to expansion of the interface until γ_T reaches a small positive value. Since $(\gamma_{o/w})_a$ is of the order of 15–20 mN m^{-1}, surface pressures of this order are required for γ_T to approach a value of zero.

The above duplex film theory can explain the nature of the microemulsion: The surface pressures at the oil and water sides of the interface depend on the interactions of the hydrophobic and hydrophilic potions of the surfactant molecule at both sides respectively. If the hydrophobic groups are bulky in nature relative to the hydrophilic groups, then for a flat film such hydrophobic groups tend to crowd forming a higher surface pressure at the oil side of the interface; this results in bending and expansion at the oil side forming a W/O microemulsion. An example for a surfactant with bulky hydrophobic groups is Aerosol OT (dioctyl sulphosuccinate). If the hydrophilic groups are bulky, such as is the case with ethoxylated surfactants containing more than 5 ethylene oxide units, crowding occurs at the water side of the interface. This produces an O/W microemulsion.

6.3.2 Solubilization theories

These concepts were introduced by Shinoda and co-workers [6] who considered microemulsions to be swollen micelles that are directly related to the phase diagram of their components.

Consider the phase diagram of a three-component system of water, ionic surfactant and medium chain alcohol as described in Fig. 6.4. At the water corner and at low alcohol concentration, normal micelles (L_1) are formed since in this case there are more surfactant than alcohol molecules. At the alcohol (cosurfactant) corner, inverse micelles (L_2) are formed, since in this region there are more alcohol than surfactant molecules.

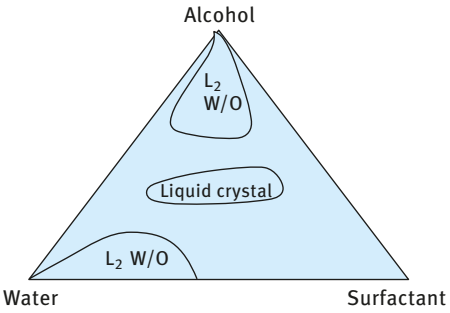

Fig. 6.4: Schematic representation of three-component phase diagram.

These L_1 and L_2 are not in equilibrium but are separated by a liquid crystalline region (lamellar structure with equal number of surfactant and alcohol molecules). The L_1 region may be considered an O/W microemulsion, whereas the L_2 may be considered a W/O microemulsion.

Addition of a small amount of oil miscible with the cosurfactant, but not with the surfactant and water, changes the phase diagram only slightly. The oil may be simply solubilized in the hydrocarbon core of the micelles. Addition of more oil leads to fundamental changes of the phase diagram as illustrated in Fig. 6.5 whereby 50 : 50 of W : O are used. To simplify the phase diagram, the $^{50}W/^{50}O$ are presented on one corner of the phase diagram.

Near the cosurfactant (co) corner the changes are small compared to the three-phase diagram (Fig. 6.5). The O/W microemulsion near the water–surfactant (sa) axis is not in equilibrium with the lamellar phase, but with a non-colloidal oil + cosurfactant phase. If co is added to such a two-phase equilibrium at fairly high surfactant concentration all oil is taken up and a one-phase microemulsion appears. Addition of co at low sa concentration may lead to separation of an excess aqueous phase before all oil is taken up in the microemulsion. A three-phase system is formed, containing a microemulsion that cannot be clearly identified as W/O or W/O and that presumably is similar to the lamellar phase swollen with oil or to a more irregular intertwining

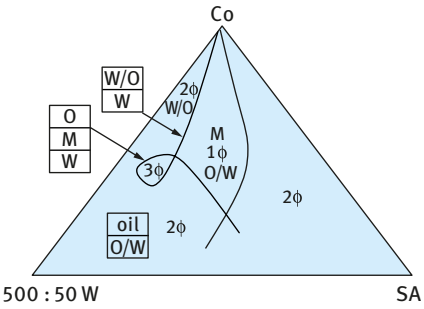

Fig. 6.5: Schematic representation of the pseudo-ternary phase diagram of oil/water/surfactant/cosurfactant.

of aqueous and oily regions (bicontinuous or middle phase microemulsion). The interfacial tensions between the three phases are very low ($0.1–10^{-4}$ mN m^{-1}). Further addition of co to the three-phase system makes the oil phase disappear and leaves a W/O microemulsion in equilibrium with a dilute aqueous sa solution. In the large one-phase region continuous transitions from O/W to middle phase to W/O microemulsions are found.

Solubilization can also be illustrated by considering the phase diagrams of nonionic surfactants containing poly(ethylene oxide) (PEO) head groups. Such surfactants do not generally need a cosurfactant for microemulsion formation. A schematic representation of oil and water solubilization by nonionic surfactants is given in Fig. 6.6.

At low temperatures, the ethoxylated surfactant is soluble in water and at a given concentration is capable of solubilizing a given amount of oil. The oil solubilization increases rapidly with increasing temperature near the cloud point of the surfactant. This is illustrated in Fig. 6.6 (a) which shows the solubilization and cloud point curves of the surfactant. Between these two curves, an isotropic region of O/W solubilized system exists. At any given temperature, any increase in the oil weight fraction above

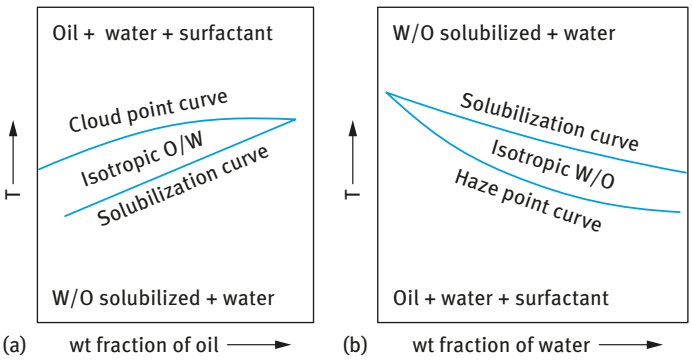

Fig. 6.6: Schematic representation of solubilization: (a) oil solubilized in a nonionic surfactant solution; (b) water solubilized in an oil solution of a nonionic surfactant.

the solubilization limit results in oil separation (oil solubilized + oil). At any given surfactant concentration, any increase in temperature above the cloud point results in separation into oil, water and surfactant.

If one starts from the oil phase with dissolved surfactant and adds water, solubilization of the latter takes place and solubilization increases with a reduction of temperature near the haze point. Between the solubilization and haze point curves, an isotropic region of W/O solubilized system exists (Fig. 6.6 (b)). At any given temperature, any increase in water weight fraction above the solubilization limit results in water separation (W/O solubilized + water). At any given surfactant concentration, any decrease in temperature below the haze point results in separation into water, oil and surfactant.

With nonionic surfactants, both types of microemulsions can be formed depending on the conditions. With such systems temperature is the most crucial factor since the solubility of surfactant in water or oil depends on temperature. Microemulsions prepared using nonionic surfactants have a limited temperature range.

6.4 Thermodynamic theory of microemulsion formation

Spontaneous formation of a microemulsion with a decrease of free energy can only be expected if the interfacial tension is so low that the remaining free energy of the interface is over compensated for by the entropy of dispersion of the droplets in the medium [7, 8]. This concept forms the basis of the thermodynamic theory proposed by Ruckenstein and Chi and Overbeek [7, 8].

6.4.1 Reason for combining two surfactants

Single surfactants do lower the interfacial tension γ, but in most cases the critical micelle concentration (cmc) is reached before γ is close to zero. Addition of a second surfactant of a completely different nature (i.e. predominantly oil soluble such as an alcohol) then lowers γ further and very small, even transiently negative values may be reached [9]. This is illustrated in Fig. 6.7 which shows the effect of addition of the cosurfactant on the γ–log C_{sa} curve. It can be seen that addition of cosurfactant shifts the whole curve to low γ values and the cmc is shifted to lower values.

For a multicomponent system i, each with an adsorption Γ_i (mol m^{-2}, referred to as the surface excess), the reduction in γ, i.e. dγ, is given by the following expression,

$$d\gamma = -\sum \Gamma_i \, d\mu_i = -\sum \Gamma_i RT \, d \ln C_i, \tag{6.4}$$

where μ_i is the chemical potential of component i, R is the gas constant, T is the absolute temperature and C_i is the concentration (mol dm^{-3}) of each surfactant component.

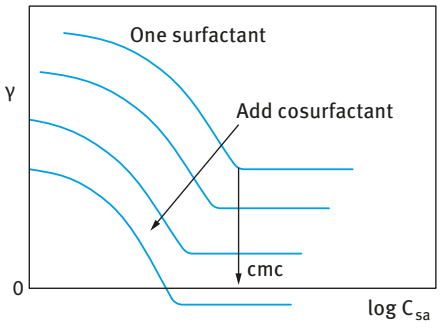

Fig. 6.7: γ–log C_{sa} curves for surfactant + cosurfactant.

The reason for the lowering of γ when using two surfactant molecules can be understood from a consideration of the Gibbs adsorption equation for multicomponent systems [9]. For two components sa (surfactant) and co (cosurfactant), equation (6.4) becomes,

$$d\gamma = -\Gamma_{sa} RT \, d \ln C_{sa} - \Gamma_{co} RT \, d \ln C_{co}. \tag{6.5}$$

Integration of equation (6.5) gives,

$$\gamma = \gamma_0 - \int_0^{C_{sa}} \Gamma_{sa} RT \, d \ln C_{sa} - \int_0^{C_{co}} \Gamma_{co} RT \, d \ln C_{co} \tag{6.6}$$

which clearly shows that γ_0 is lowered by two terms, from both surfactant and cosurfactant.

The two surfactant molecules should adsorb simultaneously and they should not interact with each other, otherwise they lower their respective activities. Thus, the surfactant and cosurfactant molecules should vary in nature, one predominantly water soluble (such as an anionic surfactant) and predominantly oil soluble (such as a medium chain alcohol).

In some cases a single surfactant may be sufficient for lowering γ far enough for microemulsion formation to become possible, e.g. Aerosol OT (sodium diethyl hexyl sulphosuccinate) and many nonionic surfactants.

6.4.2 Free energy of formation of microemulsions

A simple model was used by Overbeek [9] to calculate the free energy of formation of a model W/O microemulsion: the droplets were assumed to be of equal size. The droplets are large enough to consider the adsorbed surfactant layer to have constant composition.

The microemulsion is prepared in a number of steps and for each step one calculates the Helmholtz free energy F. This was chosen since the pressure inside the drop is higher by the Laplace pressure $2\gamma/a$ (where a is the droplet radius) than the pressure in the medium.

A summary of the four steps involved in the preparation of a model W/O microemulsion is given below:

(i) Prepare the oil phase in its final concentration,

$$F_1 = \sum n_i' \mu_i' - p_1 V_1, \tag{6.7}$$

where n_i' and μ_i' are the amount and chemical potential of oil and cosurfactant in the continuous phase, without droplets being mixed in. p_1 is the atmospheric pressure and V_1 is the volume of the oil phase.

(ii) Prepare the aqueous phase in its final concentration,

$$F_2 = \sum n_i' \mu_i' - p_1 V_2, \tag{6.8}$$

where i are now water, surfactant and salt and V_2 is the volume of the water phase.

(iii) Form the water phase into droplets close packed in the oil phase (i.e. with a packing fraction $\phi = 0.74$) and add all the adsorbed material,

$$F_3 = \gamma A + \Gamma_{sa} A \left[\mu_{sa}' + \left(2\frac{\gamma}{a} \right) \bar{V}_{sa} \right] + \Gamma_i A \mu_i, \tag{6.9}$$

where i refers to cosurfactant and oil.

The oil must be negatively adsorbed in order to keep the volume of the adsorption layer zero (in accordance with the Gibbs dividing surface). It is assumed in equation (6.9) that the Gibbs plane (the surface of tension in this case) lies close to the surface (where $\Gamma_{water} = 0$)

(iv) Allow the close-packed emulsion to expand to its final concentration (volume fraction ϕ),

$$F_4 = n_{dr} RT f(\phi). \tag{6.10}$$

n_{dr} is the amount of drops (in moles) and $f(\phi)$ is a function of ϕ. $f(\phi)$ may be simply written as

$$f(\phi) = \ln \phi - \ln 0.74. \tag{6.11}$$

More accurately $f(\phi)$ may be calculated using a hard-sphere model [10],

$$f(\phi) = \ln \phi + \phi \left[\frac{4 - 3\phi}{(1 - \phi)^2} \right] - 19.25. \tag{6.12}$$

Combining equations (6.7)–(6.12) gives the Helmholtz free energy of the complete emulsion. The free energy is minimized with respect to a change in the interfacial area A. This involves transfer of adsorbed components to or from the interface, thereby changing the bulk concentration and thus γ; the result is,

$$\gamma = -\text{const} \times \frac{1}{a^2} \times g(\phi), \tag{6.13}$$

where $g(\phi)$ is similar but not identical to $f(\phi)$.

The droplet radius a can be calculated from a knowledge of the total interfacial area A,

$$A = \frac{n_{sa}}{\Gamma_{sa}} - n_{sa} N_{av}(\text{area/molecule}). \tag{6.14}$$

The area per molecule of an anionic surfactant such as sodium dodecyl sulphate (SDS) varies between 0.7 to 1.1 nm^2, depending on the concentration of cosurfactant (pentanol) and salt concentration. The area per pentanol molecule is about 0.3 nm^2. This means that the average area per surfactant molecule is about 0.9 nm^2.

The radius of the droplet can be calculated from the ratio of the volume of the drop to its area,

$$a = \frac{3 \times (4/3)\pi a^3}{4\pi a^2} = \frac{3V}{A}, \tag{6.15}$$

where V is the total volume of the droplets and A is the total interfacial area.

The radius a of the microemulsion droplet has to fit both equations (6.13) and (6.15); γ is the most easily varied quantity in these equations. The correct value of γ is obtained by adaptation of C_{sa}.

According to equation (6.13), any value of a is allowed in the accessible range of γ. If γ is close to zero very large radii can be obtained, i.e. very large water/sa ratios are allowed. However, the phase diagram shows that at such high ratios demixing occurs. This analysis shows the inadequacy of the above simple model and it is necessary to add an explicit influence of the radius of curvature on the interfacial tension. The curvature effect is manifested in the packing of the tails and head groups at the O/W interface. With W/O microemulsions the packing of the short chains and the packing of the head groups will favour W/O curvature with a ratio of 3 or more for co/sa. With O/W microemulsions a ratio of sa/co of 2 or less is required. Thus O/W microemulsions need less cosurfactant than W/O microemulsions.

6.5 Factors determining W/O versus O/W microemulsions

The duplex film theory predicts that the nature of the microemulsion formed depends on the relative packing of the hydrophobic and hydrophilic portions of the surfactant molecule, which determine the bending of the interface. For example, a surfactant molecule such as Aerosol OT,

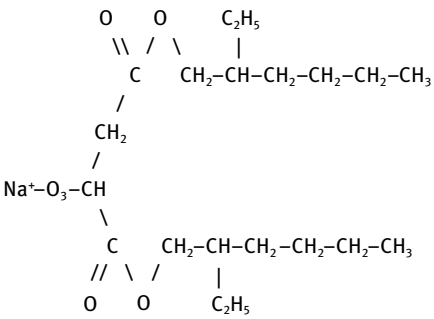

favours the formation of W/O microemulsion, without the need for a cosurfactant. As a result of the presence of a stumpy head group and large volume to length (V/l) ratio of the nonpolar group, the interface tends to bend with the head groups facing onwards, thus forming a W/O microemulsion.

The molecule has $V/l > 0.7$ which is considered necessary for formation of a W/O microemulsion. For ionic surfactants such as SDS for which $V/l < 0.7$, microemulsion formation needs the presence of a cosurfactant (the latter has the effect of increasing V without changing l).

The importance of geometric packing was considered in detail by Mitchell and Ninham [11] who introduced the concept of the packing ratio P,

$$P = \frac{V}{l_c a_0}, \tag{6.16}$$

where a_0 is the head group area and l_c is the maximum chain length.

P gives a measure of the hydrophilic–lipophilic balance. For values of $P < 1$ (usually $P \approx 1/3$), normal or convex aggregates are produced (normal micelles). For values of $P > 1$, inverse micelles are produced. P is influenced by many factors: hydrophilicity of the head group, ionic strength and pH of the medium and temperature.

P also explains the nature of the microemulsion produced using nonionic surfactants of the ethoxylate type: P increases with increasing temperature (as a result of the dehydration of the PEO chain). A critical temperature (PIT) is reached at which P reaches 1 and above this temperature inversion occurs to a W/O system.

The influence of the surfactant structure on the nature of the microemulsion can also be predicted from the thermodynamic theory. The most stable microemulsion would be that in which the phase with the smaller volume fraction forms the droplets (the osmotic pressure increases with increasing ϕ). For a W/O microemulsion prepared using an ionic surfactant such as Aerosol OT, the effective volume (hard-sphere volume) is only slightly larger than the water core volume, since the hydrocarbon tails may penetrate to a certain extent when two droplets come together. For an O/W microemulsion, the double layers may expand to a considerable extent, depending on the electrolyte concentration (the double layer thickness is of the order of 100 nm in

10^{-5} mol dm^{-3} 1 : 1 electrolyte and 10 nm in 10^{-3} mol dm^{-3} electrolyte). Thus the effective volume of O/W microemulsion droplets can be significantly higher than the core oil droplet volume and this explains the difficulty of preparing O/W microemulsions at high ϕ values when using ionic surfactants.

A schematic representation of the effective volume for W/O and O/W microemulsions is shown in Fig. 6.8.

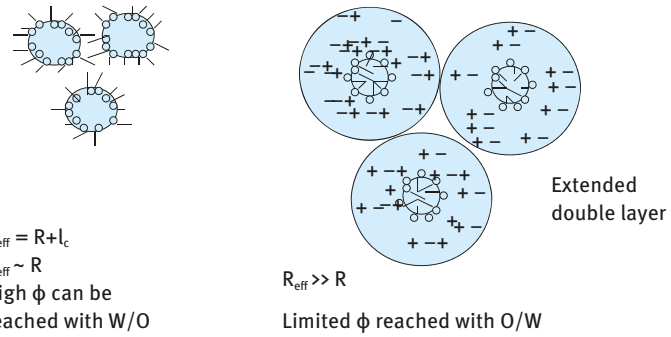

Fig. 6.8: Schematic representation of W/O and O/W microemulsion droplets.

6.6 Characterization of microemulsions using scattering techniques

Scattering techniques provide the most obvious methods for obtaining information on the size, shape and structure of microemulsions. The scattering of radiation, e.g. light, neutrons, X-rays, etc. by particles has been successfully applied for the investigation of many systems such as polymer solutions, micelles and colloidal particles. In all these methods, measurements can be made at sufficiently low concentration to avoid complications arising from particle–particle interactions. The results obtained are extrapolated to infinite dilution to obtain the desirable property such as the molecular weight and radius of gyration of a polymer coil, the size and shape of micelles, etc. Unfortunately this dilution method cannot be applied for microemulsions, which depend on a specific composition of oil, water and surfactants. The microemulsions cannot de diluted by the continuous phase since this dilution results in breakdown of the microemulsion. Thus, when applying the scattering techniques to microemulsions measurements have to be made at finite concentrations and the results obtained have to be analysed using theoretical treatments to take into account the droplet–droplet interactions.

Three scattering methods will be discussed below: time-average (static) light scattering, dynamic (quasi-elastic) light scattering referred to as photon correlation spectroscopy and neutron scattering.

6.6.1 Time-average (static) light scattering

The intensity of scattered light $I(Q)$ is measured as a function of scattering vector Q,

$$Q = \left(\frac{4\pi n}{\lambda}\right)\sin\left(\frac{\theta}{2}\right), \tag{6.17}$$

where n is the refractive index of the medium, λ is the wavelength of light and θ is the angle at which the scattered light is measured.

For a fairly dilute system, $I(Q)$ is proportional to the number of particles N, the square of the individual scattering units V_p and some property of the system (material constant) such as its refractive index,

$$I(Q) = [(\text{material constant})(\text{instrument constant})]NV_p^2 \tag{6.18}$$

The instrument constant depends on the geometry of the apparatus (the light path length and the scattering cell constant).

For more concentrated systems, $I(Q)$ also depends on the interference effects arising from particle–particle interaction,

$$I(Q) = [(\text{instrument constant})(\text{material constant})]NV_p^2P(Q)S(Q), \tag{6.19}$$

where $P(Q)$ is the particle form factor which allows the scattering from a single particle of known size and shape to be predicted as a function of Q. For a spherical particle of radius R,

$$P(Q) = \left[\frac{(3\sin QR - QR\cos QR)}{(QR)^3}\right]^2. \tag{6.20}$$

$S(Q)$ is the so-called "structure factor" which takes into account the particle–particle interaction. $S(Q)$ is related to the radial distribution function $g(r)$ (which gives the number of particles in shells surrounding a central particle) [12],

$$S(Q) = 1 - \frac{4\pi N}{Q}\int_0^\infty [g(r) - 1]r\sin QR\,\mathrm{d}r. \tag{6.21}$$

For a hard-sphere dispersion with radius R_{HS} (which is equal to $R + t$, where t is the thickness of the adsorbed layer),

$$S(Q) = \frac{1}{[1 - NC(2QR_{HS})]}, \tag{6.22}$$

where C is a constant.

One usually measures $I(Q)$ at various scattering angles θ and then plots the intensity at some chosen angle (usually 90°), i_{90} as a function of the volume fraction ϕ of the dispersion. Alternatively, the results may be expressed in terms of the Rayleigh ratio R_{90},

$$R_{90} = \left(\frac{i_{90}}{I_0}\right)r_s^2. \tag{6.23}$$

I_0 is the intensity of the incident beam and r_s is the distance from the detector.

$$R_{90} = K_0 MCP(90)S(90). \tag{6.24}$$

K_0 is an optical constant (related to the refractive index difference between the particles and the medium). M is the molecular mass of scattering units with weight fraction C.

For small particles (as is the case with microemulsions) $P(90) \approx 1$ and,

$$M = \frac{4}{3}\pi R_c^3 N_A, \tag{6.25}$$

where N_A is Avogadro's constant.

$$C = \phi_c \rho_c, \tag{6.26}$$

where ϕ_c is the volume fraction of the particle core and ρ_c is their density.

Equation (6.24) can be written in the simple form,

$$R_{90} = K_1 \phi_c R_c^3 S(90), \tag{6.27}$$

where $K_1 = K_0(4/3)N_A \rho_c^2$.

Equation (6.27) shows that to calculate R_c from R_{90} one needs to know $S(90)$. The latter can be calculated using equations (6.21) and (6.22).

The above calculations were obtained using a W/O microemulsion of water/xylene/sodium dodecyl benzene sulphonate (NaDBS)/hexanol [11]. The microemulsion region was established using the quaternary phase diagram. W/O microemulsions were produced at various water volume fractions using increasing amounts of NaDBS: 5, 10.9, 15 and 20 %. The results for the variation of R_{90} with the volume fraction of the water core droplets at various NaDBS concentrations are shown in Fig. 6.9. With the exception of the 5 % NaDBS results, all the others showed an initial increase in R_{90} with increasing ϕ, reaching a maximum at a given ϕ, after which R_{90} decreases with a further increase in ϕ. These results were used to calculate R as a function of ϕ using the hard-sphere model discussed above (equation (6.27)). This is also shown in Fig. 6.9. It can be seen that with increasing ϕ, at constant surfactant concentration, R increases (the ratio of surfactant to water decreases with increasing ϕ). At any volume fraction of water, an increase in surfactant concentration results in a decrease in the microemulsion droplet size (the ratio of surfactant to water increases).

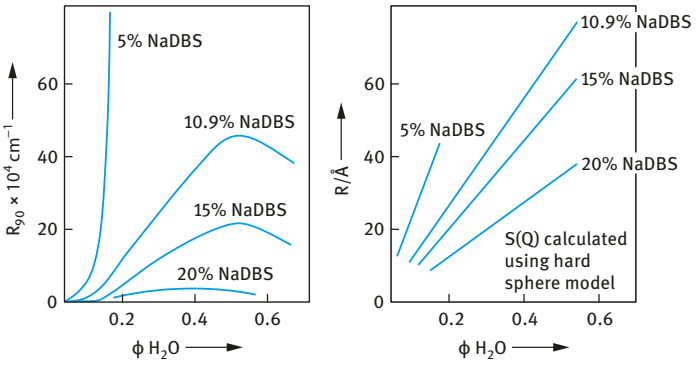

Fig. 6.9: Variation of R_{90} and R with the volume fraction of water for a W/O microemulsion based on xylene–water–NaDBS–hexanol.

6.6.2 Calculation of droplet size from interfacial area

If one assumes that all surfactant and cosurfactant molecules are adsorbed at the interface, it is possible to calculate the total interfacial area of the microemulsion from a knowledge of the area occupied by surfactant and cosurfactant molecules.

$$\begin{aligned}\text{total interfacial area} = {} & \text{total number of surfactant molecules} \\ & \times \text{area per surfactant molecule } A_s \\ & + \text{total number of cosurfactant molecules} \\ & \times \text{area per cosurfactant molecule } A_{co}.\end{aligned}$$

The total interfacial area A per kg of microemulsion is given by the expression,

$$A = \frac{(n_s N_A A_s + n_{co} N_A A_{co})}{\phi}. \tag{6.28}$$

n_s and n_{co} are the number of moles of surfactant and cosurfactant.

A is related to the droplet radius R (assuming all the droplets are of the same size) by,

$$A = \frac{3}{R\rho} \tag{6.29}$$

Using reasonable values for A_s and A_{co} (30 Å^2 for NaDBS and 20 Å^2 for hexanol) R was calculated and the results were compared with those obtained using light scattering results. Two conditions were considered:

(a) all hexanol molecules were adsorbed 1A1;
(b) part of the hexanol adsorbed to give a molar ratio of hexanol to NaDBS of 2 : 1 (1A2).

Good agreement is obtained between the light scattering data and R calculated from interfacial area particularly for 1A2.

6.6.3 Dynamic light scattering (photon correlation spectroscopy, PCS)

In this technique one measures the intensity fluctuation of light scattered by the droplets as they undergo Brownian motion [13]. When a light beam passes through a colloidal dispersion, an oscillating dipole movement is induced in the particles, thereby radiating the light. Due to the random position of the particles, the intensity of scattered light, at any instant, appear as random diffraction ("speckle" pattern). As the particles undergo Brownian motion, the random configuration of the pattern will fluctuate, such that the time taken for an intensity maximum to become a minimum (the coherence time), corresponds approximately to the time required for a particle to move one wavelength λ. Using a photomultiplier of active area about the diffraction maximum (i.e. one coherent area) this intensity fluctuation can be measured. The analogue output is digitized using a digital correlator that measures the photocount (or intensity) correlation function of scattered light.

The photocount correlation function $G^{(2)}(\tau)$ is given by,

$$g^{(2)} = B[1 + \gamma^2 g^{(1)}(\tau)]^2, \tag{6.30}$$

where τ is the correlation delay time.

The correlator compares $g^{(2)}(\tau)$ for many values of τ.

B is the background value to which $g^{(2)}(\tau)$ decays at long delay times. $g^{(1)}(\tau)$ is the normalized correlation function of the scattered electric field and γ is a constant (≈ 1).

For monodispersed non-interacting particles,

$$g^{(1)}(\tau) = \exp(-\Gamma\gamma). \tag{6.31}$$

Γ is the decay rate or inverse coherence time, that is related to the translational diffusion coefficient D,

$$\Gamma = DK^2, \tag{6.32}$$

where K is the scattering vector,

$$K = \left(\frac{4\pi n}{\lambda_0}\right)\sin\left(\frac{\theta}{2}\right). \tag{6.33}$$

The particle radius R can be calculated from D using the Stokes–Einstein equation,

$$D = \frac{kT}{6\pi\eta_0 R}, \tag{6.34}$$

where η_0 is the viscosity of the medium.

The above analysis only applies for very dilute dispersions. With microemulsions which are concentrated dispersions, corrections are needed to take into account the interdroplet interaction. This is reflected in plots of $\ln g^{(1)}(\tau)$ versus τ which become nonlinear, implying that the observed correlation functions are not single exponentials.

As with time-average light scattering, one needs to introduce a structure factor in calculating the average diffusion coefficient. For comparative purposes, one calculates the collective diffusion coefficient D which can be related to its value at infinite dilution D_0 by [14],

$$D = D_0(1 + \alpha\phi), \tag{6.35}$$

where α is a constant that is equal to 1.5 for hard spheres with repulsive interaction.

6.6.4 Neutron scattering

Neutron scattering offers a valuable technique for determining the dimensions and structure of microemulsion droplets. The scattering intensity $I(Q)$ is given by,

$$I(Q) = (\text{instrument constant})(\rho - \rho_0)NV_p^2P(Q)S(Q), \tag{6.36}$$

where ρ is the mean scattering length density of the particles and ρ_0 is the corresponding value for the solvent.

One of the main advantages of neutron scattering over light scattering is the Q range at which one operates: with light scattering, the range of Q is small (≈ 0.0005–$0.0015\ \text{Å}^{-1}$) while for small angle neutron scattering the Q range is large (0.02–$0.18\ \text{Å}^{-1}$). In addition, neutron scattering can give information on the structure of the droplets.

As an illustration Fig. 6.10 shows plots of $I(Q)$ versus Q for W/O microemulsions (xylene/water/NaDBS/hexanol) [15].

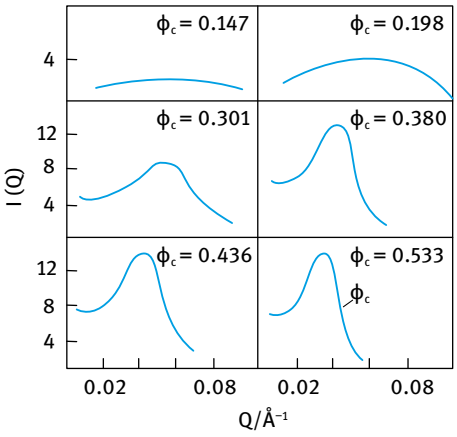

Fig. 6.10: $I(Q)$ versus Q for W/O microemulsions at various water volume fractions.

The Q values at the maximum can be used to calculate the lattice spacing using Bragg's equation. Alternatively, one can use a hard-sphere model to calculate $S(Q)$ and then fit the data of $I(Q)$ versus Q to obtain the droplet radius R.

6.6.5 Contrast matching for determining the structure of microemulsions

By changing the isotopic composition of the components (e.g. using deuterated oil and H_2O–D_2O) one can match the scattering length density of the various components: By matching the scattering length density of the water core with that of the oil, one can investigate the scattering from the surfactant "shell". By matching the scattering length density of the surfactant "shell" and the oil, one can investigate the scattering from the water core.

6.7 Characterization of microemulsions using conductivity

Conductivity measurements may provide valuable information on the structural behaviour of microemulsions. In the early applications of conductivity measurements, the technique was used to determine the nature of the continuous phase. O/W microemulsions should give fairly high conductivity (that is determined by that of the continuous aqueous phase) whereas W/O microemulsions should give fairly low conductivity (that is determined by that of the continuous oil phase).

As an illustration Fig. 6.11 shows the change in electrical resistance (reciprocal of conductivity) with the ratio of water to oil (V_w/V_o) for a microemulsion system prepared using the inversion method [16]. Fig. 6.11 indicates the change in optical clarity and birefringence with the ratio of water to oil.

At low V_w/V_o, a clear W/O microemulsion is produced with a high resistance (oil continuous). As V_w/V_o increases, the resistance decreases, and in the turbid region, hexanol and lamellar micelles are produced. Above a critical ratio, inversion occurs and the resistance decreases producing O/W microemulsion.

Conductivity measurements were also used to study the structure of the microemulsion, which is influenced by the nature of the cosurfactant. This is illustrated in Fig. 6.12 for two systems based on water/toluene/potassium oleate/butanol and water/hexadecane/potassium oleate/hexanol [17]. The difference between the two systems is in the nature of the cosurfactant, namely butanol (C_4 alcohol) and hexanol (C_6 alcohol). The first system based on butanol shows a rapid increase in κ above a critical water volume fraction value, whereas the second system based on hexanol shows much lower conductivity values with a maximum and minimum at two water volume fractions values ϕ'_w and ϕ''_w.

In the first case (when using butanol), the κ–ϕ_w curve can be analysed using the percolation theory of conductivity [18]. In this model, the effective conductivity is practically zero as long as the volume fraction of the conductor (water) is below a critical value ϕ_w^p (the percolation threshold). Beyond this value, κ suddenly takes a non-zero value and it increases rapidly with a further increase in ϕ_w.

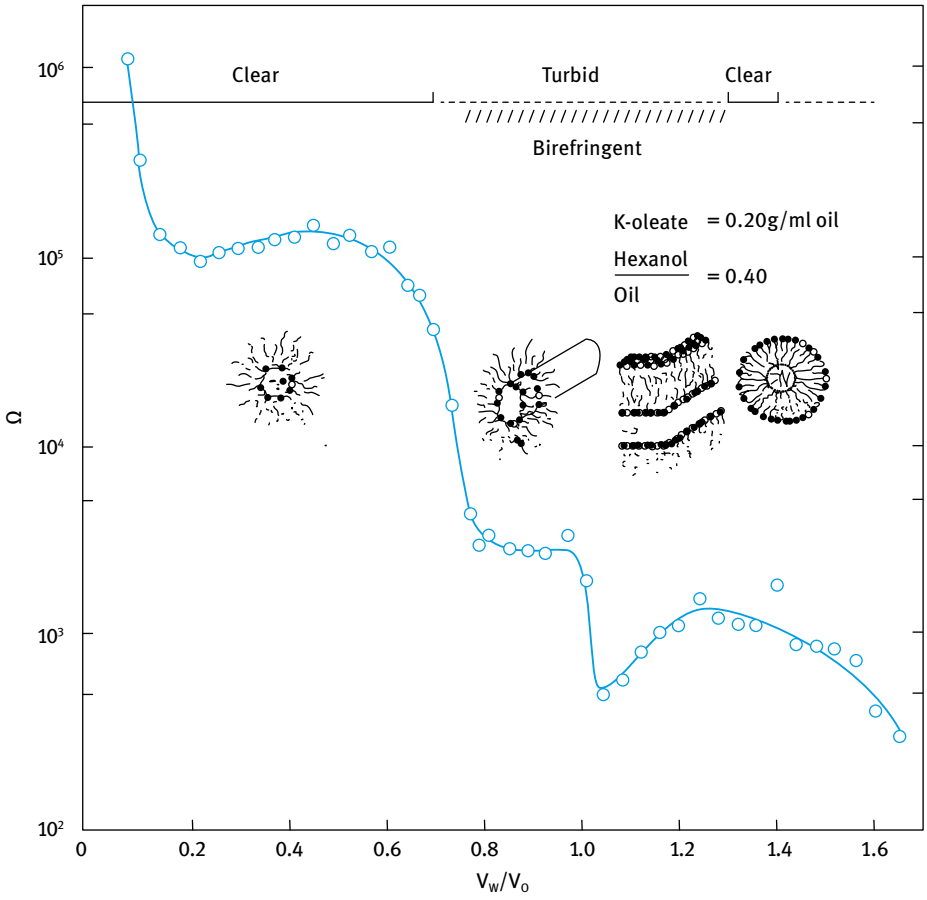

Fig. 6.11: Electrical resistance versus V_w/V_o.

In the above case (percolating microemulsions), the following equation was theoretically derived.

$$\kappa = \begin{cases} (\phi_w - \phi_w^p)^{8/5} & \text{when } \phi_w > \phi_w^p; \\ (\phi_w^p - \phi_w)^{-0.7} & \text{when } \phi_w < \phi_w^p. \end{cases} \tag{6.37}$$

By fitting the conductivity data to equation (6.37), ϕ_w^p was found to be 0.176 ± 0.005 in agreement with the theoretical value.

The second system based on hexanol does not fit the percolation theory (non-percolating microemulsion). The trend of the variation of κ with water volume fraction is due to more subtle changes in the system on changing ϕ_w. The initial increase in κ with increasing ϕ_w can be ascribed to enhanced surfactant solubilization with added water. Alternatively it could be due to an increase in surfactant dissociation

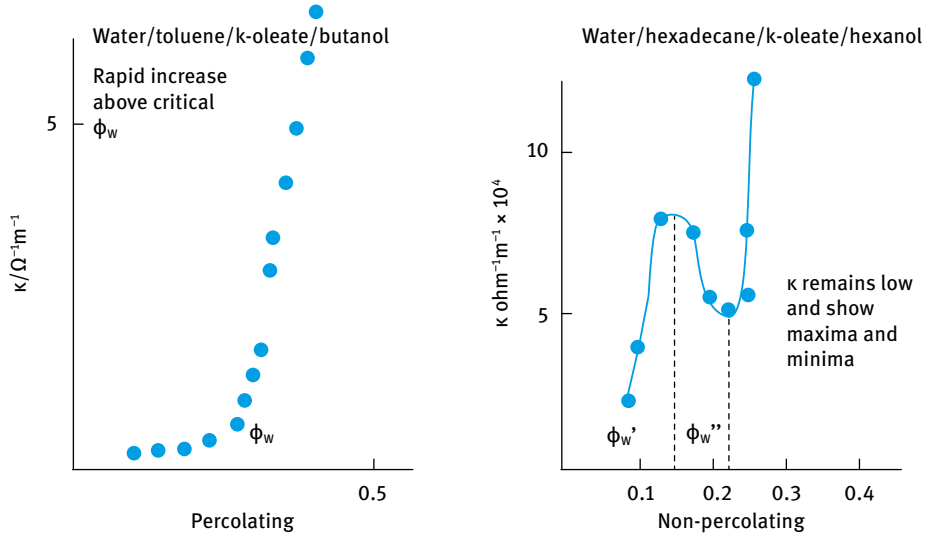

Fig. 6.12: Conductivity versus water volume fraction for two W/O microemulsion systems.

on the addition of water. Beyond the maximum, addition of water mainly causes micelle swelling, i.e. a definite water core (microemulsion droplets) begins to be formed, which may be considered a dilution process leading to a decrease in conductivity. The decrease in κ beyond the maximum may be due to the replacement of the hydrated surfactant-cosurfactant aggregates with microemulsion droplets. The sharp increase in κ beyond the minimum must be associated with a facilitated path for ion transport (formation of non-spherical droplets resulting from swollen micelle clustering and subsequent cluster interlinking).

A systematic study of the effect of cosurfactant chain length on the conductive behaviour of W/O microemulsions was carried out by Clausse and his co-workers [19]. The cosurfactant chain length was gradually increased from C_2 (ethanol) to C_7 (heptanol). The results for the variation of κ with ϕ_w are shown in Fig. 6.13. With the short chain alcohols ($C < 5$), the conductivity shows a rapid increase above a critical ϕ value. With longer chain alcohols, namely hexanol and heptanol, the conductivity remains very low up to a high water volume fraction. With the short chain alcohols, the system shows percolation above a critical water volume fraction. Under these conditions the microemulsion is "bicontinuous". With the longer chain alcohols, the system is non-percolating and one can define definite water cores. This is sometimes referred to as a "true" microemulsion.

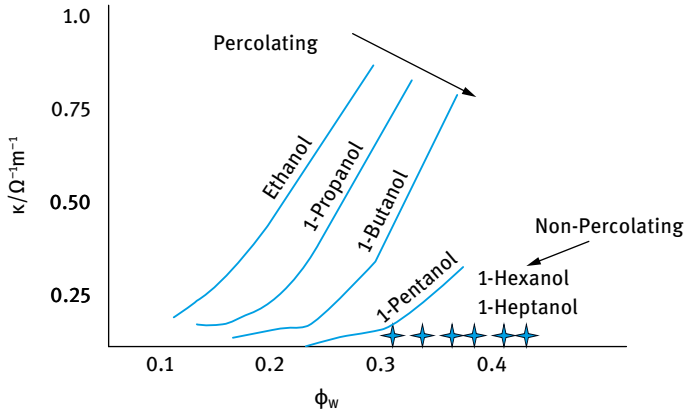

Fig. 6.13: Variation of conductivity with water volume fraction for various cosurfactants.

6.8 NMR measurements

Lindman and co-workers [20–22] demonstrated that the organization and structure of microemulsions can be elucidated from self-diffusion measurements of all the components (using pulse gradient or spin echo NMR techniques). Within a micelle, the molecular motion of the hydrocarbon tails (translational, reorientation and chain flexibility) is almost as rapid as in a liquid hydrocarbon. In a reverse micelle, water molecules and counterions are also highly mobile. For many surfactant-water systems, there is a distinct spatial separation between hydrophobic and hydrophilic domains. The passage of species between different regions is an improbable event and this occurs very slowly.

Thus, self-diffusion, if studied over macroscopic distances, should reveal whether the process is rapid or slow depending on the geometrical properties of the inner structure. For example, a phase that is water continuous and oil discontinuous should exhibit rapid diffusion of hydrophilic components, while the hydrophobic components should diffuse slowly. An oil continuous but water discontinuous system should exhibit rapid diffusion of the hydrophobic components. One would expect that a bicontinuous structure should give rapid diffusion of all components.

Using the above principle, Lindman and co-workers [20–22] measured the self-diffusion coefficients of all components consisting of various components, with particular emphasis to the role of the cosurfactant. For microemulsions consisting of water, hydrocarbon, an anionic surfactant and a short chain alcohol (C_4 and C_5), the self-diffusion coefficient of water, hydrocarbon and cosurfactant was quite high, of the order of 10^{-9} m^2 s^{-1}, i.e. two orders of magnitude higher than the value expected for a discontinuous medium (10^{-11} m^2 s^{-1}). This high diffusion coefficient was attributed to three main effects: bicontinuous solutions, easily deformable and flexible interface

and absence of any large aggregates. With microemulsions based on long chain alcohols (e.g. decanol), the self-diffusion coefficient for water was low, indicating the presence of definite (closed) water droplets surrounded by surfactant anions in the hydrocarbon medium. Thus, NMR measurements could clearly distinguish between the two types of microemulsion systems.

6.9 Formulation of microemulsions

The formulation of microemulsions or micellar solutions, like that of conventional macroemulsions is still an art. In spite of the exact theories that explain the formation of microemulsions and their thermodynamic stability, the science of microemulsion formulation has not advanced to the point where one can predict with accuracy what happens when the various components are mixed. The very much higher ratio of emulsifier to disperse phase which differentiates microemulsions from macroemulsions appears at first sight to make the application of various formulation techniques less critical. However, in the final stages of the formulation one immediately realizes that the requirements are very critical due to the greater number of parameters involved.

The mechanics of forming microemulsions differ from those used in making macroemulsions. The most important difference lies in the fact that putting more work into a macroemulsion or increasing emulsifier usually improves its stability. This is not so for microemulsions. Formation of a microemulsion depends on specific interactions of the molecules of oil, water and emulsifiers. These interactions are not precisely known. If such specific interactions are not realized, no amount of work nor excess emulsifier can produce the microemulsion. If the chemistry is right microemulsification occurs spontaneously.

One should remember that for microemulsions the ratio of emulsifier to oil is much higher than that used for macroemulsions. This emulsifier used is at least 10 % based on the oil and in most cases it can be as high as 20–30 %. The W/O systems are made by blending the oil and emulsifier with some heating if necessary. Water is added to the oil–emulsifier blend to produce the microemulsion droplets and the resulting system should appear transparent or translucent. If the maximum amount of water that can be microemulsified is not high enough for the particular application, one should try other emulsifiers to reach the required composition.

The most convenient way of producing an O/W microemulsion is to blend the oil and emulsifier and the pour the mixture into water with mild stirring. In the case of waxes, both oil/emulsifier blend and the water must be at higher temperature (above the melting point of the wax). If the melting point of the wax is above the boiling temperature of water, the process can be carried out at high pressure. Another technique to mix the ingredients is to make a crude macroemulsion of the oil and one of the emulsifiers. By using low volumes of water, a gel is formed and the system can then be

titrated with the co-emulsifier until a transparent system is produced. This system may be further diluted with water to produce a transparent or translucent microemulsion.

Four different emulsifier selection methods can be applied for formulation of microemulsions:

(i) the hydrophilic–lipophilic balance (HLB) system;
(ii) the phase inversion temperature (PIT) method;
(iii) the cohesive energy ratio (CER) concept;
(iv) partitioning of cosurfactant between the oil and water phases.

The first two methods are essentially the same as those used for selection of emulsifiers for macroemulsions, described in detail in Chapter 2. However, with microemulsions one should try to match the chemical type of the emulsifier with that of the oil. The cosurfactant portioning plays a major role in microemulsion formation. According to the thermodynamic theory of microemulsion formation, the total interfacial tension of the mixed film of surfactant and cosurfactant must approach zero. The total interfacial tension is given by the following equation,

$$\gamma_T = \gamma_{(O/W)} - \pi, \tag{6.38}$$

where $(\gamma_{O/W})_a$ is the interfacial tension of the oil in the presence of alcohol cosurfactant and π is the surface pressure. $(\gamma_{O/W})_a$ seems to reach a value of 15 mN m^{-1} irrespective of the original value of $\gamma_{O/W}$. It seems that the cosurfactant which is predominantly oil soluble distributes itself between the oil and the interface and this causes a change in the composition of the oil which now is reduced to 15 mN m^{-1}.

Measuring the partition of the cosurfactant between the oil and the interface is not easy. A simple procedure to select the most efficient cosurfactant is to measure the oil/water interfacial tension $\gamma_{O/W}$ as a function of cosurfactant concentration. The lower the percentage of cosurfactant required to lower $\gamma_{O/W}$ to 15 mN m^{-1} the better the candidate.

References

[1] Hoar TP, Schulman JH. Nature. 1943;152:102.
[2] Prince LM. Microemulsion theory and practice. New York: Academic Press; 1977.
[3] Danielsson I, Lindman B. Colloids and Surfaces. 1983;3:391.
[4] Schulman JH, Stoeckenius W, Prince LM. J Phys Chem. 1959;63:1677.
[5] Prince LM. Adv Cosmet Chem. 1970;27:193.
[6] Shinoda K, Friberg S. Adv Colloid Interface Sci. 1975;4:281.
[7] Ruckenstein E, Chi JC. J Chem Soc Faraday Trans II. 1975;71:1690.
[8] Overbeek JTG. Faraday Disc Chem Soc. 1978;65:7.
[9] Overbeek JTG. de Bruyn PL, Verhoeckx F. In: Tadros TF, editor. Surfactants. London: Academic Press; 1984. p. 111–132.
[10] Carnahan NF, Starling KE. J Chem Phys. 1969;51:635.

[11] Mitchell DJ, Ninham BW. J Chem Soc Faraday Trans II. 1981;77:601.
[12] Baker RC, Florence AT, Ottewill RH, Tadros TF. J Colloid Interface Sci. 1984;100:332.
[13] Ashcroft NW, Lekner J. Phys Rev. 1966;45:33.
[14] Pusey PN. In: Green JHS, Dietz R, editors. Industrial polymers: Characterisation by molecular weights. London: Transcripta Books; 1973.
[15] Cazabat AN, Langevin D. J Chem Phys. 1981;74:3148.
[16] Cebula DJ, Ottewill RH, Ralston J, Pusey P. J Chem Soc Faraday Trans I. 1981;77:2585.
[17] Lagourette B, Peyerlasse J, Boned C, Clausse M. Nature. 1969;281:60.
[18] Kilpatrick S. Mod Phys. 1973;45:574.
[19] Clausse M, Peyerlasse J, Boned C, Heil J, Nicolas-Margantine L, Zrabda A. In: Mittal KL, Lindman B, editors. Solution properties of surfactants. Vol. 3. Plenum Press; 1984. p. 1583.
[20] Lindman B, Winnerstrom H. In: Borschke FL, editor. Topics in current chemistry 87. Heidelberg: Springer-Verlag; 1980. p. 1–83.
[21] Winnerstrom H, Lindman B. Phys Rep. 1970;52:1.
[22] Lindman B, Stilbs P, Moseley ME. J Colloid Interface Sci. 1981;83:569.

7 Controlled-release formulations

7.1 Introduction

Controlled-release formulations offer a number of advantages, in particular for pharmaceuticals and agrochemicals, of which the following are worth mentioning:

(i) improvement of residual activity;
(ii) reduction of application dosage;
(iii) stabilization of the core active ingredient (AI) against environmental degradation;
(iv) reduction of mammalian toxicity;
(v) reduction of phytotoxicity with agrochemicals;
(vi) reduction of fish toxicity with agrochemicals;
(vii) reduction of environmental pollution with agrochemicals.

One of the main advantages of using controlled-release formulations, in particular microcapsules, is the reduction of physical incompatibility when several drugs are used and when mixtures are used with agrochemicals in the spray tank. They also can reduce biological antagonism when mixtures are applied in the field.

Several types of controlled-release systems can be identified:

(i) Microcapsules with particles in the size range 1–100 µm that consist of a distinct capsule wall (mostly a polymer) surrounding the active ingredient core.
(ii) Microparticles (size range 1–100 µm) consisting of a matrix in which the active ingredient (AI) is uniformly dissolved or dispersed.
(iii) Granules with matrix particles of 0.2–2.0 mm with the active ingredient uniformly dissolved or dispersed within the matrix.

In this chapter I will give a brief account of the different types of slow release systems [1].

7.2 Microencapsulation

Microencapsulation of chemicals is mainly carried out by interfacial condensation, in situ polymerization and coacervation. Interfacial condensation [2] is perhaps the most widely used method for encapsulation in industry. The AI, which may be oil soluble, oil dispersible or an oil itself, is first emulsified in water using a convenient surfactant or polymer. A hydrophobic monomer A is placed in the oil phase (oil droplets of the emulsion) and a hydrophilic monomer B is placed in the aqueous phase. The two monomers interact at the interface between the oil and the aqueous phase forming a capsule wall around the oil droplet. Two main types of systems may be identi-

https://doi.org/10.1515/9783110587968-008

fied. For example, if the material to be encapsulated is oil soluble, oil dispersible or an oil itself, an oil-in-water (O/W) emulsion is first prepared. In this case the hydrophobic monomer is dissolved in the oil phase which forms the dispersed phase. The role of surfactant in this process is crucial since an oil–water emulsifier (with high hydrophilic–lipophilic balance, HLB) is required. Alternatively a polymeric surfactant such as partially hydrolyzed polyvinyl acetate (referred to as polyvinyl alcohol, PVA) or an ethylene oxide-propylene oxide-ethylene oxide, PEO–PPO–PEO (Pluronic) block copolymer can be used. The emulsifier controls the droplet size distribution and hence the size of capsules formed. On the other hand, if the material to be encapsulated is water soluble, a water-in-oil (W/O) emulsion is prepared using a surfactant with low HLB number or an A–B–A block copolymer of polyhydroxystearic acid–polyethylene oxide–polyhydroxystearic acid (PHS–PEO–PHS). In this case the hydrophilic monomer is dissolved in the aqueous internal phase droplets.

In interfacial polymerization, the monomers A and B are polyfunctional monomers capable of causing polycondensation or polyaddition reaction at the interface [2]. Examples of oil-soluble monomers are polybasic acid chloride, bis-haloformate and polyisocyanates, whereas water-soluble monomers can be polyamine or polyols. Thus, a capsule wall of polyamide, polyurethane or polyurea may be formed. Some trifunctional monomers are present to allow crosslinking reactions. If water is the second reactant with polyisocyanates in the organic phase, polyurea walls are formed. The latter modification has been termed in situ interfacial polymerization [3].

One of the most useful microencapsulation processes, that is commonly used with agrochemicals, involves reactions that produce formation of urea-formaldehyde (UF) resins. Urea along with other ingredients such as amines, maleic anhydride copolymers or phenols is added to the aqueous phase that contains oily droplets of the active ingredient that is to be encapsulated. Formaldehyde or formaldehyde oligomers are added and the reaction conditions are adjusted to form UF condensates, sometimes referred to as aminoplasts, that should preferentially wet the disperse phase [1]. The reaction is continued to completion over several hours. Fairly high activity products can be obtained. A modification of this technique is the use of etherified UF resins. The UF prepolymers are dissolved in the organic phase, along with the active ingredient, through the use of protective colloids (such as PVA), and the reaction is initiated through temperature and acid catalyst. This promotes the formation of the shell in the organic phase adjacent to the interface between the bulk-oil phase droplets and the aqueous phase solution [1].

It should be mentioned that the role of surfactants in the encapsulation process is very important. Apart from their direct role in the preparation of microcapsule dispersions, surfactants can be used to control the release of the active ingredient (AI) from the microcapsule dispersion. For example, Wade et al. [5] have shown that the efficacy of an edifenphos suspension can be improved by addition of a surfactant either to the aqueous medium or to the core. This was attributed to the possible solubilization of the AI by the surfactant micelles, thus increasing the release rate.

7.3 Mechanism of release of active ingredient from microcapsules

There are generally two mechanisms for release of the active ingredient (AI) from a capsule:

(i) diffusion of the AI through the microcapsule wall;
(ii) destruction of the microcapsule wall by either physical means, e.g. mechanical power, or by chemical means, e.g. hydrolysis, biodegradation, thermal degradation, etc.

The release behaviour is controlled by several factors such as particle size, wall thickness, type of wall material, wall structure (porosity, degree of polymerization, crosslink density, additives, etc.), type of core material (chemical structure, physical state, presence or absence of solvents) and amount or concentration of the core material. The release behaviour is determined by interaction of these factors and optimization is essential for achieving the desired release rate.

In order to get better performance of the microcapsule for biological efficacy, time-dependent or site-specific release is desirable. It is essential in this case to develop various functional microcapsules that are specific to the target. Temperature, pH, light, or enzyme responsive microcapsules are desirable.

The simplest release kinetics of microcapsules is diffusion controlled as predicted by Fick's first law. The amount of AI that diffuses through the wall of a microcapsule, $\mathrm{d}m/\mathrm{d}t$ (mol s^{-1}), is proportional to the diffusion coefficient D, the surface area A and the concentration gradient $\mathrm{d}c/\mathrm{d}x$, where $\mathrm{d}c$ is the difference in concentration between the inside and outside wall and $\mathrm{d}x$ is the thickness of the capsule wall,

$$\frac{\mathrm{d}m}{\mathrm{d}t} = -DA\frac{\mathrm{d}c}{\mathrm{d}x}. \tag{7.1}$$

Equation (7.1) clearly shows that the release rate increases with increasing A (i.e. when using small capsules) and decreasing $\mathrm{d}x$ (thinner capsule wall). To decrease the rate of diffusion one has to use larger capsules and thicker capsule walls.

7.4 Encapsulation by phase separation from aqueous solution

There are four types of encapsulation utilizing the system of phase separation from aqueous solution [2]:

(i) complex coacervation or phase separation resulting from two oppositely charged colloids neutralizing one another;
(ii) simple coacervation where a non-electrolyte such as alcohol causes formation of a separate polymer-rich phase;
(iii) salt coacervation where a polymer separates as a result of a salting-out process;
(iv) precipitation and insolubilization of a polymer by changing the pH of the aqueous solution system.

An example of complex coacervation [4] is the interaction between gelatin and gum arabic. In this case a dispersion of oil in a dilute solution of gelatin-gum arabic mixture is prepared. Gelatin usually has an isoelectric point (IEP) at pH ≈ 4.8, whereas gum arabic, which contains only carboxylic groups, is usually negative over a wide range of pH values. Thus, by lowering the pH to a value below the IEP of gelatin, say to pH = 4.0, the gelatin acquires a positive charge and become coacervated with gum arabic forming capsules around the oil droplets. Various other anionic polyelectrolytes may be used such as sodium alginate, agar, polyvinyl benzene sulphonic acid, etc. In general, effective materials include polymers, surface active agents and organic compounds which have acid groups in the molecule [2].

Encapsulation by phase separation can also be applied in nonaqueous media. This is particularly suitable for encapsulation of water-soluble materials. A W/O emulsion of the active ingredient is dissolved in the water droplets using an oil-soluble polymer. Phase separation of the oil-soluble polymer may be induced by addition of another polymer, nonsolvent or by changing the temperature.

Salt coacervation is best exemplified by the formation of calcium alginate capsules. In this process a drop of a solution, an emulsion or suspension containing the AI and sodium alginate is dropped into a solution of calcium chloride. When the drop touches the calcium chloride solution, a membrane of calcium alginate forms instantaneously, maintaining the drop shape in this aqueous/aqueous system. Calcium ions diffuse in, gelling the entire drop. This drop is then placed in a solution of a polycation which displaces the calcium ions from the outer surface, forming a permanent membrane. This capsule is then placed in sodium citrate, which slowly solubilizes the calcium through the formation of a soluble citrate complex, ungelling the internal portion of the drop. By controlling the molecular weight of the reactants and the times of reaction, the thickness and size selectivity of the permanent wall can be controlled over a wide range.

7.5 Microencapsulation of solid particles

This is by far the most challenging process of encapsulation since one has to coat the particles individually without any aggregation. These particles cover the size range 0.1–5 μm with an average of 1–2 μm. Clearly, when encapsulating these particles one has to make sure that the smallest size fraction is retained without any aggregation. This is vital for biological efficacy since the smaller particles are more effective for biological control (due to their higher solubility when compared with the larger particles). Beestan [5] suggested an injection treatment coating method for encapsulation of solid particles of agrochemicals. This method utilizes air at sonic velocity to atomize the coating material and accelerate the particles in such a manner that they become coated on all surfaces. The liquid coating material may be melted wax or resins, solutions of polymers or coating materials or suspensions of film-forming solids such as

polymer latexes. Coating is accomplished by metering the solid particles in the shear zone concurrently with metering the liquid coating material into the air stream. The latter is accelerated to the speed of sound through a restriction zone to give a shear zone of sufficient intensity to affect coating. The mixing action within the shear zone coats the solid particles individually with the coating material. On-line particle size measurement of the encapsulated solid particles showed that the particle size range of the solid particles remain virtually unchanged by this injection treatment coating process, indicating that individual particles of all sizes are discretely coated.

Another method that can be applied to encapsulate solid particles is a modification of the coacervation process described above. In this method a technique of solvent evaporation is used to precipitate the polymers as intact coatings. The solid particles are suspended in a solvent solution of the polymer and emulsified into a liquid. The emulsion is then heated to evaporate the solvent causing the polymer to insolubilize as a coating around the suspended particles. Alternatively, a nonsolvent for the polymer is added to the suspension of particles in polymer solution, causing the solvent to phase separate and the polymers to insolubilize to coatings

7.6 Controlled-release of agrochemicals from matrix-based microparticles

Matrix-based microparticles are of three main types [6]:

(i) Matrix powders where the active ingredient (AI) is dispersed throughout the matrix and the mixture is ground (if necessary to form a powder that can be applied as wettable powder). Surface active agents are incorporated to aid wetting and dispersion of the microparticles. The matrices used include polymers such as lignin, starch, proteins; high molecular weight natural polymers such as waxes, cyclodextrin; synthetic polymers such as urea formaldehyde resins; or acrylic acid polymers. Inorganic materials such as glass, silica or diatomaceous earth can also be used. These inorganic materials can also act as carriers.

(ii) Carriers plus matrix where the particles are based on a porous powder that is used as a carrier. Two types can be distinguished, namely co-loaded (where the AI/matrix mixture is loaded into the carrier) and postcoated (where the AI is loaded into the carrier and the matrix is then loaded separately).

(iii) Matrix emulsions where the microparticles are made by emulsifying a hot solution of the AI plus matrix, typically in water. On cooling, the emulsion droplets solidify producing an aqueous suspension of the microparticles.

Generally speaking, one component of the formulation, the “matrix”, will be responsible for the controlled release of the formulation. It is convenient to consider the controlled release as being due to interaction among the AI, the matrix and the environment. Matrix systems where the AI is uniformly dispersed through a matrix ma-

terial are the basis of commercial formulations [7]. Three models may be used for describing the behaviour of such systems. The first two mechanisms apply where the AI is uniformly dispersed throughout the matrix and is essentially impermeable to water or the external environment. Leaching of the AI occurs at the edge of the particle, setting up a concentration gradient within the particle that provides the driving force for diffusion of the AI to the edge of the particle and into the external environment. In such a system, the rate of release is governed by the solubility of the AI in the matrix, the diffusion coefficient for the transport of the AI through the matrix and the geometry of the particle. Matrix particles usually contain pores and cracks, thus increasing the effective surface area between the particle and the external environment and hence the release rate. The second mechanism applies to rigid, often glassy matrices where diffusion of the AI within the matrix of the active is negligible. Leaching is controlled by surface exposure of the AI through biological or chemical degradation of the matrix. The third mechanism applies to systems where the matrix material is permeable to the external environment, e.g. water. This corresponds to a system where the AI is dispersed in a latex. In this case water permeates the matrix through a combination of capillary and osmotic effects. The AI dissolves and diffuses to the edge of the particle into the surrounding medium. The process is diffusion controlled and is governed by the solubility and diffusion coefficient of the AI in water.

7.7 Mechanism of controlled-release from microparticles

The release of AI from conventional formulations generally follows an exponential decay, i.e. the release rate is proportional to the concentration of the AI remaining in the formulation. This decay follows first-order kinetics, which means that the initial concentration in the environment is initially very high (often resulting in an undesirable toxic effect) and decreases rapidly to a low (ineffective) level. In contrast, a controlled-release formulation generally exhibits lower initial concentrations and a longer time before the concentration decreases to an ineffective level. This is schematically illustrated in Fig. 7.1, which clearly shows that when using a conventional formulation

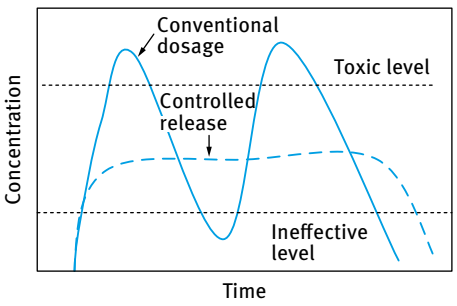

Fig. 7.1: Release of active ingredient from conventional and controlled-release formulations.

several treatments are required for biological control. During these treatments the AI concentration may reach an undesirably high concentration which is above the toxic limit. In contrast, a controlled-release formulation maintains an effective concentration that is sufficient for bioefficacy without reaching the toxic limit. Thus, with a conventional treatment a higher dose of AI is required to maintain bioefficacy. This dose is significantly reduced when using a controlled-release formulation. The high AI concentrations reached with conventional formulations can also have adverse toxic effects on humans, birds, fish, etc.

Most controlled-release systems rely on diffusion of AI through a rate controlling membrane or polymer matrix. Transport through a polymer membrane or matrix occurs by a solution–diffusion process, whereby the AI first dissolves in the polymer and then diffuses across the polymer to the external surface, where the concentration is lower. As discussed before, the process follows Fick's first law of diffusion (equation (7.1)).

The rate of AI release from controlled-release systems can follow a variety of patterns, ranging from first-order (exponential) decay (as with conventional systems) to zero-order kinetics in which the release rate is constant over most of the lifetime of the device. In the latter case the release rate decreases proportionally to the square root of time. A comparison of the release kinetics is shown in Fig. 7.2. As can be clearly seen the zero-order kinetics (membrane-coated reservoir) results in lower peak concentration and more extended release when compared with the case of first-order kinetics.

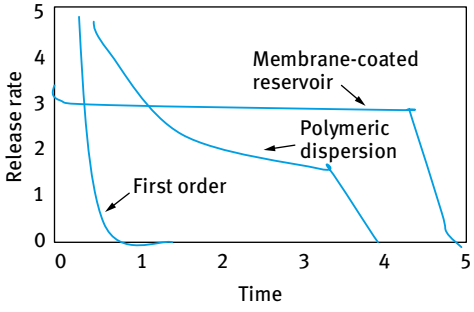

Fig. 7.2: Comparison of release kinetics observed from controlled-release formulations.

As mentioned before, the most common types of controlled-release microparticles are membrane-coated reservoirs and polymeric matrices. A reservoir system consists of a core of pure or saturated AI surrounded by a rate-controlling membrane (polymer shells). The AI is released from the reservoir system by diffusion through the rate-controlling membrane at a constant rate (zero-order kinetics) and this follows Fick's law. For a spherical capsule with outer and inner radii r_2 and r_1 and hence a membrane thickness of $(r_2 - r_1)$ the release rate at time t, $\mathrm{d}M_t/\mathrm{d}t$, is given by the following equation,

$$\frac{\mathrm{d}M_t}{\mathrm{d}t} = 4\pi D \frac{\mathrm{d}c}{\mathrm{d}x} \frac{r_2 r_1}{(r_2 - r_1)}, \tag{7.2}$$

where D is the diffusion coefficient of the AI and dc/dx is the concentration gradient within the membrane.

The release rate remains constant as long as D and dc/dx remain constant. However, the latter values are temperature dependent and hence the release rate will increase with increasing temperature. In many cases the release rate is doubled for every 10 °C increase in temperature. In addition, dc/dx remains constant as long as the activity of the AI remains constant within the reservoir. If the activity of the AI decreases as a result of release of the chemical, the release rate will decrease.

Another important factor that affects the release rate of membrane-coated reservoir type microparticles is the polydispersity of the system. The release rate from each microparticle may be constant and hence initially the release rate may also be constant. However, with time the release rate may change as a result of polydispersity. The quantity of AI in the microparticle is a function of its volume, i.e. the cube of the radius, but the release rate is a function of the radius. Thus, the duration which is approximately equal to the mass of the AI divided by the release rate is a function of the square of the radius. Thus, smaller microparticles become depleted before larger ones and this results in a decrease of the overall release rate from a collection of microparticles with different sizes.

It should also be mentioned that to maintain a constant release rate, the membrane must remain intact. In general, large microparticles and those with high loading of AI are more susceptible to rupture resulting in rapid release. With matrix-type microparticles where the AI is dispersed or dissolved in a polymeric matrix, the release of the AI occurs by diffusion through the matrix to the surface and hence the process follows Fick's law (equation (7.1). However, the release kinetics can depend on the quantity of the AI and whether this is dispersed or dissolved in the matrix.

7.8 Controlled release from granules

Many agrochemicals are formulated as water dispersible granules (WG) which disperse quickly and completely when added to water. The main advantage of WGs is that they avoid the use of solvents thus reducing the risk during manufacture and to farm workers during application. In addition they can be applied for slow release as will be discussed below.

Several processes can be applied to produce WGs of insoluble AI:

(i) Those in which the starting materials are essentially dry and are subsequently made wet and then redried.
(ii) Those in which the starting materials are wet and are granulated and dried.

A typical composition of a WG is one or two AIs, dispersing agent, suspending agent, wetting agent, binder (such as lignosulphonate or a gum) and a filler (mineral filler or water-soluble salt).

As mentioned above, granulation is carried out using a dry or wet route process. Several dry route processes are possible such as pan granulation, fluid-bed granulation, Schugi granulator, extrusion and peg or pin granulator [8]. The wet route process can be carried out by spray drying or spray granulation [8].

Approaches to achieving controlled release from granules fall into two main categories:

(i) the matrix (monolith) with the AI dispersed throughout the structure;
(ii) the reservoir in which a polymeric coating entraps the AI with or without a support [9].

Particle size and uniformity are very important, especially in applications where the duration of release is critical. Three types of granule dimensions can be distinguished, namely fine granules 0.3–2.5 mm in diameter, microgranules 0.1–0.6 mm and macrogranules 2–6 mm. A formulation containing a range of particle sizes (from dusts to macrogranules) will have an extended period of effectiveness. A controlled-release system based on a monolithic polymer granule made from extruding the AI with a release-rate-modifying inert material ("porisogen") in a thermoplastic matrix can play an important role for pest management for periods up to 2–3 years following a single treatment of a non-persistent agrochemical.

Although the above approach based on synthetic polymers is the most successful of the controlled-release granules, natural polymers have shown great success in matrix formulations for AI delivery. Examples of natural polymers are crosslinked starch, polysaccharides, crosslinked alginates and cellulose derivatives. To provide effective delay of release, alginate gels crosslinked with calcium require the incorporation of absorbents such as silica, alumina, clays or charcoal. Further control of the release rate could be achieved by combining kaolin clay with linseed oil in the granule. Other gel forming polymers include carboxymethyl cellulose stabilized with gelatin and crosslinked with cupric or aluminium ions. Coating of granules with rate-controlling polymer film can also be applied. Controlled delivery of agrochemicals has also been obtained with superabsorbent acrylamide and acrylate polymers.

The biodegradability of the formulating material is an important aspect of controlled release for environmental applications. Several synthetic and natural polymers used for formulating granules are biodegradable. The delivery of bioactives from controlled-release granules can be enhanced by inclusion of biosurfactants.

Several lignin-based granules have been introduced for controlled release of several AIs. Lignin is a polyphenolic material that occurs in the cell wall of most terrestrial plants, where it is strongly associated with carbohydrates. It is a polymer produced by random dehydrogenation of a number of phenolic precursors linked to the polysaccharide component of the plant cell. This produces a complex structure without any regular repeating monomer. Lignin is separated from lignocellulosic plants by physical or chemical means.

Several agrochemicals are formulated as granules using lignin, in particular for oil applications. The AI is characterized by some physicochemical properties such as moderate sorption on soil components, low volatility, moderate to high melting points, crystallinity and low to moderate water solubility. Such properties make them compatible with alkali lignins for preparing matrices by melting the components together. This produces a glassy matrix upon cooling.

The compatibility of a lignin and an agrochemical can be assessed by observing a film of the melt mixture under the microscope for presence of unsolvated lignin particles. Where solvation occurs, the melting point of the agrochemical is depressed and this can be determined using differential scanning calorimetry (DSC). The density of the glassy adhesive matrix is usually lower than that of the lignin and often less than that of the AI. This can be explained by the presence of voids or pores that cannot be observed by microscopy.

The effect of water on the matrix formulation varies according to the agrochemical compatibility with the lignin and the ratio of AI to lignin. With highly compatible AI such as diuron the surface of the matrix changes from dark brown to dull light brown on exposure to water. With further exposure some swelling occurs and the outer region is very porous. Diffusion of diuron is enhanced compared to that in the unswollen glassy interior. The swelling and water uptake depends to a large extent on the lignin type used.

The mechanism of release from lignin matrix granules intended for use in soil and aqueous media is studied by immersing the granule in water under static, stirred or flowing conditions. Granules prepared from various lignin types always show release rates that decrease with time. This is illustrated in Fig. 7.3 which also shows the dependency on lignin type.

The release kinetics fitted the generalized model [9],

$$\frac{M_t}{M_z} = kt^n + c, \tag{7.3}$$

where M_t/M_z is the proportion of AI released at time t, the constant k incorporates the polymer properties, the exponent n characterizes the transport mechanism, and c is a constant.

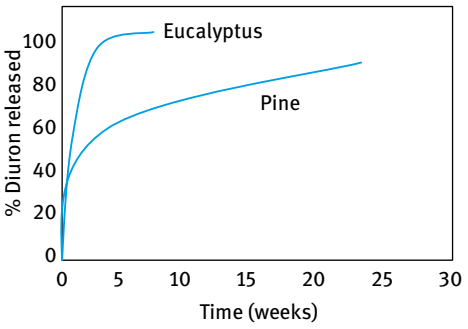

Fig. 7.3: Percentage release of diuron (50 %) from granules based on two different lignin types.

The results of Fig. 7.3 could be fitted to equation (7.3) giving an exponent n ranging from 0.35 to 0.53 indicating that the release is mainly diffusion controlled.

References

[1] Scher HB. Controlled-release delivery systems for pesticides. New York: Marcel Dekker; 1999.
[2] Kondo A. Microcapsule processing and technology. New York: Marcel Dekker; 1979.
[3] Morgan PW, Kvolek SL. J Polym Sci. 1947;2:90.
[4] Bunderberg de Jong HC. Complex colloid system. In: Ktuyt HR, editor. Colloid Science. Vol. II. Amsterdam: Elsevier; 1949.
[5] Beetsman GB. In: Scher HB, editor. Controlled-release delivery systems for pesticides. New York: Marcel Dekker; 1999.
[6] Park DJ, Jackson WR, McKinnon IR, Marshall M. Controlled-release delivery systems for pesticides. In: Scher HB, editor. Controlled-release delivery systems for pesticides. New York: Marcel Dekker; 1999.
[7] Bahadir M, Pfister G. Controlled release formulations of pesticides. In: Bowers WS, Ebing W, Martin D, editors. Controlled release, biochemical effects of pesticides and inhibition of plant pathogenic fungi. Berlin:Springer-Verlag; 1990. p. 1–64.
[8] Woodford AR. Dispersible granules. In: Van Valkenberg W, Sugavanan B, Khetan SK, editors. Pesticide Formulation. Vienna: UNIDO; New Delhi: New Age International (P) Ltd.; 1998. Chapter 9.
[9] Wilkins RM, editor. Controlled delivery of crop protection agents. London: Taylor and Francis; 1990.

8 Solid dosage formulations

8.1 Introduction

Solid dosage forms are one of the most important systems used in the chemical industry, e.g. pharmaceuticals, food and speciality products. The formulation of such solid dosage forms requires the formation of the desired structure, as well as its controlled breakdown during end use by the consumer [1]. The preparation of these systems requires an understanding of the fundamental chemistry and materials science, e.g. the biological activity in a pharmaceutical product, taste in a food, etc. The material must be produced in a form that has the correct structure and on usage and delivery one must prove that this structure is correct. It is, therefore, important to obtain information on the structure by using techniques such as electron microscopy and spectroscopy.

In this chapter, I will start with a section on agglomerated products which are frequently used in instant foods (e.g. coffee), agrochemicals and detergent powders. The structure of the agglomerated product is made by agglomeration of smaller constituent particles. In some cases, the agglomerated product is further processed by compaction to produce a tablet, as is the case with many pharmaceutical products. The process of agglomeration is briefly described. The next section will deal with the process of compaction which is sometimes referred to as "dry agglomeration" since in this case no liquid binders are necessary for the agglomeration process. The last section will deal with the use of solid dosage forms in the pharmaceutical industry. Three main types are used, namely tablets, hard and soft gelatin capsules and sustained-release pellets.

8.2 Agglomeration

Three steps are used in the agglomeration (granulation) process [1]; in the first stage the active ingredients are mixed with one or more excipients (materials other than the active are added to provide bulk and/or to improve processability and properties of the final product). A liquid binder may be added in order to promote agglomeration, but any solvent added with the binder must be removed at a later stage. The last step involves drying using tray driers or fluidized bed dryers, as will be discussed below.

The main objectives of granulation are to improve the flow properties and compression characteristics of the mix, and to prevent segregation of the constituents [2]. Granulation may be considered a size enlargement process during which small particles are formed into larger, physically strong agglomerates in which the original particles can be identified. In wet granulation processes, a liquid binder is sprayed onto the particles as they are agitated in a tumbling drum, a fluidized bed, a high-

https://doi.org/10.1515/9783110587968-009

shear mixer or similar device. Agglomeration results from the collision between two or more wet particles leading to the formation of moving liquid bridges and wet granulation. If the cohesion strength is greater than the break-up forces, the solidification of liquid bridges produces the agglomerates. Thus, the growth mechanism depends on the relative magnitude of the binding forces depending on the local phenomena taking place at the solid surface. These phenomena depend on the properties of the solution and solid particles. The break-up forces depend on the process variables that affect growth kinetics and granule properties by modifying the mixing intensity and the drying rate [2].

Granulation has been described in four principal mechanisms [3]:

(i) layering, where the powder mix added to the granulation adheres to existing granules forming a surface layer and increasing the granule size;
(ii) crushing and layering, where some granules break into fragments that adhere to other granules forming a layer of material over the surviving granule;
(iii) coalescence, where two or more granules join to form a larger granule;
(iv) abrasion transfer, where the abraded material caused by attrition of granules adheres to other granules, thereby increasing their size.

However, Lister et al. [4] considered granulation as a combination of only three sets of rate processes:

(i) wetting and nucleation, where the liquid binder is brought into contact with a dry powder bed, and is distributed through the bed to give a distribution of nuclei granules;
(ii) condensation and growth, where collision between two granules and feed powder, or a granule and the equipment leads to granule compaction and growth;
(iii) attrition and breakage, where wet or dried granules break due to impact, wear or compaction in the granulators or during subsequent product handling.

These mechanisms of granulation are controlled by the forces giving rise to the cohesion of particles and the phenomena of adhesion and cohesion.

The mechanism of bonding in the wet state depends on capillary and interfacial forces between the particles. Immobile adsorbed surface liquid serves to reduce surface imperfections and increase particle–particle contact by decreasing the effective interparticle distance. Once sufficient liquid is added, granulation shifts from an immobile surface liquid state to a mobile liquid film state. However, the granules can exist in a number of different states of liquid saturation [5], as is illustrated in Fig. 8.1.

In the pendular state, particles are held together by a liquid bridge at their contact points: pendular bonds. The capillary state occurs when all voids are filled with the liquid and the surface liquid is drawn back into pores under capillary action. The funicular state is a transition between the pendular and capillary state, where the voids are not fully saturated with liquid. The droplet state occurs when the liquid completely surrounds the granule, resulting in an external phase consisting of liquid, with an

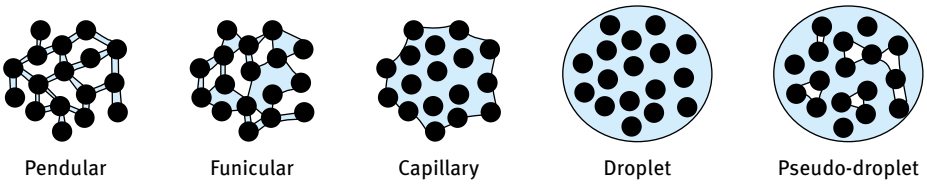

Fig. 8.1: States of liquid content in agglomerate during wet granulation.

internal solid phase. It is also possible to have a pseudo-droplet state where unfilled voids remain trapped inside the droplet. During granulation, it is possible to shift from the pendular state through to the droplet state, either due to the continuous addition of liquid binder and/or consolidation reducing the granule porosity.

The relative strength of the bonds that form during granulation by agitation affects both the mechanism and kinetics of granule growth and such final product properties as friability, dissolution rate and density. It is dominated by three forces, namely static surface tension forces, dynamic forces due to the liquid viscosity and frictional forces. These forces can be evaluated by a capillary number Ca that is defined by the ratio between viscous forces and the capillary force,

$$Ca = \frac{\eta_I U}{\gamma_{LV}} \tag{8.1}$$

where η_I is the binder viscosity, γ_{LV} is the binder surface tension and U is the velocity. According to Ennis et al. [6], the viscous term made a negligible contribution to bridge strength for $Ca < 10^{-3}$ but became dominant for $Ca > 1$.

The static strength of a pendular liquid bridge consists of two components as illustrated in Fig. 8.2.

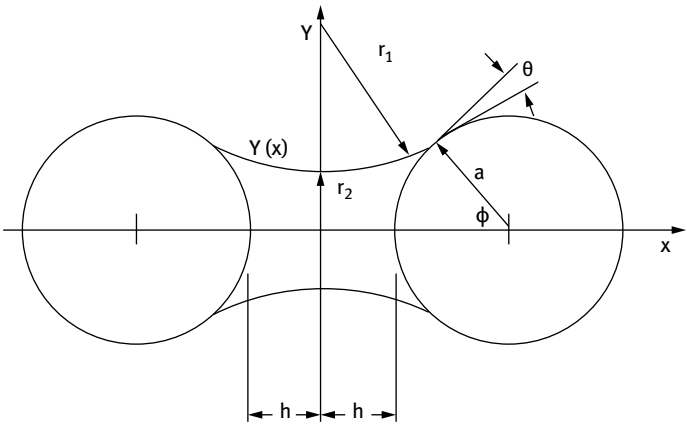

Fig. 8.2: Schematic diagram of two spheres with radius $a(= d_p/2)$ in pendular bond.

There is a capillary suction pressure ΔP_{cap} caused by the curvature of the liquid interface and a force due to the interfacial tension γ_{LV} acting around the perimeter of the bridge cross section. ΔP_{cap} is given by the Laplace–Young equation,

$$\Delta P_{cap} = \frac{2\gamma_{LV}}{r} = \gamma_{LV}\left(\frac{1}{r_1} - \frac{1}{r_2}\right), \tag{8.2}$$

where r_1 and r_2 are the two principal radii of curvature which can be used to calculate the bridge curvature r.

It is common to approximate the liquid bridge profile as a toroid; however, a toroid does not have a constant mean surface curvature. Thus, the interfacial tension and capillary pressure terms are better evaluated at the contact line with one of the spheres from the following equation,

$$F = \Delta P_{cap} a^2 \sin^2 \phi + 2a \sin(\phi) \sin(\phi + \theta), \tag{8.3}$$

where F is the bridge force.

Willet et al. [7] numerically solved the full Laplace–Young equation and then fitted an empirical expression to the result. For $V/a^3 < 0.001$ (where V is the bridge volume) they found that,

$$F = \frac{2\pi a \gamma_{LV} \cos\theta}{1 + 2.1\left(\frac{h^2 a}{V}\right)^{0.5} + 10\left(\frac{h^2 a}{V}\right)}. \tag{8.4}$$

At the maximum contact between two spheres, $h = 0$,

$$F = 2\pi a \gamma_{LV} \cos\theta. \tag{8.5}$$

This means that the bridge force is directly proportional to the liquid adhesion tension $\gamma_{LV} \cos\theta$ of the system.

Rumpf [8] developed a model for predicting the tensile strength of a liquid-bound granule and he assumed the granules are a matrix of equi-sized spheres that failed by sudden rupture of liquid bridges between every particle across the whole fracture plane. For a granule in the funicular and capillary states (Fig. 8.1), the static tensile strength σ_t is given by [8],

$$\sigma_t = Sk \frac{\gamma_{LV} \cos\theta}{a_p}\left(\frac{1 - \varepsilon}{\varepsilon}\right), \tag{8.6}$$

where S is the liquid pore saturation, k is a material constant (for uniform spheres $k = 6$), a_p is the surface average particle radius, ε is the granule porosity and θ is the liquid–solid contact angle.

The strength of a dynamic pendular liquid bridge between two spheres F_{vis} can be calculated using lubrication theory [8],

$$F_{vis} = \frac{3\eta_L a^2}{8L} U_0, \tag{8.7}$$

where η_L is the liquid viscosity, a is the particle radius, U_0 is the relative velocity of particles and L is the gap distance between the spheres.

Theoretical and experimental results obtained by Ennis et al. [6] demonstrated that the cohesive strength of the dynamic liquid bridges may exceed that of the static strength by at least one order of magnitude due to the additional energy dissipation resulting from the binder viscosity. Both capillary and viscous contributions significantly affect the binding mechanism of colliding particles. In order to establish the regimes of granulation, Ennis et al. [9] defines the Stokes number, St_v, as the ratio of the kinetic energy between colliding particles to the viscous dissipation brought about by the pendular bond,

$$St_v = \frac{8\rho_p a U_0}{18\eta}, \tag{8.8}$$

where a is the harmonic mean granule radius of the two spheres, ρ_p the particle density and η the viscosity of the binding liquid.

The above model predicts that collisions will result in coalescence when the viscous Stokes number (St_v) is less than some critical Stokes number, (St_v^*) where,

$$St_v^* = \left(1 + \frac{1}{l}\right) \ln\left(\frac{h}{h_a}\right), \tag{8.9}$$

where l is the particle coefficient of restitution, h is the thickness of the binder layer and h_a is a measure of the particle's surface asperities as illustrated in Fig. 8.3.

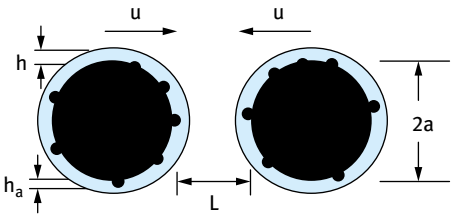

Fig. 8.3: Schematic of model used by Ennis et al. [9].

There granulation regimes can be defined depending on the relative magnitudes of St_v and St_v^*:

(i) $St_v \ll St_v^*$, noninertial regime (all collisions successful);
(ii) $St_v = St_v^*$, inertial regime (some collisions successful);
(iii) $St_v \gg St_v^*$, coating regime (no collisions successful).

8.3 Types of granulators

The process of wet granulation involves three steps, namely blending (to achieve a homogeneous blend), liquid binder addition and wet massing or distribution of the liquid. Two main types of granulation processes are generally used, namely fluid-bed granulators and high-shear mixers and these are summarized below.

Fluid-bed granulation is a process by which granule particles are produced in a single piece of equipment by spraying a binder as solution, suspension, or melt onto a fluidized powder bed. The latter is a bed of solid particles with a stream of air or gas passing upward through the particles at a rate fast enough to set them in motion. This velocity is higher than the incipient fluidized velocity, which is known as the minimum fluidization velocity (U_{min}) but lower than the entrainment velocity A. Rapid drying is claimed to be the advantage of this system.

The mechanism of formation of a granule and subsequent growth progresses in three stages, namely nucleation, transition and ball growth. At the start of the spraying stage, primary particles form nuclei held together by liquid bridges in the pendular state. The size of these nuclei depends on the droplet size of the binder solution. As liquid addition continues, more and more nuclei agglomerate and continue the transition from the pendular state to the capillary state. The specificity of the fluid-bed granulation process is the competition between liquid addition and drying steps. When the granulating liquid is introduced onto a fluidized bed, the primary particles are wetted and form, together with the binder, relatively loose and very porous agglomerates. Densification of these agglomerates is brought about solely by the capillary forces due to the liquid bridges. Therefore, it is important that the quantity of liquid sprayed onto the bed should be relatively large compared with that used in high-shear granulation. Therefore, drying becomes a fundamental step in fluidized-bed granulation.

Several authors [10–12] have reported a description of the growth mechanism in fluidized beds. Atomized liquid from the nozzle tends to spread over the particle surface, as long as there is an adequate wettability of particles by the liquid. If the droplet size is less than the particle size, two situations can be distinguished:

(i) Fast drying before collision between the particles; the growth occurs by layering.
(ii) Collision of two or more particles leading to the formation of a liquid bridge.

If the cohesion strength is weak in comparison with the break-up forces induced by the fluidized bed, the break-up of the bridges could lead to the formation of individual wet particles that can be dried and grown by the layering mechanism. On the contrary, the solidification of liquid bridges occurs due to evaporation of the solvent and the agglomerates become stabilized. The strength of the binder determines whether these particles stay as agglomerates. If the binding forces are in excess of the break-up forces, either in the wet state or in the dry state, uncontrolled growth will proceed to an overwetted bed. Alternatively, if the liquid droplets are too large with respect to the particles, with uneven liquid distribution, then wet agglomerates can develop by formation of liquid bridges. If wet agglomerates are too strong to be fragmented and too large to be fluidized, then large regions of the bed may defluidize and stick together as large wet clumps. This phenomenon is termed “wet quenching”. If the break-up forces completely predominate, the agglomerate may break down to smaller agglomerates or individual particles with a small amount of coating material attached

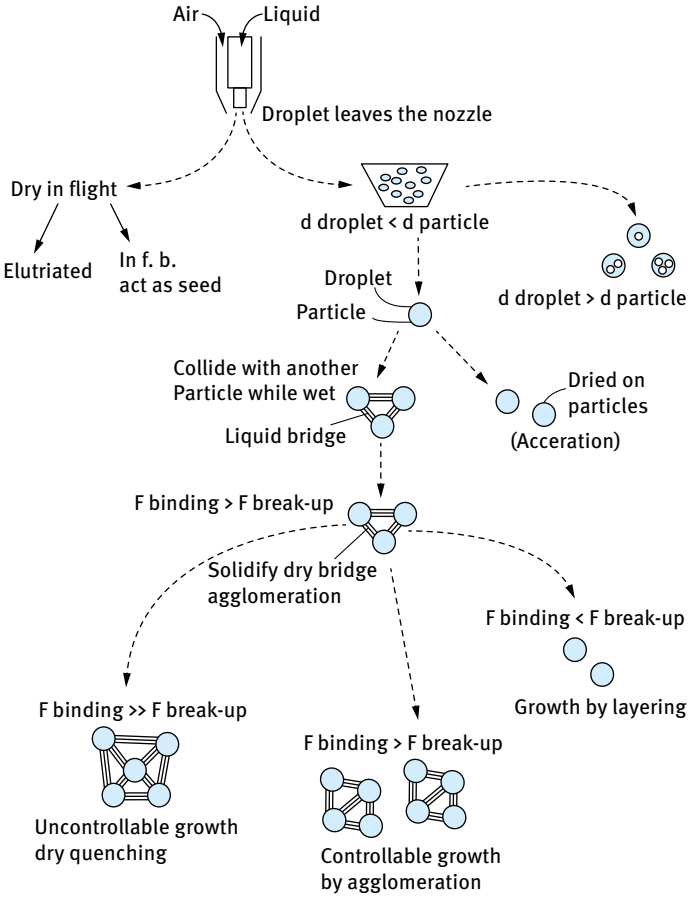

Fig. 8.4: Mechanism of granulation in fluid bed [2, 12].

to the surface of each. Hence, the interaction between build-up and break-up forces and consequently the strength of solid and liquid bridges between particles plays a crucial role in determining the mechanism of growth.

Fig. 8.4 shows a schematic representation of the mechanism of granulation in a fluid bed [2, 12].

It should be mentioned that good control of the fluid-bed agglomeration process is difficult [2]. Wetting, mixing and drying of particles take place simultaneously in the same apparatus. These different elementary processes affect each other and consequently the influence of each one on the growth kinetics is difficult to characterize. It is necessary to understand the important mechanisms involved and their relation to each other, to be able to control the granulation process. It is important to carry out systematic studies on the design of the fluid-bed granulator, the nature of the binder, the process-related variables (atomizer location, hydrodynamic and thermal

behaviour of fluidized bed in the presence of a submerged spray, atomizing air flow rate, fluidizing air velocity, liquid flow rate), product variables (liquid binder surface tension and contact angle and viscosity, particle shape and size, particle porosity).

High-shear mixer granulation is performed using the following steps:

(i) Dry mixing of the powders until the desired degree of uniformity is achieved. This is obtained by controlling the impeller speed and mixing time.
(ii) Addition of liquid binder by either pumping or pouring the liquid through the lid of the mixer, or by spraying it onto the mass through a pneumatic or binary nozzle.
(iii) Wet mixing following binder addition and this requires additional energy until the desired consistency is obtained.
(iv) Drying after granulation; the material is dried by the transfer of heat through conduction from the jacket bowl to the product.

Agitation may be applied by slowly rotating the bowl or operating the impeller at low speed either continuously or intermittently throughout the drying stage. Caution must be exercised to avoid granule breakdown during drying.

The main advantages of granulation in high-shear mixers are [13]:

(i) short processing time;
(ii) less liquid binder compared to fluid-bed granulators, thus requiring shorter time for drying;
(iii) highly cohesive materials can be granulated which are difficult to fluidize and agglomerate in a fluid bed;
(iv) voluminous materials can be densified by granulation;
(v) control of granule porosity by massing time and impact of the agitators.

The granulation process in high-shear mixers can be monitored by determining the power consumption profile [2] as schematically illustrated in Fig. 8.5. In phase I initial wetting of the powder occurs and moisture becomes absorbed by the powder particles without formation of liquid bridges. In this phase the power consumption does not increase, indicating that particle growth is insignificant. In phase II, liquid bridges are formed between the particles and the first granules and this is accompanied by an increase in power consumption. In phase III the power consumption levels off and addition of granulating liquid results in filling of the interparticle voids and formation of coarser granules. The agglomerates are growing in size and a marked increase in power consumption occurs. In phase IV large areas in the particulate system are completely filled with liquid and the power consumption increases and drops before reaching point S_5. At this point the liquid saturation is equal to 100 %. In phase V after an increase in power consumption (due to an artefact), the power consumption drops due to the formation of a suspension by the excess of liquid.

In order to calculate the corresponding amounts of granulating liquid in different compositions, it is necessary to introduce a dimensionless amount of granulating liquid π which is defined as the degree of saturation of the interparticulate void space

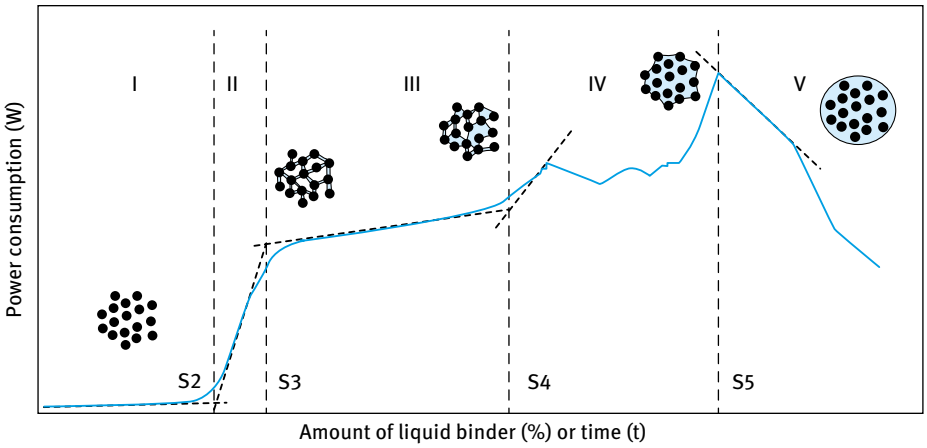

Fig. 8.5: Power consumption profile [2].

between the solid materials [14],

$$\pi = \frac{S - S_2}{S_5 - S_2}, \tag{8.10}$$

where S is the amount of granulating liquid, S_2 is the amount of granulating liquid necessary, which corresponds to moisture equilibrium at approximately 100 % relative humidity, and S_5 is the complete saturation of interparticulate void space before slurry is formed. Leunberger et al. [14] stated that the use of π enables a direct comparison of the agglomerating properties of different starting materials.

As with the fluid-bed granulation process, high-shear mixing granulation is sensitive to process and product variables. The most important process variables that control agglomeration are the moisture content, impeller speed, liquid flow rate and wet massing time. The most important product variables are the liquid binder surface tension (and contact angle), wettability and viscosity.

8.4 Compaction of solids

The compaction process is often referred to as “dry agglomeration”, since no liquid binders are necessary for the agglomeration process. The main objective of compaction is to reduce the bulk density of the powder, improving handling properties and avoiding segregation after a mixing process or production of agglomerates with a defined shape such as tablets [2]. The main binding force in compaction is van der Waals attraction. Compaction processes are based on a compression of the powder between two surfaces or processing through an orifice in extrusion.

The powders that are compressed to form compacts can be of three main categories:

(i) powders that form robust and stable compacts when a small pressure is applied;
(ii) powders that form compacts but show a tendency towards capping or lamination;
(iii) powders that resist forming a compact such as glass spheres or sand.

Whereas powders of the first category can be compressed to 100 % compact, the other two categories require a solid formulation in order to overcome their unpleasant compression properties. Thus these powders are mixed with appropriate additives or excipients before carrying out the compaction process.

The process of compaction of powders starts with a rearrangement of the particles [15] which is limited by the minimum porosity. This is illustrated in Fig. 8.6, which shows the basic mechanisms of the compaction process [2].

With increasing the pressure the bulk density increases, the porosity decreases and air is disposed. In the next step. deformation or fragmentation of the particles occurs and this leads to consolidation of the material. Plastic and viscoelastic and deformation are the most important mechanisms in compaction of powders. Elastic deformation is the main mechanism responsible for capping or lamination [15]. With increasing time under pressure, plastic deformation occurs thus improving bonding and stability. With further increasing the time under pressure, weaker compacts may be produced due to little plastic deformation. If consolidation is mainly based on fragmentation, the compaction speed will not affect the strength of the compacts. In this case the most important bonding mechanism is van der Waals force. These effects should be taken into account when developing a formulation and considering additives.

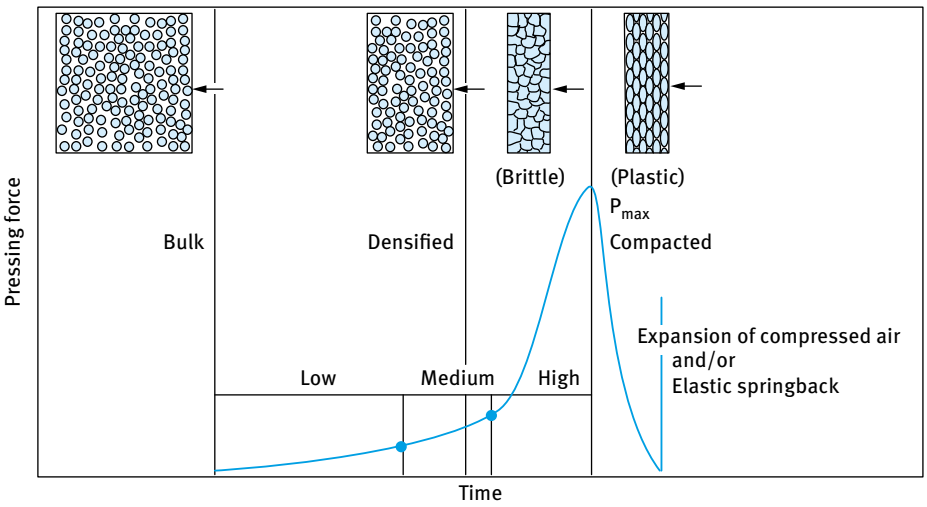

Fig. 8.6: Basic compaction mechanisms.

In most cases compaction is carried out at room temperature, but depending on the process and product specification compaction may be carried out at higher temperatures (up to 1,000 °C) [2]. The throughput in compaction processes varies widely. High value products such as pharmaceuticals may be produced in small quantities of some kilograms per hour. Bulk chemicals or ores may be compacted at much higher throughput, reaching 100 t/h.

8.5 Solid dosage formulations in the pharmaceutical industry

Three main types are commonly used in the pharmaceutical industry [16], namely tablets (which are mostly used for oral drug administration), hard and soft gelatin capsules and sustained-release pellets [16]. In this section, I will first consider the formulation of tablets that can be obtained by simple compression of the active ingredient (AI) powder. However in most cases, direct compression of the AI powder may not be easy, in particular with substance of poor self-compressibility and tablets that require a high drug dose and tablets with low drug content where uniformity becomes important. In these cases, a granulation process is required before compression to form the tablets. The disintegration of tablets in the gastric fluid is discussed at a fundamental level with particular reference to the substances that can be used to aid the disintegration process. The dissolution rate of the drug following tablet disintegration is very important and requires fundamental discussion. The process of tablet coating, that is required for aesthetic and protective purposes, is briefly described. The next section will give a summary of the formation of hard-shell and soft-shell gelatin capsules. The last section will deal with the formulation of sustained-release tablets and the process of the release pattern expected.

8.5.1 Formulation of tablets

As mentioned above, tablets are the most popular of all dosage forms [16]. They have the advantage that they are convenient and inexpensive to deliver a dosed amount of AI with great accuracy. However, a certain amount of operational expense is involved in preparing a drug for delivery to the die and suitable compression. It would be advantageous if the powder could be simply mixed and compressed. In cases where the major portion of the dosage form is an inert excipient, suitable selection of this excipient can make this possible, and this is known as direct compression. Originally, spray dried lactose was used but more recently this is being replaced with microcrystalline cellulose and this is mixed with the drug, glidant, disintegrant and lubricant. The powder blend is placed in the hopper of a tablet machine and simply compressed.

Although the direct compression technique is popular, many products have to be made by granulation methods which serve three main purposes, namely improved

flow, uniform AI distribution and aiding the bonding together of the tablet. As mentioned above, the steps involved in the granulation process consist of transfer of the powder to a mixer, blending, adding granulation solution, coarse milling of the wet granulate, drying and milling. The wet granules can be dried by placing them on trays, although this method is not very efficient and is now replaced by fluid-bed drying. The drying time depends on the velocity with which dry air passes over the wet surface and on the thickness of the stagnant layers on the surface to be dried. By monitoring the exit air temperature, a sudden increase will indicate that drying is complete. This avoids the danger of over-drying which exists in all tray drying processes.

Milling of granulations is usually accomplished by means of hammer mills. Sometimes, granulators are used in which the wet powder is forced through a semi-circular wire mesh screen by an oscillating head. In milling of wet granulations through hammer mills, screens with large openings or no screens at all are used. In dry milling, the strength of the granule is important; poor granulations may give powders (i.e. all fines) which will not flow or compress. The particle size distribution and the strength of the granules are very important. In general, a strong granule will produce a strong tablet. However, a high granulation strength may give rise to compression difficulties. Therefore, it is necessary to have a method for testing the strength of granulations to arrive at the optimum level. The breaking strength of an individual granule can be measured by placing it on a flat plate on the Labjack and raising it until it touches another flat plate which is fixed on the underside of the pan of a chemical balance. Lead shot is then poured onto the pan until the point is reached where the granule breaks. By determining the weight of the lead shot, the breaking strength of the granule is arrived at. Using this method, it was found that the granule strength increases with decreasing particle size.

For a tablet to maintain uniformity, the granules must flow into the die prior to compression in a reproducible manner. In addition, the granules must be able to find their closest packing with ease. The final criterion of whether a granulation is a mechanically good one or not is whether it performs well under tableting conditions.

One of the fundamental aspects of tablet formation is to consider the solids behaviour under compression. This was considered by Leigh et al. [17] who showed that for a perfectly elastic body, when axial loading occurs, a force will be transmitted radically of the value,

$$\tau = \nu\sigma, \tag{8.11}$$

where σ is the axial force, τ is the radial force and ν is the Poisson ratio.

The above relation is shown schematically in Fig. 8.7.

Fig. 8.7 shows that when the axial force is released the redial force returns to zero, and a tablet produced in such a process would be free to move out of its die.

Many solids show the presence of a yield stress as illustrated in Fig. 8.8. In this case, if the force is increased beyond the yield point A_1, then deformation starts, and σ becomes a function of τ depending on the yield value (similar to a pseudoplastic

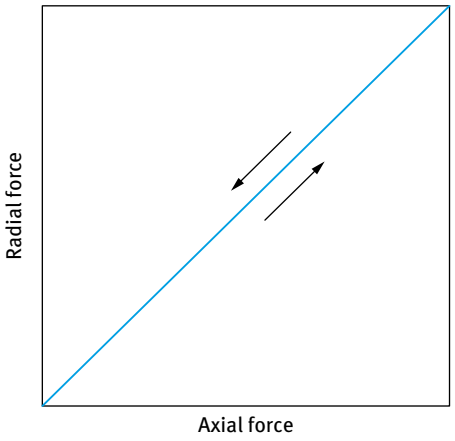

Fig. 8.7: Expected compression cycle for an elastic body.

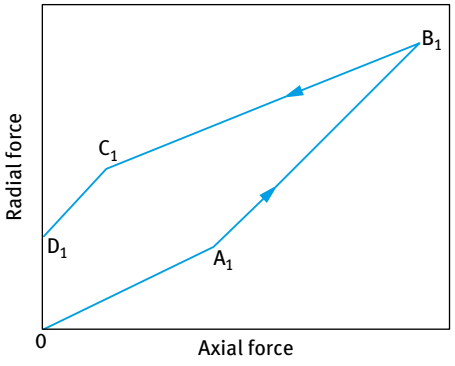

Fig. 8.8: Expected compression cycle when a (constant) yield stress occurs [2].

system). In Fig. 8.8, the yield value is obtained by extrapolating the line AB to zero radial force and the functionality here is assumed to be linear. In equation (8.11), the factor v is less than unity [17, 18]. In the area beyond the yield point, the slope is unity, and we have

$$\tau = \sigma - s, \tag{8.12}$$

where s is the yield value.

If the axial load is released at point B_1 in Fig. 8.8, then the radial force will decrease at v times the rate of axial force decrease (i.e. the line B_1C_1 is parallel to line OA_1). A point C $(\sigma_1 \tau_1)$ will be reached where,

$$\tau_1 = \sigma_1 + s. \tag{8.13}$$

Yield will take place again and a further decrease is according to line C_1D_1 with unity slope. The equation for this line is,

$$\tau - (\sigma_1 + s) = \sigma - \sigma_1 \tag{8.14}$$

or,

$$\tau = \sigma + s. \tag{8.15}$$

In this case, the body will exert the force s on the die wall after compression. However, the force may be less because the point B_1 may be sufficiently low so that point C_1 is not reached (on the right of the radial force axis).

Another point that is worth considering is the die wall pressure, i.e. the part of pressure that goes into a horizontal component. Many tablet machines provide a maximum diameter beyond which they will not be able to withstand lateral pressures. Also the compressed tablet has to be pulled out; this is the result of the horizontal component and the fact that there was not complete elastic recovery, which in turn is responsible for the fact that once the tablet is out of the die, it cannot be placed back in again. Lubricants are added to reduce the ejection pressure. Instrumental presses exist that allows elastic measurement of ejection pressure so that the optimum level of lubricant can be determined. The lubricant decreases the cohesion and, therefore, a minimum of lubricant must be applied, which may also have an effect on tablet dissolution.

A schematic representation of the tableting process is shown in Fig. 8.9 which also shows the related force/displacement time plots. The raw material is filled in the die after the lower punch has moved at the lowest position. Afterwards, the upper punch compresses the raw material while the lower punch remains at the lowest position. Then the upper punch is lifted off and the lower punch moves the tablet upwards. Finally the tablet is removed and the next tableting cycle starts [2].

With modern tableting machines up to 1,490,000 tablets per hour can be produced. This is only possible with excellent formulated feed materials. It is essential to ensure free flowing and deaeration supporting feed material for the tableting machine. The surface and bulk properties of the powder, as well as those of excipients and additives are very important for tableting pharmaceutical products. The same is true for catalysts and laundry detergents.

One of the most important values for characterizing tablet production is the compression pressure p calculated by dividing the compression force F by the punch tip area,

$$p = \frac{F}{A}. \tag{8.16}$$

The porosity ε of the tablet can be calculated from the particle density ρ_p and the density of the tablet ρ_c,

$$\varepsilon = 1 - \frac{\rho_\mathrm{c}}{\rho_\mathrm{p}}. \tag{8.17}$$

Heckel [19] introduced a density–pressure relationship in powder compaction,

$$\ln \frac{1}{1 - D^*} = C_1 p + C_2, \tag{8.18}$$

where D^* is the relative density (density of compact ρ_c to the density of the material ρ_p) that changes with the pressure applied on the compact C_1 and C_2. Roberts and

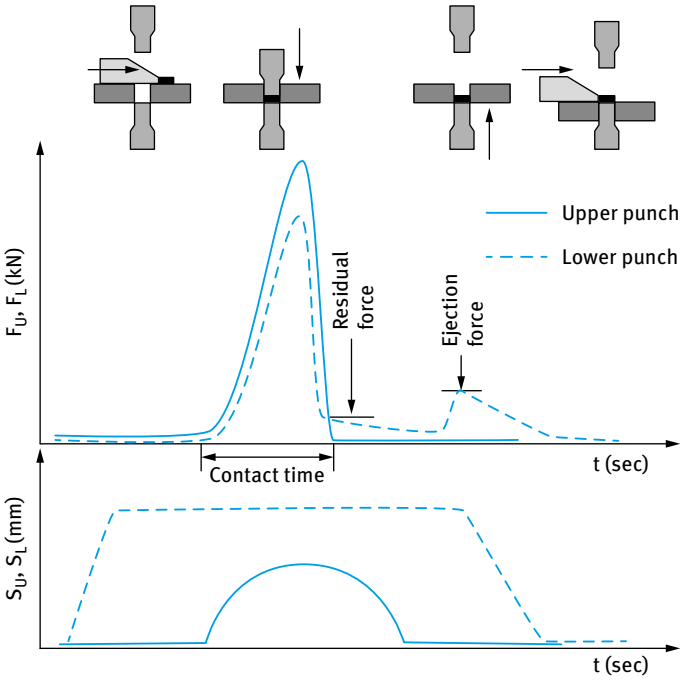

Fig. 8.9: Schematic representation of the tableting process and related force/displacement-time plots.

Rowe [20] expanded the above relationship by introducing the speed of compaction. Equation (8.18) shows that a plot of $\ln(1/1 - D^*)$ versus p is linear and this allows one to obtain the constants C_1 and C_2. By using the Heckel equation and the related plots, it is possible to distinguish between three different volume reduction mechanisms, A, B and C [21] as illustrated in Fig. 8.10.

The size fractions of type A show different initial packing. The plots of type A remain parallel with increasing pressure. After particle rearrangement, type A behaviour is related to plastic flow. In type B, fragmentation powder densification occurs

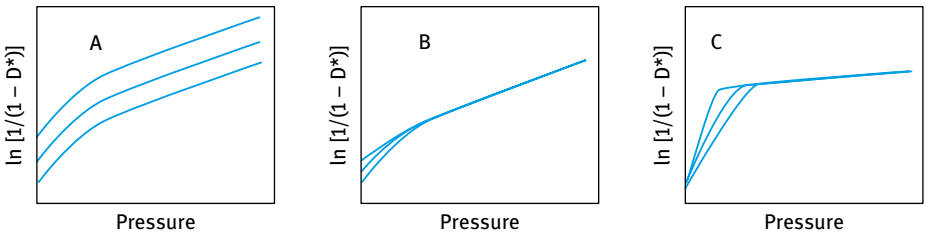

Fig. 8.10: Types of density–pressure relationship in powder compaction.

and at the beginning the plots are slightly curved. With increasing pressure they become coincident. The compaction mechanism of type C is also plastic flow. Contrary to type A the volume reduction is very small and the curves become coincident after a steep rise at the beginning.

The volume reduction due to compression consumes energy. The work of compression can be calculated using the force–displacement data illustrated in Fig. 8.9. Fig. 8.11 shows typical plots of the force–displacement of compression and decompression.

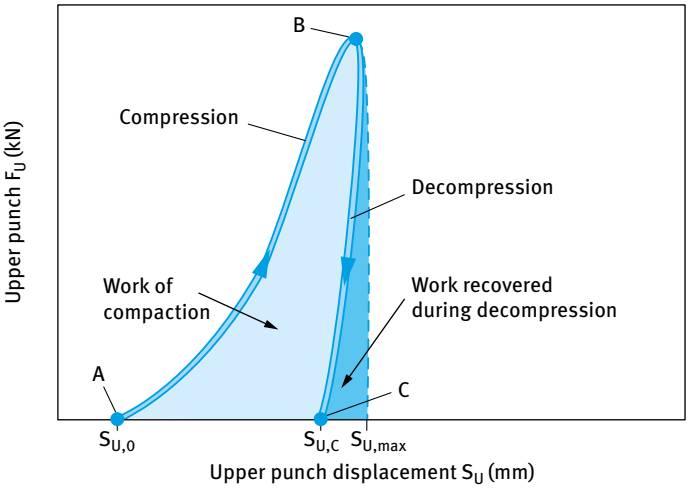

Fig. 8.11: Force–displacement plots for compression and decompression.

The total work during compression phase A → B can be calculated by integrating the upper punch force F_U between the first contact $S_{U,0}$ and the maximum displacement $S_{U,max}$,

$$E_{total} = \int_{S_{U,0}}^{S_{U,max}} F_U(S_U)\,ds. \tag{8.19}$$

During decompression phase B → C work is recovered due to the elastic behaviour of the compact. In this phase a vertical expansion of the tablet can be measured using a force acting on the upper punch. When moving back the upper punch loses contact with the surface of the tablet at a certain point. At this point the force F_U ($S_{U,C}$) becomes zero and the elastic work recovered is given by,

$$E_{total} = \int_{S_{U,C}}^{S_{U,max}} F_U(S_U)\,ds. \tag{8.20}$$

By subtracting the elastic work from the total work, one can calculate the plastic work, E_{plast},

$$E_{\text{plast}} = E_{\text{total}} - E_{\text{elast}}. \tag{8.21}$$

The elasticity describes the elastic behaviour of the material compacted,

$$\text{elasticity} = \left(\frac{E_{\text{elast}}}{E_{\text{total}}}\right) \times 100. \tag{8.22}$$

Control of product properties such as size, weight, shape, porosity, disintegration time, and dissolution time are very important in the tableting process. The mechanical properties such as friability and hardness are also very important. One of the most important mechanical tablet properties is the tensile strength σ_s which can be calculated by a diametrical compression test applying a force F on a tablet with diameter D and thickness t [21],

$$\sigma_s = \frac{2F}{\pi t D} \tag{8.23}$$

In general, the tablet properties are influenced by properties of the primary particles, processing of the primary particles, amount and properties of additives and excipients, humidity, temperature, post-treatment (e.g. de-dusting and coating), etc. With decreasing particle size of the primary particles, the tensile strength increases in most cases. Designing the particle size distribution using agglomeration processes can improve the tableting properties. The microstructure of the granules is affected by the production process. In most cases granules produced by high-shear mixing processes produce a more homogeneous structure when compared with granules produced using fluid-bed processes. Pre-compression, tableting speed, deaeration and time of application of contact pressure can also affect the tablet properties [2].

The hardness of tablets is usually checked by commercial hardness testers [16]. The crushing strength is defined as the particular force of compression that, when applied diametrically, just causes the tablet to fracture. In general the tablet is positioned on a fixed anvil; a force is then applied by means of a moving plate. Hardness is a function of compression force. In general there is no influence of hardness on dissolution rate when hydrophilic gums are used for specific sustained release [16].

Tablet defects such as picking, capping and splitting, and spotting are sometimes observed. In picking, part of the surface of the tablet is missing and this can be attributed to very wet granulation, poorly polished punches, too much play between punch and die and insufficient lubricant. Capping and splitting range from the presence of hairline cracks in the wall of the tablet to the top (convex) part being missing. This is attributed to high pressure, excess fines, too weak a granule, too dry a granulation, presence of unfavourable polymorphic forms or crystal habits or too high compression rate. Poor punch surfaces and improper lubrication can also contribute to these defects. Spotting may be due to chemical changes, dirt (often from seals in mixers) and high moisture content (that causes mould growth).

The uniformity of tablets is tested by calculating the coefficients of uniformity (the reciprocal of the coefficient of variation) of weight, thickness and hardness as functions of the percent of fines in the granulation process. Uniformity is not only a function of granulation quality, but also of machine performance [16].

An important property worth considering in tablet manufacture is the heat of compression. This is caused by several factors:

(i) In the initial bed of powder, only one point of contact exists between any two particles. Upon application of pressure, the bed consolidates by particles sliding over one another; the extent of which depends on the frictional properties of the material surfaces.
(ii) In the next stage of compression, elastic and plastic deformation occurs and this is associated with energy consumption.
(iii) Compression involves a certain amount of fragmentation which at moderate pressures causes an increase in surface and at very high pressures a decrease.
(iv) Removal from the die of the upper punch at the late stage of the compression cycle.
(v) The actual ejection of the tablet has energy requirements associated with it.

The above energy consumption is reflected in a linear increase of tablet temperature with increasing pressure applied [22] as schematically represented in Fig. 8.12.

The logarithm of the absolute temperature also shows a linear response to the reciprocal of the machine speed as illustrated in Fig. 8.13.

8.5.2 Tablet disintegration

It has always been assumed that the more rapidly tablets fall apart in the gastric juice, the more available they should be. It is obvious that tablet operation, in particular the granulation process and hardness, must somehow affect disintegration. For example, hardness of tablets is dependent on the compression force [23] as illustrated in Fig. 8.14.

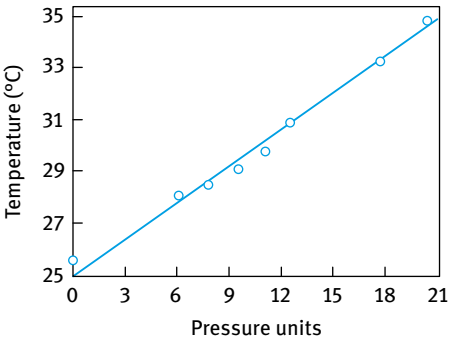

Fig. 8.12: Linear response of tablet temperature to applied pressure.

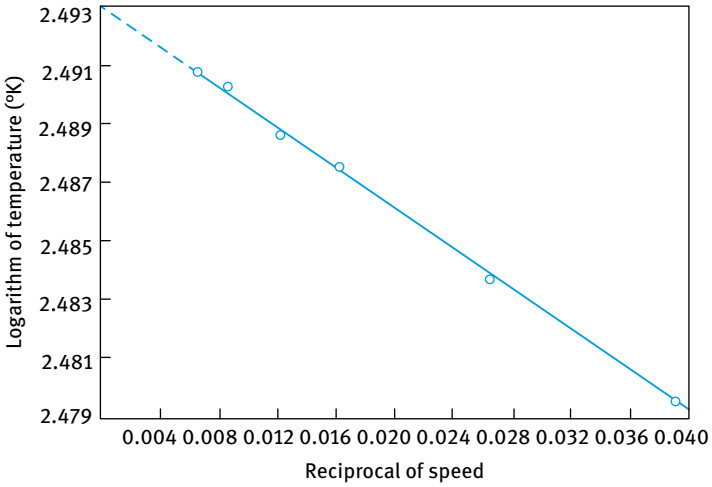

Fig. 8.13: log T (K) versus reciprocal of machine speed.

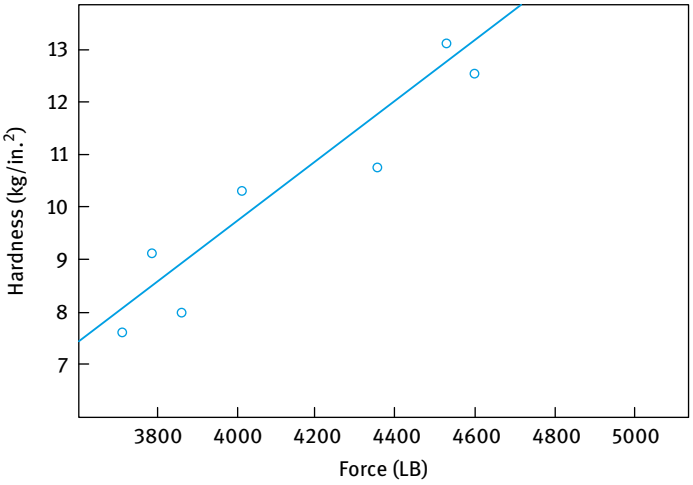

Fig. 8.14: Linear response of tablet hardness to compression force.

The hardness h is related to the compression force F by the following relationship,

$$F = F_\infty[1 - \exp(-k'h)] \approx F_\infty k'h. \tag{8.24}$$

The disintegration time t is related to hardness by,

$$t = t_\infty[1 - \exp(-kF_\infty k'k)] \tag{8.25}$$

which for large values of $kF_\infty k'$ becomes,

$$t = \text{const} \times h. \tag{8.26}$$

For reducing the disintegration time of tablets, excipients (disintegrants) need to be added. This is illustrated in Fig. 8.15, which shows the variation of disintegration time with compression force for tablets containing various concentrations (%) of starch [24].

At low starch concentrations (1–8 %) the disintegration time t shows an exponential increase with increasing tablet compression force F and this follows the following relationship,

$$t = t_{\infty}[1 - \exp(-kF))]. \tag{8.27}$$

However, at high starch concentration (15 and 30 %) the disintegration time is almost constant and independent of compression force. The results of Fig. 8.15 show the reduction of disintegration time with increasing concentration of the disintegrant (starch in this case).

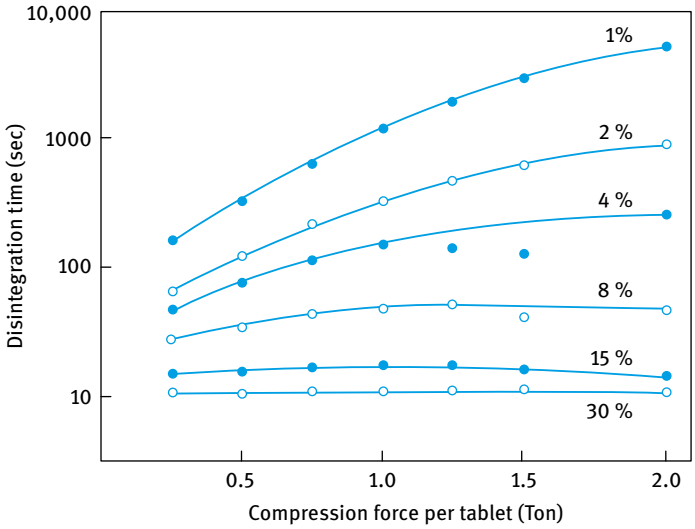

Fig. 8.15: Variation of disintegration time with compression force at various starch concentrations (%).

The most common disintegrants are resins, alginic acid and corn starch. The former two act by swelling. Commons et al. [25] showed that when starch is used as disintegrant (added with lubricants), it appears in the channels between the granules. Starch is a somewhat incompressible substance and it acts by an increase in porosity. Curlin et al. [26] suggested that disintegration of compressed tablets containing corn starch may be attributed to capillary action. Several factors must be considered when using starch as a disintegrant [16], namely pH, electrolyte concentration, pepsin, surfactants, etc. The concentrations of dissolved electrolyte, pH and pepsin have little

effect on swelling of starch. Surfactants aid wetting and increase permeability. Untreated or unmodified starch will not swell sufficiently to cause tablet disintegration. Irreversible hydration of starch hinders tablet disintegration; the starch gelatinizes on the tablet surface and the interior portion of the tablet remains dry and this hinders disintegration.

8.5.3 Drug dissolution rates from tablets

One of the most important aspects of using tablets for drugs is bioavailability, which is affected by the tablet's disintegration and to large extent by its rate of dissolution after disintegration [16]. A tablet's disintegration does not guarantee that the active ingredient goes into solution. It is necessary to design in vitro tests that can predict ranks of performance in vivo. In other words if a drug dissolves more rapidly say from tablet A than tablet B, then peak blood levels should be higher and/or time of onset more rapid and/or available for tablet A. The test should be one in which a tablet is somehow presented in the test liquid (water, 0.1 mol dm^{-3} HCl, 0.1 mol dm^{-3} NaOH, artificial gastric or intestinal fluid) and the drug concentration C is measured as a function of time t. Usually the dissolution rate dC/dt follows Fick's law of diffusion,

$$\frac{dC}{dt} = KA(C_s - C), \tag{8.28}$$

where K is the dissolution rate constant, A is the surface area and C_s is the saturation amount in the test liquid.

Equation (8.28) shows that when $C = C_s$ the rate dC/dt will be zero. Integration of equation (8.28) gives,

$$\ln\left(1 - \frac{C}{C_s}\right) = -KAt \tag{8.29}$$

or,

$$C = C_s[1 - \exp(-KAt)]. \tag{8.30}$$

Equation (8.30) will hold out if $C_s > C_0$ (sink conditions), where C_0 is the amount in milligrams present in the tablet. However if the opposite is the case, then equation (8.30) holds until $C = C_s$, but then no more material will dissolve. Some typical dissolution rates for tablets containing various lubricants [26] are shown in Fig. 8.16.

For drugs that have different polymorphic forms, the metastable polymorph has a higher dissolution rate (dC/dt) and higher saturation solubility C_s. Once seeded with the more stable form, the solution will behave as a supersaturated solution and the amount in solution will decrease with time asymptotically towards the thermodynamic solubility.

Several factors affect the dissolution of the drug, e.g. agitation (laminar versus turbulent flow), temperature (that follows Arrhenius type since the diffusion coefficient varies in this fashion), viscosity (that affects the diffusion-controlled dissolution), complexation and solubilizing agents in the liquid phase [16].

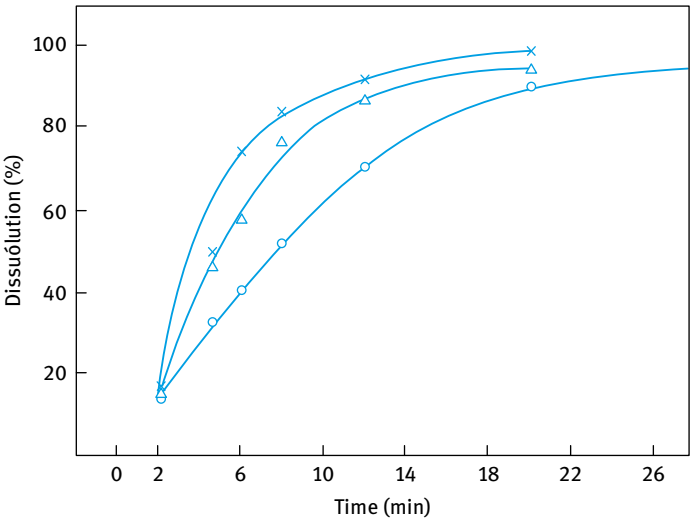

Fig. 8.16: Dissolution rates for tablets containing various lubricants. (○) magnesium stearate; (△) hydrogenated vegetable oil; (×) soluble lubricant.

It should be mentioned that addition of a solubilizer (e.g. micellar species) to a poorly absorbed drug may not necessarily aid its biological availability, because activity (and hence in vivo transport) depends on the concentration of free, not free plus micellar, species. Solid solution in polyethylene glycol may increase both in vitro dissolution rates and in vivo bioavailability. Lubricant generally decreases the dissolution rate due to formation of a hydrophobic thin film on the surface of the particles. Increased hardness of the tablets also decreases the dissolution rate.

8.5.4 Effect of porosity on release rates

An important factor that affects the release rate is the porosity of the matrix of the tablet. If the rate of dissolution is diffusion controlled, then the number of grams of drug released per unit area Q is related to the porosity ε by the equation [27],

$$Q = \left[\left(\frac{D\varepsilon}{\tau}\right)(2A - \varepsilon C_s)C_s t\right]^{1/2}, \tag{8.31}$$

where D is the diffusion coefficient, τ is the tortuosity, A is the amount of drug per unit volume and C_s is the solubility of the drug in the liquid.

However, Singh et al. [28] found that for salicylic acid in polyethylene, the rates did not follow equation (8.31) and they concluded that diffusion was not the rate-controlling factor but that the release was limited by the rate or extent of penetration of the liquid into the matrix according to the Washburn equation [29],

$$P_i = -\left(\frac{4}{d_i}\right)\gamma \cos\theta, \tag{8.32}$$

where P_i is the smallest net pressure necessary to effect penetration, d_i is the smallest diameter of a pore that can be penetrated at P_i, γ is the surface tension of the liquid and θ is the contact angle of the interface between solid and liquid. Equation (8.32) only holds if $\theta > 90°$, which was the case for the system in question. Using a nitrogen tank, pressure was then added and the release rates of salicylic acid was measured as a function of applied pressure as illustrated in Fig. 8.17.

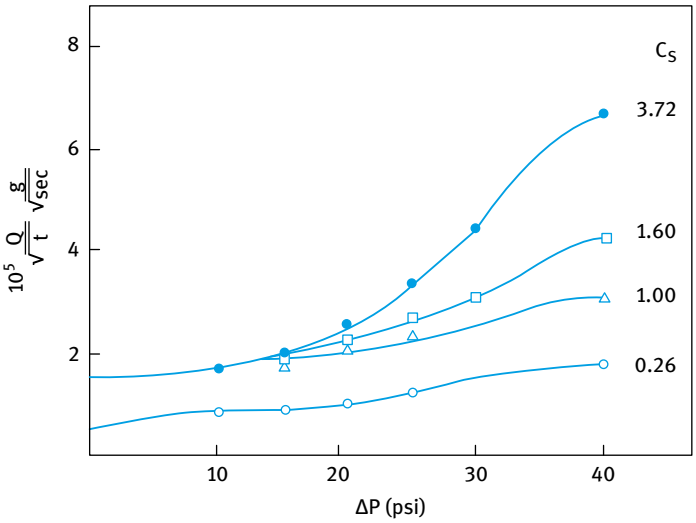

Fig. 8.17: Effect of pressure on release rates.

All the curves in Fig. 8.17 show the same trend, namely an inflection point at about 25 psi. If small amounts of polysorbate are added to the liquid, so that the contact angle is still > 90°, the pressure falls by about 10–15 psi, which is in agreement with the Washburn equation and also in agreement with porosimeter data which show that the pore distribution has a peak about 0.3–2 µm.

8.5.5 Tablet coating

Tablet coating is undertaken for protective and aesthetic purposes. Protection against oxygen, moisture and light is provided by depositing sugar on the outside of the tablet. Coating is carried out in coating cans which range from 8-inch laboratory models to 42-inch or larger diameter production units. Syrups of various compositions are poured into the tablets in small proportions and hot air is blown onto the tablets to

evaporate the water and leave solids (e.g. sugar) deposited on the tablets. The process of coating is usually carried out in several steps to deposit many coats [16]:

(i) a sealing coat of, e.g. shellac (applied in alcoholic solution), which serves to prevent moisture from the first syrup coat penetrating into the core or kernel;
(ii) build-up coats serve to give the tablet bulk and round out the edges, which eventually disappear;
(iii) smoothing coats for a smooth appearance (usually sugar syrup);
(iv) colour coats, usually sugar syrup suspensions of lake dyes;
(v) finishing coats;
(vi) polishing coats usually carnauba wax and beeswax applied in an organic solvent to give the tablets shine;
(vii) a printing coat if desired.

Wurster coating [16] employs fluidization and simultaneous spraying of coating liquids. It is sometimes desirable to have a tablet that passes through the stomach intact and then disintegrates in the small intestine. In this case, the sealing coat is made of an acid-insoluble, alkaline-soluble material, e.g. cellulose acetate phthalate.

8.6 Hard and soft-shell gelatin capsules

Hard-shell capsules have been in existence for more than 50 years [16]. They are produced by dipping rods into gelatin melt at controlled viscosity and temperature, drying them by exposing them (in a continuous set-up) to a stream of air of controlled temperature and humidity, and cutting and removing them. Gelatin and machine parameters are quite critical since a 10^{-5}-inch variation in thickness will make a joint too tight or too loose. For the filling operation, it is first necessary to separate the two halves. This is accomplished by feeding the capsules into a hopper under which two tightly fitted plates are positioned. Capsules fall down a chute where by means of a wedge (as illustrated in Fig. 8.18) they are oriented unidirectionally so that they feed into the plates (rings) right side up. The plates are then separated and the lower plate placed under and rotated under a hopper (which can be swung in and out) containing the powder to be filled. The powder flows under gravity or with the aid of an auger.

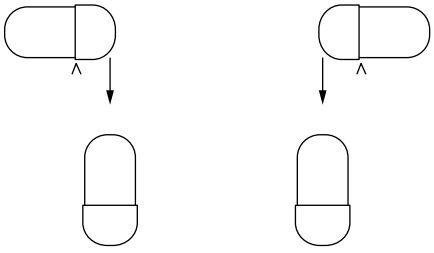

Fig. 8.18: Principle of alignment of capsules.

After one rotation, the hopper is swung away, the plate is removed, the two plates are brought together, and the capsule parts are brought together and ejected by a set of male pegs that fit the holes in the ring. In the automatic machines, capsules are separated and fed into separate hoppers and the powder fill is accomplished by vacuum and then deposited in the lower half of the capsule. Several capsule sizes are commercially available and the fill weights relate to the sizes available.

Several in vivo tests have shown that the capsules do not necessarily give better bioavailability [16]. The in vitro dissolution patterns from capsule formulations showed that the lubricant (magnesium stearate) and fillers (lactose or dicalcium phosphate) affect dissolution greatly [16]. In instances where slow dissolution occurred, the contents of the capsule had a tendency to remain as a wet plug after the dissolution of the gelatin. Thus, drug dissolution was limited by erosion, solution and diffusion rates of the drug and capsule powder mass. The poor water penetration of the powder plug was shown to be due to the magnesium stearate content.

The thickness of the capsule shell is of importance as far as the fit of the top and bottom halves is concerned. It is, therefore, necessary to determine the capsule thickness. One should also recognize that gelatin contains some water under normal environmental conditions and this may transfer to hygroscopic contents in a hard-shell capsule. This correlates with the water vapour diffusion through a hard-shell capsule. Hard-shell capsule operations are preferred in rooms with at most 20 % relative humidity. The capsules are polished in a coating pan with salt after completion. Printing is possible on special machines and is best performed prior to filling.

Soft-shell capsules are produced by using a gel of gelatin and glycerol which is made under vacuum at about 20 °C and then transferred to a holding tank where it is held at 50–70 °C. It is then transferred to a hopper with an adjustable side which allows the gelatin to flow at desired thickness onto a casting drum 5 ft in diameter. The drum rotates slowly (at 4–6 rpm); the gelatin is cast in two parallel films, one of which is stripped and guided to roll (the die roll) positioning right under the measuring roll. Vacuum draws the gelatin around a cylindrically protruding die which is slightly larger than the cavity in the measuring roll. As the cavity lines up with the die, pressure is applied to it, and the powder plug falls into the die, then continues to rotate; after a 30–40° rotation, it comes into contact with the second film which has to be guided to the pressure roll; the two films are sealed together by the pressure and cut by the edge of the die. They are ejected by compressed air and blown into a coating pan where they are tumbled to shape (stearyl alcohol being used as a conspergent). The capsules are then trayed and dried at 10 % relative humidity in large drying rooms. Empty capsules are floated off in isopropanol; “leakers”, i.e. capsules that have a pinhole in the seal, will eject air as they dry and hence shrink and become hard, and can be easily removed by inspection.

The most important parameters that affect soft gelatin capsules are film thickness, gelatin temperature, casting drum speed, temperature of encapsulation and moisture content of the gelatin [16]. Fill weight can be adjusted and controlled partly by vacuum

and partly by having available a set of measuring rolls with varying depths. Since large amounts of "web" are produced (the part of the films not used when the capsules are cut out) and this is used in part of the following gelatin melts, the latter quality may vary. Gelatin web denatures on storage, getting harder and more difficult to melt and seal. Drying to a specific moisture content of capsules is important since capsules which are too dry are brittle and capsules that are too moist stick together, having a tendency to discolour (by promoting diffusion of water-soluble ingredients into the shell) and possess poor chemical stability when moisture active ingredients are present in the capsule shell. The drying patterns are complicated by the fact that at the early stage moisture migrates both out into the dry atmosphere and into the fill. After about 2–3 hours, the constant rate period sets in and the drying endpoints coincide with the end of the constant drying period. To minimize moisture transfer from the shell to the fill, an internal film (Piccolyte) is applied; this alleviates but does not eliminate the problem of moisture migration into the fill. The physical tests performed on the capsules involve moisture tests and friability tests; the latter consist in dropping container capsules 8 ft through a tube onto a hard surface; at least ten falls without breakage are required. Fill weights are monitored every 15 min on control charts, as are film thickness. In most cases the fill is a liquid suspension which forces the gelatin into dies of exact dimensions. When oxygen and moisture-sensitive products are used, the active ingredient is suspended in an oil.

8.7 Sustained-release pellets

It is possible to make tablets which do not disintegrate but rather "peel off" a layer at time. These so-called "erosion tablets" will release their medication by a cube-root law. They suffer from the fact that gastric emptying time may depend on many factors and therefore that reproducible biological effects are difficult to envisage [6]. A more popular system (less prone to these variations) are the sustained-release pellets, since here probably all the pellets would not pass out of the stomach at one time.

The sustained-release pellets are produced as follows. The drug is applied as multiple coats of syrup suspension to non-pareil seeds (of uniform size, e.g. 16–20 mesh) of sized sugar which has been rounded in a coating pan with sugar syrup and subsequently dried. Coats of beeswax and glycerol monostearate are applied by dissolving the waxes in a volatile organic solvent and spraying the solution on the pellets.

Using the pellets, the sustained-release pattern is more readily controlled. The principle is to divide a daily dose into many (say 20) pellets and design their release so that, for example, one fourth is released immediately, one fourth after 6 h, one fourth after 12 h and one fourth after 18 h. This is idealized but is approached by some delayed-action preparations. The problem with this approach is that the absorption constants after 6 and 12 h are not liable to be the same as at time zero. If a sustained-release product is developed, the release is usually tested in vitro by subjecting the

preparation to 1 h in artificial gastric juice. The amount released is checked by a suitable assay procedure on a small quantity of the gastric juice. Half of it is removed and replaced with artificial intestinal juice and this is assayed after 1 h; then half of the test fluid is removed and replaced with artificial intestinal juice and so on. In this fashion, the first hr will be a test in gastric juice and subsequent tests will consist of: second hour 1 : 1, third hour 1 : 3, fourth hour 1 : 7 and fifth hour 1 : 15 ratios of gastric to intestinal fluids. However, good in vitro release curves are not a guarantee of good in vivo performance. Fortunately, the in vitro release curve may give a good control procedure and may specify that 30–40 % is released in the first half hour, 60–70 % after 3 h and 90–100 % after 8 h.

The release pattern to be expected can be investigated by considering the stages involved in diffusion of the drug out of the pellet.

(i) A volume V of liquid diffuses into each pellet and (instantaneously) dissolves the drug in the seed.

(ii) Thereafter, the drug diffuses out following Fick's law of diffusion,

$$\frac{\mathrm{d}C}{\mathrm{d}t} = -ACD \tag{8.33}$$

where C is the drug concentration inside the pellet, A is the (inside) surface area (assumed to be the same for all fractions) and D is the diffusion coefficient (which is inversely proportional to the thickness).

Step (i) requires different times for different cuts and the lag time is proportional to the thickness (number of coats) in each fraction. This is illustrated in Tab. 8.1.

Tab. 8.1: Parameters for sustained release in four fractions.

Number of coats	Lag time	Diffusion parameter (DA)
1	τ	DA
2	2τ	$DA/2$
3	3τ	$DA/3$
4	4τ	$DA/4$

Integrating equation (8.33) gives,

$$\ln\left(\frac{C}{C_0}\right) = -AD(t-\tau), \tag{8.34}$$

where C_0 is the amount of drug in the pellet, or

$$\frac{C}{C_0} = \exp[-AD(t-\tau)] \tag{8.35}$$

for the first coat and,

$$\frac{C}{C_0} = \exp[-(AD/i)(t - \tau i)] \tag{8.36}$$

for the i-th coat, where nothing diffuses out at times less than τi.

At $t = \tau i$,

$$C = C_0 = \frac{Q}{Vn}, \tag{8.37}$$

where Q is the amount of drug on n originally coated non-pareil seeds.

The amount released for the first fraction is then,

$$\frac{1}{4}n(C_0 - CV) = \frac{1}{4Q}\left[1 - \left(\frac{C}{C_0}\right)\right] = \{1 - \exp[-AD(t - \tau)]\} \tag{8.38}$$

and for the i-th cut,

$$\frac{1}{4}\{1 - \exp[-(AD/i)(t - \tau i)]\}, \tag{8.39}$$

so that the total release is given by,

$$x = \frac{1}{4}Q\sum_{i=1}^{4}\{1 - \exp[-(AD/i)(t - \tau i)]\}, \tag{8.40}$$

or in general for n cuts 4 is replaced by n; τ gets smaller the larger the n.

The sustained-release pattern for pellets coated with four thicknesses of sustained-release is shown in Fig. 8.19 (lower curve). For comparison, the pattern for uncoated pellets (equivalent to an initial dose) is also shown in Fig. 8.19 (upper curve).

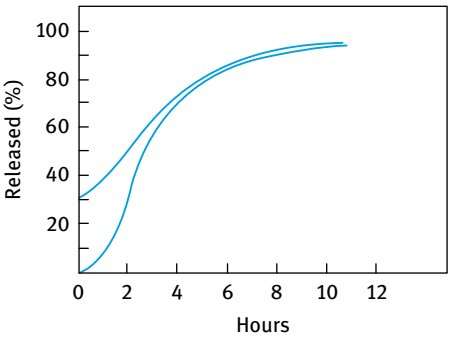

Fig. 8.19: Sustained-release pattern for pellets coated with four thicknesses of sustained-release coat.

References

[1] Seville JPK, Fryer PJ, Norton IT. In: Brockel U, Meier W, Wagner G, editors. Product design and engineering. Vol. 1. Weinheim: Wiley-VCH; 2007. Chapter 6.
[2] Hemati M, Benali M, Diguet S. In: Brockel U, Meier W, Wagner G, editors. Product design and engineering. Vol. 1. Weinheim: Wiley-VCH; 2007. Chapter 8.
[3] Sastry KVS, Fuerstenau DW. Powder Technology. 1973;7:97.
[4] Lister JD, Ennis BJ, Iveson SM, Hapgood K. Powder Technol. 2001;117:3.
[5] Newitt DM, Conway-Jones JM. Trans I Chem Eng. 1958;36:422.
[6] Ennis BJ, Tardos GI, Pfeffer R. Chem Eng Sci. 1990;45:3071.
[7] Willet CD, Adams MJ, Johnson SA, Seville JPK. Langmuir. 2001;16:9396.
[8] Adams MJ, Edmondson B. Force between particles in continuous and discrete liquid media. In: Briscoe BJ, Adams MJ, editors. Tribology in particulate techbology. 1987. p. 154–172.
[9] Ennis BJ, Tardos GI, Pfeffer R. Powder Technology. 1991;65:257.
[10] Nalimov SP. J Appl Chem USSR. 1977;50:1682.
[11] Hemati M, Cherif R, Saleh K, Pont V. Powder Technol. 2003;130:18.
[12] Maroglou A, Nienow AW. Powder Metall. 1986;29:291.
[13] Holm P. High shear mixer granulation. In: Parikh DM, editor. Handbook of pharmaceutical granulation technology. Vol. 81. New York: Marcel Dekker; 1997,. p. 151–204.
[14] Leunberger L, Luy B, Studer J. STP Pharm. 1990;6:303.
[15] Pietsch W. Agglomeration in industry. Weinheim: Wiley-VCH; 2005.
[16] Carstensen JT. Theory of pharmaceutical systems. Vol. II. New York: Academic Press; 1973.
[17] Leigh S, Carless JE, Burt B. J Pharm Sci. 1967;56:888.
[18] Long WM. Powder Met. 1960;6:173.
[19] Heckel RW. Trans Metallurgical Soc AIME. 1961;221:671.
[20] Roberts RJ, Rowe RC. Chem Eng Sci. 1987;42:903.
[21] Alderborn G, Nystrom C. Pharmaceutical powder compaction technology. New York: Marcel Dekker; 1975.
[22] Hanus EJ, King LD. J Pharm Sci. 1968;57:677.
[23] Goodhart FW, Mayorga G, Mills MN, Ninger F. J Pharm Sci. 1968;57:1770.
[24] Kennon L, Swintosky JV. J Amer Pharm Ass Soc. 1958;47:397.
[25] Commons KC, Bergen A, Walker GC. J Pharm Sci. 1968;57:1254.
[26] Marlowe E, Shangraw RF. J Pharm Sci. 1967;56:499.
[27] Desai SJ, Singh P, Simonelli AP, Higuchi WI. J Pharm Sci. 1966;55:1224,1230.
[28] Singh P, Desai SJ, Simonelli AP, Higuchi WI. J Pharm Sci. 1968;57:217.
[29] Washburn EW. Proc Nat Acad Sci USA. 1921;7:115.

9 Assessments of the stability of formulations

9.1 Introduction

For full characterization of the properties of formulations, three main types of investigations are needed:

(i) Fundamental investigations of the system at a molecular level. This requires investigating the structure of the solid/liquid interface [1], namely the structure of the electrical double layer (for charge stabilized suspensions), adsorption of surfactants [2], polymers and polyelectrolytes and conformation of the adsorbed layers (e.g. the adsorbed layer thickness) [3]. It is important to know how each of these parameters changes with the conditions, such as temperature, solvency of the medium for the adsorbed layers and effect of addition of electrolytes. These fundamental investigations have been discussed in detail in Chapters 4, 5, 6, 7, 8 and 9 of Vol. 1.

(ii) Investigations of the state of the suspension on standing, namely flocculation rates, flocculation points with sterically stabilized systems, spontaneity of dispersion on dilution and Ostwald ripening or crystal growth. The latter was disused in detail in Chapter 10 of Vol. 1.

(iii) Investigations of emulsion coalescence that were discussed in Chapter 11 of Vol. 1.

(iv) Investigations of phase inversion for emulsions, discussed in Chapter 12 of Vol. 1. All these phenomena require accurate determination of the particle size distribution as a function of storage time.

(v) Bulk properties of the suspension, which are particularly important for concentrated systems. This requires measuring the rate of sedimentation and equilibrium sediment height as discussed in Chapter 13 of Vol. 1. More quantitative techniques are based on assessments of the rheological properties of the suspension (without disturbing the system, i.e. without its dilution and measurement under conditions of low deformation) and how these are affected by long-term storage. This subject is discussed in detail in Chapter 14 of Vol. 1.

A useful parameter for describing the charge and potential distribution in charge stabilized systems is the electrokinetic or zeta potential [4] which will be described below.

Several techniques are available for obtaining information on particle and droplet size distribution in diluted systems [5].

9.2 Measuring particle and droplet size distributions

These measurements carried out as a function of time and temperature are essential for the assessment of flocculation, Ostwald ripening and coalescence (in case of emulsions) of the formulation. It is essential to dilute the concentrated formulation with its

https://doi.org/10.1515/9783110587968-010

own dispersion medium in order not to affect the state of the dispersion during examination. The dispersion medium can be obtained by centrifugation of the formulation whereby the supernatant liquid is produced at the top (with suspensions) or bottom (with most emulsions) of the centrifuge tube. Care should be taken when diluting the concentrated system with its supernatant liquid (i.e. with minimum shear). Several techniques may be applied for measuring particle and droplet size distributions and these are summarized below [6].

9.2.1 Optical microscopy

This is by far the most valuable tool for a qualitative or quantitative examination of the formulation. Information on the size, shape, morphology and aggregation of particles can be conveniently obtained with minimum time required for sample preparation. Since individual particles can be directly observed and their shape examined, optical microscopy is considered as the only absolute method for particle characterization. However, optical microscopy has some limitations: The minimum size that can be detected since the practical lower limit for accurate measurement of particle size is 1.0 μm, although some detection may be obtained down to 0.3 μm. Image contrast may not be good enough for an observation, particularly when using a video camera which is mostly used for convenience. The contrast can be improved by decreasing the aperture of the iris diaphragm but this reduces the resolution. The contrast of the image depends on the refractive index of the particles relative to that of the medium. Hence the contrast can be improved by increasing the difference between the refractive index of the particles and the immersion medium. Unfortunately, changing the medium for the suspension is not practical since this may affect the state of the dispersion. Fortunately, water with a refractive index of 1.33 is a suitable medium for most organic particles or droplets with a refractive index usually > 1.4.

The ultramicroscope, by virtue of dark field illumination, extends the useful range of optical microscopy to small particles not visible in a bright light illumination. Dark field illumination utilizes a hollow cone of light at a large angle of incidence. The image is formed by light scattered from the particles against a dark background. Particles about 10 times smaller than those visible by bright light illumination can be detected. However, the image obtained is abnormal and the particle size cannot be accurately measured. For that reason, the electron microscope (see below) has displaced the ultramicroscope, except for dynamic studies by flow ultramicroscopy.

Three main attachments to the optical microscope are possible.

9.2.1.1 Phase contrast

This utilizes the difference between the diffracted waves from the main image and the direct light from the light source. The specimen is illuminated with a light cone

and this illumination is within the objective aperture. The light illuminates the specimen and generates zero-order and higher orders of diffracted light. The zero-order light beam passes through the objective and a phase plate which is located at the objective back focal plane. The difference between the optical path of the direct light beam and that of the beam diffracted by a particle causes a phase difference. The constructive and destructive interferences result in brightness changes which enhance the contrast. This produces sharp images allowing one to obtain particle size measurements more accurately. The phase contrast microscope has a plate in the focal plane of the objective back focus. Instead of a conventional iris diaphragm, the condenser is equipped with a ring matched in its dimension to the phase plate.

9.2.1.2 Differential interference contrast (DIC)

This gives a better contrast than the phase contrast method. It utilizes a phase difference to improve contrast but the separation and recombination of a light beam into two beams is accomplished by prisms. DIC generates interference colours and the contrast effects indicate the refractive index difference between the particle and medium.

9.2.1.3 Polarized light microscopy

This illuminates the sample with linearly or circularly polarized light, either in a reflection or transmission mode. One polarizing element, located below the stage of the microscope, converts the illumination to polarized light. The second polarizer is located between the objective and the ocular and is used to detect polarized light. Linearly polarized light cannot pass the second polarizer in a crossed position, unless the plane of polarization has been rotated by the specimen. Various characteristics of the specimen can be determined, including anisotropy, polarization colours, birefringence, polymorphism, etc.

9.2.1.4 Sample preparation for optical microscopy

A drop of the formulation is placed on a glass slide and covered with a cover glass. As mentioned above, the dispersion medium (that can be obtained by centrifugation and/or filtration of the suspension) should be used as the diluent in order to avoid aggregation. At low magnifications the distance between the objective and the sample is usually adequate for manipulating the sample, but at high magnification the objective may be too close to the sample. An adequate working distance can be obtained, while maintaining high magnification, by using a more powerful eyepiece with a low power objective. For formulations encountering Brownian motion (when the particle or droplet size is relatively small), microscopic examination of moving particles can become difficult. In this case one can record the image on a photographic film or video tape or disc (using computer software).

9.2.1.5 Particle size measurements using optical microscopy

The optical microscope can be used to observe dispersed particles or droplets and flocs. Particle or droplet sizing can be carried out using manual, semiautomatic or automatic image analysis techniques. In the manual method (which is tedious) the microscope is fitted with a minimum of 10× and 43× achromatic or apochromatic objectives equipped with a high numerical apertures (10×, 15× and 20×), a mechanical XY stage, a stage micrometre and a light source. The direct measurement of particle or droplet size is aided by a linear scale or globe-and-circle graticule in the ocular. The linear scale is useful mainly for spherical particles, with a relatively narrow particle size distribution. Globe-and-circle graticules are used to compare the projected particle area with a series of circles in the ocular graticule. The size of spherical particles or droplets can be expressed by the diameter, but for irregularly shaped particles various statistical diameters are used. One of the difficulties with the evaluation of dispersions by optical microscopy is the quantification of data. The number of particles or droplets in at least six different size ranges must be counted to obtain a distribution. This problem can be alleviated by the use of automatic image analysis which can also give an indication on the floc size and its morphology.

9.2.2 Electron microscopy

Electron microscopy utilizes an electron beam to illuminate the sample. The electrons behave as charged particles which can be focused by annular electrostatic or electromagnetic fields surrounding the electron beam. Due to the very short wavelength of electrons, the resolving power of an electron microscope exceeds that of an optical microscope by ≈ 200 times. The resolution depends on the accelerating voltage which determines the wavelength of the electron beam and magnifications as high as 200,000 can be reached with intense beams, but this could damage the sample. Mostly the accelerating voltage is kept below 100–200 kV and the maximum magnification obtained is below 100,000. The main advantage of electron microscopy is the high resolution, sufficient for resolving details separated by only a fraction of a nanometre. The increased depth of field, usually by about 10 μm or about 10 times that of an optical microscope, is another important advantage of electron microscopy. Nevertheless, electron microscopy also has some disadvantages such as sample preparation, selection of the area viewed and interpretation of the data. The main drawback of electron microscopy is the potential risk of altering or damaging the sample that may introduce artefacts and possible aggregation of the particles during sample preparation. The suspension has to be dried or frozen and the removal of the dispersion medium may alter the distribution of the particles. If the particles do not conduct electricity, the sample has to be coated with a conducting layer, such as gold, carbon or platinum to avoid negative charging by the electron beam. Two main types of electron microscopes are used: transmission and scanning.

9.2.2.1 Transmission Electron Microscopy (TEM)

TEM displays an image of the specimen on a fluorescent screen and the image can be recorded on a photographic plate or film. TEM can be used to examine particles in the range 0.001–5 µm. The sample is deposited on a Formvar (polyvinyl formal) film resting on a grid to prevent charging of the simple. The sample is usually observed as a replica by coating with an electron transparent material (such as gold or graphite). The preparation of the sample for TEM may alter the state of dispersion and cause aggregation. Freeze fracturing techniques have been developed to avoid some of the alterations of the sample during sample preparation. Freeze fracturing allows the dispersions to be examined without dilution and replicas can be made of dispersions containing water. It is necessary to have a high cooling rate to avoid the formation of ice crystals.

9.2.2.2 Scanning Electron Microscopy (SEM)

SEM can show particle topography by scanning a very narrowly focused beam across the particle surface. The electron beam is directed normally or obliquely at the surface. The backscattered or secondary electrons are detected in a raster pattern and displayed on a monitor screen. The image provided by secondary electrons exhibits good three-dimensional detail. The backscattered electrons, reflected from the incoming electron beam, indicate regions of high electron density. Most SEMs are equipped with both types of detectors. The resolution of the SEM depends on the energy of the electron beam which does not exceed 30 kV and hence the resolution is lower than that obtained by TEM. A very important advantage of SEM is elemental analysis by energy dispersive X-ray analysis (EDX). If the electron beam impinging on the specimen has sufficient energy to excite atoms on the surface, the sample will emit X-rays. The energy required for X-ray emission is characteristic of a given element and since the emission is related to the number of atoms present, quantitative determination is possible.

Scanning transmission electron microscopy (STEM) coupled with EDX has been used for the determination of metal particle sizes. Specimens for STEM were prepared by ultrasonically dispersing the sample in methanol and one drop of the suspension was placed onto a Formvar film supported on a copper grid.

9.2.3 Confocal laser scanning microscopy (CLSM)

CLSM is a very useful technique for the identification of formulations. It uses a variable pinhole aperture or variable width slit to illuminate only the focal plane by the apex of a cone of laser light. Out-of-focus items are dark and do not distract from the contrast of the image. As a result of extreme depth discrimination (optical sectioning) the resolution is considerably improved (up to 40 % when compared with optical microscopy).

The CLSM technique acquires images by laser scanning or uses computer software to subtract out-of-focus details from the in-focus image. Images are stored as the sample is advanced through the focal plane in elements as small as 50 nm. Three-dimensional images can be constructed to show the shape of the particles.

9.2.4 Scanning probe microscopy (SPM)

SPM can measure physical, chemical and electrical properties of the sample by scanning the particle surface with a tiny sensor of high resolution. Scanning probe microscopes do not measure a force directly; they measure the deflection of a cantilever which is equipped with a tiny stylus (the tip) functioning as the probe. The deflection of the cantilever is monitored by

(i) a tunnelling current,
(ii) laser deflection beam from the back side of the cantilever,
(iii) optical interferometry,
(iv) laser output controlled by the cantilever used as a mirror in the laser cavity,
(v) change in capacitance.

SPM generates a three-dimensional image and allows calibrated measurements in three (x, y, z) coordinates. SPM not only produces a highly magnified image, but provides valuable information on sample characteristics. Unlike EM which requires vacuum for its operation, SPM can be operated under ambient conditions and, with some limitation, in liquid media.

9.2.5 Scanning tunnelling microscopy (STM)

STM measures an electric current that flows through a thin insulating layer (vacuum or air) separating two conductive surfaces. The electrons are visualized to "tunnel" through the dielectric and generate a current, I, that depends exponentially on the distance, s, between the tiny tip of the sensor and the electrically conductive surface of the sample. The STM tips are usually prepared by etching a tungsten wire in an NaOH solution until the wire forms a conical tip. Pt/Ir wire has also been used. In the contrast current imaging mode, the probe tip is raster-scanned across the surface and a feedback loop adjusts the height of the tip in order to maintain a constant tunnel current. When the energy of the tunnelling current is sufficient to excite luminescence, the tip-surface region emits light and functions as an excitation source of subnanometre dimensions. In situ STM has revealed a two-dimensional molecular lamellar arrangement of long chain alkanes adsorbed on the basal plane of graphite. Thermally induced disordering of adsorbed alkanes was studied by variable temperature STM and atomic scale resolution of the disordered phase was claimed by studying the quenched high-temperature phase.

9.2.6 Atomic force microscopy (AFM)

AFM allows one to scan the topography of a sample using a very small tip made of silicon nitride. The tip is attached to a cantilever that is characterized by its spring constant, resonance frequency and a quality factor. The sample rests on a piezoceramic tube which can move the sample horizontally (x, y motion) and vertically (z motion). The displacement of the cantilever is measured by the position of a laser beam reflected from the mirrored surface on the top side of the cantilever. The reflected laser beam is detected by a photodetector. AFM can be operated in either a contact or a non-contact mode. In the contact mode the tip travels in close contact with the surface, whereas in the non-contact mode the tip hovers 5–10 nm above the surface.

9.3 Scattering techniques

These are by far the most useful methods for characterizing formulations and in principle they can give quantitative information on the particle size distribution, floc size and shape. The only limitation of the methods is the need to use sufficiently dilute samples to avoid interference such as multiple scattering which makes interpretation of the results difficult. However, recently backscattering methods have been designed to allow one to measure the sample without dilution. In principle one can use any electromagnetic radiation such as light, X-ray or neutrons but in most industrial labs only light scattering is applied (using lasers).

9.3.1 Light scattering techniques

These can be conveniently divided into the following classes:

(i) Time-average light scattering; static or elastic scattering.
(ii) Turbidity measurements which can be carried out using a simple spectrophotometer.
(iii) Light diffraction technique.
(iv) Dynamic (quasi-elastic) light scattering that is usually referred as photon correlation spectroscopy. This is a rapid technique that is very suitable for measuring submicron particles or droplets (nanosize range).
(v) Backscattering techniques that are suitable for measuring concentrated samples.

Application of any of these methods depends on the information required and availability of the instrument.

9.3.1.1 Time-average light scattering

In this method a dispersion that is sufficiently diluted to avoid multiple scattering is illuminated by a collimated light (usually laser) beam and the time-average intensity of scattered light is measured as a function of scattering angle θ. Static light scattering is termed elastic scattering. Three regimes can be identified.

Rayleigh regime

In the Rayleigh regime the particle radius R is smaller than $\lambda/20$ (where λ is the wavelength of incident light). The scattering intensity is given by the equation,

$$I(Q) = [\text{instrument constant}][\text{material constant}]NV_p^2. \tag{9.1}$$

Q is the scattering vector that depends on the wavelength of light λ used and is given by,

$$Q = \left(\frac{4\pi n}{\lambda}\right)\sin\left(\frac{\theta}{2}\right), \tag{9.2}$$

where n is the refractive index of the medium.

The material constant depends on the difference between the refractive index of the particle or droplet and that of the medium. N is the number of particles and V_p is the volume of each particle. Assuming that the particles are spherical one can obtain the average size using equation (9.1).

The Rayleigh equation reveals two important relationships:

(i) The intensity of scattered light increases with the square of the particle volume and consequently with the sixth power of the radius R. Hence the scattering from larger particles may dominate the scattering from smaller particles.

(ii) The intensity of scattering is inversely proportional to λ^4. Hence a decrease in the wavelength will substantially increase the scattering intensity.

Rayleigh–Gans–Debye regime (RGD) $\lambda/20 < R < \lambda$

The RGD regime is more complicated than the Rayleigh regime and the scattering pattern is no longer symmetrical about the line corresponding to the 90° angle but favours forward scattering ($\theta < 90°$) or backscattering ($180° > \theta > 90°$). Since the preference for forward scattering increases with increasing particle size, the ratio $I_{45°}/I_{135°}$ can indicate the particle size.

Mie regime $R > \lambda$

The scattering behaviour is more complex than the RGD regime and the intensity exhibits maxima and minima at various scattering angles depending on particle size and refractive index. The Mie theory for light scattering can be used to obtain the particle size distribution using numerical solutions. One can also obtain information on particle shape.

9.3.2 Turbidity measurements

Turbidity (total light scattering technique) can be used to measure particle size, flocculation and particle sedimentation. This technique is simple and easy to use; a single or double beam spectrophotometer or a nephelometer can be used.

For nonabsorbing particles the turbidity τ is given by,

$$\tau = (1/L)\ln(I_0/I), \tag{9.3}$$

where L is the path length, I_0 is the intensity of incident beam and I is the intensity of transmitted beam.

The particle size measurement assumes that the light scattered by a particle is singular and independent of other particles. Any multiple scattering complicates the analysis. According to the Mie theory the turbidity is related to the particle number N and their cross section πr^2 (where r is the particle radius) by

$$\tau = Q\pi r^2 N, \tag{9.4}$$

where Q is the total Mie scattering coefficient. Q depends on the particle size parameter α (which depends on particle diameter and wavelength of incident light λ) and the ratio of refractive index of the particles and medium m.

Q depends on the particle size parameter α (which depends on particle diameter and wavelength of incident light) and the ratio of refractive index of the particles and medium. Q depends on α in an oscillatory mode and exhibits a series of maxima and minima whose position depends on m. For particles with $R < (1/20)\lambda$, $\alpha < 1$ and it can be calculated using the Rayleigh theory. For $R > \lambda$, Q approaches 2 and between these two extremes, the Mie theory is used. If the particles are not monodisperse (as is the case with most practical systems), the particle size distribution must be taken into account. Using this analysis one can establish the particle size distribution using numerical solutions.

9.3.3 Light diffraction techniques

This is a rapid and nonintrusive technique for determining a particle or droplet size distribution in the range 2–300 μm with good accuracy for most practical purposes. Light diffraction gives an average diameter over all particle orientations as randomly oriented particles pass the light beam. A collimated and vertically polarized laser beam illuminates a particle dispersion and generates a diffraction pattern with the undiffracted beam in the centre. The energy distribution of diffracted light is measured by a detector consisting of light sensitive circles separated by isolating circles of equal width. The angle formed by the diffracted light increases with decreasing particle size. The angle-dependent intensity distribution is converted by Fourier optics into a

spatial intensity distribution $I(r)$.The spatial intensity distribution is converted into a set of photocurrents and the particle size distribution is calculated using a computer. Several commercial instruments are available, e.g. Malvern Mastersizer (Malvern, UK), Horriba (Japan) and Coulter LS Sizer (USA). A schematic illustration of the set-up is shown in Fig. 9.1.

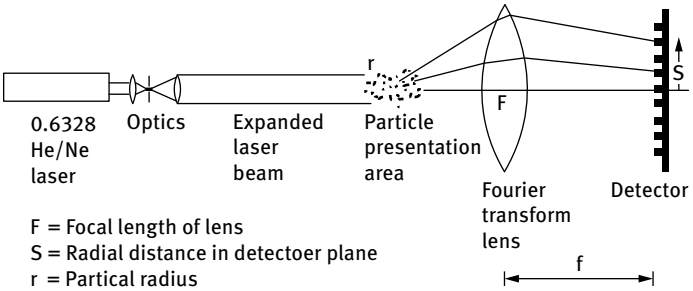

Fig. 9.1: Schematic illustration of light diffraction particle sizing system.

In accordance with the Fraunhofer theory (which was introduced by Fraunhofer over 100 years ago), the special intensity distribution is given by,

$$I(r) = \int_{X_{\min}}^{X_{\max}} N_{\text{tot}} q_0(x) I(r, x)\, \mathrm{d}x, \tag{9.5}$$

where $I(r, x)$ is the radial intensity distribution at radius r for particles of size x, N_{tot} is the total number of particles and $q_0(x)$ describes the particle size distribution.

The radial intensity distribution $I(r, x)$ is given by,

$$I(r, x) = I_0 \left(\frac{\pi x^2}{2f} \right)^2 \left(\frac{J_i(k)}{k} \right)^2. \tag{9.6}$$

With $k = (\pi x r)/(\lambda f)$, r is the distance to the centre of the disc, λ is the wavelength, f is the focal length, and J_i is the first-order Bessel function.

The Fraunhofer diffraction theory applies to particles or droplets whose diameter is considerably larger than the wavelength of illumination. As shown in Fig. 9.1, an HeNe laser is used with $\lambda = 632.8$ nm for particle or droplet sizes mainly in the 2–120 µm range. In general, the diameter of the sphere-shaped particle should be at least four times the wavelength of the illumination light. The accuracy of a particle or droplet size distribution determined by light diffraction is not very good if a large fraction of particles with diameter < 10 µm is present in the formulation. For small particles or droplets (diameter < 10 µm) the Mie theory is more accurate if the necessary optical parameters such as refractive index of particles and medium, and the light absorptivity of the dispersed particles are known. Most commercial instruments combine

light diffraction with forward light scattering to obtain a full particle size distribution covering a wide range of sizes.

As an illustration Fig. 9.2 shows the result of particle sizing using a six component mixture of standard polystyrene lattices (using a Mastersizer).

Most practical dispersions are polydisperse and generate a very complex diffraction pattern. The diffraction pattern of each particle or droplet size overlaps with diffraction patterns of other sizes. The particles or droplets of different sizes diffract light at different angles and the energy distribution becomes a very complex pattern. However, manufacturers of light diffraction instruments (such as Malvern, Coulters and Horriba) have developed numerical algorithms relating diffraction patterns to particle or droplet size distributions.

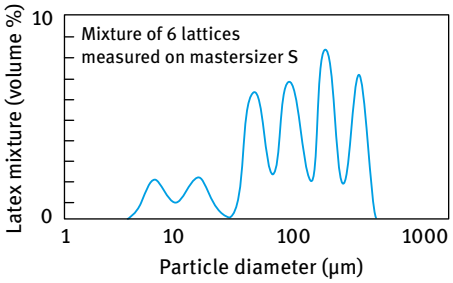

Fig. 9.2: Single measurement of a mixture of six standard lattices using the Mastersizer.

Several factors can affect the accuracy of Fraunhofer diffraction:

(i) Particles or droplets smaller than the lower limit of Fraunhofer theory.
(ii) Non-existent "ghost" particles in a particle or droplet size distribution obtained by Fraunhofer diffraction applied to systems containing particles with edges, or a large fraction of small particles or droplets (below 10 μm).
(iii) Computer algorithms that are unknown to the user and vary with the manufacturer software version.
(iv) The composition-dependent optical properties of the particles and dispersion medium.
(v) If the density of all particles is not the same, the result may be inaccurate.

9.3.4 Dynamic light scattering – photon correlation spectroscopy (PCS)

Dynamic light scattering (DLS) is a method that measures the time-dependent fluctuation of scattered intensity. It is also referred to as quasi-elastic light scattering (QELS) or photon correlation spectroscopy (PCS). The latter is the most commonly used term for describing the process since most dynamic scattering techniques employ autocorrelation.

PCS is a technique that utilizes Brownian motion to measure the particle or droplet size. As a result of Brownian motion of dispersed particles or droplets the intensity of scattered light undergoes fluctuations that are related to the velocity of the particles. Since larger particles move less rapidly than smaller ones, the intensity fluctuation (intensity versus time) pattern depends on particle size as is illustrated in Fig. 9.3. The velocity of the scatterer is measured in order to obtain the diffusion coefficient.

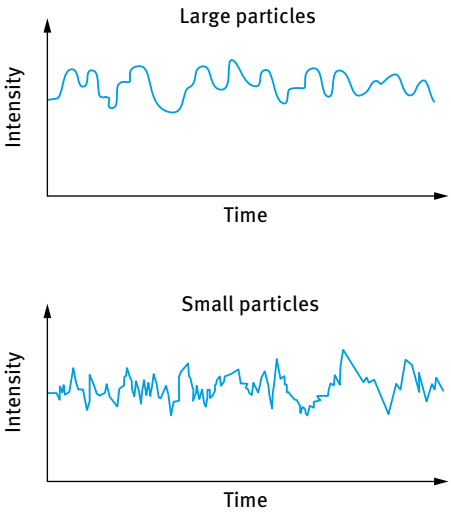

Fig. 9.3: Schematic representation of the intensity fluctuation for large and small particles.

In a system where Brownian motion is not interrupted by sedimentation or creaming or particle–particle or droplet–droplet interaction, the movement of particles or droplets is random. Hence, the intensity fluctuations observed after a large time interval do not resemble those fluctuations observed initially, but represent a random distribution of particles. Consequently, the fluctuations observed at large time delay are not correlated with the initial fluctuation pattern. However, when the time differential between the observations is very small (a nanosecond or a microsecond) both positions of particles are similar and the scattered intensities are correlated. When the time interval is increased, the correlation decreases. The decay of correlation is dependent on particle size. The smaller the particles are, the faster is the decay.

The fluctuations in scattered light are detected by a photomultiplier and are recorded. The data containing information on particle motion are processed by a digital correlator. The latter compares the intensity of scattered light at time t, $I(t)$, to the intensity at a very small time interval τ later, $I(t + \tau)$, and it constructs the second-order autocorrelation function $G_2(\tau)$ of the scattered intensity,

$$G_2(\tau) = \langle I(t)I(t + \tau)\rangle. \tag{9.7}$$

The experimentally measured intensity autocorrelation function $G_2(\tau)$ depends only on the time interval τ, and is independent of t, the time when the measurement started.

PCS can be measured in a homodyne where only scattered light is directed to the detector. It can also be measured in heterodyne mode where a reference beam split from the incident beam is superimposed on scattered light. The diverted light beam functions as a reference for the scattered light from each particle.

In homodyne mode, $G_2(\tau)$ can be related to the normalized field autocorrelation function $g_1(\tau)$ by,

$$G_2(\tau) = A + Bg_1^2(\tau), \tag{9.8}$$

where A is the background term designated as the baseline value and B is an instrument-dependent factor. The ratio B/A is regarded as a quality factor of the measurement or the signal-to-noise ratio and expressed sometimes as the % merit.

The field autocorrelation function $g_1(\tau)$ for a monodisperse suspension decays exponentially with τ,

$$g_1(\tau) = \exp(-\Gamma\tau), \tag{9.9}$$

where Γ is the decay constant (s^{-1}).

Substituting equation (9.9) into equation (9.8) yields the measured autocorrelation function,

$$G_2(\tau) = A + B\exp(-2\Gamma\tau). \tag{9.10}$$

The decay constant Γ is linearly related to the translational diffusion coefficient D_T of the particle,

$$\Gamma = D_T q^2. \tag{9.11}$$

The modulus q of the scattering vector is given by,

$$q = \frac{4\pi n}{\lambda_0}\sin\left(\frac{\theta}{2}\right), \tag{9.12}$$

where n is the refractive index of the dispersion medium, θ is the scattering angle and λ_0 is the wavelength of the incident light in vacuum.

PCS determines the diffusion coefficient and the particle or droplet radius R is obtained using the Stokes–Einstein equation,

$$D = \frac{kT}{6\pi\eta R}, \tag{9.13}$$

where k is the Boltzmann constant, T is the absolute temperature and η is the viscosity of the medium.

The Stokes–Einstein equation is limited to non-interacting, spherical and rigid spheres. The effect of particle or droplet interaction at relatively low particle concentration c can be taken into account by expanding the diffusion coefficient into a power series of concentration,

$$D = D_0(1 + k_D c), \tag{9.14}$$

where D_0 is the diffusion coefficient at infinite dilution and k_D is the virial coefficient that is related to particle interaction. D_0 can be obtained by measuring D at several particle number concentrations and extrapolating to zero concentration.

For polydisperse dispersions, the first-order autocorrelation function is an intensity-weighted sum of autocorrelation function of particles contributing to the scattering,

$$g_1(\tau) = \int_0^\infty C(\Gamma) \exp(-\Gamma\tau)\, d\Gamma. \tag{9.15}$$

$C(\Gamma)$ represents the distribution of decay rates.

For narrow particle or droplet size distributions, cumulant analysis is usually satisfactory. The cumulant method is based on the assumption that for monodisperse suspensions $g_1(\tau)$ is monoexponential. Hence the log of $g_1(\tau)$ versus τ yields a straight line with a slope equal to Γ,

$$\ln g_1(\tau) = 0.5 \ln(B) - \Gamma\tau, \tag{9.16}$$

where B is the signal-to-noise ratio.

The cumulant method expands the Laplace transform about an average decay rate,

$$\langle\Gamma\rangle = \int_0^\infty \Gamma C(\Gamma)\, d\Gamma. \tag{9.17}$$

The exponential in equation (9.16) is expanded about an average and integrated term,

$$\ln g_1(\tau) = \langle\Gamma\rangle\tau + (\mu_2\tau^2)/2! - (\mu_3\tau^3)/3! + \cdots. \tag{9.18}$$

An average diffusion coefficient is calculated from $\langle\Gamma\rangle$ and the polydispersity (termed the polydispersity index) is indicated by the relative second moment, $\mu_2/\langle\Gamma\rangle^2$. A constrained regulation method (CONTIN) yields several numerical solutions to the particle size distribution and this is normally included in the software of the PCS machine.

PCS is a rapid, absolute and non-destructive method for particle size measurements. It has some limitations. The main disadvantage is the poor resolution of particle size distribution. Also it suffers from the limited size range (absence of any creaming or sedimentation) that can be accurately measured. Several instruments are commercially available, e.g. by Malvern, Brookhaven, Coulters, etc.

9.3.5 Backscattering techniques

This method is based on the use of fibre optics, sometimes referred to as fibre optic dynamic light scattering (FODLS) and it allows one to measure at high particle or droplet number concentrations. FODLS employs either one or two optical fibres. Alternatively, fibre bundles may be used. The exit port of the optical fibre (optode) is immersed in

the sample and the scattered light in the same fibre is detected at a scattering angle of 180° (i.e. backscattering).

The above technique is suitable for on-line measurements during manufacture of a suspension or emulsion. Several commercial instruments are available, e.g. Lesentech (USA).

9.4 Electrokinetic and zeta potential measurements

There are essentially two techniques for measuring the electrophoretic mobility and zeta potential, namely laser velocimetry and electroacoustic technique. The laser velocimetry method is suitable for particles that undergo Brownian motion. As discussed above the light scattered by particles will show intensity fluctuations as a result of Brownian diffusion (Doppler shift). If an electric field is placed at right angles to the incident light and in the plane defined by the incident and observation beam, the line broadening is unaffected but the centre frequency of the scattered light is shifted to an extent determined by the electrophoretic mobility. The shift is very small compared to the incident frequency (≈ 100 Hz for and incident frequency of $\approx 6 \times 10^{14}$ Hz) but with a laser source it can be detected by heterodyning (i.e. mixing) the scattered light with the incident beam and detecting the output of the difference frequency. A homodyne method may be applied in which case a modulator to generate an apparent Doppler shift at the modulated frequency is used. To increase the sensitivity of the laser Doppler method, the electric fields are much higher than those used in conventional electrophoresis. The Joule heating is minimized by pulsing the electric field in opposite directions. The Brownian motion of the particles also contributes to the Doppler shift and an approximate correction can be made by subtracting the peak width obtained in the absence of an electric field from the electrophoretic spectrum. An HeNe laser is used as the light source and the output of the laser is split into two coherent beams which are cross-focused in the cell to illuminate the sample. The light scattered by the particle, together with the reference beam is detected by a photomultiplier. The output is amplified and analysed to transform the signals to a frequency distribution spectrum. At the intersection of the beams, interferences of known spacing are formed.

The magnitude of the Doppler shift $\Delta\nu$ is used to calculate the electrophoretic mobility u using the following expression,

$$\Delta\nu = \left(\frac{2n}{\lambda_0}\right)\sin\left(\frac{\theta}{2}\right)uE, \tag{9.19}$$

where n is the refractive index of the medium, λ_0 is the incident wavelength in vacuum, θ is the scattering angle and E is the field strength.

The zeta potential ζ is calculated from the mobility u using the Smoluchowski equation [6] that is applicable when the particle radius R is much higher than the

double layer thickness ($1/\kappa$, where κ is the Debye–Hückel parameter, Chapter 7) that is the case with most suspensions with $R > 0.5\,\mu m$ and ($1/\kappa < 10\,nm$, i.e. with 1 : 1 electrolyte concentration $> 10^{-3}\,mol\,dm^{-3}$),

$$u = \frac{2}{3}\frac{\varepsilon_r \varepsilon_0 \zeta}{\eta}. \tag{9.20}$$

Several commercial instruments are available for measuring electrophoretic light scattering:

(i) The Coulter DELSA 440SX (Coulter Corporation, USA) is a multi-angle laser Doppler system employing heterodyning and autocorrelation signal processing. Measurements are made at four scattering angle (8, 17, 25 and 34°) and the temperature of the cell is controlled by a Peltier device. The instrument reports the electrophoretic mobility, zeta potential, conductivity and particle size distribution.

(ii) Malvern (Malvern Instruments, UK) has two instruments: The ZetaSizer 3000 and ZetaSizer 5000: The ZetaSizer 3000 is a laser Doppler system using crossed beam optical configuration and homodyne detection with photon correlation signal processing. The zeta potential is measured using laser Doppler velocimetry and the particle size is measured using photon correlation spectroscopy (PCS). The ZetaSizer 5000 uses PCS to measure both
   (a) movement of the particles in an electric field for zeta potential determination,
   (b) random diffusion of particles at different measuring angles for size measurement on the same sample.

   In both instruments, a Peltier device is used for temperature control.

An alternative method that can be applied on more concentrated dispersions is the electroacoustic technique. The mobility of a particle in an alternating field is termed dynamic mobility, to distinguish it from the electrophoretic mobility in a static electric field. The principle of the technique is based on the creation of an electric potential by a sound wave transmitted through an electrolyte solution, as described by Debye [7]. The potential, termed the ionic vibration potential (IVP), arises from the difference in the frictional forces and the inertia of hydrated ions subjected to ultrasound waves. The effect of the ultrasonic compression is different for ions of different masses and the displacement amplitudes are different for anions and cations. Hence the sound waves create periodically changing electric charge densities. Debye's original theory was extended to include electrophoretic, relaxation and pressure gradient forces [8, 9].

A much stronger effect can be observed in colloidal dispersions. The sound waves transmitted by the suspension of charged particles generate an electric field because the relative motion of the two phases is different. The displacement of a charged particle from its environment by ultrasound waves generates an alternating potential, termed colloidal vibration potential (CVP). The IVP and CVP are both called ultrasound vibration potential (UVP).

The converse effect, namely the generation of sound waves by an alternating electric field [10] in a colloidal dispersion, can be measured and is termed the electrokinetic sonic amplitude (ESA). The theory for the ESA effect has been developed by O'Brian and co-workers [11–15]. Dynamic mobility can be determined by measuring either UVP or ESA, although in general ESA is the preferred method. Several commercial instruments are available for measuring dynamic mobility:

(i) the ESA-8000 system from Matec Applied Sciences that can measure both CVP and ESA signals;
(ii) the Pen Kem System 7000 Acoustophoretic titrator that measures the CVP, conductivity, pH, temperature, pressure amplitude and sound velocity.

In the ESA system (from Matec) and the AcoustoSizer (from Colloidal Dynamics) the dispersion is subjected to a high frequency alternating field and the ESA signal is measured. The ESA-8000 operates at constant frequency of ≈ 1 MHz and the dynamic mobility and zeta potential (but not particle size) are measured. The AcoustoSizer operates at various frequencies of the applied electric field and can measure particle mobility, zeta potential and particle size.

The frequency synthesizer feeds a continuous sinusoidal voltage into a grated amplifier that creates a pulse of sinusoidal voltage across the electrodes in the dispersion. The pulse generates sound waves which appear to emanate from the electrodes. The oscillation, the back-and-forth movement of the particle caused by an electric field is the product of the particle charge times the applied field strength. When the direction of the field is alternating, particles in the dispersion between the electrodes are driven away towards the electrodes. The magnitude and phase angle of the ESA signal created is measured with a piezoelectric transducer mounted on a solid nonconductive (glass) rod attached to the electrode as illustrated in Fig. 9.4. The purpose of this nonconductive acoustic delay line is to separate the transducer from the high-frequency electric field in the cell. Three pulses of the voltage signal are recorded as schematically shown in Fig. 9.5.

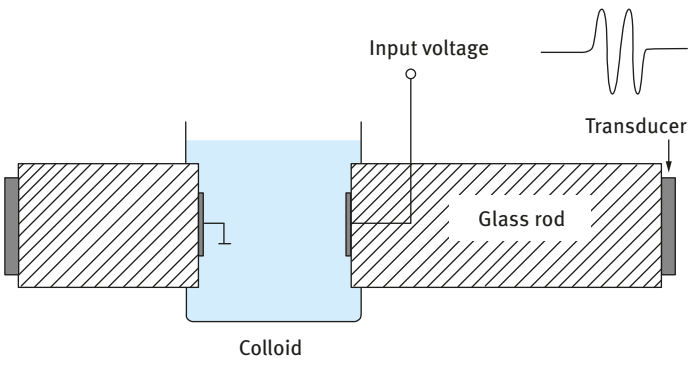

Fig. 9.4: Schematic representation of the AcoustoSizer cell.

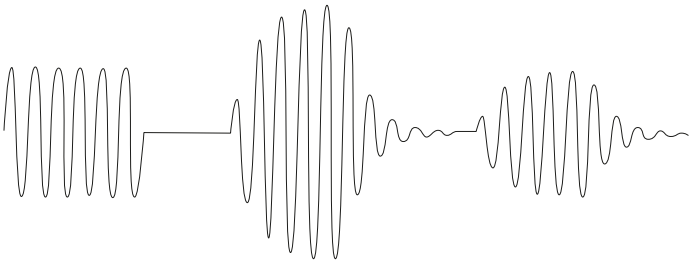

Fig. 9.5: Signals from the right-hand transducer.

The first pulse of the signal, shown on the left, is generated when the voltage pulse is applied to the sample and is unrelated to the ESA effect. This first pulse of the signal is received before the sound has sufficient time to pass down the glass rod and is an electronic crosstalk deleted from data processing. The second and third pulses are ESA signals. The second pulse is detected by the nearest electrode. This pulse is used for data processing to determine the particle size and zeta potential. The third pulse originates from the other electrode and is deleted.

In addition to the electrodes, the sample cell of the ESA instruments also houses sensors for pH, conductivity and temperature measurements. It is also equipped with a stirrer and the system is linked to a digital titrator for dynamic mobility and zeta potential measurements as a function of pH.

To convert the ESA signal to dynamic mobility one needs to know the density of the disperse phase and dispersion medium, the volume fraction of the particles and the velocity of sound in the solvent. As shown before, to convert mobility to zeta potential one needs to know the viscosity of the dispersion medium and its relative permittivity. Because of the inertia effects in dynamic mobility measurements, the weight average particle size has to be known.

For dilute suspensions with a volume fraction $\phi = 0.02$, the dynamic mobility, u_d, can be calculated from the electrokinetic sonic amplitude $A_{ESA}(\omega)$ using the following expression [9, 10],

$$A_{ESA}(\omega) = Q(\omega)\phi(\Delta\rho/\rho)(u_d), \tag{9.21}$$

where ω is the angular frequency of the applied field, $\Delta\rho$ is the density difference between the particle (with density ρ) and the medium. $Q(\omega)$ is an instrument-related coefficient independent of the system being measured.

For a dilute dispersion of spherical particles with $\phi < 0.1$, a thin double layer ($\kappa R > 50$) and narrow particle size distribution (with standard deviation < 20 % of the mean size), u_d can be related to the zeta potential ζ by the equation [8],

$$u_d = \frac{2\varepsilon\zeta}{3\eta} G\left(\frac{\omega R^2}{\nu}\right)[1 + f(\lambda, \omega)], \tag{9.22}$$

where ε is the permittivity of the liquid (that is equal to $\varepsilon_r\varepsilon_0$, defined before), R is the particle radius, η is the viscosity of the medium, λ is the double layer conductance and ν is the kinematic viscosity ($= \eta/\rho$). G is a factor that represents particle inertia, which reduces the magnitude of u_d and increases the phase lag in a monotonic fashion as the frequency increases. This inertia factor can be used to calculate the particle size from electroacoustic data. The factor $[1 + f(\lambda, \omega)]$ is proportional to the tangential component of the electric field and dependent on the particle permittivity and a surface conductance parameter λ. For most suspensions with large κR, the effect of surface conductance is insignificant and the particle permittivity/liquid permittivity $\varepsilon p/\varepsilon$ is small. In most cases where the ionic strength is at least 10^{-3} mol dm^{-3} and a zeta potential < 75 mV, the factor $[1 + f(\lambda, \omega)]$ assumes the value 0.5. In this case the dynamic mobility is given by the simple expression,

$$u_d = \frac{\varepsilon\zeta}{\eta} G(\alpha). \tag{9.23}$$

Equation (9.23) is identical to the Smoluchowski equation, except for the inertia factor $G(\alpha)$.

The equation for converting the ESA amplitude, A_{ESA}, to dynamic mobility is given by,

$$u_d = \frac{A_{ESA}}{\phi v_s \Delta\rho} G(\alpha)^{-1}. \tag{9.24}$$

The zeta potential ζ is given by,

$$\zeta = \frac{u_d \eta}{\varepsilon} G(\alpha)^{-1} = \frac{A_{ESA}}{\phi v_s \Delta\rho} G(\alpha)^{-1}. \tag{9.25}$$

For a polydisperse system $\langle u_d \rangle$ is given by,

$$\langle u_d(\omega) \rangle = \int_0^\infty u(\omega, R) p(R)\, dR, \tag{9.26}$$

where $u(\omega, R)$ is the average dynamic mobility of particles with radius R at a frequency ω, and $pR\,dR$ is the mass fraction of particles with radii in the range $R \pm dR/2$.

The ESA measurements can also be applied for determining particle size from particle mobilities in a dispersion. The electric force acting upon a particle is opposed by the hydrodynamic friction and inertia of the particles. At low frequencies of alternating electric field, the inertial force is insignificant and the particle moves in the alternating electric field with the same velocity as it would have moved in a constant field. The particle mobility at low frequencies can be measured to calculate the zeta potential. At high frequencies the inertia of the particle increases causing the velocity of the particle to decrease and the movement of the particle to lag behind the field. This is illustrated in Fig. 9.6 which shows the variation of applied field and particle velocity with time. Since inertia depends on particle mass, both of these effects depend on the particle

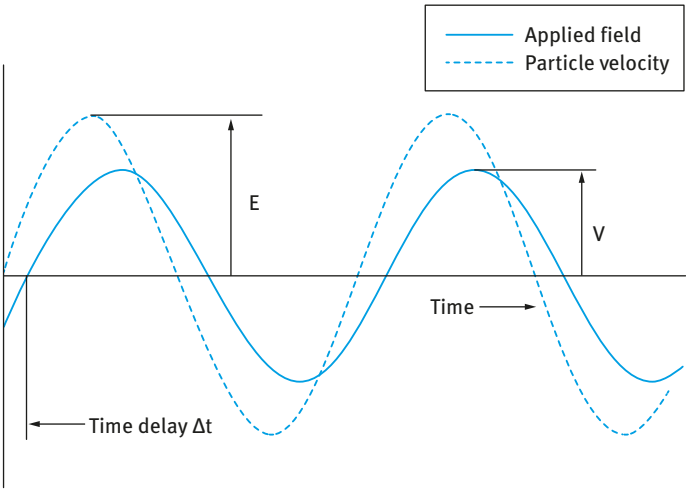

Fig. 9.6: Variation of applied field and particle velocity with time at high frequency.

mass and consequently on its size. Hence both zeta potential and particle size can be determined from the ESA signal, if the frequency of the alternating field is sufficiently high. This is the method that is provided by the AcoustoSizer from Colloidal Dynamics.

Several variables affect the ESA measurements and these are listed below:

(i) Particle concentration range: Very dilute suspensions generate a weak signal and are not suitable for ESA measurements. The magnitude of the ESA signal is proportional to the average particle mobility, the volume fraction of the particles ϕ and the density difference between the particles and the medium $\Delta\rho$. To obtain a signal that is at least one order of magnitude higher than the background electrical noise (≈ 0.002 mPa M/V) the concentration and/or the density difference have to be sufficiently large. If the density difference between the particles and medium is small, e.g. polystyrene latex with $\Delta\rho \approx 0.05$ then a sufficiently high concentration ($\phi > 0.02$) is needed to obtain a reasonably strong ESA signal. The accuracy of the ESA measurement is also not good at high ϕ values. This is due to the nonlinearity of the ESA amplitude–ϕ relationship at high ϕ values. Such a deviation becomes appreciable at $\phi > 0.1$. However, reasonable values of zeta potential can be obtained from ESA measurements up to $\phi = 0.2$. Above this concentration, the measurements are not sufficiently accurate and the results obtained can only be used for qualitative assessment.

(ii) Electrolyte effects: Ions in the dispersion generate electroacoustic (IVP) potential and the ESP signal is therefore a composite of the signals created by the particles and ions. However, the ionic contribution is relatively small, unless the particle concentration is low, their zeta potential is low and the ionic concentration is high. The ESA system is therefore not suitable for dynamic mobility and zeta potential measurements in systems with electrolyte concentration higher than 0.3 mol dm^{-3} KCl.

(iii) Temperature: Since the viscosity of the dispersion decreases by ≈ 2 % per °C and its conductivity increases by about the same amount, it is important that temperature be accurately controlled using a Peltier device. Temperature control should also be maintained during sample preparation, for example when the suspension is sonicated. To avoid overheating, the sample should be cooled in an ice bath at regular intervals during sonication.

(iv) Calibration and accuracy: The electroacoustic probe should be calibrated using a standard reference dispersion such as polystyrene latex or colloidal silica (Ludox). The common sources of error are unsuitable particle concentration (too low or too high), irregular particle shape, polydispersity, electrolyte signals, temperature variations, sedimentation, coagulation and entrained air bubbles. The latter in particular can cause erroneous ESA signal fluctuations resulting from weakening of the sound by the air bubbles. In many cases the zeta potential results obtained using the ESA method do not agree with those obtained using other methods such as microelectrophoresis or laser velocimetry. However, the difference seldom exceeds 20 % and this makes the ESA method more convenient for measuring in many industrial methods. The main advantages are the speed of measurement and the dispersion does not need to be diluted, which could change the state of the suspension.

9.5 Measuring the rate of flocculation

Two general techniques may be applied for measuring the rate of flocculation of dispersions, both of which can only be applied for dilute systems. The first method is based on measuring the scattering of light by the particles or droplets. For monodisperse particles or droplets with a radius that is less than $\lambda/20$ (where λ is the wavelength of light) one can apply the Rayleigh equation, whereby the turbidity τ_0 is given by,

$$\tau_0 = A' n_0 V_1^2, \tag{9.27}$$

where A' is an optical constant (which is related to the refractive index of the particle and medium and the wavelength of light) and n_0 is the number of particles, each with a volume V_1.

By combining the Rayleigh theory with the Smoluchowski–Fuchs theory of flocculation kinetics [6, 16], one can obtain the following expression for the variation of turbidity with time,

$$\tau = A' n_0 V_1^2 (1 + 2 n_0 k t), \tag{9.28}$$

where k is the rate constant of flocculation

The second method for obtaining the rate constant of flocculation is by direct particle or droplet counting as a function of time. For this purpose optical microscopy or image analysis may be used, provided the particle size is within the resolution limit

of the microscope. Alternatively, the particle or droplet number may be determined using electronic devices such as the Coulter Counter or the flow ultramicroscope.

The rate constant of flocculation is determined by plotting $1/n$ versus t, where n is the number of particles after time t, i.e.,

$$\left(\frac{1}{n}\right) = \left(\frac{1}{n_0}\right) + kt. \tag{9.29}$$

The rate constant k of slow flocculation is usually related to the rapid rate constant k_0 (the Smoluchowski rate) by the stability ratio W,

$$W = \left(\frac{k}{k_0}\right). \tag{9.30}$$

One usually plots log W versus log C (where C is the electrolyte concentration) to obtain the critical coagulation concentration (CCC), which is the point at which $\log W = 0$.

A very useful method for measuring flocculation is to use the single-particle optical method. The particles or droplets of the formulation dispersed in a liquid flow through a narrow uniformly illuminated cell. The dispersion is made sufficiently dilute (using the continuous medium) so that particles or droplets pass through the cell individually. A particle or droplet passing through the light beam illuminating the cell generates an optical pulse detected by a sensor. If the particle or droplet size is greater than the wavelength of light (> 0.5 μm), the peak height depends on the projected area of the particle or droplet. If the particle or droplet size is smaller than 0.5 μm, the scattering dominates the response. For particles or droplets > 1 μm, a light obscuration (also called blockage or extinction) sensor is used. For particles or droplets smaller than 1 μm, a light scattering sensor is more sensitive.

The above method can be used to determine the size distribution of aggregating dispersions. The aggregated particles or droplets pass individually through the illuminated zone and generate a pulse which is collected at small angle (< 3°). At sufficiently small angles, the pulse height is proportional to the square of the number of monomeric units in an aggregate and independent of the aggregate shape or its orientation.

9.6 Measuring incipient flocculation

This can be done for sterically stabilized dispersions, when the medium for the chains becomes a θ-solvent. This occurs, for example, on heating an aqueous dispersion stabilized with poly(ethylene oxide) (PEO) or poly(vinyl alcohol) chains. Above a certain temperature (the θ-temperature) that depends on electrolyte concentration, flocculation of the dispersion occurs. The temperature at which this occurs is defined as the critical flocculation temperature (CFT).

This process of incipient flocculation can be followed by measuring the turbidity of the dispersion as a function of temperature. Above the CFT, the turbidity of the dispersion rises very sharply. For this purpose, the cell in the spectrophotometer that is used to measure the turbidity is placed in a metal block that is connected to a temperature programming unit (which allows one to increase the temperature rise at a controlled rate).

9.7 Measuring Ostwald ripening

Ostwald ripening is the result of the difference in solubility S between small and large particles or droplets. The smaller particles or droplets have larger solubility than the larger particles or droplets. The effect of particle or droplet size on solubility is described by the Kelvin equation [17],

$$S(r) = S(\infty)\exp\left(\frac{2\sigma V_m}{rRT}\right), \tag{9.31}$$

where $S(r)$ is the solubility of a particle or droplet with radius r, $S(\infty)$ is the solubility of a particle or droplet with infinite radius, σ is the solid/liquid or liquid/liquid interfacial tension, V_m is the molar volume of the disperse phase, R is the gas constant and T is the absolute temperature.

For two particles or droplets with radii r_1 and r_2,

$$\frac{RT}{V_m}\ln\left(\frac{S_1}{S_2}\right) = 2\sigma\left(\frac{1}{r_1} - \frac{1}{r_2}\right). \tag{9.32}$$

R is the gas constant, T is the absolute temperature, V_m is the molar volume of the disperse phase and σ is the solid/liquid or liquid/liquid interfacial tension.

To obtain a measure of the rate of crystal growth, the particle or droplet size distribution of the dispersion is followed as a function of time, using either a Coulter Counter, a Mastersizer or an optical disc centrifuge. One usually plots the cube of the average radius versus time which gives a straight line from which the rate of Ostwald ripening can be determined (the slope of the linear curve),

$$r^3 = \frac{8}{9}\left[\frac{S(\infty)\gamma V_m D}{\rho RT}\right]t. \tag{9.33}$$

D is the diffusion coefficient of the disperse phase in the continuous phase and ρ is the density of the particles.

9.8 Measuring the rate of coalescence for emulsions

As mentioned in Chapter 11 of Vol. 1, the driving force for emulsion coalescence is the thinning and disruption of the liquid film between the droplets. When two emulsion

droplets come into contact, say in a cream layer or a floc, or even during Brownian collision, the liquid film between them undergoes some fluctuation in thickness; the thinnest part of the film will have the highest van der Waals attraction and this is the region where coalescence starts. Alternatively, the surfaces of the emulsion droplets may undergo fluctuation producing waves, which may grow in amplitude; the strongest van der Waals attraction is at the apices of these fluctuations and coalescence occurs by further growth of the fluctuation. One may define a critical film thickness below which coalescence occurs.

The rate of coalescence is determined by the rate at which the film thins and this usually follows a first-order kinetics,

$$N = N_0 \exp(-Kt), \tag{9.34}$$

where N is the number of droplets after time t, N_0 is the number at zero time and K is the rate constant of coalescence.

Alternatively one can measure the average droplet diameter d as a function of time,

$$d = d_0 \exp(Kt). \tag{9.35}$$

Providing the emulsion does not undergo any flocculation, the coalescence rate can be simply measured by following the number of droplets or average diameter as a function of time. A given volume of the emulsion is carefully diluted into the isotone solution of the Coulter Counter and the number of droplets is measured. The average diameter can be obtained using laser diffraction methods (e.g. using the Mastersizer). By following this procedure at various time periods, one can obtain the coalescence rate constant K.

Usually one plots $\log N$ or $\log d$ versus t and the slope of the line in the initial period gives the rate of coalescence K. Clearly, the higher the value of K, the higher the coalescence of the emulsion. An accelerated test may be used by subjecting the system to higher temperatures; usually the rate of coalescence increases with increasing temperature (although this is not always the case). One should be careful in the dilution procedure, particularly if the oil is significantly soluble (say greater than 10 ppm) in the isotone solution or in the tank of the Mastersizer. In this case, one should saturate the solution with the oil before diluting the concentrated emulsion for droplet counting or sizing.

9.9 Assessing sedimentation or creaming of dispersions

As mentioned in Chapter 13 of Vol. 1 most suspensions undergo sedimentation on standing due to gravity and the density difference $\Delta\rho$ between the particles and dispersion medium. This is particularly the case when the particle radius exceeds 50 nm and when $\Delta\rho > 0.1$. In this case Brownian diffusion cannot overcome the gravity force

and sedimentation occurs, resulting in an increasing particle concentration from the top to the bottom of the container.

With emulsions where the oil density is usually lower than that of the medium, creaming usually occurs. However, with water-in-oil emulsions, the density of the aqueous phase is usually higher than that of the oil dispersion medium and in this case sedimentation occurs.

As discussed in Chapter 13 of Vol. 1 to prevent particle sedimentation, "thickeners" (rheology modifiers) are added in the continuous phase. The same applies for prevention of creaming of emulsions. The sedimentation of a suspension is characterized by the sedimentation rate, sediment volume, the change of particle size distribution during settling and the stability of the suspension to sedimentation. Creaming of an emulsion is also characterized by the rate of creaming, the cream volume (height), the change of droplet size distribution during creaming and the stability of the emulsion, e.g. its flocculation, Ostwald ripening and coalescence.

Assessing the sedimentation of a suspension depends on the force applied to the particles in the suspension, namely gravitational, centrifugal and electrophoretic. The sedimentation processes are complex and subject to various errors in sedimentation measurements [5]. A suspension is usually agitated before measuring sedimentation, to ensure an initially homogeneous system of particles in random motion. Vigorous agitation or the use of ultrasonic cavitation must be avoided to prevent any breakdown of aggregates and change of the particle size distribution.

Several physical measurements can be applied to assess sedimentation and these methods have been described in detail by Kissa [5]. The simplest method is to measure the density of the settling suspension at a known depth using a hydrometer. Unfortunately this simple method is highly invasive due to the disturbance of the suspension by the hydrometer. A more accurate method is to use sedimentation balances, whereby the sediment accumulated at the base of the sedimentation column is collected and weighed. Manometric methods that use a capillary side arm for measuring the difference between the densities of the pure sedimentation fluid and that of the suspension can also be applied.

Several electrical methods can be applied to assess sedimentation. Most suspensions have complex electrical permittivities and may require measurement of both the capacitance and conductivity to determine the solid volume fraction at depth h and time t. This method has the advantage of being non-invasive since the sensing electrodes do not have to be in direct contact with the dispersion. A more convenient method is to use ultrasound probes at various heights from the top to the bottom of the sedimentation tube as discussed below. Ultrasound velocity and attenuation depend on the volume fraction of the suspension, allowing one to obtain the solids content as a function of height in the sedimentation tube. An alternative optical technique is to measure the backscattering of near infrared at various heights from the sedimentation tube. A commercially available apparatus, namely the Turboscan, can be used for this purpose.

Several other techniques have been designed to monitor sedimentation of suspensions of which photosedimentation, X-ray sedimentation and laser anemometry are perhaps worth mentioning. The simplest sedimentation test is based on visual observation of settling. The turbidity of the suspension is estimated visually, or the height of the sediment and sediment volume are recorded as a function of time. This visual estimation of sedimentation is only qualitative but is adequate in many practical situations. However, the characterization of suspensions and the determination of particle size distributions require quantitative sedimentation methods. Instrumental techniques have been developed for measuring the turbidity of the suspension as a function of time, either by measuring the turbidity of the bulk suspension or by withdrawing a sample at a given height of the settling suspension. The earlier instruments used for measuring the turbidity of suspensions, called nephelometers, have evolved into instruments with a more sophisticated optical system. Photosedimentometers monitor gravitational particle sedimentation by photoelectric measurement of incident light under steady-state conditions. A horizontal beam of parallel light is projected through a suspension in a sedimentation column to a photocell. Double-beam photosedimentometers using matched photocells, one for the sample and the other for the reference beam, were developed later. A more sophisticated method was later introduced, using linear charge-coupled photodiode array as the image sensor to convert the light intensity attenuated by the particles into an electric signal. The output of each of the photodetectors is handled by a computer independently. Hence the settling distance between any point in the liquid and the surface of the liquid can be measured accurately without using a mechanical device. As a consequence, the particle measurement is rapid, requiring only about 5 minutes to determine a particle size distribution. The use of fibre optics has made it possible to scan the sedimentation column without moving parts or with a fibre optic probe that is moved inside the sedimentation column.

Laser anemometry, also described as laser Doppler velocity measurement (LVD) is a sensitive technique that can extend the range of photosedimentation methods. It has been applied in a sedimentometer to measure particle sizes as low as 0.5 μm.

X-ray sedimentometers measure X-ray absorption to determine concentration gradients in sedimenting suspensions. The use of X-ray and γ-rays has been proposed as transmittance probes that correlate transmitted radiation with the density of suspension. X-ray transmittance T is directly related to the weight of particles by an exponential relationship, analogous to the Lambert–Beer law governing transmittance of visible radiation,

$$\ln T = -A\phi_s, \tag{9.36}$$

where A is a particle-, medium- and equipment constant and ϕ_s is the volume fraction of particles in the suspension.

The concentration of particles remaining in the liquid at various sedimentation depths is determined by using a finely collimated beam of X-rays. The time required

for the sedimentation measurement is shortened by continuously changing the effective sedimentation depth. The concentration of particles remaining at various depths is measured as a function of time. X-ray sedimentometers can be used for particles containing elements with atomic numbers above 15 and, therefore, the method cannot be applied to measure sedimentation of organic pigments.

It should be mentioned that gravitational sedimentation is often too slow, particularly if the particles are small and have a density that is not appreciably higher than that of the medium. Application of a centrifugal force accelerates sedimentation allowing one to obtain results within a reasonable time. However, the data obtained by centrifugation do not always correlate with those resulting from settling under gravity. This is particularly the case with suspensions that are weakly flocculated, where the loose structure may break up on application of a centrifugal force. The interaction between the particles may also change on application of a high gravitational force. This casts doubt on the use of centrifugation as an accelerated test for predicting sedimentation.

The practical measurement of creaming or sedimentation of emulsions is hindered by the opacity of the emulsions [18]. If there is any variation in the speed of the droplets due to polydispersity or density variation, the slower moving fraction obscures the movement of the faster droplets. Analysis of creaming or sedimentation rates needs a knowledge of the droplet concentration with height and time. Two methods can be applied to obtain such information, namely the use of backscattering of near infrared (NIR) and measuring ultrasound velocity as a function of height in the tube containing the emulsion. A schematic representation of an instrument that can be used for such measurements, namely the Turbiscan is shown in Fig. 9.7. This technique consists in sending photons (light) into the sample. After being scattered by the emulsion droplets these photons emerge from the sample and are detected by the measurement device of the Turbiscan. A mobile reading head, composed of an NIR diode and two detectors (transition T and backscattering BS), scans a cell containing the emulsion. The Turbiscan software then enables one to interpret the obtained data easily. The measurement enables the quantification of several parameters, as BS and T values are linked to droplet average diameter (d) and volume fraction (ϕ),

$$BS = f\left(\frac{d}{\phi}\right). \tag{9.37}$$

Two kinds of signal, including transmission light and backscattering light could be achieved as illustrated in Fig. 9.8 for a sample of 20 ml glass vial with a height of 42 mm. The signal value is obtained every 40 μm of the sample and once takes about 20 s. In general, the signal value of transmitted light is used to analyse clear liquid, whereas that of backscattered light is used to analyse non-clear liquids or samples with high concentration.

The transmission intensity $T(\lambda, r_i)$, where λ is the mean free path of photons and r_i is the inner radius of the vial, is related to the transmission T_0 of the continuous

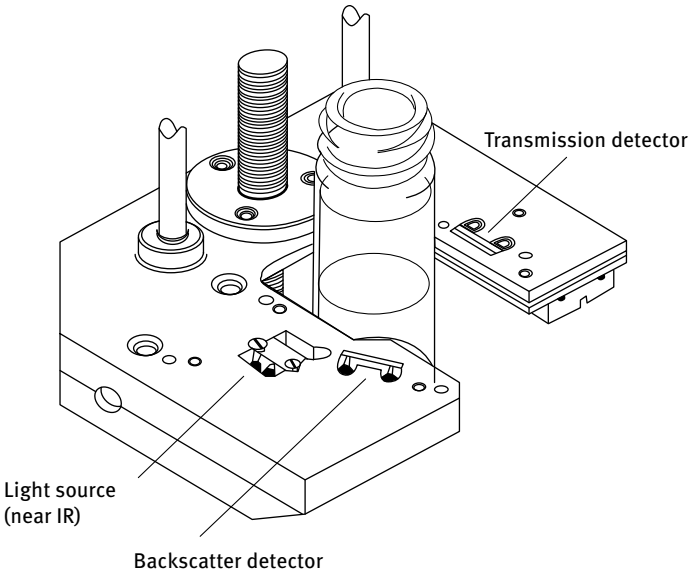

Fig. 9.7: Schematic representation of the Turbiscan.

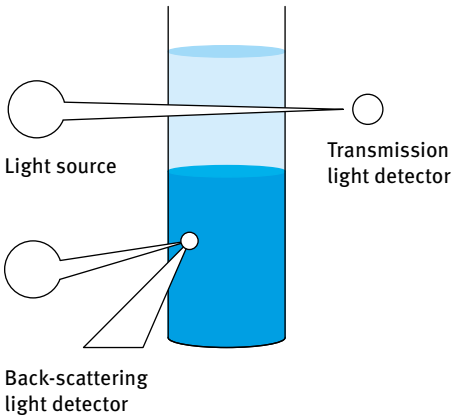

Fig. 9.8: Schematic diagram and parameters of Turbiscan.

phase by the expression,

$$T(\lambda, r_i) = T_0 \exp -\frac{2r_i}{\lambda} \tag{9.38}$$

and,

$$\lambda(d, \phi) = \frac{2d}{3\phi Q_s}, \tag{9.39}$$

where d is the average particle size, ϕ is the volume concentration of disperse phase and Q_s is the optical parameter according to the Mie theory.

According to equations (9.38) and (9.39) T is affected by the average particle diameter and mean free path of the photons. The change in transmission intensity over time and height can be calculated using the following expressions.

$$T_i = \frac{\sum_{H_l}^{H_u} [Scan_i(h) - Scan_0(h)]}{H_u - H_l}, \tag{9.40}$$

$$\Delta T = T_i - T_0, \tag{9.41}$$

where T_i is the average transmission intensity (time is i) and T_0 is the average intensity of transmission (time 0), H_u is the upper limit, H_l is the lower limit, $Scan_i(h)$ is the intensity of scanning light at time i and height h, $Scan_0$ is the intensity of scanning light at time 0 and height h.

ΔT shows the average transmitted intensity and is appropriate to use when the transmitted intensity changes over height are small. *TSI* can be calculated using the following expression,

$$TSI = \sum_i \frac{\sum_h [Scan_i(h) - Scan_{i-1}(h)]}{H}, \tag{9.42}$$

where H is the sample height from bottom of the cell to the meniscus and $Scan_{i-1}(h)$ is the intensity of scanning light at time $i - 1$ and height h.

A schematic representation of an ultrasonic method is shown in Fig. 9.9. The velocity of ultrasound through an emulsion is sensitive to composition [18]. This is the principle of the ultrasound monitor, shown in Fig. 9.9, which measures the ultrasonic velocity as a function of height.

The time-of-flight of a pulse of ultrasound is measured across a rectangular sample cell immersed in a thermostated water bath. The time-of-flight data are converted to ultrasonic velocity by reference to measurements made in two calibration fluids. The ultrasonic velocity data may be used to calculate the volume fraction of the oil using simple mixing theory.

The speed at which ultrasound propagates through an emulsion is a complex function of the droplet volume fraction, size and properties of the droplets and continuous phase. However, when the droplets are much smaller than the wavelength of ultrasound and there is a significant difference between the speed of sound in the bulk dispersed and continuous phases, the effect of volume fraction greatly outweighs all other effects so that the speed of ultrasound V may be calculated by assuming the system behaves like a simple mixture using the equation,

$$V = \left(\frac{V_c^2}{\left(1 - \phi\left(1 - \frac{\rho_d}{\rho_c}\right)\right)\left(1 - \phi\left(1 - \frac{\rho_c V_c^2}{\rho_d V_d^2}\right)\right)} \right)^{1/2}, \tag{9.43}$$

where ρ_d, ρ_c, V_d and V_c are the densities and speeds of ultrasound through the dispersed and continuous phases respectively and ϕ is the volume fraction of the dispersed phase.

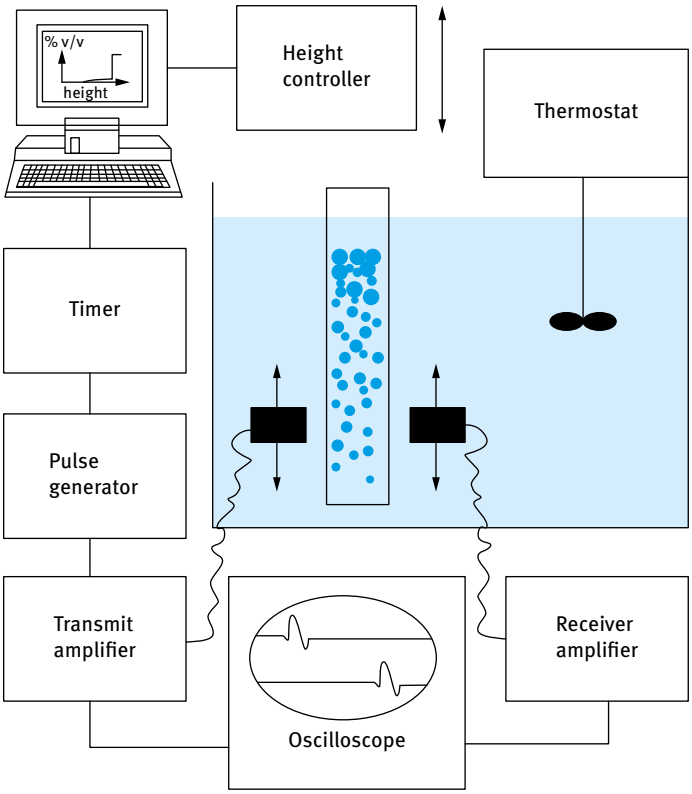

Fig. 9.9: Schematic representation of the ultrasonic creaming meter.

9.10 Bulk properties of suspensions and emulsions. Equilibrium sediment volume (or height) and redispersion

For a "structured" suspension or emulsion, obtained by "controlled" flocculation or addition of "thickeners" (such polysaccharides, clays or oxides), the "flocs" sediment or cream at a rate depending on their size and porosity of the aggregated mass. After this initial sedimentation or creaming, compaction and rearrangement of the floc structure occurs, a phenomenon referred to as consolidation.

Normally in sediment or cream volume measurements, one compares the initial volume V_0 (or height H_0) with the ultimately reached value V (or H). A colloidally stable suspension or emulsion gives a "close-packed" structure with relatively small sediment or cream volume. A weakly "flocculated" or "structured" suspension or emulsion gives a more open sediment or cream and hence a higher sediment or cream volume. Thus by comparing the relative sediment or cream volume V/V_0 or height H/H_0, one can distinguish between a stable and flocculated suspension or emulsion.

9.11 Methods for evaluating formulations without dilution – rheological techniques

Evaluating the stability/instability of suspensions or emulsion without any dilution (which can cause significant changes in the structure of the system) requires carefully designed techniques that should cause as little disturbance to the structure. The most powerful techniques that can be applied in any industrial laboratory are rheological measurements [19–25]. These measurements provide accurate information on the state of the system such as sedimentation or creaming and flocculation. These measurements are also applied for predicting the long-term physical stability of the suspension. The various rheological techniques that can be applied were described in Chapter 14 of Vol. 1. Three types of measurements can be applied:

(i) Steady state shear stress σ–shear rate γ measurements. This requires the use of a shear rate controlled instrument. The results obtained can be fitted to models to obtain the yield value σ_β and the viscosity η as a function of shear rate. Time effects (thixotropy) can also be investigated.

(ii) Constant stress (creep) measurements: a constant stress is applied on the system and the strain γ or compliance J (γ/σ) is followed as a function of time. By measuring creep curves at increasing stress values one can obtain the residual (zero shear) viscosity $\eta(0)$ and the critical stress σ_{cr} that is the stress above which the structure starts to break down. σ_{cr} is sometimes referred to as the "true" yield value.

(iii) Dynamic (oscillatory) measurements: A sinusoidal stress or strain with amplitudes σ_0 and γ_0 is applied at a frequency ω (rad s^{-1}) and the stress and strain are simultaneously measured. For a viscoelastic system, as is the case with most formulations, the stress and strain amplitudes oscillate with the same frequency but out of phase. The phase angle shift δ is measured from the time shift of the strain and stress sine waves. From σ_0, γ_0 and δ one can obtain the complex modulus $|G^*|$, the storage modulus G' (the elastic component) and the loss modulus G'' (the viscous component). The results are obtained as a function of strain amplitude and frequency.

9.12 Application of rheological techniques for the assessment and prediction of the physical stability of suspensions [21]

9.12.1 Rheological techniques for assessing sedimentation or creaming and syneresis

As mentioned in Chapter 13 of Vol. 1, sedimentation or creaming is prevented by addition of "thickeners" that form a "three-dimensional elastic" network in the continuous phase. If the viscosity of the elastic network, at shear stresses (or shear rates) com-

parable to those exerted by the particles or droplets, exceeds a certain value, then sedimentation is completely eliminated.

The shear stress, σ_p, exerted by a particle (force/area) can be simply calculated,

$$\sigma_p = \frac{(4/3)\pi R^3 \Delta\rho g}{4\pi R^2} = \frac{\Delta\rho R g}{3}. \tag{9.44}$$

For a 10 μm radius particle or droplet with a density difference $\Delta\rho$ of 0.2 g cm^{-3}, the stress is equal to,

$$\sigma_p = \frac{0.2 \times 10^3 \times 10 \times 10^{-6} \times 9.8}{3} \approx 6 \times 10^{-3} \text{ Pa}. \tag{9.45}$$

For smaller particles or droplets smaller stresses are exerted. Thus, to predict sedimentation or creaming, one has to measure the viscosity at very low stresses (or shear rates). These measurements can be carried out using a constant stress rheometer (Carrimed, Bohlin, Rheometrics, Haake or Physica). Usually one obtains good correlation between the rate of creaming or sedimentation, υ, and the residual viscosity $\eta(0)$ as will be described below. Above a certain value of $\eta(0)$, υ becomes equal to 0. Clearly, to minimize sedimentation or creaming one has to increase $\eta(0)$; an acceptable level for the high shear viscosity η_∞ must be achieved, depending on the application. In some cases, a high $\eta(0)$ may be accompanied by a high η_∞ (which may not be acceptable for the application, for example if spontaneous dispersion on dilution is required). If this is the case, the formulation chemist should look for an alternative thickener.

Another problem encountered with many dispersions is that of "syneresis", i.e. the appearance of a clear liquid film at the top of the container. "Syneresis" occurs with most "flocculated" and/or "structured" (i.e. those containing a thickener in the continuous phase) dispersions. "Syneresis" may be predicted from measuring the yield value (using steady state measurements of shear stress as a function of shear rate) as a function of time or using oscillatory techniques (whereby the storage and loss modulus are measured as a function of strain amplitude and frequency of oscillation). The oscillatory measurements are perhaps more useful since to prevent separation the bulk modulus of the system should balance the gravity forces that is given by $h\rho\Delta g$ (where h is the height of the disperse phase, $\Delta\rho$ is the density difference and g is the acceleration due to gravity). The bulk modulus is related to the storage modulus G'. A more useful predictive test is to calculate the cohesive energy density of the structure E_c described in Chapter 14 of Vol. 1.

The separation of a formulation decreases with increasing E_c as will be discussed below. The value of E_c that is required to stop complete separation depends on the particle or droplet size distribution, the density difference between the particle or droplet and the medium as well as on the volume fraction ϕ of the dispersion.

As mentioned above, thickeners reduce creaming or sedimentation by increasing the residual viscosity $\eta(0)$ which must be measured at stresses compared to those exerted by the droplets or particles (mostly less than 0.1 Pa). At such low stresses, $\eta(0)$ increases very rapidly with increasing "thickener" concentration. This rapid increase is

not observed at high stresses and this illustrates the need for measurement at low stresses (using constant stress or creep measurements). This will be illustrated below.

9.12.2 Assessing flocculation using rheological techniques

Steady state rheological investigations may be used to investigate the state of flocculation of a dispersion. Weakly flocculated dispersions usually show thixotropy and the change of thixotropy with applied time may be used as an indication of the strength of this weak flocculation. These methods are only qualitative and one cannot use the results in a quantitative manner. This is due to the possible breakdown of the structure on transferring the formulation to the rheometer and also during the uncontrolled shear experiment. Better techniques to study flocculation of a formulation are constant stress (creep) or oscillatory measurements. By careful transfer of the sample to the rheometer (with minimum shear) the structure of the flocculated system may be maintained.

A very important point that must be considered in any rheological measurement is the possibility of "slip" during the measurements. This is particularly the case with highly concentrated dispersions, whereby the flocculated system may form a "plug" in the gap of the platens leaving a thin liquid film at the walls of the concentric cylinder or cone-and-plate geometry. This behaviour is caused by some "syneresis" of the formulation in the gap of the concentric cylinder or cone and plate. To reduce "slip" one should use roughened walls for the platens. A vane rheometer may also be used.

Steady state shear stress–shear rate measurements are by far the most commonly used method in many industrial laboratories. Basically the dispersion is stored at various temperatures and the yield value σ_β and plastic viscosity η_{pl} are measured at various intervals of time. Any flocculation in the formulation should be accompanied by an increase in σ_β and η_{pl}. A rapid technique to study the effect of temperature changes on the flocculation of a formulation is to carry out temperature sweep experiments, running the samples from say 5–50 °C. The trend in the variation of σ_β and η_{pl} with temperature can quickly give an indication on the temperature range at which a dispersion remains stable (during that temperature range σ_β and η_{pl} remain constant).

If Ostwald ripening occurs simultaneously, σ_β and η_{pl} may change in a complex manner with storage time. Ostwald ripening results in a shift of the particle size distribution to higher diameters. This has the effect of reducing σ_β and η_{pl}. If flocculation occurs simultaneously (having the effect of increasing these rheological parameters), the net effect may be an increase or decrease of the rheological parameters. This trend depends on the extent of flocculation relative to Ostwald ripening and/or coalescence. Therefore, following σ_β and η_{pl} with storage time requires knowledge of Ostwald ripening. Only in the absence of these latter breakdown processes can one use rheological measurements as a guide to assessing flocculation.

Constant stress (creep) experiments are more sensitive for following flocculation. A constant stress σ is applied on the system and the compliance J (Pa^{-1}) is plotted as a function of time. These experiments are repeated several times increasing the stress from the smallest possible value (that can be applied by the instrument), increasing the stress in small increments. A set of creep curves are produced at various applied stresses. From the slope of the linear portion of the creep curve (after the system reaches a steady state), the viscosity at each applied stress, η_σ, is calculated. A plot of η_σ versus σ allows one to obtain the limiting (or zero shear) viscosity $\eta(0)$ and the critical stress σ_{cr} (which may be identified with the "true" yield stress of the system. The values of $\eta(0)$ and σ_{cr} may be used to assess the flocculation of the dispersion on storage. If flocculation occurs on storage (without any Ostwald ripening), the values of $\eta(0)$ and σ_{cr} may show a gradual increase with increasing storage time. As discussed in the previous section (on steady state measurements), the trend becomes complicated if Ostwald ripening occurs simultaneously (both have the effect of reducing $\eta(0)$ and σ_{cr}).

The above measurements should be supplemented by particle size distribution measurements of the diluted dispersion (making sure that no flocs are present after dilution) to assess the extent of Ostwald ripening. Another complication may arise from the nature of the flocculation. If flocculation occurs in an irregular way (producing strong and tight flocs), $\eta(0)$ may increase, while σ_{cr} may show some decrease and this complicates the analysis of the results. In spite of these complications, constant stress measurements may provide valuable information on the state of the dispersion on storage.

Carrying out creep experiments and ensuring that a steady state is reached can be time consuming. One usually carries out a stress sweep experiment, whereby the stress is gradually increased (within a predetermined time period to ensure that one is not too far from reaching the steady state) and plots of η_σ versus σ are established. These experiments are carried out at various storage times (say every two weeks) and temperatures. From the change of $\eta(0)$ and σ_{cr} with storage time and temperature, one may obtain information on the degree and the rate of flocculation of the system. Clearly, interpreting the rheological results requires expert knowledge of rheology and measurement of the particle size distribution as a function of time.

One main problem in carrying the above experiments is sample preparation. When a flocculated dispersion is removed from the container, care should be taken not to cause much disturbance to that structure (minimum shear should be applied on transferring the formulation to the rheometer). It is also advisable to use separate containers for assessments of flocculation; a relatively large sample is prepared and this is then transferred to a number of separate containers. Each sample is used separately at a given storage time and temperature. One should be careful in transferring the sample to the rheometer. If any separation occurs in the formulation the sample is gently mixed by placing it on a roller. It is advisable to use as minimum shear as possible when transferring the sample from the container to the rheometer

(the sample is preferably transferred using a "spoon" or by simple pouring from the container). The experiment should be carried out without an initial pre-shear.

Another rheological technique for assessing flocculation is oscillatory measurement. One carries out two sets of experiments.

9.12.2.1 Strain sweep measurements

In this case, the oscillation is fixed (say at 1 Hz) and the viscoelastic parameters are measured as a function of strain amplitude. G^*, G' and G'' remain virtually constant up to a critical strain value, γ_{cr}. This region is the linear viscoelastic region. Above γ_{cr}, G^* and G' start to fall, whereas G'' starts to increase; this is the nonlinear region. The value of γ_{cr} may be identified with the minimum strain above which the "structure" of the dispersion starts to break down (for example breakdown of flocs into smaller units and/or breakdown of a "structuring" agent).

From γ_{cr} and G', one can obtain the cohesive energy E_c (J m^{-3}) of the flocculated structure. E_c may be used in a quantitative manner as a measure of the extent and strength of the flocculated structure in a dispersion. The higher the value of E_c the more flocculated the structure is. Clearly E_c depends on the volume fraction of the dispersion as well as the particle size distribution (which determines the number of contact points in a floc). Therefore, for quantitative comparison between various systems, one has to make sure that the volume fraction of the disperse particles is the same and the dispersions have very similar particle size distribution. E_c also depends on the strength of the flocculated structure, i.e. the energy of attraction between the droplets. This depends on whether the flocculation is in the primary or secondary minimum. Flocculation in the primary minimum is associated with a large attractive energy and this leads to higher values of E_c when compared with the values obtained for secondary minimum flocculation (weak flocculation). For a weakly flocculated dispersion, such as is the case with secondary minimum flocculation of an electrostatically stabilized system, the deeper the secondary minimum, the higher the value of E_c (at any given volume fraction and particle size distribution of the dispersion). With a sterically stabilized dispersion, weak flocculation can also occur when the thickness of the adsorbed layer decreases. Again the value of E_c can be used as a measure of flocculation; the higher the value of E_c, the stronger the flocculation. If incipient flocculation occurs (on reducing the solvency of the medium for the change to worse than θ-condition) a much deeper minimum is observed and this is accompanied by a much larger increase in E_c.

To apply the above analysis, one must have an independent method for assessing the nature of the flocculation. Rheology is a bulk property that can give information on interparticle interaction (whether repulsive or attractive) and to apply it in a quantitative manner one must know the nature of these interaction forces. However, rheology can be used in a qualitative manner to follow the change of the formulation on storage. Providing the system does not undergo any Ostwald ripening, the change of the

moduli with time and in particular the change of the linear viscoelastic region may be used as an indication of flocculation. Strong flocculation is usually accompanied by a rapid increase in G' and this may be accompanied by a decrease in the critical strain above which the "structure" breaks down. This may be used as an indication of formation of "irregular" and tight flocs which become sensitive to the applied strain. The floc structure will entrap a large amount of the continuous phase and this leads to an apparent increase in the volume fraction of the dispersion and hence an increase in G'.

9.12.2.2 Oscillatory sweep measurements

In this case, the strain amplitude is kept constant in the linear viscoelastic region (one usually takes a point far from γ_{cr} but not too low, i.e. in the midpoint of the linear viscoelastic region) and measurements are carried out as a function of frequency. Both G^* and G' increase with increasing frequency and ultimately above a certain frequency, they reach a limiting value and show little dependency on frequency. G'' is higher than G' in the low frequency regime; it also increases with increasing frequency and at a certain characteristic frequency ω^* (that depends on the system) it becomes equal to G' (usually referred to as the crossover point), after which it reaches a maximum and then shows a reduction with a further increase in frequency.

From ω^* one can calculate the relaxation time τ of the system,

$$\tau = \frac{1}{\omega^*}. \tag{9.46}$$

The relaxation time may be used as a guide for the state of the dispersion. For a colloidally stable dispersion (at a given particle size distribution), τ increases with increasing volume fraction of the disperse phase, ϕ. In other words, the crossover point shifts to lower frequency with increasing ϕ. For a given dispersion, τ increases with increasing flocculation, providing the particle size distribution remains the same (i.e. no Ostwald ripening).

The value of G' also increases with increasing flocculation, since aggregation of particles usually results in liquid entrapment and the effective volume fraction of the dispersion shows an apparent increase. With flocculation, the net attraction between the particles also increases and this results in an increase in G'. The latter is determined by the number of contacts between the particles and the strength of each contact (which is determined by the attractive energy).

It should be mentioned that in practice one may not obtain the full curve, due to the frequency limit of the instrument and also measurement at low frequency is time consuming. Usually one obtains part of the frequency dependency of G' and G''. In most cases, one has a more elastic than viscous system.

Most disperse systems used in practice are weakly flocculated and they also contain "thickeners" or "structuring" agents to reduce sedimentation and to acquire the

right rheological characteristics for the application, e.g. in hand creams and lotions. The exact values of G' and G'' required depend on the system and its application. In most cases a compromise has to be made between acquiring the right rheological characteristics for the application and the optimum rheological parameters for long-term physical stability. The application of rheological measurements to achieve these conditions requires a great deal of skill and understanding of the factors that affect rheology.

9.13 Predicting creaming, sedimentation, flocculation and coalescence of formulations

9.13.1 Predicting creaming and sedimentation – accelerated tests and their limitations [21]

Several tests have been designed to accelerate the process of sedimentation or creaming, the most commonly used methods are based on increasing temperature or subjecting the suspension or emulsion to high g forces (using a high-speed centrifuge).

With increasing temperature, the viscosity of the system usually decreases and hence sedimentation or creaming is accelerated. The assumption is usually made that if a suspension or emulsion does not show any sedimentation, creaming or separation at 50 °C for say one month, the system will show no separation at ambient temperatures for more than one year.

The above method is only valid if the formulation viscosity η follows the Arrhenius equation that predicts a linear increase in $\ln \eta$ with $(1/T)$, where T is the absolute temperature. Most practical formulations do not follow such a plot due to the possible phase changes or flocculation that may occur at high temperatures. With many surfactant systems, such phase changes may result in the formation of liquid crystalline phases that have higher viscosity at high temperatures and hence no separation results at high temperatures, although that could occur at ambient conditions.

The second accelerated test is to apply high gravity (g) force; this method, if carefully studied, may offer a better accelerated method. This has been particularly applied to emulsions. The assumption is also made here that by increasing the g force the rate of sedimentation or creaming is significantly increased and this could be applied to predict the process from measurements at short time periods.

In a centrifuge, the gravity force is given by,

$$g = \omega^2 x, \tag{9.47}$$

where x is the mean distance of the centrifuge tube from the axis of rotation and ω is the angular velocity ($\omega = 2\pi\nu$, where ν is the number of revolutions per second). Note that if the centrifuge tube is not small compared to x, then the applied centrifugal field cannot be considered to be uniform over the length of the tube.

Modern analytical ultracentrifuges allow one to follow the separation of emulsions in a quantitative manner. With typical O/W emulsions, three layers are generally observed:

(i) a clear aqueous phase;
(ii) an opaque phase consisting of distorted polyhedral oil droplets;
(iii) a clear separated oil phase, resulting from coalescence of the polyhedra.

The degree of emulsion stability may be taken as the volume of the opaque phase remaining after time t. Alternatively, one may use the volume of oil separated at infinite time as an index for stability.

A simple expression may be used to treat the data in a quantitative manner,

$$\frac{t}{V} = \frac{1}{bV_\infty} + \frac{1}{V_\infty}, \tag{9.48}$$

where V is the volume of oil separated at time t, V_∞ is the extrapolated volume at infinite time and b is a constant.

A plot of t/V versus t should give a straight line from which b and V_∞ may be calculated. These two parameters may be taken as indices for emulsion stability.

A more rigorous procedure to studying emulsion stability using the ultracentrifuge is to observe the system at various speeds of rotation. At relatively low centrifuge speeds one may observe the expected opaque cream layer. At sufficiently high centrifuge speeds, one may observe a coalesced oil layer and a cream layer which are separated by an extra layer of deformed oil droplets. This deformed layer looks like a "foam", i.e. it consists of oil droplets separated by thin aqueous films.

For certain emulsions, one may find that by increasing the centrifuge speed, the "foam"/cream layer boundary does not move. Under conditions where there is an equilibrium between the "foam"/cream layer, one may conclude that there is no barrier to be overcome in forming the foam layer from the cream layer. This implies that in the foam layer, the aqueous film separating two oil droplets thins to a "black" film under the action of van der Waals forces. The boundary between the foam layer and the coalesced layer is associated with a force (or pressure) barrier.

One may observe the minimum centrifuge speed that is necessary to produce a visible amount of coalesced oil after say 30 minutes of centrifugation. This centrifuge speed may be used to calculate the "critical pressure" that needs to be applied to induce coalescence.

9.13.2 Rheological techniques for predicting sedimentation or creaming and syneresis

Sedimentation or creaming is prevented by addition of "thickeners" that form a "three-dimensional elastic" network in the continuous phase. If the viscosity of the elastic network, at shear stresses (or shear rates) comparable to those exerted

by the particles or droplets, exceeds a certain value, then creaming or sedimentation is completely eliminated.

As mentioned above, the shear stress, σ_p, exerted by a particle (force/area) can be simply calculated using equation (9.39). For a 10 μm radius particle with a density difference $\Delta\rho$ of 0.2 g cm^{-3}, the stress is equal to 6×10^{-3} Pa. For smaller particles smaller stresses are exerted. Thus, to predict creaming or sedimentation, one has to measure the viscosity at very low stresses (or shear rates). These measurements can be carried out using a constant stress rheometer (Carrimed, Bohlin, Rheometrics, Haake or Physica).

Usually one obtains good correlation between the rate of creaming or sedimentation v and the residual viscosity $\eta(0)$. This is illustrated in Fig. 9.10. Above a certain value of $\eta(0)$, υ becomes equal to 0. Clearly, to minimize creaming or sedimentation one has to increase $\eta(0)$; an acceptable level for the high shear viscosity η_∞ must be achieved, depending on the application. As mentioned above, in some cases, a high $\eta(0)$ may be accompanied by a high η_∞ (which may not be acceptable for the application, for example if spreading of a dispersion on the skin is required). If this is the case, the formulation chemist should look for an alternative thickener.

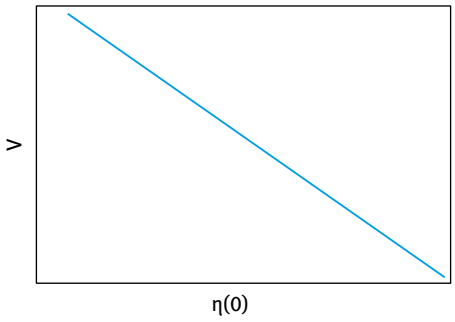

Fig. 9.10: Variation of creaming or sedimentation rate with residual viscosity.

Another problem encountered with many dispersions is that of "syneresis", i.e. the appearance of a clear liquid film at the bottom (if creaming is the case) or the top (if sedimentation is the case) of the container. "Syneresis" occurs with most "flocculated" and/or "structured" (i.e. those containing a thickener in the continuous phase) dispersions.

"Syneresis" may be predicted from measuring the yield value (using steady state measurements of shear stress as a function of shear rate) as a function of time or using oscillatory techniques (whereby the storage and loss modulus are measured as a function of strain amplitude and frequency of oscillation).

The oscillatory measurements are perhaps more useful since to prevent separation the bulk modulus of the system should balance the gravity forces that is given by $h\Delta\rho g$ (where h is the height of the disperse phase, $\Delta\rho$ is the density difference and g is the acceleration due to gravity).

The bulk modulus is related to the storage modulus G'. A more useful predictive test is to calculate the cohesive energy density of the structure E_c that is given by the following equation,

$$E_c = \int_0^{\gamma_{cr}} G'\gamma \, d\gamma = \frac{1}{2} G'\gamma_{cr}^2. \tag{9.49}$$

The separation of a formulation decreases with increasing E_c. This is illustrated in Fig. 9.11 which schematically shows the reduction in percentage separation with increasing E_c. The value of E_c that is required to stop complete separation depends on the particle or droplet size distribution, the density difference between the particle or droplet and the medium as well as on the volume fraction ϕ of the dispersion.

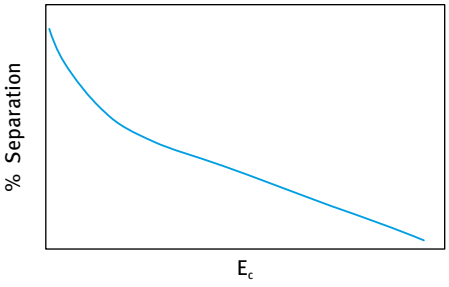

Fig. 9.11: Schematic representation of the variation of percentage separation with E_c.

9.13.3 Examples of correlation of sedimentation or creaming with residual (zero shear) viscosity

9.13.3.1 Model suspensions of aqueous polystyrene latex [26]

The sedimentation rate is a complex function of the volume fraction ϕ. This was tested using polystyrene latex suspensions with radius $R = 1.55\ \mu m$ in 10^{-3} mol dm^{-3} NaCl.

One may be able to correlate the change in the rate of sedimentation with increasing ϕ with the viscosity of the suspension as predicted by the Dougherty–Krieger equation [27],

$$\frac{v}{v_0} \propto \frac{\eta_0}{\eta}, \tag{9.50}$$

$$\frac{v}{v_0} = \alpha \frac{\eta_0}{\eta}, \tag{9.51}$$

where α is a constant.

$$\frac{v}{v_0} = \left[1 - \left(\frac{\phi}{\phi_p}\right)\right]^{-[\eta]\phi_p}, \tag{9.52}$$

where ϕ_p is the maximum packing fraction and $[\eta]$ is the intrinsic viscosity.

Equation (9.52) was tested for polystyrene dispersions as illustrated in Fig. 9.12.

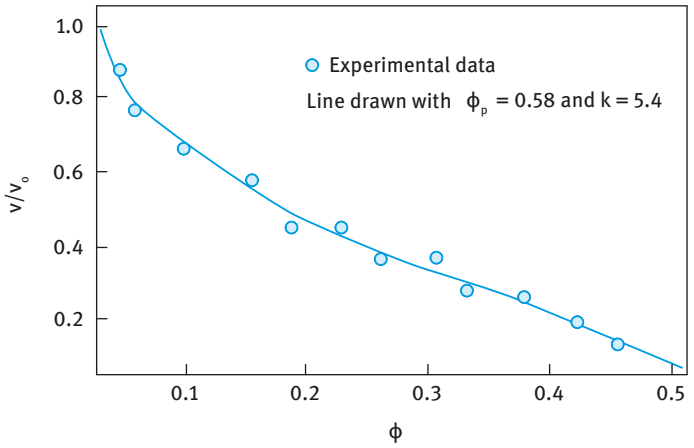

Fig. 9.12: Variation of sedimentation rate with volume fraction for polystyrene dispersions.

To reduce creaming or sedimentation one usually adds high molecular weight material, e.g. hydroxyethyl cellulose or xanthan gum (Kelzan, Keltrol or Rhodopol). Above a critical concentration, C^*, such polymer solutions show non-Newtonian flow in aqueous solution. This is illustrated in Fig. 9.13, which shows the variation of shear stress and viscosity with shear rate [21]. Fig. 9.14 shows the variation of log η with log C to illustrate the onset of free coil overlap. Before overlap $\eta \propto C$, whereas after overlap $\eta \propto C^{3.4}$. Two limiting Newtonian viscosities are identified:

(i) residual (zero shear) viscosity $\eta(0)$;
(ii) Newtonian high shear rate viscosity η_∞.

$\eta(0)$ can be several orders of magnitude (10^3–10^5) higher than η_∞ and such high $\eta(0)$ can significantly reduce creaming or sedimentation.

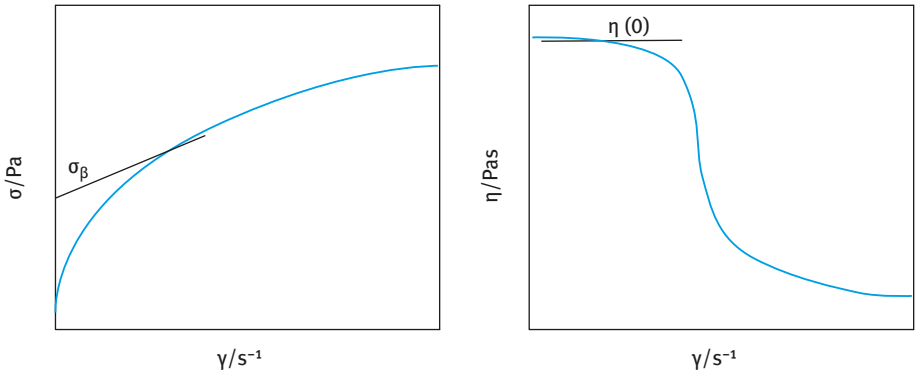

Fig. 9.13: Flow behaviour of "thickeners".

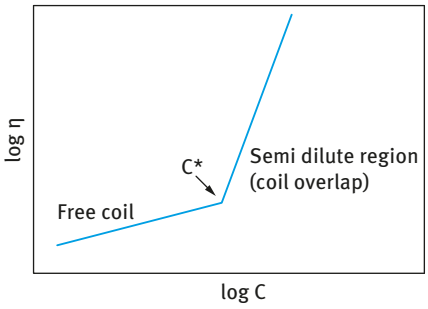

Fig. 9.14: Variation of log η with log C.

As mentioned above, thickeners reduce creaming or sedimentation by increasing the residual viscosity $\eta(0)$ which must be measured at stresses compared to those exerted by the droplets or particles (mostly less than 0.1 Pa). At such low stresses, $\eta(0)$ increases very rapidly with increasing "thickener" concentration. This rapid increase is not observed at high stresses and this illustrates the need for measurements at low stresses (using constant stress or creep measurements). As an illustration Fig. 9.15 shows the variation of η with applied stress σ for ethyl hydroxyethyl cellulose (EHEC), a thickener that is applied in some formulations [26].

It can be seen that the limiting residual viscosity increases rapidly with increasing EHEC concentration. A plot of sedimentation rate for 1.55 μm PS latex particles versus $\eta(0)$ is shown in Fig. 9.16 which shows an excellent correlation [26]. In this case a value of $\eta(0) \geq 10$ Pa s is sufficient for reducing the rate of sedimentation to 0.

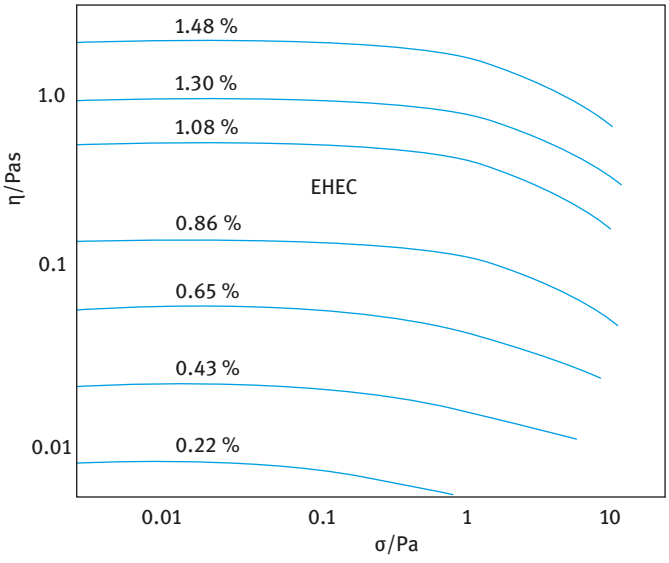

Fig. 9.15: Constant stress (creep) measurements for PS latex dispersions as a function of EHEC concentration.

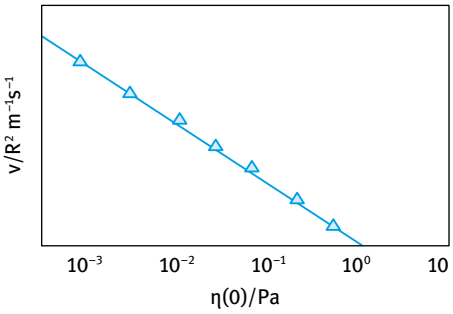

Fig. 9.16: Sedimentation rate versus $\eta(0)$.

9.13.3.2 Predicting emulsion creaming [28]

For the above purpose some model emulsions were prepared using mixtures of oils and commercial surfactants. The oil phase of the emulsion consisted of 10 parts Arlamol HD (Isohexadecane), 2 parts of Estol 3603 (Caprylic/capric triglyceride), one part of sunflower oil (Florasen 90, helanthus Annus) and 1 part of avocado oil (Persea Gratissima).

Two emulsifier systems were used for the preparation of oil-in-water (O/W) emulsions. The first emulsifier was Pluronic PEF 127, an A–B–A block copolymer of polyethylene oxide, PEO (the A chains, about 100 EO units each) and propylene oxide PPO (the B chain, about 55 PO units). The second emulsifier system was Arlatone V-100 which is a nonionic emulsifier system made of a blend of Steareth-100 (stearyl alcohol with 100 EO units), Steareth-2 (stearyl alcohol with 2 EO units), glyceryl stearate citrate, sucrose and a mixture of two polysaccharides, namely mannan and xanthan gum (Keltrol F, supplied by Kelco). In some emulsions, xanthan gum was used as a thickener. All emulsions contained a preservative (Nipaguard BPX).

The rate of creaming and cream volume were measured using graduated cylinders. The creaming rate was assessed by comparing the cream volume V_c with that of the maximum value V_∞ obtained when the emulsion was stored at 55 °C. The time $t_{0.3}$ taken to reach a value of $V_c/V_\infty = 0.3$ (i.e. 30 % of the maximum rate) was calculated [29].

All rheological measurements were carried out using a Physica UDS 200 (Universal Dynamic Spectrometer). A cone and plate geometry was used with a cone angle of 2°. The emulsions were also investigated using optical microscopy and image analysis.

Fig. 9.17 shows the results for creaming rates obtained at various temperatures, using a 20/80 O/W emulsion stabilized with Pluronic PEF 127. As is clear, $t_{0.3}$ decreases with increasing temperature.

The most useful method to predict creaming is to use constant stress (creep) measurements. From these measurements one can obtain the residual (zero shear) viscosity $\eta(0)$. Results were obtained for 20/80 v/v % emulsions as a function of Arlatone V-100 concentration. The results are shown in Fig. 9.18 after several periods of time of storage (1 day, 1 week, 2 weeks and 1 month). $\eta(0)$ showed a large decrease after

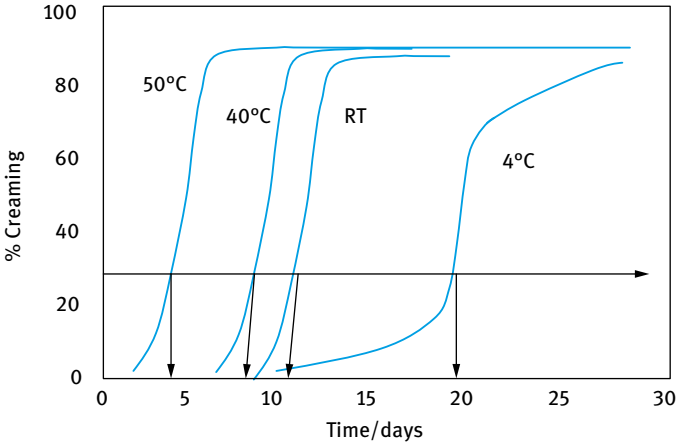

Fig. 9.17: Percentage creaming versus time at various temperatures.

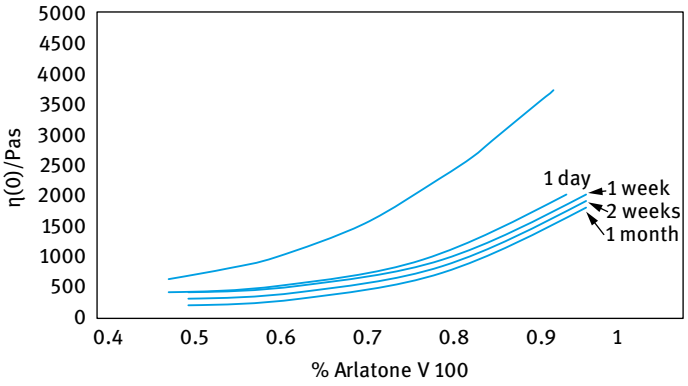

Fig. 9.18: Variation of residual viscosity with Arlatone V-100 concentration at various storage times.

1 day which could be due to equilibration of the structure. The results after 1 week, 2 weeks and 1 month are close to each other. There is a significant increase in $\eta(0)$ when the Arlatone V-100 concentration increased above 0.8 %. The creaming rate of the emulsion also showed a sharp decrease above 0.8 % Arlatone V-100 indicating the correlation between $\eta(0)$ and creaming rate.

A very useful method for predicting creaming is to measure the cohesive energy density as given by equation (9.49). As an illustration Fig. 9.19 shows the variation of cohesive energy density E_c with Arlatone V-100 concentration. The results clearly show a rapid increase in E_c above 0.8 % Arlatone V-100. E_c seems to show a decrease in the values after storage for 2 weeks. This may be due a small increase in droplet size (as a result of some coalescence) which results in a reduction in the cohesive energy density. This small increase in droplet size could not be detected by microscopy since the change was very small.

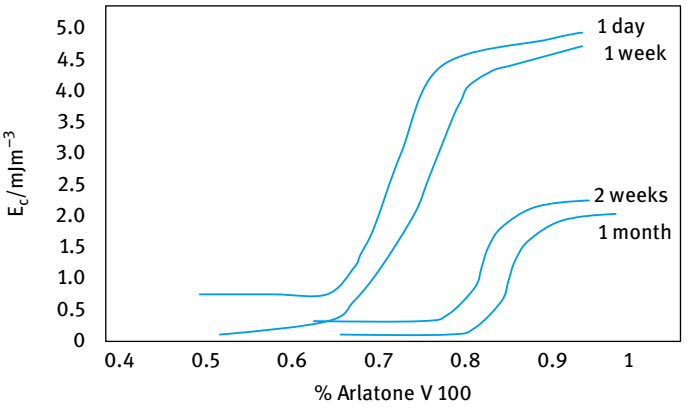

Fig. 9.19: Variation of E_c with % Arlatone V-100 in the emulsion.

9.13.3.3 Predicting flocculation using rheological techniques

Steady state rheological investigations may be used to investigate the state of flocculation of a dispersion. Weakly flocculated dispersions usually show thixotropy and the change of thixotropy with applied time may be used as an indication of the strength of this weak flocculation. These methods are only qualitative and one cannot use the results in a quantitative manner. This is due to the possible breakdown of the structure on transferring the formulation to the rheometer and also during the uncontrolled shear experiment. Better techniques to study flocculation of a formulation are constant stress (creep) or oscillatory measurements. By careful transfer of the sample to the rheometer (with minimum shear) the structure of the flocculated system may be maintained.

As mentioned above, a very important point that must be considered in any rheological measurement is the possibility of "slip" during the measurements. This is particularly the case with highly concentrated dispersions, whereby the flocculated system may form a "plug" in the gap of the platens leaving a thin liquid film at the walls of the concentric cylinder or cone-and-plate geometry. This behaviour is caused by some "syneresis" of the formulation in the gap of the concentric cylinder or cone and plate. To reduce "slip" one should use roughened walls for the platens. A vane rheometer may also be used.

Steady state shear stress–shear rate measurements are by far the most commonly used methods in many industrial laboratories. Basically the dispersion is stored at various temperatures and the yield value σ_β and plastic viscosity η_{pl} are measured at various intervals of time [21]. Any flocculation in the formulation should be accompanied by an increase in σ_β and η_{pl}.

A rapid technique to study the effect of temperature changes on the flocculation of a formulation is to carry out temperature sweep experiments, running the samples from say 5–50 °C. The trend in the variation of σ_β and η_{pl} with temperature can quickly

give an indication on the temperature range at which a dispersion remains stable (during that temperature range σ_β and η_{pl} remain constant).

If Ostwald ripening and/or coalescence occur simultaneously, σ_β and η_{pl} may change in a complex manner with storage time. Ostwald ripening and/or coalescence result in a shift of the particle size distribution to higher diameters. This has the effect of reducing σ_β and η_{pl}. If flocculation occurs simultaneously (having the effect of increasing these rheological parameters), the net effect may be an increase or decrease of the rheological parameters. This trend depends on the extent of flocculation relative to Ostwald ripening and/or coalescence. Therefore, following σ_β and η_{pl} with storage time requires knowledge of Ostwald ripening and/or coalescence. Only in the absence of these latter breakdown processes can one use rheological measurements as a guide to assessing flocculation.

Constant stress (creep) experiments can also be applied to predict flocculation. Basically a constant stress σ is applied on the system and the compliance J (Pa^{-1}) is plotted as a function of time. These experiments are repeated several times increasing the stress from the smallest possible value (that can be applied by the instrument), increasing the stress in small increments. A set of creep curves are produced at various applied stresses. From the slope of the linear portion of the creep curve (after the system reaches a steady state), the viscosity at each applied stress, η_σ, is calculated. A plot of η_σ versus σ allows one to obtain the limiting (or zero shear) viscosity $\eta(0)$ and the critical stress σ_{cr} (which may be identified with the "true" yield stress of the system. The values of $\eta(0)$ and σ_{cr} may be used to assess the flocculation of the dispersion on storage [21].

If flocculation occurs on storage (without any Ostwald ripening or coalescence), the values of $\eta(0)$ and σ_{cr} may show a gradual increase with increasing storage time. As discussed in the previous section (on steady state measurements), the trend becomes complicated if Ostwald ripening and/or coalescence occur simultaneously (both have the effect of reducing $\eta(0)$ and σ_{cr}).

The above measurements should be supplemented by particle size distribution measurements of the diluted dispersion (making sure that no flocs are present after dilution) to assess the extent of Ostwald ripening and/or coalescence. Another complication may arise from the nature of the flocculation. If flocculation occurs in an irregular way (producing strong and tight flocs), $\eta(0)$ may increase, while σ_{cr} may show some decrease and this complicates the analysis of the results. In spite of these complications, constant stress measurements may provide valuable information on the state of the dispersion on storage.

Carrying out creep experiments and ensuring that a steady state is reached can be time consuming. One usually carries out a stress sweep experiment, whereby the stress is gradually increased (within a predetermined time period to ensure that one is not too far from reaching the steady state) and plots of η_σ versus σ are established.

The above experiments are carried out at various storage times (say every two weeks) and temperatures. From the change of $\eta(0)$ and σ_{cr} with storage time and tem-

perature, one may obtain information on the degree and the rate of flocculation of the system. Clearly, interpreting the rheological results requires expert knowledge of rheology and measurement of the particle size distribution as a function of time.

One main problem in carrying the above experiments is sample preparation. When a flocculated dispersion is removed from the container, care should be taken not to cause much disturbance to that structure (minimum shear should be applied on transferring the formulation to the rheometer). It is also advisable to use separate containers for assessments of the flocculation; a relatively large sample is prepared and this is then transferred to a number of separate containers. Each sample is used separately at a given storage time and temperature. One should be careful in transferring the sample to the rheometer. If any separation occurs in the formulation the sample is gently mixed by placing it on a roller. It is advisable to use as minimum shear as possible when transferring the sample from the container to the rheometer (the sample is preferably transferred using a "spoon" or by simple pouring from the container). The experiment should be carried out without an initial pre-shear.

Dynamic (oscillatory) measurements can also be used to predict flocculation [21]. As mentioned above, in oscillatory measurements one carries out two sets of experiments.

Strain sweep measurements

In this case, the oscillation is fixed (say at 1 Hz) and the viscoelastic parameters are measured as a function of strain amplitude. G^*, G' and G'' remain virtually constant up to a critical strain value, γ_{cr}. This region is the linear viscoelastic region. Above γ_{cr}, G^* and G' starts to fall, whereas G'' starts to increase; this is the nonlinear region. The value of γ_{cr} may be identified with the minimum strain above which the "structure" of the dispersion starts to break down (for example breakdown of flocs into smaller units and/or breakdown of a "structuring" agent). From γ_{cr} and G', one can obtain the cohesive energy E_c (J m^{-3}) of the flocculated structure using equation (9.49). E_c may be used in a quantitative manner as a measure of the extent and strength of the flocculated structure in a dispersion. The higher the value of E_c the more flocculated the structure is.

Clearly E_c depends on the volume fraction of the dispersion as well as the particle size distribution (which determines the number of contact points in a floc). Therefore, for quantitative comparison between various systems, one has to make sure that the volume fraction of the disperse particles is the same and the dispersions have very similar particle size distribution. E_c also depends on the strength of the flocculated structure, i.e. the energy of attraction between the droplets. This depends on whether the flocculation is in the primary or secondary minimum. Flocculation in the primary minimum is associated with a large attractive energy and this leads to higher values of E_c when compared with the values obtained for secondary minimum flocculation (weak flocculation). For a weakly flocculated dispersion, such as the case with sec-

ondary minimum flocculation of an electrostatically stabilized system, the deeper the secondary minimum, the higher the value of E_c (at any given volume fraction and particle size distribution of the dispersion).

With a sterically stabilized dispersion, weak flocculation can also occur when the thickness of the adsorbed layer decreases. Again the value of E_c can be used as a measure of the flocculation – the higher the value of E_c, the stronger the flocculation. If incipient flocculation occurs (on reducing the solvency of the medium for the change to worse than θ-condition) a much deeper minimum is observed and this is accompanied by a much larger increase in E_c.

To apply the above analysis, one must have an independent method for assessing the nature of the flocculation. Rheology is a bulk property that can give information on the interparticle interaction (whether repulsive or attractive) and to apply it in a quantitative manner one must know the nature of these interaction forces. However, rheology can be used in a qualitative manner to follow the change of the formulation on storage.

Providing the system does not undergo any Ostwald ripening and/or coalescence, the change of the moduli with time and in particular the change of the linear viscoelastic region may be used as an indication of flocculation. Strong flocculation is usually accompanied by a rapid increase in G' and this may be accompanied by a decrease in the critical strain above which the "structure" breaks down. This may be used as an indication of formation of "irregular" and tight flocs which become sensitive to the applied strain. The floc structure will entrap a large amount of the continuous phase and this leads to an apparent increase in the volume fraction of the dispersion and hence an increase in G'.

Oscillatory sweep measurements

In this case, the strain amplitude is kept constant in the linear viscoelastic region (one usually takes a point far from γ_{cr} but not too low, i.e. in the midpoint of the linear viscoelastic region) and measurements are carried out as a function of frequency. Both G^* and G' increase with increase in frequency and ultimately above a certain frequency, they reach a limiting value and show little dependence on frequency. G'' is higher than G' in the low frequency regime; it also increases with increase in frequency and at a certain characteristic frequency ω^* (that depends on the system) it becomes equal to G' (usually referred to as the crossover point), after which it reaches a maximum and then shows a reduction with further increase in frequency.

From ω^* one can calculate the relaxation time τ of the system as given by equation (9.46). The relaxation time may be used as a guide for the state of the dispersion. For a colloidally stable dispersion (at a given particle size distribution), τ increases with increasing volume fraction of the disperse phase, ϕ. In other words, the crossover point shifts to lower frequency with increasing ϕ. For a given dispersion, τ increases

with increasing flocculation, providing the particle size distribution remains the same (i.e. no Ostwald ripening and/or coalescence).

The value of G' also increases with increasing flocculation, since aggregation of particles usually results in liquid entrapment and the effective volume fraction of the dispersion shows an apparent increase. With flocculation, the net attraction between the particles also increases and this results in an increase in G'. The latter is determined by the number of contacts between the particles and the strength of each contact (which is determined by the attractive energy).

It should be mentioned that in practice one may not obtain the full curve, due to the frequency limit of the instrument and also measurement at low frequency is time consuming. Usually one obtains part of the frequency dependency of G' and G''. In most cases, one has a more elastic than viscous system.

Most disperse systems used in practice are weakly flocculated and they also contain "thickeners" or "structuring" agents to reduce creaming or sedimentation and to acquire the right rheological characteristics for application, e.g. in hand creams and lotions. The exact values of G' and G'' required depend on the system and its application. In most cases a compromise has to be made between acquiring the right rheological characteristics for application and the optimum rheological parameters for long-term physical stability. Application of rheological measurements to achieve these conditions requires a great deal of skill and understanding of the factors that affect rheology.

9.13.4 Examples of applications of rheology for predicting flocculation

Hunter and Nicol [30] studied the flocculation and restabilization of kaolinite suspensions using rheology and zeta potential measurements. Fig. 9.20 shows plots of the yield value σ_β and electrophoretic mobility as a function of cetyl trimethyl ammonium bromide (CTAB) concentration at pH = 9.

σ_β increases with increasing CTAB concentration, reaching a maximum at the point where the mobility reaches zero (the isoelectric point, IEP, of the clay) and then decreases with a further increase in CTAB concentration. This trend can be explained on the basis of flocculation and restabilization of the clay suspension.

Initial addition of CTAB causes a reduction in the negative surface charge of the clay (by adsorption of CTA^+ on the negative sites of the clay). This is accompanied by a reduction in the negative mobility of the clay. When complete neutralization of the clay particles occurs (at the IEP) maximum flocculation of the clay suspension occurs and this is accompanied by a maximum in σ_β. On further increasing CTAB concentration, further adsorption of CTA^+ occurs, resulting in charge reversal and restabilization of the clay suspension. This is accompanied by a reduction in σ_β.

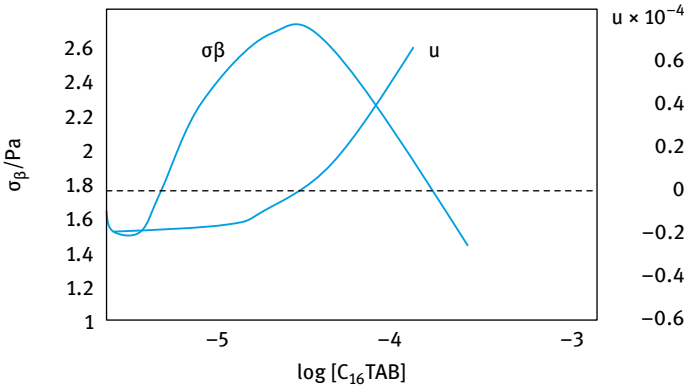

Fig. 9.20: Variation of yield value σ_β and electrophoretic mobility u with C_{16} TAB concentration.

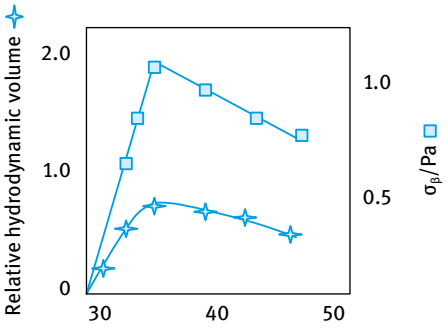

Fig. 9.21: Variation of σ_β and hydrodynamic volume with temperature.

Neville and Hunter [31] also studied the flocculation of polymethylmethacrylate (PMMA) latex stabilized with poly(ethylene oxide) (PEO). Flocculation was induced by adding electrolyte and/or increasing temperature. Fig. 9.21 shows the variation of σ_β with increasing temperature at constant electrolyte concentration.

It can be seen that σ_β increases with increasing temperature, reaching a maximum at the critical flocculation temperature (CFT) and then decreases with a further increase in temperature. The initial increase is due to the flocculation of the latex with increasing temperature, as a result of a reduction of solvency of the PEO chains with increasing temperature. The reduction in σ_β after the CFT is due to the reduction in the hydrodynamic volume of the dispersion.

The flocculation of sterically stabilized emulsions was investigated by addition of electrolyte (NaCl). Emulsions were prepared using an A–B–A block copolymer of PEO–PPO–PEO (Pluronic F127). Fig. 9.22 shows the variation of the yield value, calculated using the Herschel–Bulkley model [32] as a function of NaCl concentration at various storage times.

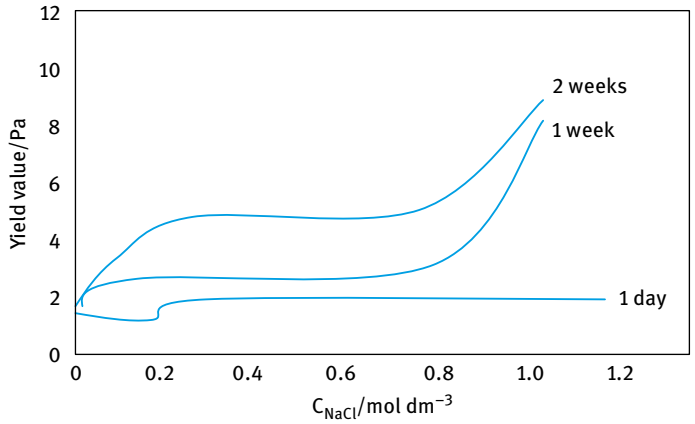

Fig. 9.22: Variation of yield value with NaCl concentration.

In the absence of NaCl, the yield value did not change with storage time over a period of 1 month, indicating absence of flocculation. In the presence of NaCl, the yield value increased with increasing storage time and this increase was very significant when the NaCl concentration was increased above 0.8 mol dm^{-3} NaCl.

The above increase in yield value indicated flocculation of the emulsion and this was confirmed by optical microscopy. The smaller increase in yield value below 0.8 mol dm^{-3} NaCl is indicative of weak flocculation and this could be confirmed by redispersion of the emulsion by gently shaking. Above 0.8 mol dm^{-3} NaCl, the flocculation was strong and irreversible. In this case, the solvency of the medium for the PEO chains becomes poor resulting in incipient flocculation.

Further evidence of flocculation was also obtained from dynamic (oscillatory) measurements. Fig. 9.23 shows the variation of G' with NaCl concentration at various storage times.

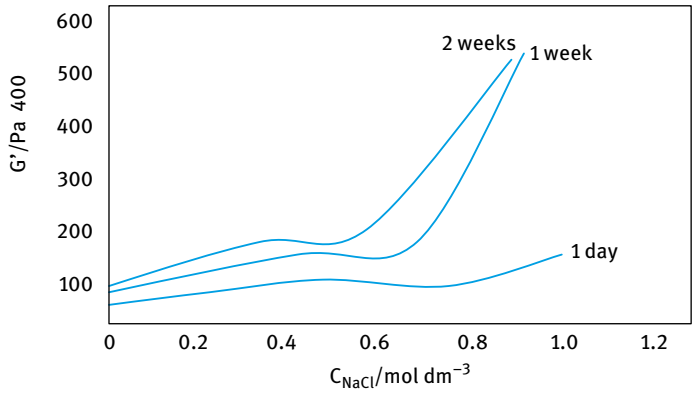

Fig. 9.23: Variation of G' with NaCl concentration.

Below 0.8 mol dm^{-3} NaCl, G' shows a modest increase with storage time over a period of two weeks indicating weak flocculation. Above 0.8 mol dm^{-3} NaCl, G' shows a rapid increase with increasing storage time indicating strong flocculation. This strong (incipient) flocculation is due to the reduction of solvency of PEO chains (worse than θ-solvent) resulting in strong attraction between the droplets which are difficult to redisperse [21].

9.13.5 Predicting emulsion coalescence using rheological techniques

As mentioned in Chapter 11 of Vol. 1, the driving force for emulsion coalescence is the thinning and disruption of the liquid film between the droplets [18]. When two emulsion droplets come into contact, say in a cream layer or a floc, or even during Brownian collision, the liquid film between them undergoes some fluctuation in thickness; the thinnest part of the film will have the highest van der Waals attraction and this is the region where coalescence starts. Alternatively, the surfaces of the emulsion droplets may undergo fluctuation producing waves, which may grow in amplitude; the strongest van der Waals attraction is at the apices of these fluctuations and coalescence occurs by further growth of the fluctuation. One may define a critical film thickness below which coalescence occurs.

The rate of coalescence is determined by the rate at which the film thins and this usually follows a first-order kinetics,

$$N = N_0 \exp(-Kt), \tag{9.53}$$

where N is the number of droplets after time t, N_0 is the number at zero time and K is the rate constant of coalescence.

Alternatively one can measure the average droplet diameter d as a function of time,

$$d = d_0 \exp(Kt). \tag{9.54}$$

Providing the emulsion does not undergo any flocculation, the coalescence rate can be simply measured by following the number of droplets or average diameter as a function of time. A given volume of the emulsion is carefully diluted into the Isotone solution of the Coulter Counter and the number of droplets is measured. The average diameter can be obtained using laser diffraction methods (e.g. using the Master Sizer). By following this procedure at various time periods, one can obtain the coalescence rate constant K.

Usually one plots log N or log d versus t and the slope of the line in the initial period gives the rate of coalescence K. Clearly, the higher the value of K, the higher the coalescence of the emulsion. An accelerated test may be used by subjecting the system to higher temperatures; usually the rate of coalescence increases with increasing temperature (although this is not always the case). One should be careful in the dilution

procedure, particularly if the oil is significantly soluble (say greater than 10 ppm) in the Isotone solution or in the tank of the Mastersizer. In this case, one should saturate the solution with the oil before diluting the concentrated emulsion for droplet counting or sizing.

Various rheological techniques can be applied for prediction of emulsion coalescence [21].

9.13.5.1 Viscosity measurements

In the absence of any flocculation, coalescence of an emulsion results in a reduction of its viscosity. At any given volume fraction of oil, an increase in droplet size results in a reduction in viscosity; this is particularly the case with concentrated emulsions. Thus by following the decrease in emulsion viscosity with time one may obtain information on its coalescence. However, one should be careful in applying simple viscosity measurements, particularly if flocculation occurs simultaneously (which results in an increase in the viscosity). It is possible in principle to predict the extent of viscosity reduction on storage, if one combines the results of droplet size analysis (or droplet number) as a function of time with the reduction in viscosity in the first few weeks.

Freshly prepared emulsions with various droplet sizes were prepared (by controlling the speed of the stirrer used for emulsification). The emulsifier concentration in these experiments should be kept constant and care should be taken that excess emulsifier is not present in the continuous phase. The viscosity of these freshly prepared emulsions is plotted versus the average droplet diameter. A master curve is produced that relates the emulsion viscosity to the average droplet size; the viscosity decreases monotonically with increase in the average droplet size.

Using the Coulter Counter or Mastersizer one can determine the rate of coalescence by plotting log of the average droplet diameter versus time in the first few weeks. This allows one to predict the average droplet diameter over a longer period (say 6–12 months). The predicted average droplet diameter is used to obtain the viscosity that is reached on storage using the master curve of viscosity versus average drop size.

The above procedure is quite useful for setting the limit of viscosity that may be reached on storage as a result of coalescence. With many creams, the viscosity of the system is not allowed to drop below an acceptable limit (which is important for the application). The limit that may be reached after one year storage may be predicted from the viscosity and rate constant measurements over the first few weeks.

9.13.5.2 Measurement of yield value as a function of time

Since the yield value σ_β of an emulsion depends on the number of contacts between the droplets, any coalescence should be accompanied by a reduction in the yield value. This trend is only observed if no flocculation occurs (this causes an increase in σ_β).

The above change measured using O/W emulsions that were stabilized with an A–B–A block copolymer of polyethylene oxide (PEO, A) and polypropylene oxide (PPO, B); Pluronic PEF 127. 60 : 40 O/W emulsions were prepared using 0.5, 1.0, 1.5, 2.0, 3, 4 and 5 % emulsifier. Fig. 9.24 shows the variation of droplet size with time at various Pluronic PEF 127 concentrations. At emulsifier concentration > 2 % there is no change of droplet size with time, indicating absence of coalescence. Below 2 % the droplet size increased with time indicating coalescence.

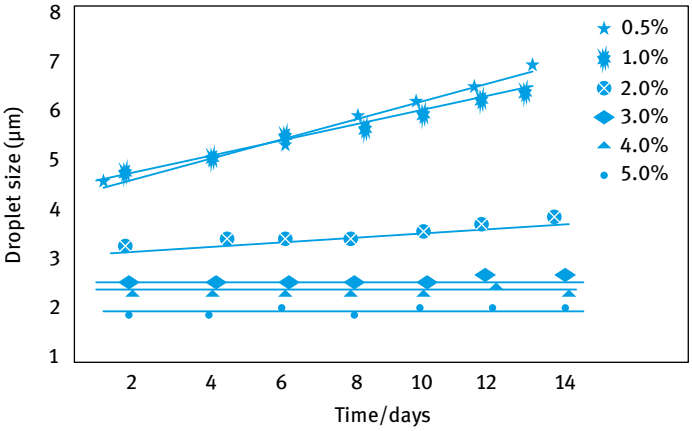

Fig. 9.24: Variation of droplet size with time at various Synperonic PEF 127 concentrations.

9.13.5.3 Measuring storage modulus G' as a function of time

This is perhaps the most sensitive method for predicting coalescence. G' is a measure of the contact points of the emulsion droplets as well as their strength. Providing no flocculation occurs (which results in an increase in G'), any reduction in G' on storage indicates coalescence.

The above trend was confirmed using the emulsions described above. The emulsions containing less than 3 % Pluronic PEF 127 showed a rapid reduction in G' when compared with those containing > 3 % which showed virtually no change in G' over 2 weeks period. This is illustrated in Fig. 9.25.

The correlation between the emulsion elastic modulus and coalescence rate can be easily represented if one calculates the relative decrease in G' after 2 weeks [21],

$$\text{relative decrease of } G' = \left(\frac{G_{\text{initial}} - G_{\text{after 2 weeks}}}{G_{\text{initial}}} \right) \times 100. \tag{9.55}$$

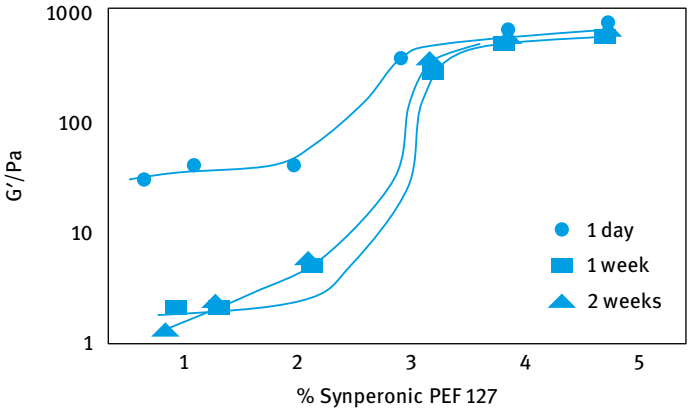

Fig. 9.25: Variation of G' with Pluronic PEF 127 concentration at various storage times.

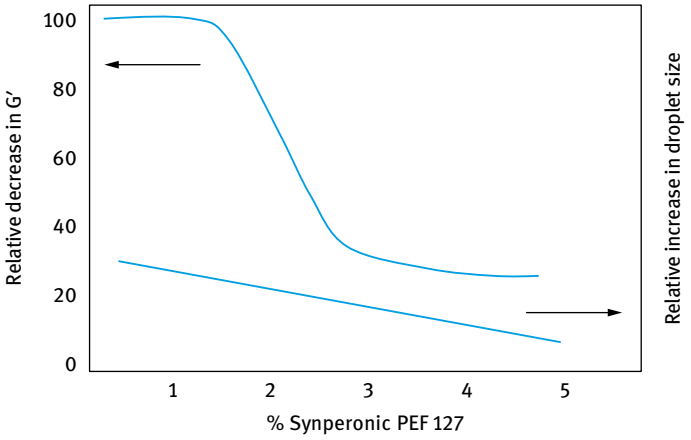

Fig. 9.26: Correlation of relative decrease in G' with relative increase in droplet size.

Fig. 9.26 shows the variation of the relative decrease of G' and relative increase in droplet size with Pluronic PEF 127 concentration. The correlation between the relative decrease in G' and relative increase in droplet size as a result of coalescence is now very clear.

The cohesive energy E_c (given by equation (9.49)) is the most sensitive parameter for assessing coalescence. Any coalescence results in a decrease in the number of contact point and causes a reduction in E_c. Using the above mentioned emulsions, E_c was found to decrease with increasing droplet size (as a result of coalescence). At and above 3 % Pluronic PEF 127, E_c remained virtually unchanged, indicating absence of coalescence. Fig. 9.27 shows the variation of the relative decrease of E_c with the relative increase in droplet size; the correlation is clear.

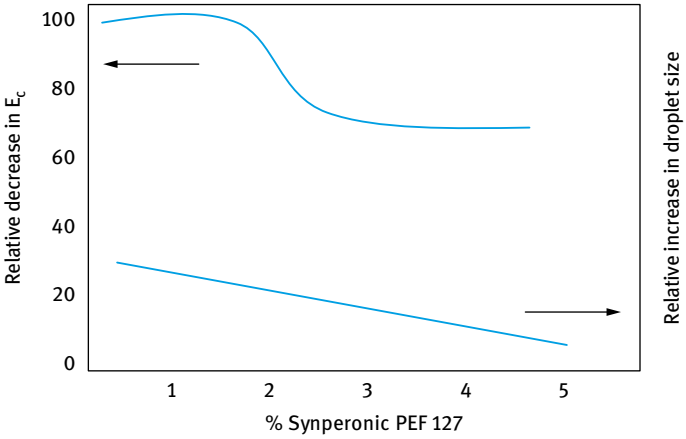

Fig. 9.27: Correlation of relative decrease in E_c with relative increase in droplet size.

References

[1] Lyklema J. In: Tadros T, editor. Solid/liquid dispersions. London: Academic Press; 1987.
[2] Parfitt GD, Rochester CH, editors. Adsorption from solution at the solid/liquid interface. London: Academic Press; 1983.
[3] Fleer GJ, Cohen-Stuart MA, Scheutjens JMHM, Cosgrove T, Vincent B. Polymers at interfaces. London: Chapman and Hall; 1993.
[4] Hunter RJ. Zeta potential in colloid science. London: Academic Press; 1981.
[5] Kissa E. Dispersions: Characterization, testing and measurement. New York: Marcel Dekker; 1999.
[6] Smoluchowski MV. Physik. Z., 17, 557, 585 (1916).
[7] Debye P. J Chem Phys. 1933;1:13.
[8] Bugosh J, Yeager E, Hovarka F. J Chem Phys. 1947;15:542.
[9] Yeager E, Bugosh J, Hovarka F, McCarthy J. J Chem Phys. 1949;17:411.
[10] Dukhin AS, Goetz PJ. Colloids and Surfaces. 1998;144:49.
[11] Oja T, Petersen GL, Cannon DC. US Patent 4,497,208 (1985).
[12] O'Brian RW. J Fluid Mech. 1988;190:71.
[13] O'Brian RW. J Fluid Mech. 1990;212:81.
[14] O'Brian RW, Garaside P, Hunter RJ. Langmuir. 1994;10:931.
[15] O'Brian RW, Cannon DW, Rowlands WN. J Colloid Interface Sci. 1995;173:406.
[16] Fuchs N. Z Physik. 1936;89:736.
[17] Thompson W (Lord Kelvin). Phil Mag. 1871;42:448.
[18] Tadros T. Emulsions. Berlin: De Gruyter; 2016.
[19] Ferry JD. Viscoelastic properties of polymers. New York: John Wiley & Sons; 1980.
[20] Mackosko CW. Rheology, Principles, Measurement and Applications. New York: Wiley-VCH; 1994.
[21] Tadros T. Rheology of Dispersions. Weinheim: Wiley-VCH; 2010.
[22] Goodwin JW, Hughes RW. Advances Colloid Interface Sci. 1992;42:303.
[23] Tadros TF. Advances Colloid and Interface Science. 1996;68:97.

[24] Goodwin JW, Hughes RW. Rheology for Chemists. Cambridge: Royal Society of Chemistry Publication; 2000.
[25] Whorlow RW. Rheological Techniques. Chichester: Ellis Horwood; 1980.
[26] Buscall R, Goodwin JW, Ottewill RH, Tadros TF. J Colloid Interface Sci. 1982;85:78.
[27] Krieger IM, Advances Colloid and Interface Sci. 1972;3:111.
[28] Tadros TF. Advances Colloid and Interface Science. 2004;108–109:227.
[29] Salager JL. Pharmaceutical emulsions and suspensions. New York: Marcel Dekker; 2000.
[30] Hunter RJ, Nicol SK. J Colloid Interface Sci. 1968;28:200.
[31] Neville PC, Hunter RJ. J Colloid Interface Sci. 1974;49:204.
[32] Herschel WH, Bulkley R. Proc Amer Soc Test Materials. 1926;26:621; Kolloid Z. 1926;39:291.

Index